U.PORTO

FEUP FACULDADE DE ENGENHARIA
UNIVERSIDADE DO PORTO

EXPERIMENTAL AND NUMERICAL ASSESSMENT OF REINFORCED CONCRETE JOINTS SUBJECTED TO SHEAR LOADING

Diogo André de Oliveira Figueira da Silva

Dissertation submitted to fulfill requirements of the degree

DOCTORATE IN CIVIL ENGINEERING – STRUCTURES

Supervisor: Professor Afonso António de Serra Neves

Co-Supervisor: Professor Rui Artur Bártolo Calçada

Co-Supervisor: Professor Carlos Filipe Ferreira de Sousa

SEPTEMBER 2017

POPH QUALIFICAR É CRESCER.
QREN QUADRO DE REFERÊNCIA ESTRATÉGICO NACIONAL PORTUGAL 2007.2013
GOVERNO DA REPÚBLICA PORTUGUESA
UNIÃO EUROPEIA Fundo Social Europeu

DOCTORAL PROGRAM IN CIVIL ENGINEERING 2016/2017

DEPARTMENT OF CIVIL ENGINEERING

Tel. +351 22 508 1901

Fax +351 22 508 1446

✉ prodec@fe.up.pt

Edited by

UNIVERSITY OF PORTO, FACULTY OF ENGINEERING

Rua Dr. Roberto Frias

4200-465 PORTO

Portugal

Tel. +351 22 508 1400

Fax +351 22 508 1440

✉ feup@fe.up.pt

http://www.fe.up.pt

To my father, God bless him

Science without religion is lame, religion without science is blind.
Albert Einstein

ACKNOWLEDGMENTS

The author acknowledges the financial support of the Portuguese Science and Technology Foundation (FCT) through the R&D&I unit CONSTRUCT and the PhD Grant SFRH/BD/65111/2009. This work has also been funded by *Agência de Inovação, S. A.*, and *Mota-Engil Engenharia e Construção*, through the research project Innovative Precast Solutions for High Speed Rail Tracks (SIPAV). Acknowledgements are extended to the Laboratory Testing of Construction Materials (LEMC) and Tribology, Vibrations and Industrial Management Unit (CETRIB) for their material support.

Finally, a personal acknowledgment message to all the people who helped in the realization of this Thesis, particularly:

- to my family, for the eternal and huge support in my academic and personal life;
- to Professors Afonso Serra Neves and Rui Calçada, scientific supervisors of this work, for sharing their experience and providing the necessary means to outdone the several tasks;
- to Professor Carlos Sousa, also scientific supervisor of this work, for all valuable scientific contributions, references and the unsurpassed way I was always encouraged and accompanied;
- to all friends, colleagues and professors who shared my academic life in a journey of learning and personal enrichment.

ABSTRACT

The knowledge about the cyclic behavior and the effects of fatigue on interfaces between concrete cast at different times, subjected to shear stress, is still very limited. This aspect is particularly relevant in structures subjected to important cyclic loads, such as railway bridges. In this context, firstly, a brief state-of-the-art on the monotonic and cyclic behavior of interfaces between concretes cast at different times is presented, especially reflecting the case of a joint between a precast beam and a cast-in-place slab, where the contact surface between the old and the new concrete is usually a free surface, left without further treatment after vibration of the old concrete. Then, the test campaign, which was aimed at obtaining experimental support for modeling the behavior of such interfaces, subjected to a high number of load cycles, is described, and the corresponding results discussed and analyzed in terms of slip and crack opening, stress variations in the monotonic tests, failure mode, and number of resisting load cycles. It was further observed that the number of resisting load cycles increases as the maximum load level decreases. Based on this evidence, an experimental S-N curve was set for this type of interface.

A concrete interface is a material discontinuity which requires special care in structural design and assessment. Therefore, the definition of design expressions, based on experimental testing data, must ensure the needed reliability depending on the type of structure and its use. In the present work, a new proposal for the design of concrete interfaces subjected to shear loading is presented for different roughness profile types. The proposal is characterized by 3 linear branches (for monotonic loading), an S-N curve (for cyclic loading) and is the result of a parametric analysis of existing experimental data (obtained by the author and also from an extensive literature search) based on statistical and probabilistic methods. Design expressions were defined in order to minimize dispersion and variability of the safety factor values for each considered experimental test, and also to assure that those values are within a target range (defined according to reliability considerations). These improvements were noticed when the new proposal was compared with the most common design code recommendations.

A nonlinear finite element model is developed to evaluate the behavior of a dowel bar subjected to monotonic loading and embedded on a single concrete block substrate. In the model, a “beam element” representation of the steel reinforcing bar is used, considering material plasticity, rotational degrees of freedom and flexural stiffness. The bar is connected

to concrete embedment through several Winkler spring elements to simulate the deformability and strength of the concrete substrate. Comparison with results from experimental tests available in literature allowed to calibrate force-displacement relations for the nonlinear Winkler spring response during an imposed dowel displacement up to 4 mm. Finally, new coefficients are included in those relations in order to account for the influence of concrete cover and confinement imposed by stirrups.

Later, the nonlinear finite element model is extended to assess the response of a concrete interface submitted to static loading. In the model, an interface element simulates aggregate interlock of the concrete joint and the “beam element” representation of the steel reinforcing bars is used. The reinforcing bars are connected to concrete embedment through several spring elements to simulate dowel action and bond along the bar length. Considering geometric non-linearity, or kinking, effect influence of the deformed reinforcing bars, each strength mechanism is modeled separately in order to determine the corresponding contribution to the joint shear stress. Comparison with experimental results available in literature allowed to determine new stress-strain relationships for the interface aggregate interlock element for two types of interface roughness profiles: monolithic concrete cracks, and interfaces between concretes cast at different times corresponding to a free surface. These new constitutive relations are suitable to be use in the case of a concrete interface with embedded reinforcing steel bars.

KEYWORDS: Concrete; Interface; Shear transfer; Cyclic loads; Experimentation; Design codes; Finite element model.

RESUMO

O conhecimento sobre o comportamento cíclico e os efeitos da fadiga nas interfaces entre betões de idades diferentes, submetidas a esforço rasante, é ainda muito limitado. Este aspeto é particularmente relevante em estruturas submetidas a cargas cíclicas importantes, tais como pontes ferroviárias. Neste contexto, em primeiro lugar, um breve estado-da-arte sobre o comportamento monotónico e cíclico de interfaces entre betões de idades diferentes é apresentado, refletindo especialmente o caso de uma junta entre uma viga pré-fabricada e a laje betonada "in situ", onde a superfície de contacto entre os betões é uma superfície livre de betonagem, sem qualquer tratamento posterior à vibração do betão de maior idade. Em seguida, a campanha de ensaios, que teve como objetivo a obtenção de apoio experimental para modelar o comportamento de tais interfaces, submetidas a um elevado número de ciclos de carga, é descrita, e os resultados correspondentes discutidos e analisados em termos de deslizamento e abertura de fenda, variações dos esforços nos ensaios monotónicos, modo de rotura, e número de ciclos de carga atingidos. Constatou-se ainda que o número de ciclos atingidos aumenta à medida que o nível máximo de carga diminui. Com base nessas evidências experimentais, uma curva S-N foi definida para este tipo de interface.

Uma interface entre dois betões é uma descontinuidade material que requer cuidados especiais no projeto e avaliação estruturais. Assim, a definição de expressões de dimensionamento, com base em dados de ensaios experimentais, deve assegurar a fiabilidade necessária, dependendo do tipo de estrutura e da sua utilização. No presente trabalho, uma nova proposta para o dimensionamento de interfaces entre betões submetidas a esforço rasante é apresentada para diferentes tipos de perfil de rugosidade. A proposta é caracterizada por três ramos lineares (para carregamentos monotónicos), uma curva S-N (para cargas cíclicas) e é o resultado de uma análise paramétrica dos dados experimentais existentes (obtidos pelo autor e também a partir de uma extensa pesquisa bibliográfica) com base em métodos estatísticos e probabilísticos. As expressões de dimensionamento foram definidas de modo a minimizar a dispersão e a variabilidade dos valores de fator de segurança para cada ensaio experimental considerado, e também para assegurar que esses valores estão dentro de um intervalo desejado (definido de acordo com considerações acerca de fiabilidade estrutural). Estes aperfeiçoamentos adquiriram uma evidência particular quando a nova proposta foi comparada com as recomendações de dimensionamento regulamentares.

Um modelo não-linear de elementos finitos é desenvolvido de modo a avaliar o comportamento do efeito de cavilha de um varão submetido a um carregamento monotónico, e embebido num único bloco de betão funcionando como substrato. No modelo, a representação dos varões de aço da armadura é considerada através de elementos de viga, considerando plasticidade material, graus de liberdade de rotação e rigidez face a momento fletores. A armadura é ligada ao betão através de vários elementos constituídos por molas Winkler para simular a deformabilidade e a resistência do substrato. A comparação com resultados experimentais disponíveis na bibliografia permitiu calibrar relações força-deslocamento para a resposta não-linear das molas Winkler ao longo de um deslizamento imposto até 4 mm. Por último, novos coeficientes são incluídos nessas expressões de modo a ter em conta a influência do recobrimento lateral e do confinamento providenciado por estribos.

Posteriormente, o modelo não-linear de elementos finitos é estendido para conseguir prever a resposta estrutural de uma interface entre betões sujeita a um carregamento estático. No modelo, um elemento de interface simula o imbricamento entre agregados na junta de betonagem e a representação dos varões de aço da armadura é considerada através de elementos de viga. A armadura é ligada ao substrato de betão através de vários elementos de mola a simular o respetivo efeito de cavilha e a aderência aço/betão ao longo do comprimento da barra. Tendo em conta a influência da não-linearidade geométrica associada à deformação dos varões, ou efeito de dobra, cada mecanismo resistente é modelado separadamente de modo a determinar-se a respetiva contribuição para o esforço rasante na junta de betonagem. A comparação com resultados experimentais disponíveis na bibliografia permitiu determinar novas relações tensão-deslocamento para o elemento de interface a simular o mecanismo de imbricamento dos agregados, para dois tipos de perfil de rugosidade de uma interface: fendas no betão monolítico, e interfaces entre betões de idades diferentes correspondentes a uma superfície livre de betonagem. Estas novas relações constitutivas são passíveis de serem usadas no caso de uma interface entre betões reforçada com armadura embebida.

PALAVRAS-CHAVE: Betão; Interface; Esforço rasante; Ações cíclicas; Instrumentação; Regulamentação; Elementos Finitos.

CONTENTS LIST

LIST OF TABLES

LIST OF FIGURES

SYMBOLS

Latin upper case letters

A_s	cross sectional area of reinforcement
C_f	aggregate effectiveness coefficient
DI	damage build-up parameter
E	effect of actions
E_c	concrete Young's modulus
E_s	reinforcement Young's modulus
F	applied force
F_s	reinforcement axial force
$F_{s,x}$	reinforcing bar force component at the interface section in the x axis direction
F_v	Winkler spring force
F_{vR}	Winkler spring peak load
$F_{vR,c}$	Winkler spring peak load when concrete is confined by stirrups
$F_{vR,split}$	Winkler spring splitting strength
I	reinforcing bar moment of inertia
K	coefficient dependent on the confinement in the concrete substrate under the reinforcing bar; parameter dependent on the interface roughness
L	interface length
L_c	curvature influencing zone length
N	number of cycles reached until fatigue failure occurs
P	probability
P_f	failure probability
R	structural resistance
R_a	average roughness
R_d	resistance design values
R_{pm}	mean peak height
R_{vm}	mean valley depth
SF_R	safety factor for structural resistance
T_R	reference period
V	shear force
V_{agg}	shear force corresponding to the aggregate interlock mechanism
V_d	dowel force
$V_{d,new}$	new concrete dowel force
$V_{d,old}$	old concrete dowel force
V_{dR}	dowel strength
$V_{dR,split}$	dowel splitting strength

Latin lower case letters

b	interface width
c	lateral concrete cover length; parameter dependent on the interface roughness
d	distance
f_c	concrete compressive strength

f_{c1} old concrete compressive strength
f_{c2} new concrete compressive strength
f_c' specified concrete compressive strength
f_c^* concrete strength under a biaxial or triaxial stress state caused by confinement due to local compression
$f_{c,c}$ concrete strength under biaxial or triaxial compression caused by confinement due to the presence of stirrups.
$f_{c,cyl}$ concrete cylinder compressive strength
f_{cc} concrete compressive strength measured in cube specimens
f_{cd} design value for the concrete compressive strength
f_{ck} characteristic value for the concrete compressive strength
f_{ct} concrete tensile strength
f_{ctd} design value for the concrete tensile strength
f_t reinforcement tensile strength
f_y reinforcement yield stress
f_{yd} design value for the reinforcement yield stress
i inclination angle of the sliding plane
k_0 elastic stiffness of the concrete substrate
k_c concrete substrate stiffness
k_{sp} Winkler spring stiffness
$k_{sp,b}$ stiffness of the springs simulating steel/concrete bond behavior
k_{sub} elastic stiffness of concrete substrate in the finite element models
n load cycle number; number of bars crossing the interface; number of tests in an experimental campaign
s slip
s_1 slip value at maximum shear stress in a monotonic test
s_{1n} slip value for which is observed an exponentially grow of interface displacements in a cyclic test
s_2 local minimum slip observed in a monotonic test
s_{2n} slip value for which is observed an interface response changing in a cyclic test
s_{c1} dowel slip at maximum force V_{dR} in specimens confined by stirrups
s_{end} slip value at the end of the tests performed to induce an initial crack at the interface
s_{max} maximum slip value
s_{min} minimum slip value
s_{new} maximum dowel vertical displacement in the new concrete
s_{old} maximum dowel vertical displacement in the old concrete
s_{sp} spring spacing
x distance between the specimen limit (or the concrete interface plane) and a certain bar cross-section
w crack opening
z height of a given point of the roughness profile from an average plane of reference

Greek upper case letters

Φ cumulative standard normal distribution function; bar diameter

Greek lower case letters

α	angle between the interface and the reinforcement axis
α_R	resistance sensitivity factor
β	reliability index
β_c	coefficient allowing for the angle of the diagonal strut
γ	volumetric weight
δ_h	relative horizontal displacement between the reinforcing bar and the surrounding concrete
δ_v	dowel vertical displacement
δ_{v1}	dowel vertical displacement at the peak load
$\delta_{v1,c}$	dowel vertical displacement at the peak load when concrete is confined by stirrups
ε_s	reinforcement strain
ε_{su}	reinforcement strain at maximum load
κ_1	coefficient of efficiency for tensile force
κ_2	coefficient for flexural resistance of reinforcement (dowel action)
μ	mean value; tangent of the angle i
ν	Poisson's ratio; reduction factor for concrete cracked in shear;
ρ	interface transverse reinforcement rate; volumetric mass density
σ	standard deviation
σ_2	confinement stress
σ_E	standard deviation of the action effect
σ_n	interface normal stress
$\sigma_{n,exp}$	σ_n values obtained from experimental tests
σ_s	reinforcement axial stress
σ_R	standard deviation of structural resistance
τ	interface shear stress
τ_2	local minimum shear stress observed in a monotonic test
τ_{agg}	shear stress due to the aggregate interlock mechanism
$\tau_{agg,exp}$	τ_{agg} values obtained from experimental tests
τ_b	bond stress
$\tau_{b,max}$	maximum bond stress
τ_c	cohesion contribution to shear stress
τ_{cr}	shear stress corresponding to the instant at which interface crack opening begins
τ_d	shear stress provided by dowel action of the transverse reinforcement
τ_f	friction contribution to shear stress
τ_{MAX}	maximum shear stress measured in tests performed to induce an initial crack at the interface
τ_{max}	maximum shear stress applied in a load cycle
τ_{min}	minimum shear stress applied in a load cycle
τ_R	interface monotonic shear resistance
τ_{Rd}	design value for the interface monotonic shear resistance
$\tau_{Rd,fat}$	fatigue design value for the interface shear resistance
ϕ	reinforcing bar diameter

χ	reinforcement curvature
χ_t	reinforcement curvature at onset of tensile strength
χ_y	reinforcement curvature at onset of section plasticization
ψ	nonlinearity coefficient for Winkler spring behavior
ω	nonlinear coefficient multiplying the concrete substrate elastic stiffness in the BEF expressions
ω_c	mechanical reinforcement ratio

ACRONYMS

Upper case letters

BEF	Beam resting on an Elastic Foundation
CETRIB	Tribology, Vibrations and Industrial Management Unit
FB	2D Fixed Bed finite element modeling approach
FCT	Portuguese Science and Technology Foundation
FE	Finite Element
FEM	Finite Element Method; Finite Element Model
ED	3D Embedded Dowel finite element modeling approach
LEMC	Laboratory Testing of Construction Materials
LVDT	Linear Variable Differential Transformer
SIPAV	Innovative Precast Solutions for High Speed Rail Tracks
ULS	Ultimate Limit State

Lower case letters

fib	fédération internationale du béton

1
INTRODUCTION

1.1 BACKGROUND

A bridge is a constructive solution developed in order to overcome certain obstacles that are in a way or a path, like a river or a road, where the structural component has a decisive weight in its design. Variables to consider in bridge design are mainly functional conditions imposed by actions related to traffic and environmental, the technology available and difficulties inherent to the obstacle to overcome, such as the valley topographic profile or the geotechnical resistance of the land.

There are several components which together form the bridge. It can be divided in terms of superstructure, which is the bridge deck, and infrastructure, the columns, foundations, abutments and support devices. In this context, the bridge deck has a specific inherent complexity in terms of design and calculation. One of the features particularly responsible for this complexity is related to its construction procedure. The adopted procedure is in many cases decisive in the choices made in design, and its consideration is indispensable in that study.

Sometimes, in order to reduce the time required for completion and to get economic benefits from the use of optimized configurations and standard solutions with great repeatability, a construction procedure based on precast structural elements is adopted. Within the various possibilities for the precast solution, decision is made considering aspects as span length, material properties and cost, available transport means and existing continuity options (Newhouse 2005). Typically, the solution consists in the use of precast concrete beams and a cast-in-place slab (see Figure 1-1). The beams have an I or U-shaped cross-section (see

Figures 1-2 and 1-3), length less than 50 m and continuity is materialized through cross-beams and the cast-in-place slab (Miller et al. 2004). Consequently, beam/slab connection, or joint, is an interface between concretes cast at different times, subjected to normal and shear stresses, that should receive particular attention in bridge design and structural analysis (see Figure 1-2). A concrete joint is a material discontinuity on the bridge deck that may require, in order to ensure safety purposes, a higher amount of transverse reinforcement comparing to the case of a bridge deck built with a one single material. A higher reinforcement rate is necessary to have a monolithic behavior, increasing stiffness and bending strength.

Figure 1-1 – Construction of a bridge deck with precast concrete beams (CPCI 2015).

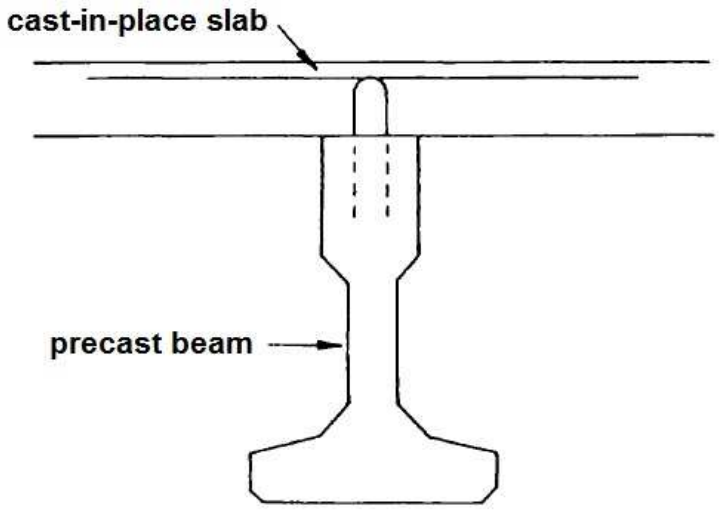

Figure 1-2 – Interface between an I-shaped precast beam and a cast-in-place slab.

Figure 1-3 – Precast U-shaped beams for bridge decks (Banagher 2015).

Systematic study of concrete joints subjected to shear loading began in the 1950s with experimental tests aiming to determine the interface strength mechanisms mobilized in shear transfer and their influence. The geometry defined for specimens typically corresponds to the classical solution of a push-off test (Hofbeck et al. 1969), where the line of action of the resultant force applied is collinear to the interface surface, thus subjected to shear stress. Tests performed in concrete beams (Patnaik 2001) and pull-off specimens (Mattock and Hawkins 1972) are also common but, in those cases, behavior is different compared to a cracked interface in a push-off specimen, where the shear stress can be determined with sufficient accuracy without any further modeling (Hsu et al. 1986).

Research on this phenomenon arose not only for precast solutions but also for structural rehabilitation and strengthening, where a concrete overlay is added to the original concrete substrate. The experimental tests serve as basis for existing recommendations and design expressions in legal codes and regulations. These recommendations relate to Ultimate Limit State (ULS), in which the interface is considered to be already cracked. In this case, bond

created by chemical reactions between concretes, Van der Waals forces and water absorption by the older concrete, is lost and shear strength decreases (Santos and Júlio 2011).

After cracking, the interface departs from monolithic behavior and shear strength is mobilized by aggregate interlock and dowel action of the transverse reinforcement (Maekawa et al. 2003). Aggregate interlock (see Figure 1-4) originates from developed stresses in contact areas between concretes (cohesion) and also from the clamping effect of transverse reinforcement (hereinafter called friction mechanism in this present dissertation), whose axial force is in equilibrium with bond stresses established in the steel/concrete interface. In turn, dowel action arises from the sum of three different mechanisms: bending stiffness of the steel bar embedded in the concrete substrate, bar shear stiffness and the non-linear geometric (kinking) effect. Interface roughness, material strength, reinforcement ratio and bar diameter are the parameters involved in these mechanisms contributing to shear transfer in the concrete joint.

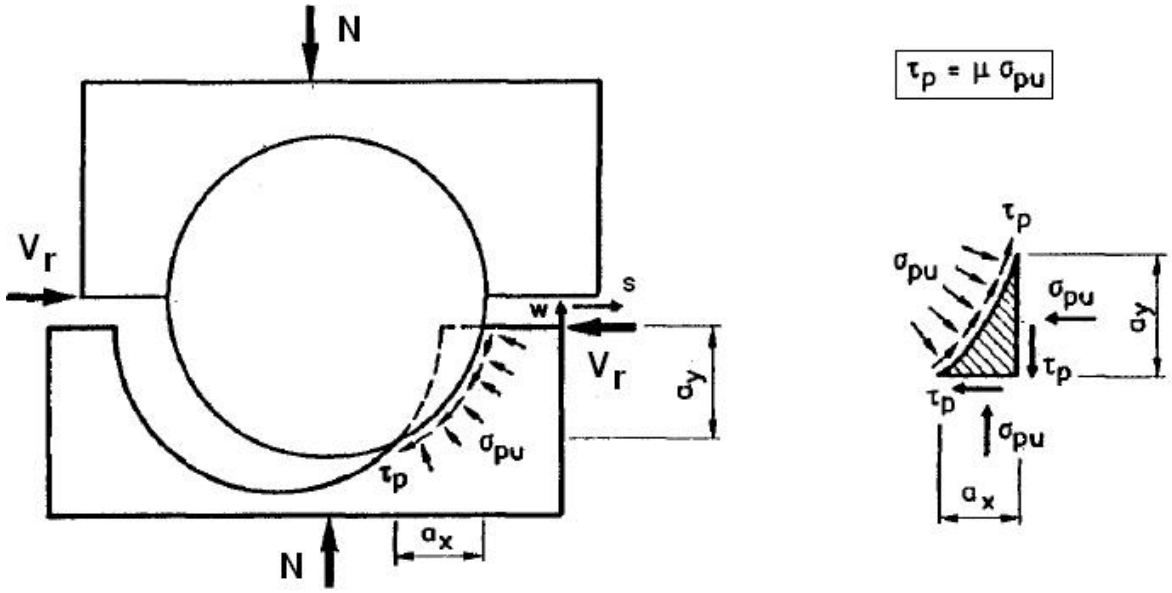

Figure 1-4 – Stresses developed in contact areas between the two concretes (Walraven 1994).

For interface roughness, surfaces may be classified (CEN 2004) as very smooth (surface cast against steel, plastic or specially prepared wooden molds), smooth (a slipformed or extruded surface, or a free surface left without further treatment after vibration), rough (surface with at least 3 mm roughness at about 40 mm spacing, achieved by raking, exposing of aggregate or other methods giving an equivalent behavior) and indented. Interfaces resulting from a crack in monolithic concrete can also be classified as a rough surface

(Mattock 2001). Usually, roughness is measured through laser scanning or mechanical contour plot instruments (Santos e Júlio 2013).

Features and advantages associated to the use of precast elements in bridge engineering gain special importance in the case of railway bridges, especially for high-speed traffic, where safety and user comfort requirements imply the construction of a very significant number of bridges along the track (see Figure 1-5). Interest in high-speed is growing and it is estimated that the number of countries to adopt this solution double in the coming years and decades (Sousa 2012). This increase is mainly due to its reliability, comfort and ability to cover vast geographical distances in a short period of time. It is also an alternative that provides clear environmental benefits in terms of pollution through the emission of "greenhouse effect" gases.

Figure 1-5 – High-speed railway bridge with precast beams (Taiwan 2015).

In railway bridges, successive train passing during lifetime period of the structure causes a high number of load cycles that may require some particular attention regarding damage associated with fatigue. In structural analysis and design, this damage can be sufficient to impose an increase in interface reinforcement rate, or other strengthening options, compared

with the case of monotonic loading. Fatigue issues are especially relevant in precast structures because optimized solutions originate slender cross-sections subjected to higher stresses. When the fatigue loading consists on several low amplitude cycles, not high enough for plastic deformation to occur, it is commonly named as a "high cycle" loading. In this case, material strength is usually characterized by an S-N curve, or Wöhler curve, relating stress amplitude with the number of load cycles applied. In turn, accumulated fatigue damage can be predicted by the Palmgren-Miner rule (CEB 1988) or fracture mechanics Paris law (Paris 1964). Plastic deformations in a structure caused by cyclic loading are typically associated with seismic actions, where high amplitude displacements are imposed and failure occurs for a few cycles ("low cycle" loading).

After this brief background description, we can conclude that the behavior of concrete interfaces subjected to normal and shear stresses is a vast subject, significant in structural analysis, involving several strength mechanisms, loading features, material properties and parameters. Therefore, it is important to define a case study or the aspects to evaluate in concrete interface behavior. In this sense, the aim and scope of the present dissertation are presented below.

1.2 AIM AND SCOPE

Although it also addresses concrete interfaces with another types of roughness profile, this present dissertation will particularly focus on interfaces between concretes cast at different times, especially reflecting the case of a joint between a precast beam and a cast-in-place slab, where the contact surface between the old and the new concrete is usually a free surface, left without further treatment after vibration of the old concrete. This case is particularly common in railway bridges, in which train passages give rise to a significant number of load cycles during the working life of the structure. Thus, behavior of those interfaces subjected to "high cycle" fatigue loading, along with monotonic loading, is a main objective.

When the joint is still uncracked, behavior is different and similar to monolithic concrete. Therefore, determination of the interface load cracking values is important and also an objective. Interface behavior analysis is performed in terms of a critical observation of experimental results, strength evaluation and numerical finite element modeling.

Due to the lack of available experimental data concerning this type of concrete joints, a new experimental campaign is designed and implemented in this present work aiming to fulfill the intended objectives and sustain conclusions. Push-off specimens are developed in order to reproduce typical interfaces between precast beams and cast-in-place slabs in railway bridge decks in terms of material properties and parameters such as reinforcement rate. A new experimental campaign is relevant because studies conducted to the present date focus mainly on cracks in monolithic concrete subjected to monotonic loading. In turn, regarding cyclic loading, research falls mostly on interfaces subjected to "low cycle" loads. Usually, study of the cyclic structural behavior focuses on determining the number of cycles achieved, before fatigue failure occurs, for each range of applied loading and also assessing the progression of displacements throughout the experimental tests. Besides addressing those aspects of greatest importance and priority, this work also aims to clarify the progression of interface slip and crack opening when these displacement values are already significantly high and the dowel action of the transverse reinforcement assumes more predominance. Another aspects to assess in fatigue behavior include influence of the minimum shear force value applied during cyclic loading, when the maximum shear force value is kept constant, and the failure modes associated with each test by observing the reinforcement condition at the end of the test.

Strength evaluation uses statistical and probabilistic methods in order to purpose new design expressions and determine structural reliability associated, depending on the type of structure and its use, number of experimental tests, the scatter of data, parameters involved and prior statistical knowledge. This evaluation also considers data obtained from experimental tests available in literature. Then, the new design expressions result from adoption of the following criteria: minimize variability of the safety factor values for each considered experimental test and assure that those values are within a target range. Applying these criteria to the tests performed by several authors on concrete interfaces, new design expressions are recommended in this Thesis depending on the interface roughness profile, concrete strength and reinforcement ratio.

In terms of numerical finite element modeling, this dissertation focuses both, and separately, on dowel action of the transverse reinforcement as well as on aggregate interlock mechanism. Due to the extension and vastness of this subject, only static loading is taken into account.

In the first case, steel bar elements with plasticity, geometric non-linearity, rotational degrees of freedom and flexural stiffness are considered. In turn, the bar is connected to concrete embedment through several Winkler spring elements to simulate the deformability and strength of the concrete substrate. New nonlinear force-displacement expressions, adjusted to experimental data available in literature, are also purposed for the springs. Those constitutive relations will be upgraded then in order to include the influence of lateral concrete cover and confinement imposed by stirrups.

Later, for aggregate interlock, new constitutive relations are presented for two types of interface roughness profiles: monolithic concrete cracks; and interfaces between concretes cast at different times corresponding to a free surface, left without further treatment after vibration of the old concrete. The new constitutive relations are calibrated on the experimental results of Walraven and Reinhardt (1981) and also on the tests performed in this present dissertation. For the purpose, a nonlinear finite element model is developed to assess the behavior of a concrete interface. Initially, a model with dowel action acting as the only strength mechanism is assumed in order to assess phenomena particularly happening in concrete joints, as crack opening and the reinforcement kinking effect. This assessment is possible with the inclusion of new springs in order to take into account steel bar/concrete embedment bond behavior. Later, an interface finite element simulating aggregate interlock is also added in the model and the new constitutive relations for this mechanism are formulated. While the ones currently available in literature can only be applied in interfaces restrained by external bars, these new constitutive relations are suitable to be use in the case of a concrete interface with embedded reinforcing steel bars.

The Thesis is divided into 5 chapters. Then, a brief description of the content of each chapter is presented.

1.3 ORGANIZATION OF THE TEXT

The present Chapter 1 displays some background about the topics discussed in this Thesis, frames its aim and scope within the state-of-art and outlines the organization of the text.

Chapter 2 presents a brief state-of-the-art on the monotonic and cyclic behavior of interfaces between concretes cast at different times. Then, the test campaign, which was

aimed at obtaining experimental support for modeling the behavior of such interfaces, subjected to a high number of load cycles, is described, and the corresponding results discussed and analyzed in terms of slip and crack opening, stress variations in the monotonic tests, failure mode, and number of resisting load cycles. An experimental S-N curve was set for this type of interface.

In Chapter 3 a new proposal for the design of concrete interfaces subjected to shear loading is purposed for different roughness profile types. Design expressions are defined in order to minimize dispersion and variability of the safety factor values for each considered experimental test, and also to assure that those values are within a target range (defined according to reliability considerations). These improvements become clear when the new proposal is compared with the most common design code recommendations.

In Chapter 4, a nonlinear finite element model is developed to assess the behavior of a dowel bar subjected to monotonic loading and embedded on a single concrete block substrate. In the model, a “beam element” representation of the steel reinforcing bar is used, and the bar is connected to concrete embedment through several Winkler spring elements. Comparison with results from experimental tests available in literature allow to calibrate constitutive relations for the nonlinear spring response. Afterwards, the influence on dowel behavior of lateral concrete cover and confinement imposed by stirrups is assessed.

Chapter 5 is dedicated to behavior nonlinear finite element modeling of concrete interfaces when subjected to monotonic loading. In the model, an interface element simulates aggregate interlock of the concrete joint and the “beam element” representation of steel reinforcing bars is used for the dowel action mechanism. Comparison with experimental results available in literature allow to determine new stress-strain relationships for the interface aggregate interlock element.

Finally, Chapter 6 contains the final remarks of this work, including its main conclusions and the prospects for future development in research.

2

EXPERIMENTAL TESTS FOR THE STUDY OF STATIC AND CYCLIC BEHAVIOR

The knowledge about the cyclic behavior and the effects of fatigue on interfaces between concrete cast at different times, subjected to shear stress, is still very limited. This aspect is particularly relevant in structures subjected to important cyclic loads, such as railway bridges. In this context, firstly, a brief state-of-the-art on the monotonic and cyclic behavior of interfaces between concretes cast at different times is presented. Then, the test campaign, which was aimed at obtaining experimental support for modeling the behavior of such interfaces, subjected to a high number of load cycles, is described, and the corresponding results discussed and analyzed in terms of slip and crack opening, stress variations in the monotonic tests, failure mode, and number of resisting load cycles. It was further observed that the number of resisting load cycles increases as the maximum load level decreases. Based on this evidence, an experimental S-N curve was set for this type of interface.

2.1 INTRODUCTION

A major practical example of an interface between concretes cast at different times is the one between a precast beam and a cast in place slab of a bridge deck. In this type of interface, the contact surface between the old and the new concrete is usually a free surface, left without further treatment after vibration of the old concrete (*fib* 2004; FIP 1982). In the case of railway bridges, train passages give rise to a significant number of load cycles during the

working life of the structure (Ribeiro 2014; Sousa et al. 2013). Therefore, the fatigue performance of such interfaces has to be properly understood and quantified.

2.1.1 STATE-OF-THE-ART

Existing knowledge regarding interfaces with the characteristics mentioned is still very limited (Mattock 2001; Randl 2013). The studies conducted to the present date focus mainly on the case of interfaces between concretes of the same age, in other words, interfaces that result from a crack in the monolithic concrete, subjected to monotonic loading (Hofbeck et al. 1969; Mansur et al. 2008; Mattock and Hawkins 1972; Mattock et al. 1975; Walraven et al. 1987). As regards interfaces between concretes cast at different ages, one of the most relevant works is that of Mattock (1976). However, in this work, the tested interfaces have undergone treatment, acquiring a roughness profile that diverges from a free surface. In turn, the study of cyclic and fatigue behavior falls mainly on interfaces subjected to low cycle loads, in other words, subjected to a limited number of high amplitude load cycles, a phenomenon that is particularly associated with actions of seismic nature (Fronteddu et al. 1998; Mattock 1981; Puntel and Saouma 2008; Tassios and Vintzeleou 1987; Walraven 1994). Research about the high-cycle fatigue behavior of concrete interfaces is scarce: Pruijssers (1988) and Gebreyouhannes et al. (2008) studied the effects of this type of loads on interfaces between concretes of the same age, and Randl et al. (2005) focused on interfaces between concretes cast at different ages which underwent a roughness treatment through jets of high pressure water.

2.1.2 INTERFACE STRENGTH MECHANISMS

An interface between two concretes forms when there is a crack, particularly a crack in the casting joint when the two concretes are of different ages. Prior to the formation of the crack, the behavior is similar to what occurs in monolithic concrete (Fardis and Chen 1986; Park and Paulay 1975). Right after cracking, the shear strength is mainly provided by aggregate interlock, divided in two different mechanisms: cohesion and the mobilization of friction. Cohesion originates from the stresses developed in the contact surfaces between the two concretes (Li et al. 1989; Walraven 1981). The friction mechanism (Figure 2-1) is raised

when a rough interface is compressed (either due to external forces or to the clamping effect of transverse reinforcement). Relative shear displacements at the interface are accompanied by crack openings, a movement which, according to a simplified shear friction theory can be represented by the sliding along a plane of inclination *i* (Birkeland and Birkeland 1966).

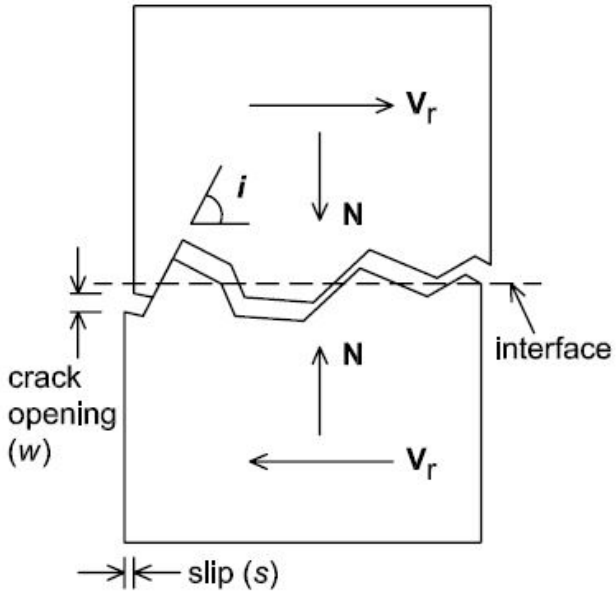

Figure 2-1 – Shear friction.

The bending deformation of transverse reinforcement crossing the interface, and associated shear stresses in the steel bars, also contributes to the interface resistance. Moreover, for large slip values, the reinforcement is progressively more inclined and additional resistance is provided by the horizontal component of the tensile force in the steel bars, the so called kinking effect (Dulacska 1972; Vintzeleou and Tassios 1986). This contribution of transverse reinforcement is called dowel action (Figure 2-2) and assumes greater influence on the interface shear strength when the slip values are quite significant.

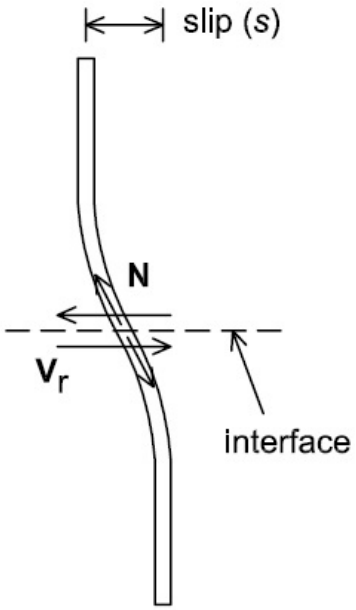

Figure 2-2 – Dowel action of the transverse reinforcement.

The shear stress on the interface, τ, then results of the superposition of the effects of cohesion, friction and dowel action, respectively:

$$\tau = c \times f_c + \mu \times \rho \times \sigma_s + \tau_d \quad (2\text{-}1)$$

where c is a parameter dependent on the roughness of the interface, f_c the compressive strength of the concrete, μ the tangent of the angle i, ρ the rate of transverse reinforcement in the interface and σ_s the axial stress in the reinforcement. The shear stress provided by the dowel action, τ_d, depends on the reinforcing bar diameter and the strength of the steel and the underlying concrete substrate (Soroushian et al. 1987). A numerical procedure for quantification of τ_d can be found in the work by Dei Poli et al. (1992).

2.1.3 CYCLIC BEHAVIOR

The study of the cyclic behavior of an interface between two concretes usually focuses on determining the number of cycles achieved for each range of applied loading and also assessing the progression of displacements throughout the experimental tests. This information allows to define proposals for the fatigue design of the interfaces and also to understand how different load amplitudes influence the structural response, including the

aforementioned parameters: number of cycles reached and the evolution of slip and crack opening.

The definition of design expressions and evaluation of the displacement evolution are aspects of greatest importance and priority in this field of study and were addressed in the work of Pruijssers (1988), Maekawa et al. (2008) and Randl et al. (2005) for interfaces with different roughness profiles from those under analysis in the present work. However, there are certainly other aspects which deserve further attention, namely, the progression of slip and crack opening when these displacement values are already significantly high and the dowel action assumes more predominance in the resistant behavior of the interface. Another aspect to note is the influence of the minimum shear force value applied during cyclic loading, when the shear force amplitude is kept constant. Finally, it is interesting to notice the fatigue failure mode associated with each test, particularly by observing the reinforcement condition at the end of the experimental test. This chapter aims at clarifying these issues, for interfaces between concretes cast at different ages.

2.2 EXPERIMENTAL PROGRAM

The experimental campaign presented here was conducted in order to study the behavior of interfaces between concretes cast at different ages, subjected to cyclic loading. The surface roughness characteristics under analysis correspond to a free surface left without any treatment after vibration. This type of surface reproduces typical interfaces between precast beams and cast-in-place slabs, in railway bridge decks, for example. The roughness profile was measured by using a mechanical contour plot device. The study was conducted by analyzing the cyclic response of the interfaces, in terms of slip and crack openings, failure mode and maximum number of cycles applied before rupture. The behavior during monotonic loading tests was also analyzed, namely as regards the variation of shear stresses for increasing slip values.

In the following paragraphs, the experimental campaign is described in detail, especially the geometry and the execution procedures of the test specimens, the material properties, the measurement system and the test setup.

2.2.1 SPECIMEN GEOMETRY

The geometry defined for the specimens (Figure 2-3) corresponds to the classical solution of the push-off type tests, where the line of action of the resultant force applied is collinear to the interface surface, thus subjected to shear stress. The old concrete was cast in two stages, with the specimen rotated 90º counterclockwise relative to the position in Figure 2-3. In the first stage, the first part of the L was cast, with dimensions of 0.45 x 0.20 x 0.15 m^3, corresponding to the old concrete. In the second stage, performed one day after so that the first stage concrete had already a satisfactory stiffness, was cast the remaining part of that L. The concrete of the second stage have similar characteristics and properties of the first stage concrete. The casting joint between the concretes of both stages has no influence on the measurements carried out in this work because it was designed not to crack in the tests performed. Finally, the new concrete was cast in a third stage, 28 days later.

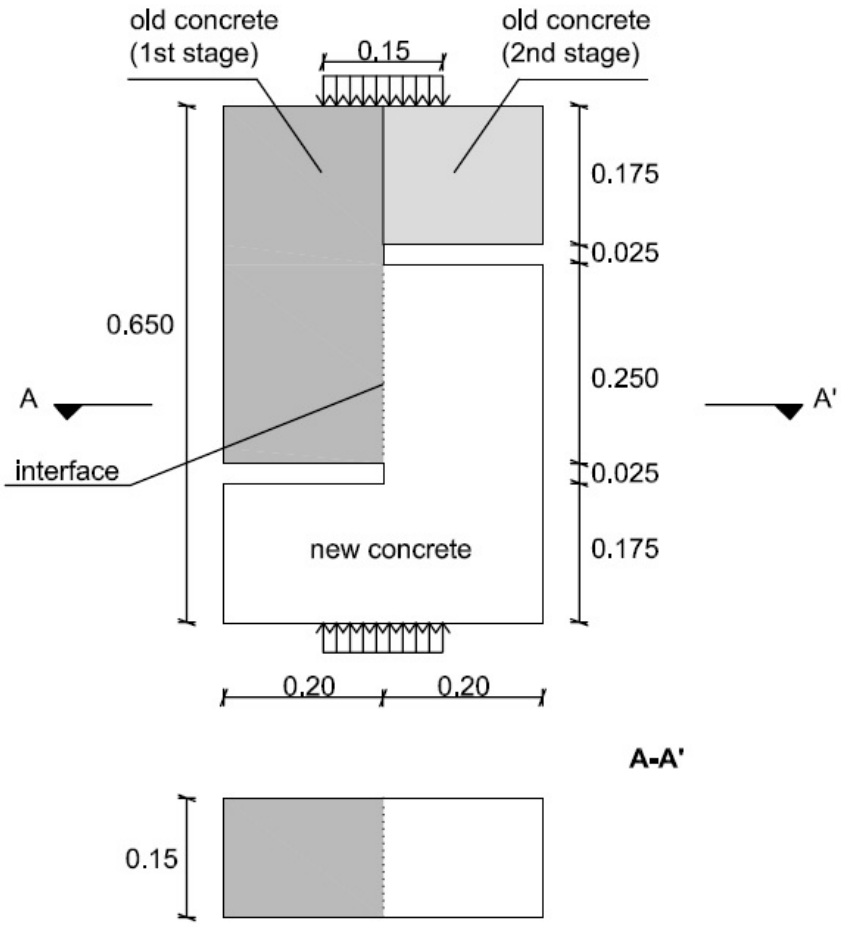

Figure 2-3 – Dimensions (in m) of the test specimens.

Figure 2-4 shows the configuration and quantities adopted for the reinforcement in each test specimen. The rate of transverse reinforcement across the interface is 1.07 %.

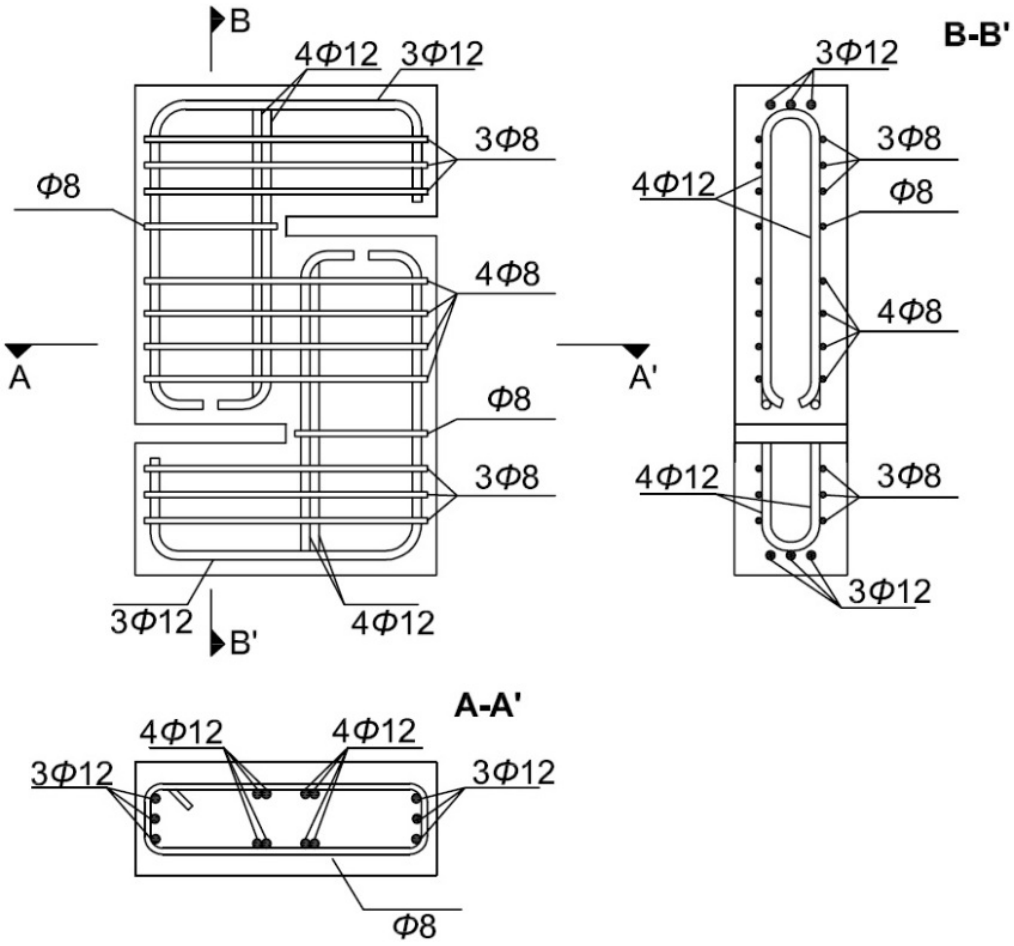

Figure 2-4 – Configuration and diameter (ϕ in mm) of the reinforcement in the test specimens.

2.2.2 MATERIAL PROPERTIES

The compressive strength f_c of the old concrete was assessed on 3 cylinders with 0.30 m high and 0.15 m in diameter at the time of the tests, corresponding to 478 days of age of the concrete (Table 2-1). The average result obtained was 67.8 MPa. For the new concrete, the average strength at 450 days was 55.3 MPa, valued on 0.15 m edge cubes (Table 2-2). The old concrete, with higher compressive strength, simulates a precast member, whereas the new concrete, with lower strength, simulates a cast-in-place element. The performance of the tests

in advanced concrete ages has particular advantages in the case of fatigue, due to the known improvements that age introduces in the behavior of concrete subjected to cyclic loading (Galloway et al. 1979). The strength at 28 days was 58.5 MPa for the old concrete and 41.5 MPa for the new concrete. In both cases, the values were determined by tests on cylinders with 0.30 m high and 0.15 m in diameter. Finally, the tensile strength f_{ct} of the new concrete was determined through direct tensile tests on cylinders of the same dimensions. The average result was 3.16 MPa (Table 2-3).

Table 2-1 – Compressive strength of the old concrete, evaluated in cylinders.

	age	f_c (MPa)			
	(days)	1	2	3	average
cylinders	28	58.0	59.0	58.5	58.5
	478	65.5	69.5	68.5	67.8

Table 2-2 – Compressive strength of the new concrete, evaluated in cubes and cylinders.

	age	f_c (MPa)			
	(days)	1	2	3	average
cubes	28	-	-	-	-
	450	55.5	56.0	54.5	55.3
cylinders	28	34.5	46.5	43.5	41.5
	450	-	-	-	-

Table 2-3 – Tensile strength of the new concrete, evaluated in cylinders.

	age	f_{ct} (MPa)			
	(days)	1	2	3	average
cylinders	28	-	-	-	-
	450	3.03	3.16	3.28	3.16

The reinforcement steel is cold worked. The 0.2 % proof-stress experimentally determined in the tensile tests was 605.4 MPa.

The surface roughness profile of the interfaces was measured in three samples corresponding to three free casting surfaces with the same size of the test specimens ($0.25\times0.15\times0.20$ m^3). For this purpose, a mechanical contour plot instrument was used (Figure 2-5). In each of the samples, 14 lines (spaced by 1 cm) were scanned. Figure 2-6 shows a typical roughness profile. The measurements allowed to determine a mean value of 0.352 mm (standard deviation $\sigma = 0.281$ mm) for the average roughness R_a, which clearly settles this type of interface in the *smooth* category ($R_a < 1.5$ mm) defined by the *fib* Model Code (*fib* 2013). The value of R_a is calculated based on the average of the deviations of the roughness profile from the average plane of reference of that same profile using the following formula:

$$R_a = \frac{1}{L\times b}\times\int_0^L\int_0^b z(x,y)\,dx\,dy \tag{2-2}$$

where L is the length of the interface, b the respective width and z the height of a given point of the roughness profile from the average plane of reference.

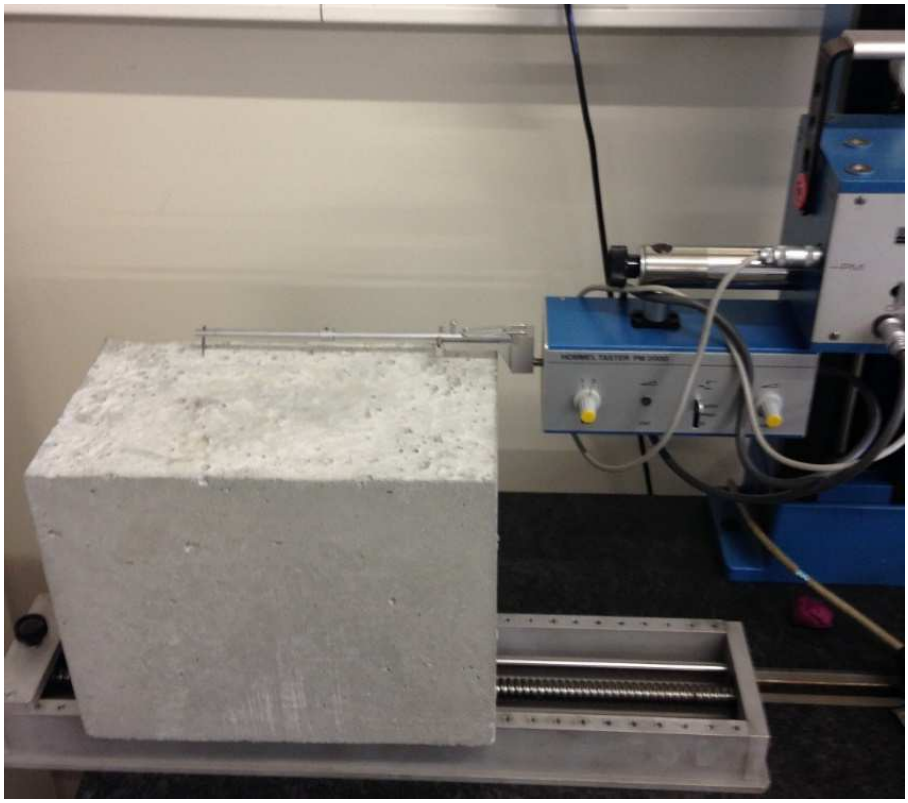

Figure 2-5 – Roughness profile measurement through a mechanical contour plot instrument.

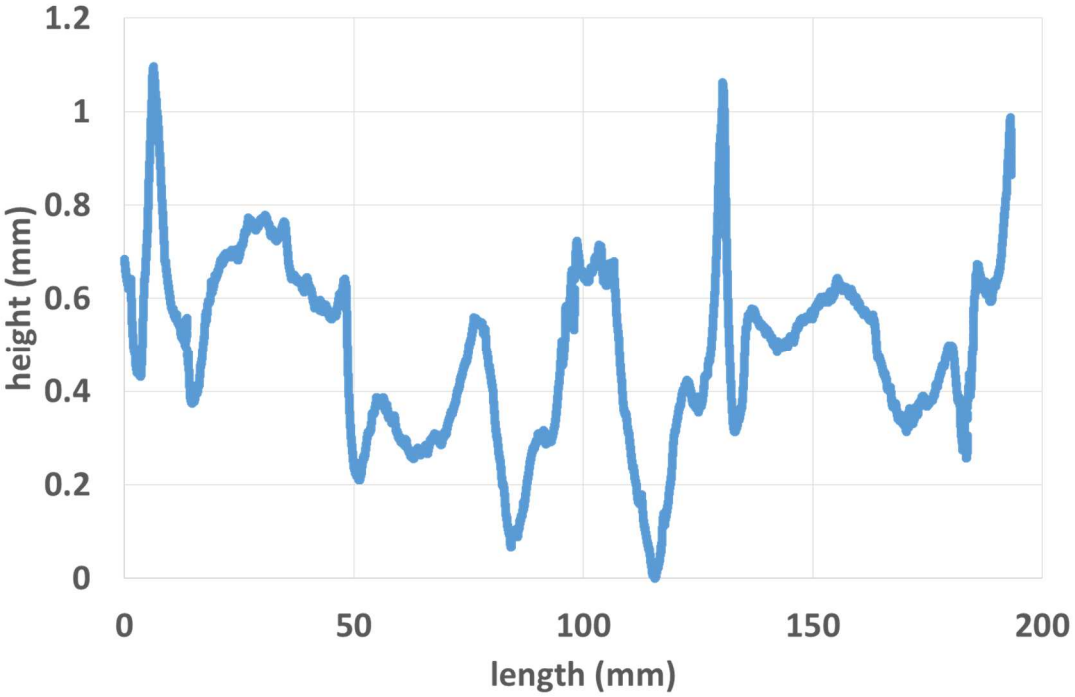

Figure 2-6 – Example of a roughness profile measured with the mechanical contour plot instrument.

2.2.3 INSTRUMENTATION

The tests were conducted in a hydraulic test machine with a capacity of 1000 kN (for tensile and compressive forces) and a gross power of 37 kW.

Figure 2-7 shows the adopted test setup. The axial load is applied through a spherical seat placed on a 15 mm thick steel plate to distribute the load over an area of 0.15×0.15 m^2. Under the steel plate, a 5 mm thick paperboard sheet (volumetric mass density ρ = 700 kg/m^3) is placed to cope with the small surface irregularities at the top of the concrete specimen. At the bottom base, a similar paperboard is also used, establishing contact with the solid metallic block coupled to the hydraulic test machine.

Figure 2-7 – Test setup.

Apart from the applied force *F*, the slip *s* and the crack opening *w* at the interface are also measured through 2 transducers of the type "Linear Variable Differential Transformer" (LVDT), arranged on each side of the specimen, totaling 4 per sample (Figure 2-8). The LVDTs have a measuring range of 10 mm, a linearity error lower than 0.025 mm, and are attached to the specimen through small and common electric cable plastic fixers. The fixers are glued to the specimen through a mortar with epoxy resin. The tips of the LVDTs are in contact with Teflon plates to minimize the friction.

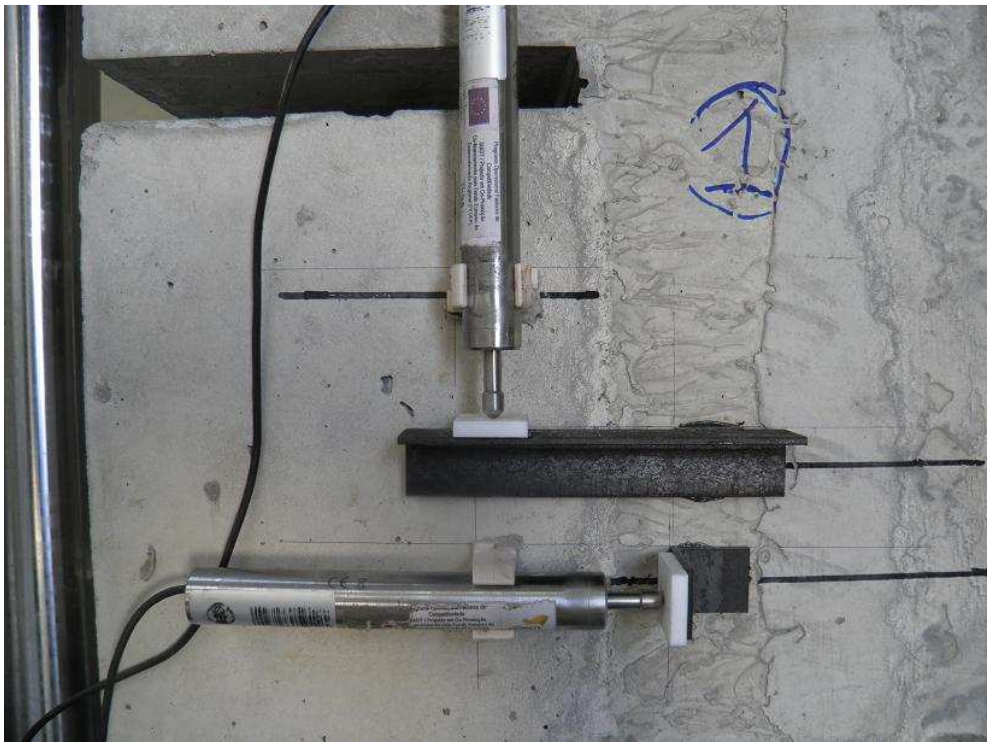

Figure 2-8 – Solution adopted for the measurement of slip and crack opening.

2.2.4 TEST PROCEDURE

The monotonic and the constant-amplitude cyclic tests are always performed in series of 3 specimens to consider the respective variability, counting a total of 15 specimens. The applied load levels are shown in Table 2-4, where τ_{max} is the maximum shear stress applied in each load cycle, τ_{min} the corresponding minimum value and τ_R the average of the maximum values recorded in the monotonic tests. Throughout the entire cyclic test these values remain unchanged. For both uncracked and cracked interfaces, the shear stress is computed as an average value:

$$\tau = \frac{F}{L \times b} \tag{2-3}$$

following the usual procedure considered in standard push-off shear tests (Hofbeck et al. 1969; Hsu et al. 1986; Mattock and Hawkins 1972).

Table 2-4 – Load levels applied in the tests.

	τ_{min} / τ_R (%)	τ_{max} / τ_R (%)	quantity
monotonic	-	-	× 3 = 3
cyclic	5	80	× 3 = 12
	25	80	
	5	70	
	5	60	

In the monotonic tests, the deformation is imposed at the rate of 0.008 mm/s. For the cyclic tests, there is an imposition of force at a frequency of 1 Hz. Both tests (monotonic and cyclic) are preceded by the application of a preliminary, monotonically increasing, load, so that an initial crack is formed in the interface. It is assumed that the initial crack is formed when the measured crack opening reaches 0.15 mm. The data acquisition rate is always 20 Hz, so that 20 measurements are recorded for each load cycle.

2.3 RESULTS

2.3.1 PRELIMINARY CRACKING LOAD

In the monotonic tests performed to induce an initial crack at the interface (Figure 2-9), an approximately linear behavior is firstly observed until a significant stiffness break occurs, thus defining the beginning of slip and crack opening. In all samples tested, the crack was almost perfectly straight along the casting joint and the average value τ_{cr} obtained for that moment was 5.075 MPa (standard deviation $\sigma = 0.886$ MPa). Then, while the energy associated with crack formation is dissipated, the shear stress increases in most of the specimens until it reaches a maximum average value τ_{MAX} of 5.729 MPa ($\sigma = 0.647$ MPa). Figure 2-9 shows the results obtained in the first 3 tests. The final average slip value at the end of the test s_{end} was 0.249 mm ($\sigma = 0.071$ mm).

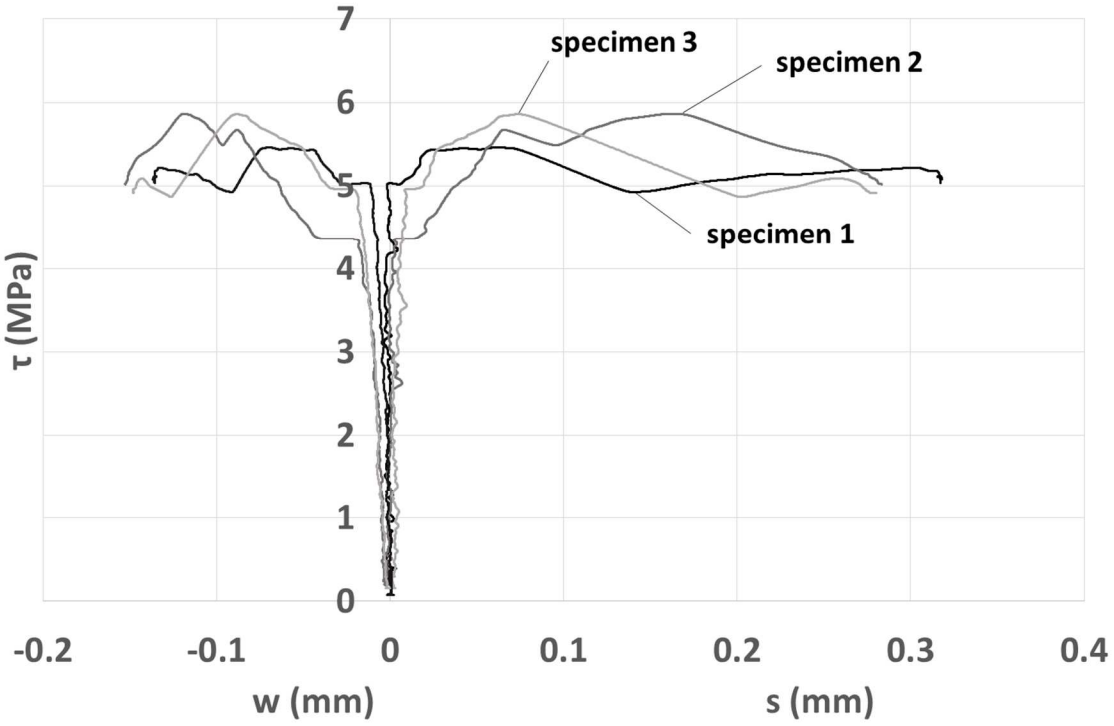

Figure 2-9 – Shear stress, slip (s) and crack opening (w) during the application of the preliminary cracking load.

2.3.2 MONOTONIC TESTS

With the interfaces already cracked, a monotonic load test was performed in 3 specimens identified as M1, M2 and M3 (results shown in Figure 2-10). A non-linear response was obtained, characterized by a continuous decrease of the roughness mobilized as the stress in the transverse reinforcement increases. The maximum shear stress is reached when the reinforcement comes into yielding (Mansur et al. 2008). The peak stress is denoted by τ_R and the corresponding slip value s_1 (results shown in Table 2-5). Then a progressive decrease of shear stress is observed, until a local minimum is reached in the slip-shear stress relationship (point with coordinates $s = s_2$ and $\tau = \tau_2$). For higher slip values, the shear stress increases again due to the predominance of the dowel action effect at this loading stage. For slip values lower than s_2, the structural response of the interface is mainly influenced by the mechanisms of cohesion and friction, which after reaching its maximum strength, begin a steady decrease. In contrast, the resistance conferred by the dowel action is always increasing.

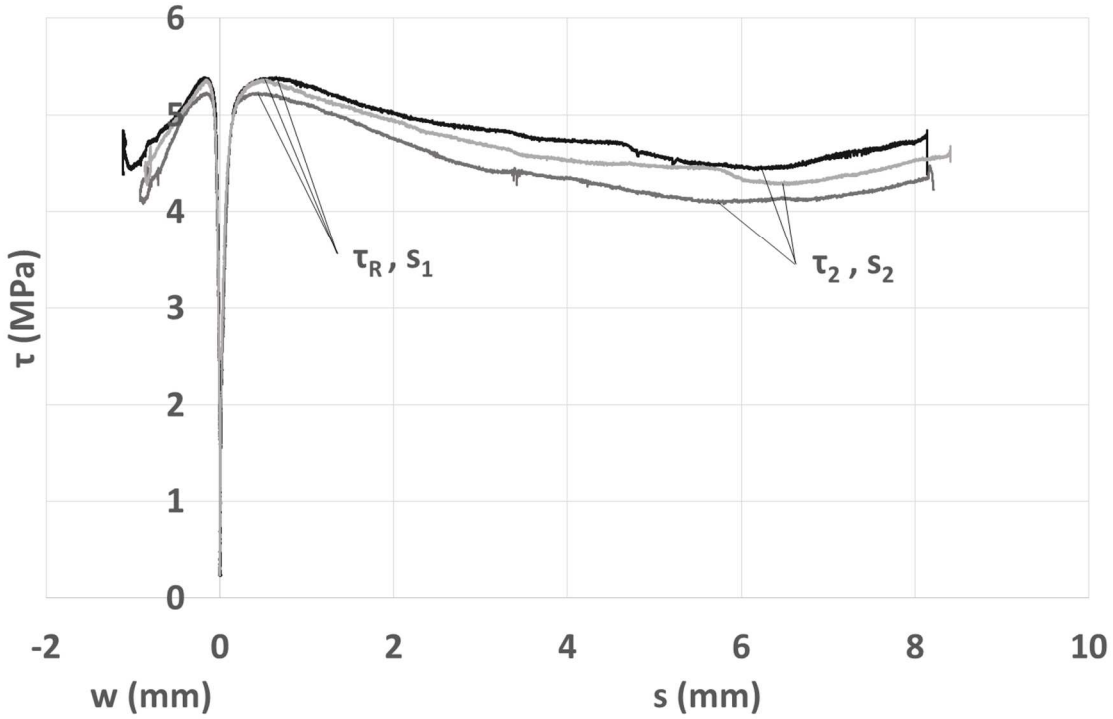

Figure 2-10 – Shear stress in the monotonic tests with the interface previously cracked.

Table 2-5 – Data relating to the 3 monotonic tests with the interface previously cracked.

specimen	τ_R (MPa)	s_1 (mm)	τ_2 (MPa)	s_2 (mm)
1	5.392	0.570	4.429	6.190
2	5.231	0.439	4.078	5.802
3	5.369	0.526	4.274	6.479
average	5.330	0.512	4.261	6.157

Finally, Figure 2-11 shows the non-linear variation of crack opening versus slip. As in Figure 2-10, a small variability is noticed in the results of the 3 tests.

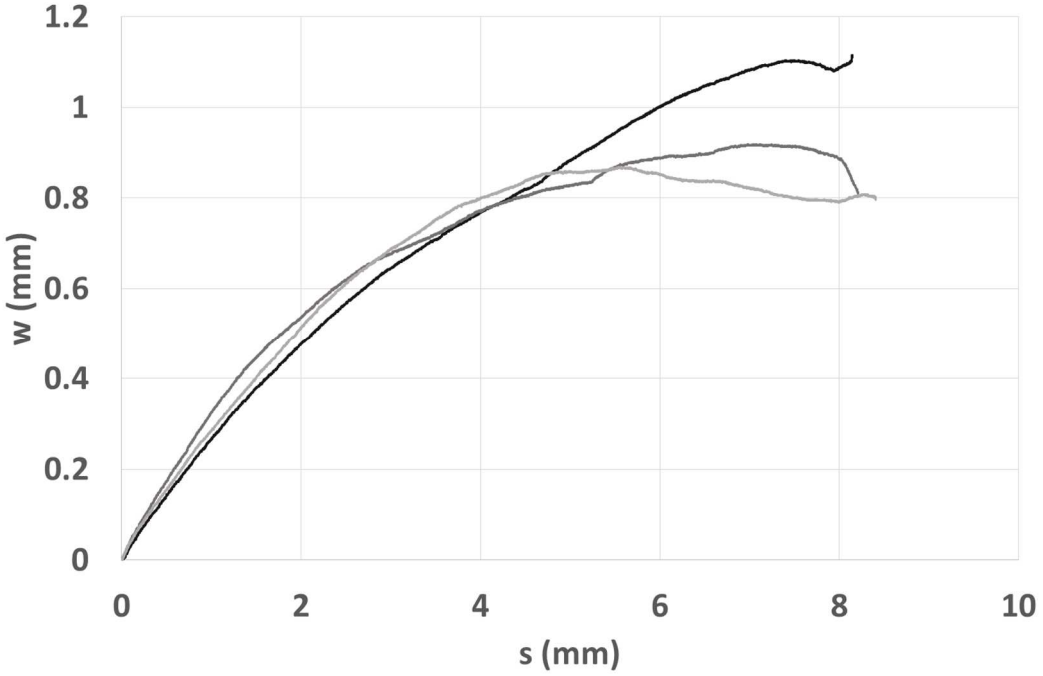

Figure 2-11 – Crack opening versus slip in the monotonic tests with interface previously cracked.

2.3.3 CYCLIC TESTS

The interface behavior was significantly different depending on the values of the applied cyclic load. Two typical and distinct behavior modes were clearly observed: one for high amplitude load cycles and another for low amplitude load cycles. The definition of "high" or "low" amplitude load cycle is made by the type of behavior observed in the tests.

2.3.3.1 HIGH AMPLITUDE LOAD CYCLES

In the cyclic tests where the loading assumes a greater amplitude ($\tau_{max}/\tau_R = 0.80$ and $\tau_{min}/\tau_R = 0.05$), 5 stages can be identified in the evolution of the maximum (s_{max}) and minimum values (s_{min}) of slip on each cycle n (Figure 2-12). In phase 1, corresponding to the initial cycles, the slip progresses with a negative second order derivative. Then, this progression is approximately linear (phase 2) to enter an exponential phase, in which the second order derivative takes a positive value (phase 3). However, instead of growing

exponentially to failure, the specimen response changes when a slip value s_{2n} is reached. The graph acquires an inflection point, revealing the beneficial contribution of a different resistance mechanism (phase 4). Similarities can be found in the results of the monotonic tests, even though the slip value that defines the transition (s_2 in the monotonic test) is slightly lower in the high amplitude fatigue tests, where the average value of s_{2n} was approximately 5.1 mm (σ = 0.7 mm). In the cyclic case, the inflection point indicates the instant at which the dowel action of the transverse reinforcement, especially the kinking effect, acquires the predominance in the resistant behavior of the interface. The path of shear stress – slip relation for some cycles of the test is shown in Figure 2-13, where it can be seen the usual cycle hysteresis in a fatigue loading.

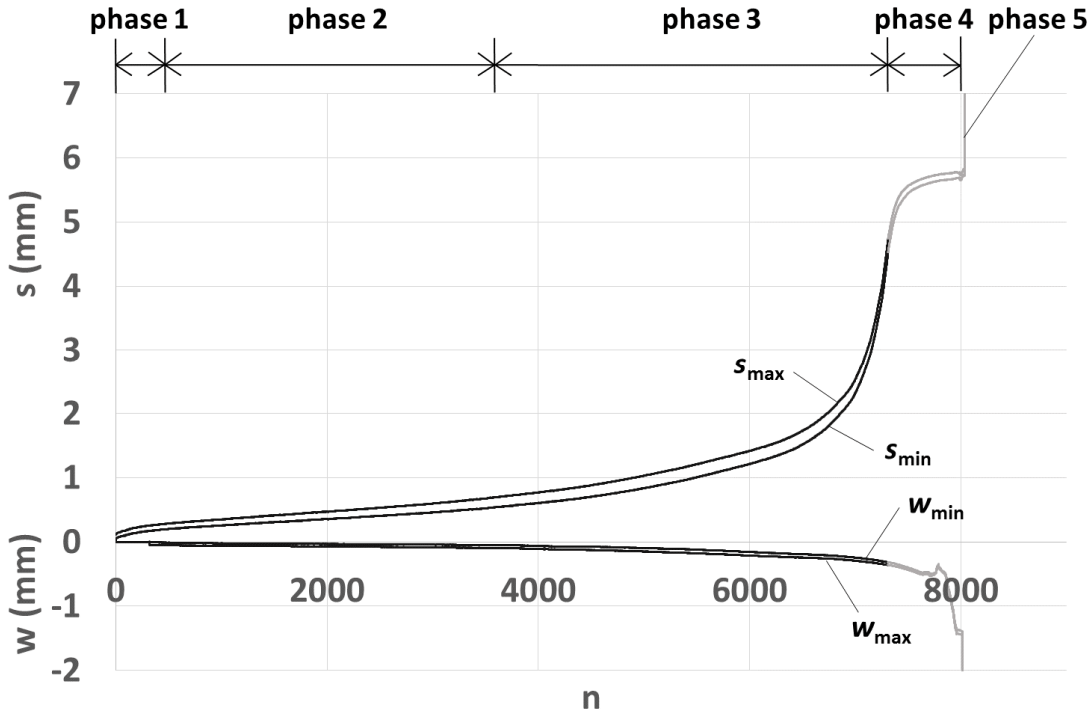

Figure 2-12 – Evolution of slip and crack opening for a high amplitude cyclic test (τ_{max}/τ_R=0.80 and τ_{min}/τ_R=0.05).

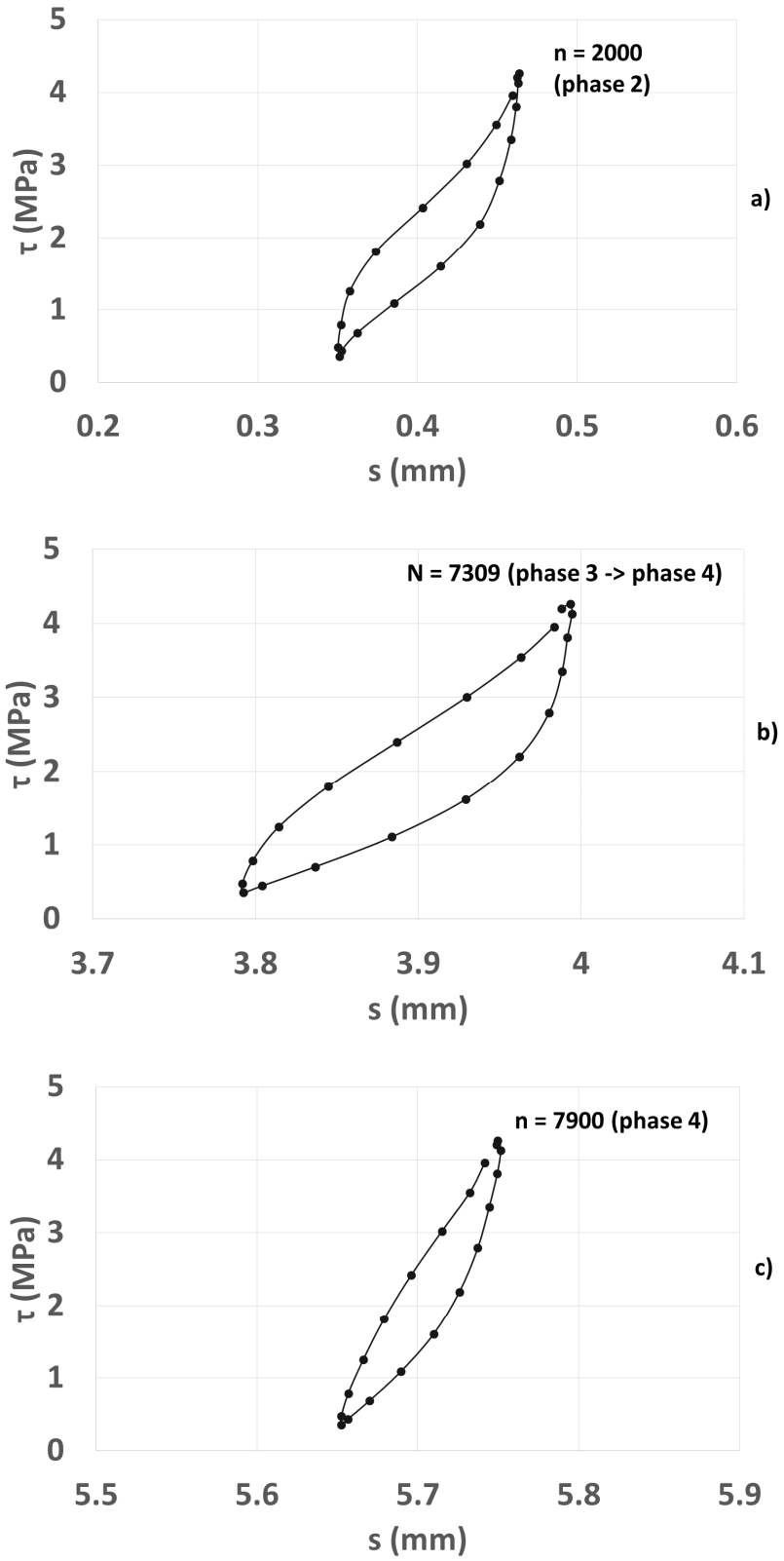

Figure 2-13 – Shear stress versus slip for the high amplitude cyclic test of Figure 2-12: a) n = 2000 (phase 2); b) N = 7309 (transition between phase 3 and phase 4); c) n = 7900 (phase 4).

Finally, a sudden detachment of the concrete cover to the reinforcement occurs (phase 5). At this point, the LVDTs glued to the concrete surface also fall and the test stops. As can be seen in Figure 2-14 (which illustrates the reinforcement shape after the surrounding concrete was removed), at the end of the test the steel bars are bent without any fracture. The same behavior was observed in all of the 3 specimens tested with this load level. As regards the crack opening, it has a nearly constant growth throughout most of the test.

Figure 2-14 – Outlook (after the surrounding concrete removal) of the reinforcement crossing an interface subjected to a high amplitude cyclic loading, at the end of the test.

2.3.3.2 LOW AMPLITUDE LOAD CYCLES

When the cyclic loads are of low amplitude ($\tau_{max}/\tau_R = 0.60$ and $\tau_{min}/\tau_R = 0.05$), there are some differences in the resistant behavior of the interfaces (Figure 2-15). In this case, only 3 stages can be identified. They correspond to the first 3 stages observed in tests with high

amplitude load cycles: phase 1 corresponds to the initial cycles in which the slip progresses with the respective second order derivative taking a negative value; phase 2, where this progression is approximately linear; and phase 3, corresponding to the last cycles, with an exponential variation and a positive second order derivative. In the case of low amplitude loads, the transition into phase 3 can be recognized more clearly. It could be concluded that the slip value corresponding to that transition, s_{1n}, is slightly higher than the slip value corresponding to the peak stress in the monotonic tests, s_1. Considering the results of all these low amplitude fatigue tests, s_{1n} takes an average value of 0.62 mm ($\sigma = 0.08$ mm). These results suggest that the slip value at the monotonic peak stress, s_1, can be taken as a safe (conservative) indicator of an upcoming fatigue failure.

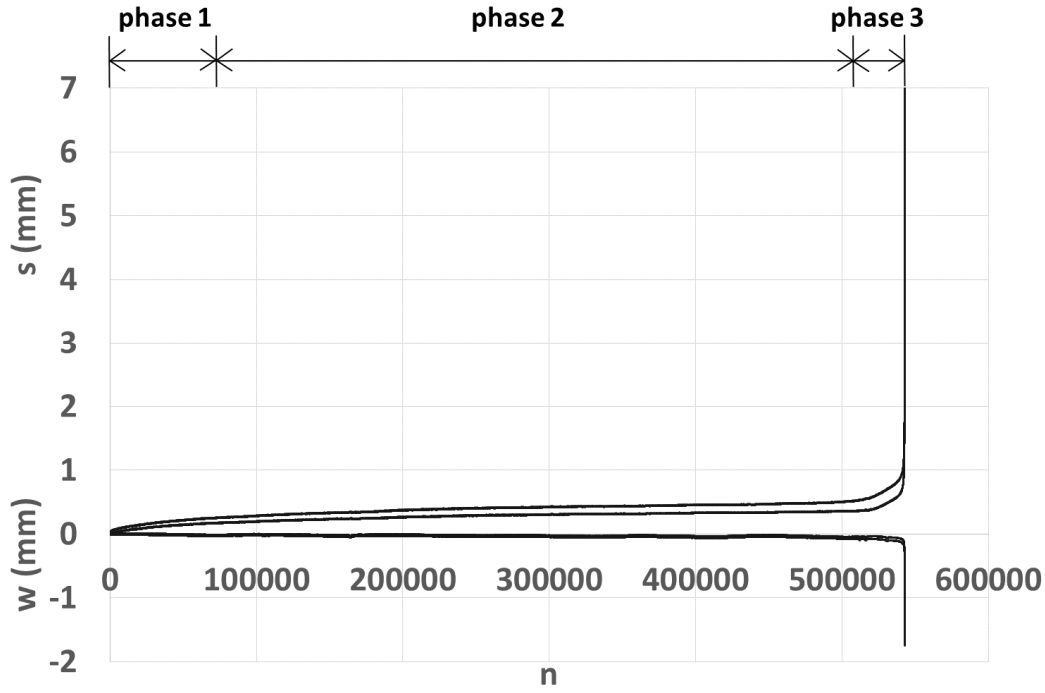

Figure 2-15 – Evolution of slip and crack opening for a low amplitude cyclic test (τ_{max}/τ_R=0.60 and τ_{min}/τ_R=0.05).

Figure 2-16 illustrates the final outlook of the transverse reinforcement, which was observed at the end of the 3 tests concerning this load level, after removal of the concrete cover. In this situation, the fracture of the steel bars at the interface zone can be clearly seen,

which explains why the kinking effect could not be mobilized when the slip reached high values.

Figure 2-16 – Outlook of the reinforcement, after the removal of the concrete cover, of an interface subjected to a low amplitude cyclic loading.

It is concluded then that when the number of cycles exceeds a certain value, the transverse reinforcement undergoes fatigue damage which affects its resistance and, therefore, the interface resistance. Figure 2-16 illustrates the classic case, and many times referenced (CEB 1988), of a fatigue failure of the steel bars, without signs of elongation and necking effects.

2.3.3.3 MEDIUM AMPLITUDE LOAD CYCLES

For medium amplitude load cycles, the interface behavior showed some variability. Of the 3 specimens subjected to cyclic loading of mean amplitude ($\tau_{max}/\tau_R = 0.70$ and $\tau_{min}/\tau_R = 0.05$),

two of them showed a similar behavior to that observed in the case of low amplitude loads (Figure 2-15), while the other one revealed a similar behavior to that observed in the case of high amplitude loads (Figure 2-12).

Figure 2-17 illustrates the influence of the applied load on the relationship between crack opening and slip. By analyzing this chart, one can see a tendency for a decrease in the crack opening when the loading is cyclic, and within the cyclic loads, a decrease when the maximum value of the applied shear stress is lower. That tendency reveals the roughness damage caused by the fatigue cycles, which gives rise to a smoother surface as the cyclic loading progresses. In smoother surfaces, the reinforcement yields for a higher value of slip. This seems to be the reason why s_{1n} is greater than s_1. Also, the roughness damage caused by fatigue loading diminishes the shear resistance due to the cohesion and friction mechanisms. That can explain why s_{2n} is lower than s_2.

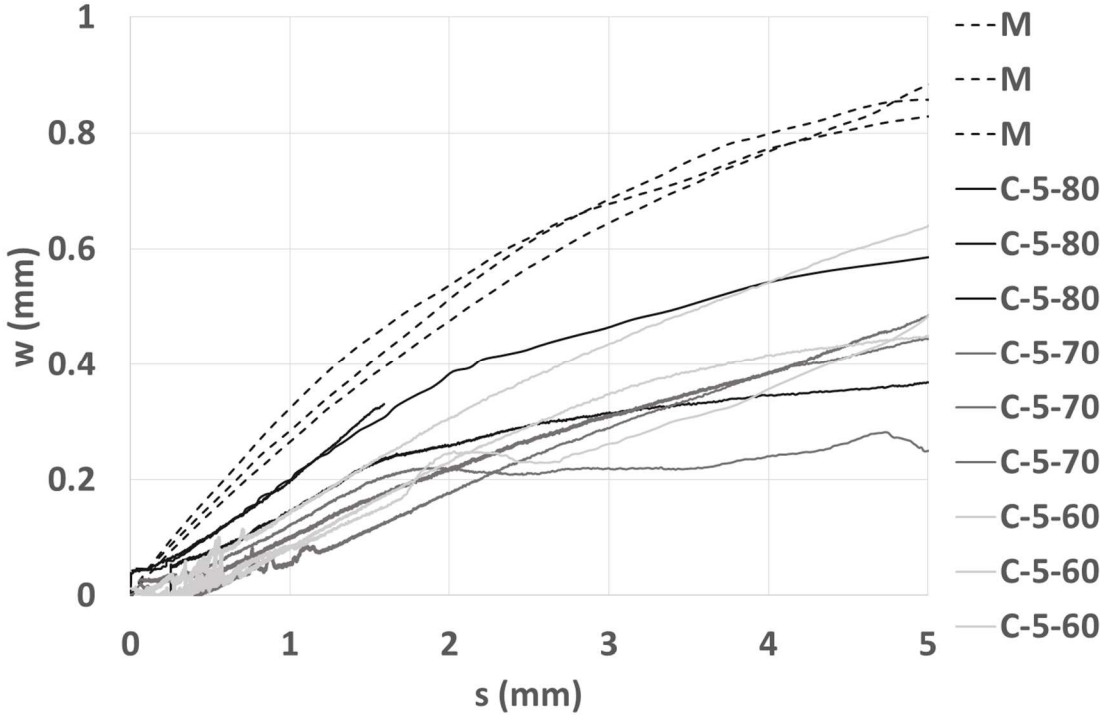

Figure 2-17 – Crack opening versus slip for both the monotonic (M) and cyclic (C) tests.

2.3.3.4 INFLUENCE OF THE LOWER LOAD LEVEL

For the 3 specimens subjected to cyclic loading varying between 25 and 80 % of the shear strength, the behavior was similar to that recorded in the specimens subjected to a high amplitude cyclic loading (Figure 2-12 and Figure 2-18). This indicates that the resistant behavior of the interface is conditioned by the maximum value of the applied action and not only by the respective amplitude. This conclusion is also reflected in the graph that indicates the variation of the crack opening versus slip (Figure 2-19). In this graph, even though a clear dependency cannot be identified, one can see that the results of tests with $\tau_{min} / \tau_R = 0.25$ tend to be closer to the values of the tests "C-5-80" than the "C-5-60". However, even so, the influence of the minimum value of the load was evident, since a higher number of cycles could be applied in the tests with $\tau_{min} / \tau_R = 0.25$, compared to the specimens "C-5-80" (Table 2-6).

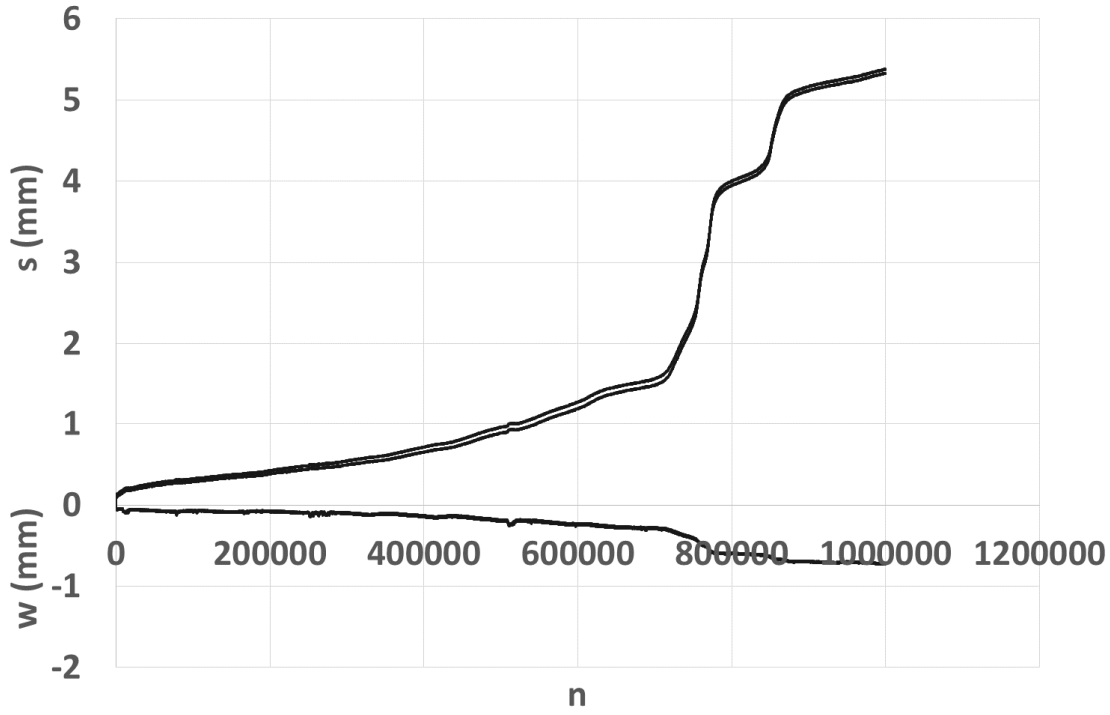

Figure 2-18 – Evolution of slip and crack opening for a cyclic test with $\tau_{max}/\tau_R = 0.80$ and $\tau_{min}/\tau_R = 0.25$.

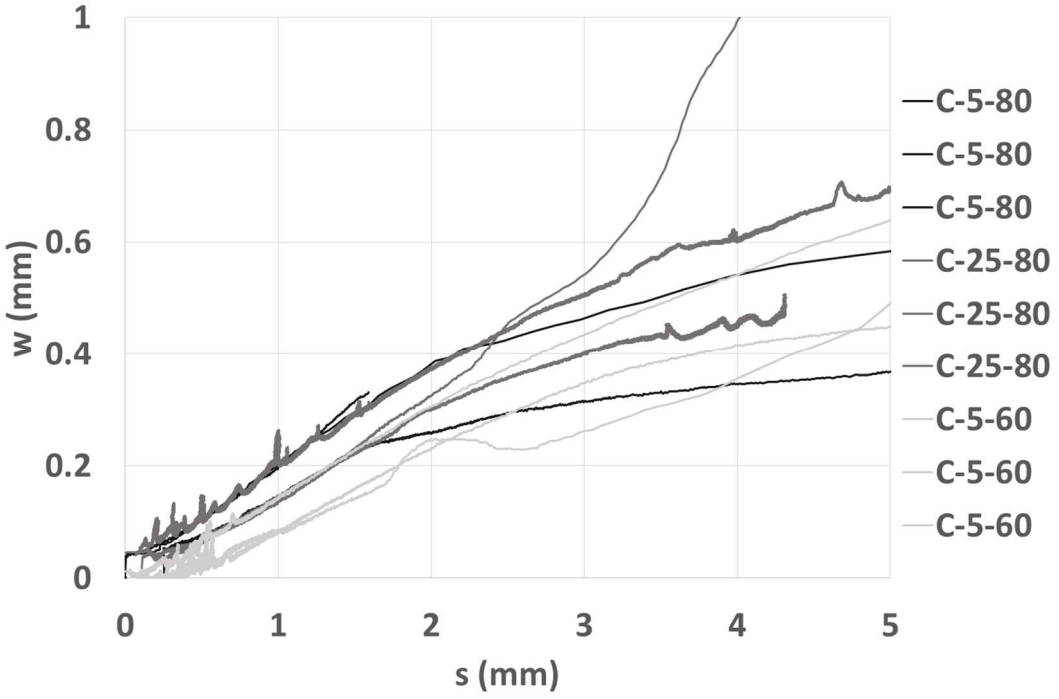

Figure 2-19 – Crack opening versus slip for 3 load levels applied in the cyclic tests.

Table 2-6 – Number of cycles applied until fatigue failure was noticed in each test performed.

τ_{min}/τ_R (%)	τ_{max}/τ_R (%)	N
5	80	89
		1063
		7309
25	80	8118
		51083
		782068
5	70	1839
		61882
		97347
5	60	364881
		542970
		988793

In Figure 2-18, aggregate interlock degradation, characterized by a very rapid growth of the slip in each cycle, occurs more than one time throughout the test, even after the dowel action mechanism gain dominance in the resistance of the interface. In both tests, the interface reached 1 million cycles without any externally visible damage and with the values of displacement still within the measurement range of the LVDTs. For this reason, after applying 10^6 load cycles, a monotonic load test was performed (Figure 2-20) aiming to determine the remaining strength of the interfaces after the fatigue damage inflicted by cyclic loading. Initially, the slip progress was slow. A clear change in the slip variation occurred when the shear stress exceeded the maximum value applied in the previous load cycles. Then, the progression of slip was significantly faster and nearly constant. The test ended when the values were still increasing and already above the average shear strength of the monotonic tests of Figure 2-10. It ended however because the concrete near the interface continually detached, exposing the reinforcement and affecting the LVDTs measurements. This phenomenon is visible in Figure 2-21, where the variation of the crack opening versus slip is not always as expected (with a negative second order derivative). In this case, once the slip reaches a certain value (~ 4.5 mm), the *s-w* relationship has a point of inflection and the second order derivative acquires a positive value, with a rapid increase of crack opening in some periods.

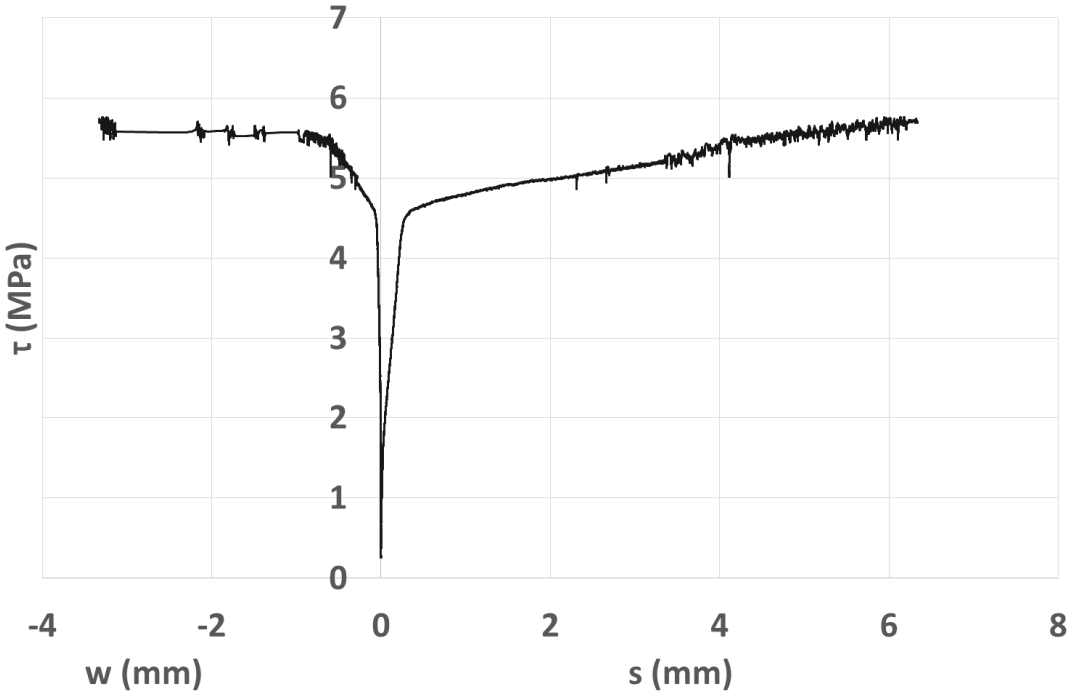

Figure 2-20 – Shear stress in the monotonic tests applied to the specimens without fatigue failure after 10^6 cycles.

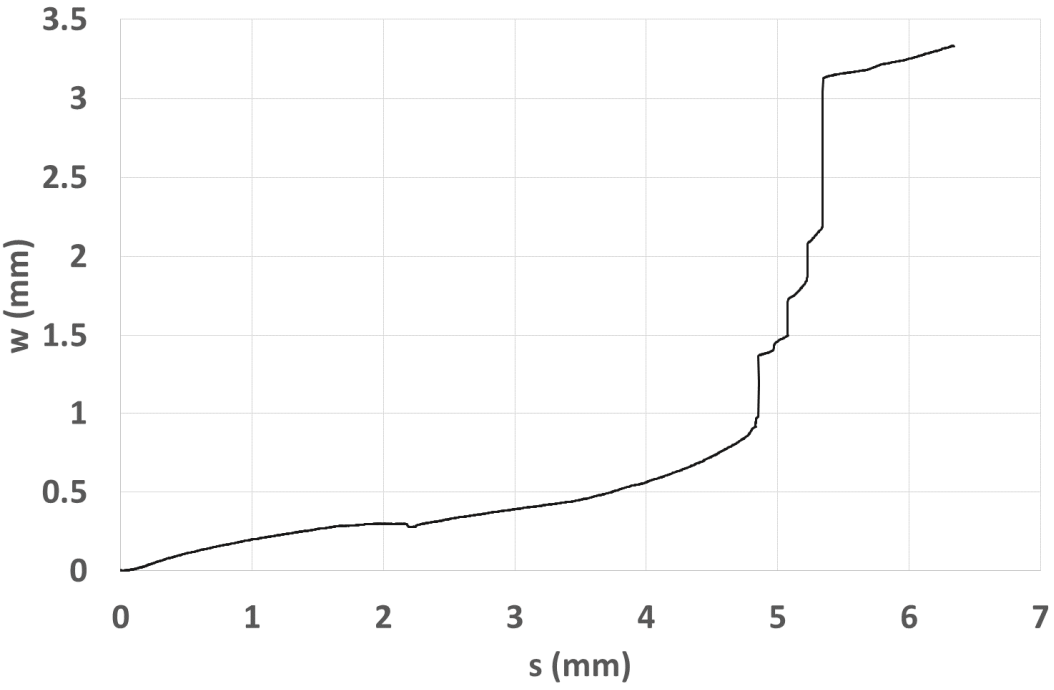

Figure 2-21 – Crack opening versus slip in the monotonic tests applied to the specimens without fatigue failure after 10^6 cycles.

Finally, it is appropriate to comment on the fact that no steel fatigue fracture was detected in the two specimens subjected to 1 million load cycles with a minimum shear stress level τ_{min} / τ_R = 0.25, contrary to what was observed in the tests with low amplitude loads (Figure 2-15 and Figure 2-16). The most likely explanation for this occurrence is that in the "C-25-80" tests a considerable slip increase occurs before the reinforcement is in danger of fatigue failure. This significant growth causes a beneficial change in the stresses acting on the steel bars. As shown before, for large slip values, the kinking effect gains predominance, and is responsible for an increased resistance provided by the steel bars crossing the interface.

2.3.3.5 STRENGTH ANALYSIS

Table 2-6 shows the number *N* of cycles reached until fatigue failure occurred in each test. While on interfaces subjected to low amplitude loads the instant of failure is evident as a brittle failure, on interfaces subjected to high amplitude loads that moment is not so clear. In this context, we consider the instant of failure as the cycle at which the first inflection point in the slip progression (transition between phases 3 and 4 of Figure 2-12) occurs. This is the moment when the dowel action effect assumes predominance in the resistant behavior of the interface and also defines the point from which the external damage on the specimens begins to be noticed. Later, after that instant, the observed behavior is considered to be a post-failure behavior, because it corresponds to very large deformations and mobilize different resistant mechanisms than those that occurred previously.

By analyzing the values shown in Table 2-6, we can notice a greater variability than that observed in monotonic load tests (Table 2-5), as expected, since this conclusion is typical in fatigue tests (Table 2-5). However, in spite of the variability, there is a clear tendency for an increased number of resisting load cycles when the applied stress amplitude decreases. The trend is visible in the S-N curve of Figure 2-22, which relates the ratio between the maximum value of the cyclic loading, τ_{max}, and the average shear strength in the monotonic loading, τ_R, with the logarithm of the number of cycles achieved in the fatigue failure, *N*. As shown before, when evaluating the interface resistant behavior, the maximum and the minimum values of the applied stress have to be taken into account, instead of considering only the stress amplitude. The S-N curve presented in Figure 2-22 corresponds to a constant value of

minimum stress level $\tau_{min}/\tau_R = 0.05$, a very low value, which provides conservative (safe) results as needed for design purposes. The derivation of the S-N curve for different minimum stress levels ($\tau_{min}/\tau_R = 0.25$ for example) is out of the scope of the present work, owing to the reduced number of specimens tested under those conditions.

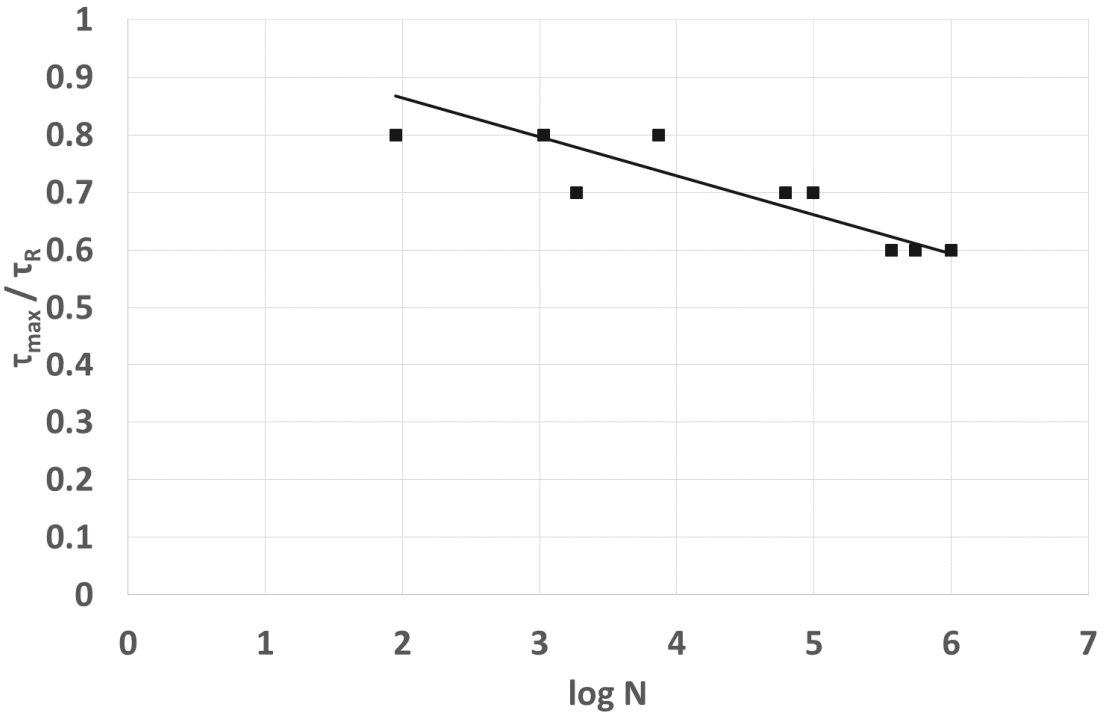

Figure 2-22 – S-N curve obtained from the performed cyclic tests

Finally, a linear trend line was fitted to the 9 results in Figure 2-22, resulting in an R^2 value equal to 0.710. Equation (2-4) predicts, in a simple and conservative way, the average number of cycles to failure achieved under constant amplitude cyclic loading, and quantifies the expected resistance for the type of interface under analysis.

$$\frac{\tau_{max}}{\tau_R} = 1 - 0.0677 \times \log N \tag{2-4}$$

2.4 CONCLUSIONS

This research provides relevant experimental information about the monotonic and cyclic resistant behavior of interfaces between concretes cast at different times, for which the existing knowledge is still very limited. For this purpose, monotonic and cyclic tests were conducted in 15 specimens designed in order to reproduce a real interface between a precast beam and a cast in place slab. The interfaces were left without further treatment after vibration of the old concrete and different, constant amplitude, load regimens were considered.

In the monotonic tests performed to induce an initial crack at the interface, it was possible to observe higher shear stress values than those that occurred in the monotonic tests with interface already cracked. In the latter, a small variability was observed in the results. Moreover, it was found that, once a certain slip value (called s_2 in the present chapter) is reached, a local minimum occurs in the slip-shear stress variation. This fact demonstrates the influence and predominance of the dowel action effect of the transverse reinforcement for large slip values.

Two main failure modes were observed in the cyclic load tests. One was observed in the case of high amplitude loads ($\tau_{max}/\tau_R = 0.80$ and $\tau_{min}/\tau_R = 0.05$), where the dowel action mechanism (particularly the kinking effect) plays an important role, even after relevant damages occur, such as severe cracking and detachment of the concrete cover to the reinforcement. In turn, in the second failure mode, which governs the response under low amplitude cyclic loads ($\tau_{max}/\tau_R = 0.60$ and $\tau_{min}/\tau_R = 0.05$), the steel bars fail due to fatigue, and the shear strength decreases abruptly (in this case, no significant damage is observed in the exterior concrete surface). It was also found that, under low amplitude cyclic loading, the slip value corresponding to the transition into the third stage (which precedes the fatigue failure) is slightly higher than the slip value corresponding to the peak stress in the monotonic tests, s_1. These results suggest that s_1, can be taken as a safe (conservative) indicator of an upcoming fatigue failure.

For medium amplitude load cycles ($\tau_{max}/\tau_R = 0.70$ and $\tau_{min}/\tau_R = 0.05$), the interface behavior showed some variability. Of the 3 specimens subjected to cyclic loading of medium amplitude, two of them showed a similar behavior to that observed in the case of low

amplitude loads, while the other one revealed a similar behavior to that observed in the case of high amplitude loads.

Conclusions could also be drawn about the evolution of crack openings. Lower crack openings are observed under cyclic loading, by comparison with monotonic loading tests. Within the cyclic loads, crack openings tend to decrease as the maximum shear stress level decreases. That tendency reveals the roughness damage caused by the fatigue cycles, which gives rise to a smoother surface as the cyclic loading progresses.

The results of cyclic tests also showed a tendency for an increased number of resisting load cycles when the applied stress amplitude decreases. Within the same amplitude, the number of resisting load cycles decreases when the minimum shear stress level increases. The S-N curve which describes the average number of cycles to failure was determined, thus quantifying the expected resistance under constant amplitude cyclic loading for the type of interface under analysis.

.

3

DESIGN RECOMMENDATIONS BASED ON STATISTICAL AND PROBABILISTIC METHODS

A concrete interface is a material discontinuity which requires special care in structural design and assessment. Therefore, the definition of design expressions, based on experimental testing data, must ensure the needed reliability depending on the type of structure and its use. In the present work, a new proposal for the design of concrete interfaces subjected to shear loading is presented for different roughness profile types. The proposal is characterized by 3 linear branches (for monotonic loading), an S-N curve (for cyclic loading) and is the result of a parametric analysis of existing experimental data (obtained by the author and also from an extensive literature search) based on statistical and probabilistic methods. Design expressions were defined in order to minimize dispersion and variability of the safety factor values for each considered experimental test, and also to assure that those values are within a target range (defined according to reliability considerations). These improvements became clearer when the new proposal was compared with the most common design code recommendations.

3.1 INTRODUCTION

A concrete interface can be found in the contact area between two concretes cast at different times or in monolithic concrete crossed by a crack. The first case represents a common situation in structural rehabilitation and strengthening (Clímaco and Regan 2001; Hartl and Feix 2011; Horvatis et al. 2010; Silfwerbrand 2003), and also in precast concrete structures, between the precast and cast-in-place concretes (FIP 1982; Tadros et al. 1993).

Since it is a material discontinuity, a concrete interface is a weak surface whose strength has to be properly quantified in structural design. Therefore, the definition of design expressions from experimental testing data must ensure the needed reliability depending on the type of structure and its use (Schneider 1997). To determine the reliability provided by the design expressions, a statistical and probabilistic approach has to be followed, depending on the number of experimental tests, the scatter of data, the parameters involved and prior statistical knowledge (ISO 1998).

This present chapter aims to determine new design expressions for calculation of concrete interface shear strength, for different roughness profile types, considering both monotonic and cyclic load cases. The proposal is the result of a parametric analysis of existing experimental data (obtained by the author and also from an extensive literature search), based on statistical and probabilistic methods. The new expressions are compared with the most common design code recommendations to evaluate the improvements achieved with the present study, which is performed in order to minimize variability of the safety factor values for each considered experimental test, and also to assure that those values are within a target range (which was established according to reliability considerations).

Firstly, it is presented a literature review regarding the calculation of the design shear strength of concrete interfaces. The literature review focuses on previously published research works and also on design code recommendations. Then, the interface strength behavior is analyzed, by using a large data set of experimental results. After that, those results are employed in the assessment and discussion of the shear strength values provided by design code expressions. Finally, new expressions for calculation of the design shear strength of concrete interfaces are proposed and justified.

3.1.1 LITERATURE REVIEW ON INTERFACE MONOTONIC STRENGTH

The first studies to evaluate interface shear strength, τ_R, were conducted by several authors (Anderson 1960; Hanson 1960; Mattock and Kaar 1961) mainly on specimens composed of two parts: a precast girder and a cast-in-place deck slab. The performed experimental tests allowed the adjustment of the following design equation:

$$\tau_R = c_1 + c_2 \times \rho \tag{3-1}$$

where c_1 and c_2 are coefficients calibrated from each experimental campaign, and ρ the reinforcement ratio.

Birkeland and Birkeland (1966) made the first attempt to model the shear transfer physical behavior on a cracked interface through friction mobilization between the concretes (shear friction theory). This mechanism arises in a compressed interface through the clamping effect of transverse reinforcement. The two concretes slide along a plane of inclination i and, according to this theory, the shear strength is then given by:

$$\tau_R = \mu \times \rho \times f_y \tag{3-2}$$

where f_y is the reinforcement yield stress and μ = tan i. The value of μ depends on the interface roughness.

Later, Hofbeck et al. (1969) developed a study based on several push-off tests of monolithic concrete cracks. The information obtained in the experimental campaign gave rise to a new design expression for this type of interface (Mattock and Hawkins 1972):

$$\tau_R = 1.38 + 0.8 \times \left(\rho \times f_y + \sigma_n \right) \leq 0.3 \times f_c \tag{3-3}$$

where τ_R is in MPa; $(\rho \times f_y + \sigma_n) \geq 1.38$ MPa; f_c is the concrete compressive strength; and σ_n is the interface normal stress. The equation maintains the shear friction theory concept, adds a fixed term of 1.38 MPa to better fit the experimental data and also considers the possibility of the friction mechanism being raised when the interface is compressed due to external forces. The upper limit $0.3 \times f_c$ expresses the shear strength for ruptures governed by concrete failure without yield of reinforcement. This failure mode occurs in interfaces with high reinforcement ratio, in which the typical behavior of cracked interfaces and the shear friction theory are not observed.

In order to determine the relative displacements (slip and crack opening) and normal stress for a certain shear loading, Walraven (1981) presented a physical model that considers, besides shear friction, the influence of the concrete strength through an aggregate interlock mechanism. This mechanism originates from the stresses developed in the contact surface between the two concretes (Walraven and Reinhardt 1981) and settled the need to evaluate more deeply the influence of concrete strength in interface shear strength. For this purpose,

Walraven et al. (1987) conducted an experimental program on monolithic concrete cracks that enabled the adjustment of a new design expression:

$$\tau_R = C_1 \times \left(\rho \times f_y\right)^{C_2} \tag{3-4}$$

where C_1 = 0.822 x $f_{cc}^{0.406}$; C_2 = 0.159 x $f_{cc}^{0.303}$; with f_{cc} and f_y in MPa. f_{cc} is the concrete compressive strength measured in cube specimens.

Commenting the technical paper published by Walraven et al. (1987), Mattock (1988) suggested a design equation that sums the two shear strength mechanisms: cohesion and friction:

$$\tau_R = 0.467 \times f_c^{0.545} + 0.8 \times \left(\rho \times f_y + \sigma_n\right) \leq 0.3 \times f_c \tag{3-5}$$

Later, Mattock (2001) presented a literature review that allowed the setting of new design expressions:

$$\tau_R = K_1 + 0.8 \times \left(\rho \times f_y + \sigma_n\right) \leq K_2 \times f_c \text{ and } K_3 \tag{3-6}$$

when (ρ x f_y + σ_n) $\geq$ (K_1 / 1.45) and

$$\tau_R = 2.25 \times \left(\rho \times f_y + \sigma_n\right) \tag{3-7}$$

when (ρ x f_y + σ_n) < (K_1 / 1.45). These equations are for cracks in monolithic concrete and also for interfaces intentionally roughened. The coefficients K_1 to K_3 depend on the type of interface. Even though a crack in monolithic high strength concrete exhibits some differences in the roughness profile due to fracture of the aggregate particles (Walraven and Stroband 1994), the design proposal remains conservative for these interfaces. Equations (3-6) and (3-7) reveal a different behavior on interfaces with a low reinforcement ratio: an improved agreement to the experimental results is obtained if the cohesion mechanism is not considered and the friction angle *i* takes a higher value. The author also presented an expression for two other interface roughness profiles, a free surface (i.e., a surface left without treatment after vibration of the old concrete) and a smooth surface (i.e., a surface cast against steel, plastic or specially prepared wooden molds):

$$\tau_R = 0.6 \times \left(\rho \times f_y + \sigma_n \right) \leq 0.2 \times f_c \text{ and } 5.5 \text{ MPa} \quad (3\text{-}8)$$

Randl (2013) included the dowel action mechanism (Dei Poli et al. 1992; Dulacska 1972) in the interface shear strength through a third term in a new design equation:

$$\tau_{Rd} = c_r \times f_{ck}^{1/3} + \mu \times \left(\sigma_n + \rho \times \kappa_1 \times f_{yd} \right) + \kappa_2 \times \rho \times \sqrt{f_{yd} \times f_{cd}} \leq \beta_c \times \upsilon \times f_{cd} \quad (3\text{-}9)$$

where f_{cd}, f_{yd} and τ_{Rd} are the design values of f_c, f_y and τ_R, respectively; f_{ck} is the characteristic value of f_c; c_r is a coefficient depending on the interface roughness; β_c is a coefficient allowing for the angle of the diagonal concrete strut; κ_1 is a coefficient of efficiency for tensile force that can be activated in reinforcement; κ_2 is a coefficient for flexural resistance of reinforcement (dowel action); and υ is a reduction factor for strength of diagonal concrete struts. In this case, the bending deformation of transverse reinforcement crossing the interface, and associated shear and bending stresses in steel bars, are also explicitly considered.

Finally, recent research works have been focusing on the study of the design coefficients depending on the interface roughness c and μ, in order to calculate them through surface roughness parameters such as the mean valley depth (Santos and Júlio 2012), R_{vm}, or the mean peak height, R_{pm} (Mohamad et al. 2015).

3.1.2 LITERATURE REVIEW ON INTERFACE CYCLIC STRENGTH

Fatigue imposed by cyclic shear loading is manifested in concrete interfaces through a progressive reduction in the material (steel and concrete) strength and also through roughness degradation in the contact surface between the two concretes. In each cycle, plastic deformations occur in that contact surface and the interface becomes smoother (Walraven 1994).

The fatigue level depends on the maximum and minimum load values and the number of cycles applied. For reversed cyclic loads, usually associated with actions of seismic nature, experimental studies were performed by several authors (Mattock 1981; Puntel and Saouma 2008; Tassios and Vintzeleou 1987) aiming to evaluate the interface behavior and strength. For non-reversed, or repeated, cyclic loads the research is scarce. Pruijssers (1988), who developed tests on monolithic concrete cracks, derived the following *S-N* curve:

$$\frac{\tau_{max}}{\tau_R} = 1 - 0.0736 \times \log N \tag{3-10}$$

which relates the ratio between the maximum value of the cyclic loading, τ_{max}, and the average shear strength under monotonic loading, τ_R, with the logarithm of the number of load cycles applied before fatigue failure, *N*. Later, an *S-N* curve was derived for a free surface by Figueira et al. (2015) (see Section 2.3.3.5).

3.2 DESIGN CODE RECOMMENDATIONS

The design code recommendations considered in the present work come from the following standards: EN 1992-1-1 (CEN 2004), EN 1992-2 (CEN 2005), ACI 318-05 (ACI 2005) and EN 1990 (CEN 2002). The former ones concern the strength of a concrete interface subjected to shear loading, while the latter presents recommendations for the definition of design expressions from experimental testing, particularly regarding target reliability indexes and the application of statistical and probabilistic methods. EN 1992-2 is considered because of its recommendations about concrete interfaces subjected to cyclic loads in bridge structures.

3.2.1 EN 1992-1-1 AND EN 1992-2

The EN 1992-1-1 design expression for the strength of concrete interfaces subjected to shear loading is:

$$\tau_{Rd} = c \times f_{ctd} + \rho \times f_{yd} \times (\mu \times \sin\alpha + \cos\alpha) + \mu \times \sigma_n \leq 0.5 \times \upsilon \times f_{cd} \tag{3-11}$$

where c and μ are coefficients depending on the roughness of the interface; f_{ctd} is the design value of axial tensile strength of concrete; α is the angle between the interface and the reinforcement axis; and υ is a reduction factor for concrete cracked in shear, equal to $0.6 \times (1 - f_{ck} / 250)$. The reinforcement should be tensioned while slip occurs and $45º \leq \alpha \leq 90º$. The proposed values for c and μ are: $c = 0.25$ and $\mu = 0.5$ for smooth interfaces; $c = 0.35$ and $\mu = 0.6$ for free surfaces; and $c = 0.45$ and $\mu = 0.7$ for rough surfaces (with at least 3 mm

roughness at about 40 mm spacing).

For cyclic loads, τ_{Rd} becomes $\tau_{Rd,fat}$ and c should be halved in the case of building structures. For bridge structures, EN 1992-2 recommends that c should be taken as 0.

3.2.2 ACI 318-05

The ACI 318-05 design expression is:

$$\tau_{Rd} = \rho \times f_y \times (\mu \times \sin\alpha + \cos\alpha) \leq 0.2 \times f_c' \text{ and } 5.5 \text{ MPa} \quad (3\text{-}12)$$

where f_c' is the specified concrete strength and $f_y \leq 420$ MPa. The proposed values for μ are: $\mu = 0.6$ for smooth and free surfaces; $\mu = 1.0$ for rough surfaces (roughened to a full amplitude of approximately 6 mm); and $\mu = 1.4$ for monolithic concrete cracks.

ACI 318-05 does not present any specific recommendation for interfaces subjected to cyclic loading.

3.2.3 EN 1990

EN 1990 presents recommendations regarding the definition of design expressions based on experimental testing results. These recommendations are consistent with ISO 2394 (1998) and *fib* Model Code (*fib* 2013). The failure probability P_f can be related with the reliability index β:

$$P_f = \Phi(-\beta) \quad (3\text{-}13)$$

where Φ is the cumulative standard normal distribution function. Equation (3-13) can also be written as the probability P of structural resistance R being inferior to the effect of actions E:

$$P(R \leq E) = \Phi(-\beta) \quad (3\text{-}14)$$

The definition of resistance design values, R_d, can be made in a convenient way through a resistance sensitivity factor, α_R:

$$P\left(R \le R_{\mathrm{d}}\right) = \Phi\left(-\alpha_{\mathrm{R}} \times \beta\right) \tag{3-15}$$

where α_R depends on the ratio between σ_E and σ_R (the standard deviations of the action effect and resistance, respectively). If $0.16 < \sigma_E / \sigma_R < 7.6$, then $\alpha_R = 0.8$. Otherwise, α_R should be taken as 1 or 0.4, depending on whether the variable with highest standard deviation is R or E, respectively.

Target values established for the index β depend on the structural failure consequence class and a reference period T_R that is usually taken as the structure design life. For the most onerous class and T_R = 50 years, EN 1990 propose a minimum value for β equal to 4.3 (corresponding to approximately $P_f = 10^{-5}$). The Standard does not recommend any values for longer reference periods, where the acceptable failure probability increases and β acquires lower values. In fatigue analyses, β can be lower than 4.3 depending on the degree of inspectability, reparability and damage tolerance (but the kind of structural detail under analysis is generally not inspectionable nor easily repairable).

The EN 1990 also presents a simplified statistical procedure for calibration of a design expression (providing design values R_d) based on experimental test data R. For this procedure, some assumptions are made including the following: $\alpha_R = 0.8$; $\beta = 3.8$; and all variables are assumed to follow either a Normal or log-Normal distribution with a known coefficient of variation. If this parameter is not known, it should be determined on the basis of some prior knowledge and/or based on the test data.

In the specific problem under analysis in this work (determination of the design shear strength for different interface types), lower P_f values were adopted for certain interface types, as will be shown below, in order to get consistent values for the design parameters for different interface types. The upper bound for the target reliability index was taken as $\beta \approx 4.75$, which corresponds to approximately $P_f = 10^{-7}$. To put this value into perspective, one can note that it is in line with the criteria proposed by CEB-FIP (1978), based on previous studies developed by CIRIA (1977), for the most adverse situation in terms of social and economic consequences, reference period and number of people within or near the structure during the period of risk. Conservative values are therefore adopted for the target reliability index, noting that concrete interfaces exist e.g. in grandstands or public buildings where consequences of failure are high (even though this is not the most common case).

Finally, one should bear in mind that, in the context of deriving design expressions based on a limited amount of test data, the calculated probabilities should not be understood as true and accurate probabilities. Instead, they should be seen as notional probabilities, which are used to establish a consistent distance to critical states (failure). The adopted methodology consists of a calibration procedure to obtain a reasonably uniform reliability for different interface types.

3.3 ANALYSIS OF EXPERIMENTAL TEST DATA

The analysis include specimens with interfaces corresponding to cracks in monolithic concrete (hereafter referred to as "cracked" interfaces, for simplicity) and also other three roughness profile types: "rough", "free" surface and "smooth". Some experimental tests on cracks in monolithic high strength concrete were found and included in the present study as well. Those specimens are hereafter referred to as "cracked*". All the tests and specimens considered in the analysis are referenced in Annex A.

The list in Annex A does not include cases in which reinforcement was installed after casting and bonded in with resin in pre-drilled holes, a particularly common situation in structural strengthening and rehabilitation, or in which a bond breaker (a coat of form oil brushed on the surface prior to applying the concrete overlay, e.g.) was used during casting, instead of cracking the interface before test through loading (Randl 1997; Randl et al. 2005). Tests performed in concrete beams (Loov and Patnaik 1994; Patnaik 2001), in pull-off specimens (Mattock and Hawkins 1972) or in uncracked interfaces (Júlio et al. 2010; Muller 2008) were not considered also. In those cases, the behavior is different compared to a cracked interface in a push-off specimen (Lenz 2012), where the shear stress can be determined with sufficient accuracy without any further modeling, and no direct stresses act on the shear plane (Hsu et al. 1986). Therefore, this study regards previously cracked interfaces in push-off specimens with reinforcement already placed before casting and without any bond breaker.

3.3.1 MONOTONIC TESTS

To model the strength behavior of an interface subjected to monotonic shear loading, a trilinear model is defined, similar to the one presented by Mattock (2001) and Mansur et al. (2008) for a smaller data set of monolithic concrete cracks than the one considered in the present study. The dowel action mechanism is not explicitly considered in the model, this being the hypothesis followed in numerous studies, as shown before. This assumption is justified by the fact that friction and dowel action mechanisms do not reach their maximum contribution at the same instant (Paulay et al. 1974), and also the limited knowledge, at the present time, about the contribution of each mechanism to interface shear strength.

The trilinear model is then given by:

$$\tau_{\mathrm{R}} = \min\left\{\tau_{\mathrm{R1}}, \tau_{\mathrm{R2}}, \tau_{\mathrm{R3}}\right\} \tag{3-16}$$

where:

$$\tau_{\mathrm{R1}} = \mu_1 \times \left(\rho \times f_{\mathrm{y}} + \sigma_{\mathrm{n}}\right) \tag{3-17}$$

$$\tau_{\mathrm{R2}} = c \times f_{\mathrm{c}} + \mu_2 \times \left(\rho \times f_{\mathrm{y}} + \sigma_{\mathrm{n}}\right) \tag{3-18}$$

$$\tau_{\mathrm{R3}} = d \times f_{\mathrm{c}} \tag{3-19}$$

For each type of interface roughness profile, coefficients c, d, μ_1 and μ_2 can be determined through the adjustment of a trend line to test data using the least squares method. This procedure becomes clearer when both terms of Equations (3-17), (3-18) and (3-19) are divided by f_{c} and presented graphically. In Figure 3-1, referring to monolithic concrete cracks, we can see that in fact shear strength varies nonlinearly with the normal stress. The following expression represents the best mathematical fitting to data using the least squares method ($R^2 = 0.8776$):

$$\frac{\tau_{\mathrm{R}}}{f_{\mathrm{c}}} = 0.0991 \times \ln\left(\frac{\rho \times f_{\mathrm{y}} + \sigma_{\mathrm{n}}}{f_{\mathrm{c}}}\right) + 0.423 \tag{3-20}$$

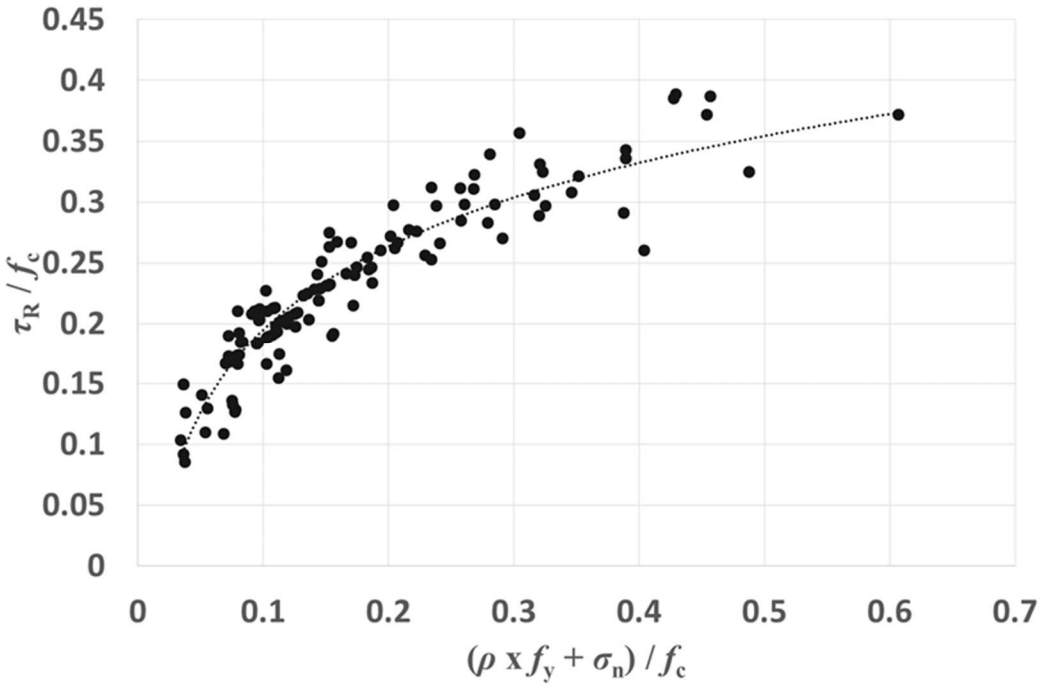

Figure 3-1 – Shear strength versus normal stress on monolithic concrete cracks.

Although it represents the best fitting to data, Equation (3-20) is more complex than Equations (3-17), (3-18) or (3-19). But the major disadvantage is that it does not give information about the physical behavior of an interface subjected to shear loading, in terms of the strength mechanisms involved and how all variables are interrelated.

Figure 3-2 shows the trilinear model adjustment to the data presented in Figure 3-1. Three different stages were defined in order to better illustrate interface shear strength behavior as a function of normal stress provided by the transverse reinforcement or an applied external force. Stage I corresponds to interfaces with low reinforcement ratio. In this stage, the cohesion mechanism is not considered and the strength is given by a shear friction model according to which the concrete blocks slide along a friction angle i_1 higher than the one observed in later stages (owing to the low concrete stress normal to the interface, in Stage I). When the reinforcement ratio grows, cohesion interacts with shear friction on interface strength (stage II). In stage III, the behavior is similar to monolithic concrete, and the shear strength does not increase for further increments of the reinforcement ratio, because the resistant behavior is governed by the concrete compressive strength.

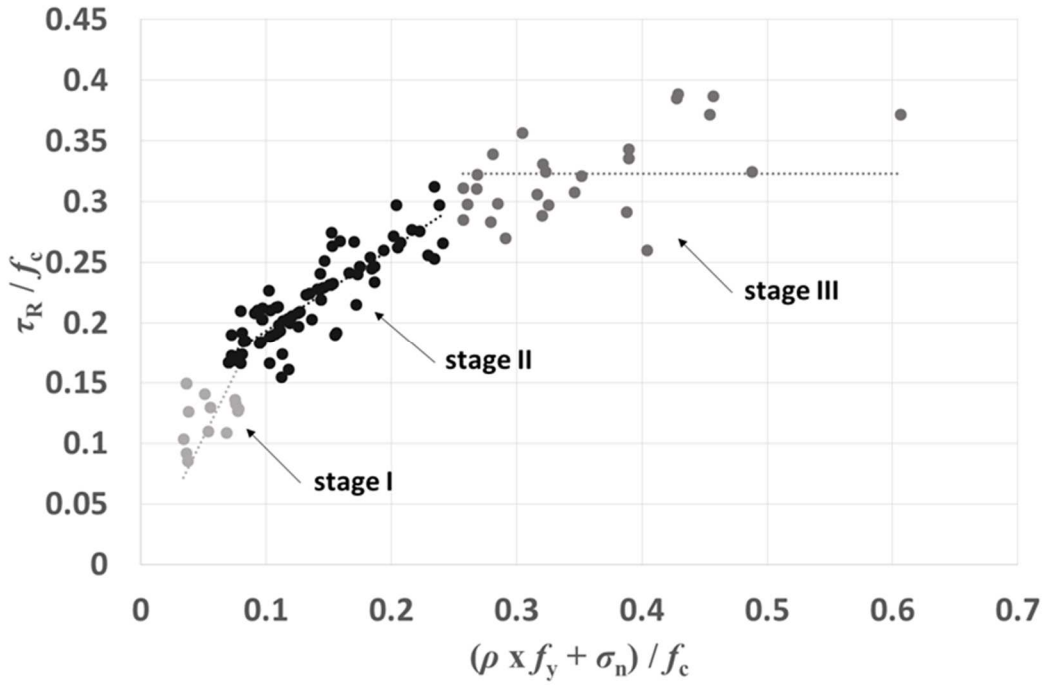

Figure 3-2 – Shear strength, divided into 3 different behavior stages, versus normal stress on monolithic concrete cracks.

Available experimental data for other roughness profile types is scarce, particularly in the case of "free" and "smooth" surfaces, where only stage II could be identified (see Figure 3-3). Values obtained for coefficients c, d and μ are shown in Table 3-1. We can notice that monolithic concrete cracks are clearly the most rough, closely followed by the case in which an interface is intentionally roughened. In a second level, we can find the "free" and "smooth" surfaces, the first presenting a higher strength than the latter. Table 3-1 also shows different results for monolithic high strength concrete cracks compared to interfaces between normal strength concretes. The results turn out to reveal the differences in the roughness profile due to fracture of high strength concrete aggregate particles.

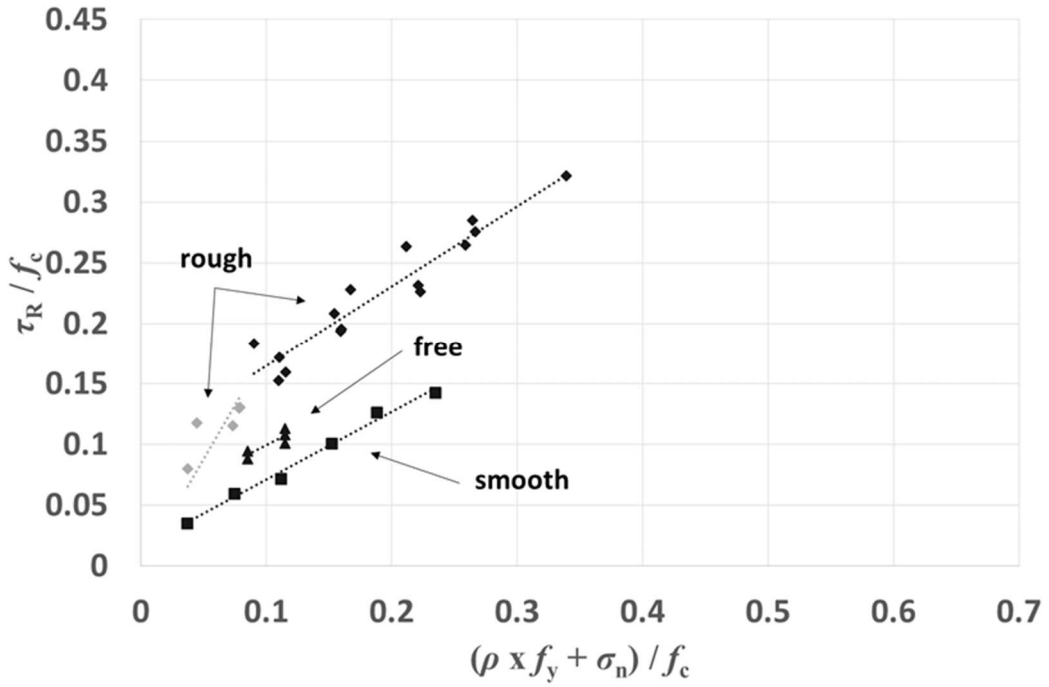

Figure 3-3 – Shear strength versus normal stress for 3 different interface roughness profiles.

Table 3-1 – Values for the shear strength factors obtained from curve fitting to available experimental results.

		μ_1	c	μ_2	d	a	b
monotonic	cracked	2.10	0.1254	0.680	0.323	-	-
	rough	1.76	0.0988	0.659	-	-	-
	free	-	0.0451	0.541	-	-	-
	smooth	-	0.0147	0.561	-	-	-
	cracked*	-	0.0523	0.934	-	-	-
cyclic	cracked	-	-	-	-	0.0695	1
	free	-	-	-	-	0.0695	1

Note: * high strength concrete

Finally, it is important to mention that for interfaces between concretes cast at different times the considered value of f_c was the average of the two concrete strengths. When only the lower value of the two is considered, the results are not so coherent: for "rough" interfaces we obtain c = 0.077 and μ_2 = 0.833 for stage II and neither stage I or stage III can be identified.

These latest values have a more pronounced discrepancy with the results regarding "cracked" interfaces, a deviation that was not noticed in some studies on this subject (Mattock 1976; Mattock 2001).

3.3.2 CYCLIC TESTS

For interfaces subjected to cyclic shear loading, an *S-N* curve is defined to model the fatigue strength behavior. Monotonic strength is reduced depending on the maximum shear value applied in the cyclic loading and the corresponding number of cycles:

$$\frac{\tau_{\max}}{\tau_{\mathrm{R}}} = b - a \times \log N \tag{3-21}$$

Equation (3-21) is similar to Equation (3-10) presented by Pruijssers (1988). Figure 3-4 shows the results obtained by Pruijssers (1988), for monolithic concrete cracks, and by Figueira et al. (2015) (see Section 2.3.3.5) for free surfaces. A great variability, typical in fatigue tests, is observed. We can also see that "free" surface results are within the cloud of the "cracked" interface ones. This conclusion allows the setting of an *S-N* curve for the two interface roughness profile types. The value obtained for the coefficient *a* was 0.0695 (see Table 3-1), with *b* previously defined as being equal to 1.

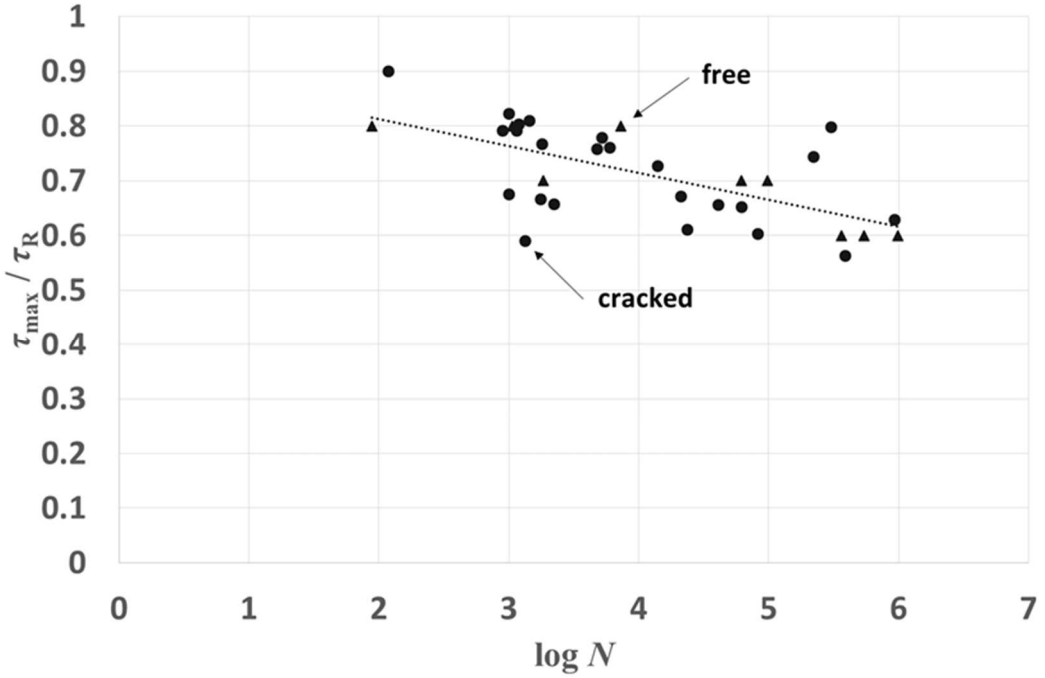

Figure 3-4 – *S-N* curve obtained from the experimental cyclic tests data.

3.4 ANALYSIS OF THE DESIGN CODE RECOMMENDATIONS

Experimental data is now compared to EN 1992 and ACI 318-05 design expressions in order to evaluate the corresponding code provisions structural reliability. In this context, it is important to mention that, when applying those expressions on interfaces between concretes cast at different times, only the lower concrete strength of the two different age concretes was introduced in the expressions. When the concrete tensile strength was not experimentally determined, *fib* Model Code (*fib* 2013) recommendations were followed to calculate it as a function of the compressive strength. For ACI 318-05 design model, f_c' was taken as the specified concrete strength by the authors of each experimental specimen considered in this present study (see Annex A). Finally, in the analysis of the EN 1992 proposal for cyclic loading, the value of coefficient *c* was taken as 0, since fatigue loading is more common in bridge structures. The comparison is established using the following formulation of Equation (3-15):

$$P\left(\mathrm{SF_R} \le 1\right) = \Phi\left(-\beta\right) \tag{3-22}$$

with $\alpha_R = 1$ (a conservative assumption, noting that the ratio between the standard deviations for the action effect and the resistance is not known) and $SF_R = \tau_R / \tau_{Rd}$ for monotonic loading or $SF_R = \tau_{max} / \tau_{Rd,fat}$ for cyclic loading. In turn, acceptable values for the reliability index β are $4.30 \leq \beta \leq 4.75$, corresponding to $10^{-7} \leq P_f \leq 10^{-5}$. This assumption is valid for monotonic and cyclic loading.

The probability P ($SF_R \leq 1$) is calculated through the adjustment of a probability distribution function. For material and structural variables, EN 1990 considers the following distributions: Normal, log-Normal, Gumbel and Weibull. These are the distributions commonly used in structural reliability analysis (Schneider 1997). However, in the present work the skew Normal distribution (Azzalini and Dalla Valle 1996) will also be considered. It has the advantage of allowing for non-zero skewness. When the number of tests n is limited, in the context of statistical determination of resistance models, EN 1990 recommends the use of a Student's t-distribution, a distribution that depends on the sample size. This European Standard suggests $n < 100$ as a criteria to define a limited number of tests. Since the mean of a t-distribution is always 0, the following substitution was implemented in the present study:

$$t = \frac{SF_R - \mu}{\sigma} \tag{3-23}$$

where μ and σ are the sample's mean value and standard deviation, respectively.

When $n \geq 100$ the probability distribution function is chosen through statistical goodness-of-fit hypothesis testing, with a null hypothesis according to which the data set follows a certain distribution. Many goodness-of-fit tests are available in literature. The Anderson-Darling test (Anderson and Darling 1954) was used in this study owing to its potential: it is a test suitable for a wide range of distribution families with parameters calculated from the data set; it also gives more weight to observations in the tails of the distribution compared to some other commonly used tests. Depending on the distribution to be tested, some authors made adjustments to the basic test statistic and proposed new p-values computing formulas. Concerning this subject, the recommendations of the following authors were considered in the study: D'Agostino and Stephens (1986) for Normal and log-Normal distributions; Shorack and Wellner (1986) for the Gumbel distribution; Lockhart and Stephens (1994) for the Weibull distribution; and Dalla Valle (2007) for the skew Normal distribution.

3.4.1 MONOTONIC TESTS

For monolithic concrete cracks, computed EN 1992 and ACI 318-05 values for the safety factor SF_R are presented in Figure 3-5 and Table 3-2. EN 1992 does not provide explicit values for roughness coefficients c and μ for this kind of interface. Therefore, since shear strength of rough surfaces is slightly lower than the shear strength of monolithic concrete cracks (as seen in Section 3.3.1 and Table 3-1), c = 0.45 and μ = 0.7 were considered. This assumption is in line with the recommendations of Mattock (2001), who proposed the same design values for both interfaces.

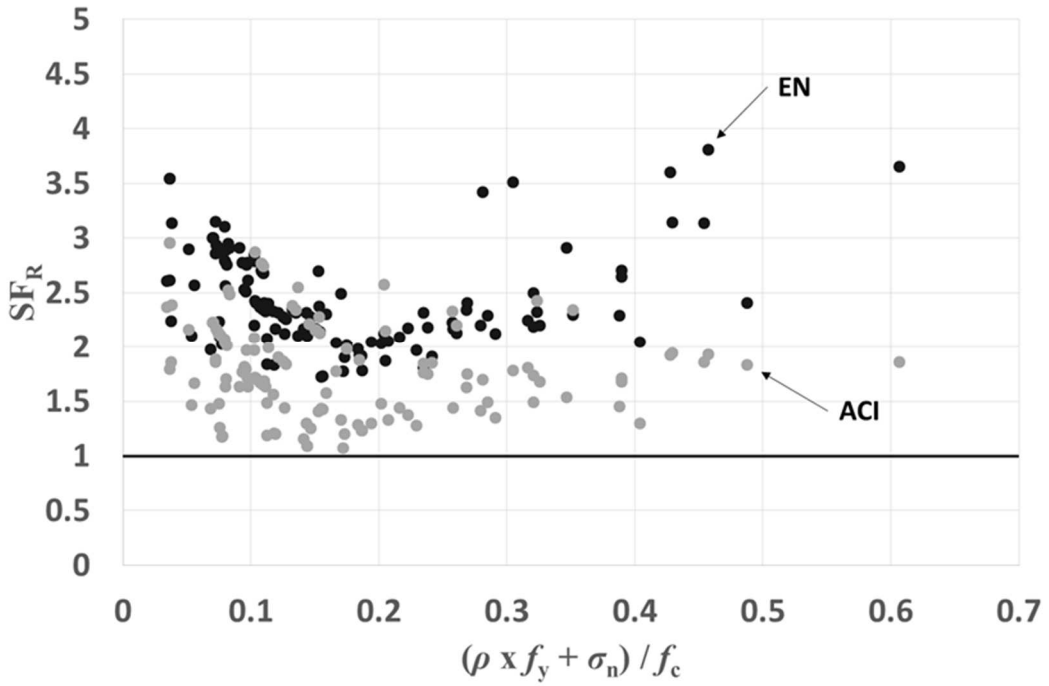

Figure 3-5 – Resistance safety factor obtained from the design expressions of EN 1992 and ACI 318-05 for monolithic concrete cracks.

Table 3-2 – Resistance safety factor values obtained from the application of EN 1992 and ACI 318-05 design expressions to interfaces with different roughness profiles (μ – average; σ – standard deviation).

		SF_R - EN		SF_R - ACI		number of tests
		μ	σ	μ	σ	
monotonic	cracked	2.45	0.442	1.81	0.425	132
	rough	2.52	0.803	1.84	0.355	20
	free	1.61	0.096	2.37	0.187	5
	smooth	1.37	0.064	1.22	0.180	6
	cracked*	2.43	0.485	2.28	0.540	18
cyclic	cracked	2.27	0.403	-	-	24
	free	1.25	0.146	-	-	9

The results in Table 3-2 and Figure 3-5 show that the EN 1992 expression is more conservative (μ = 2.45 and σ = 0.442) than ACI 318-05 expression (μ = 1.81 and σ = 0.425). In both cases, a significant variability can be seen in the results.

For the two design expressions, the skew Normal distribution was the one that best fitted the data (see Figure 3-6 and Table 3-3) with a *p*-value equal to 0.335 for EN 1992 (P ($SF_R \leq 1$) = 8.73×10^{-14}) and 0.383 for ACI 318-05 (P ($SF_R \leq 1$) = 1.27×10^{-2}). Comparing with the defined target reliability index range, we can conclude EN 1992 provides too conservative values and ACI 318-05 values that should be more reliable.

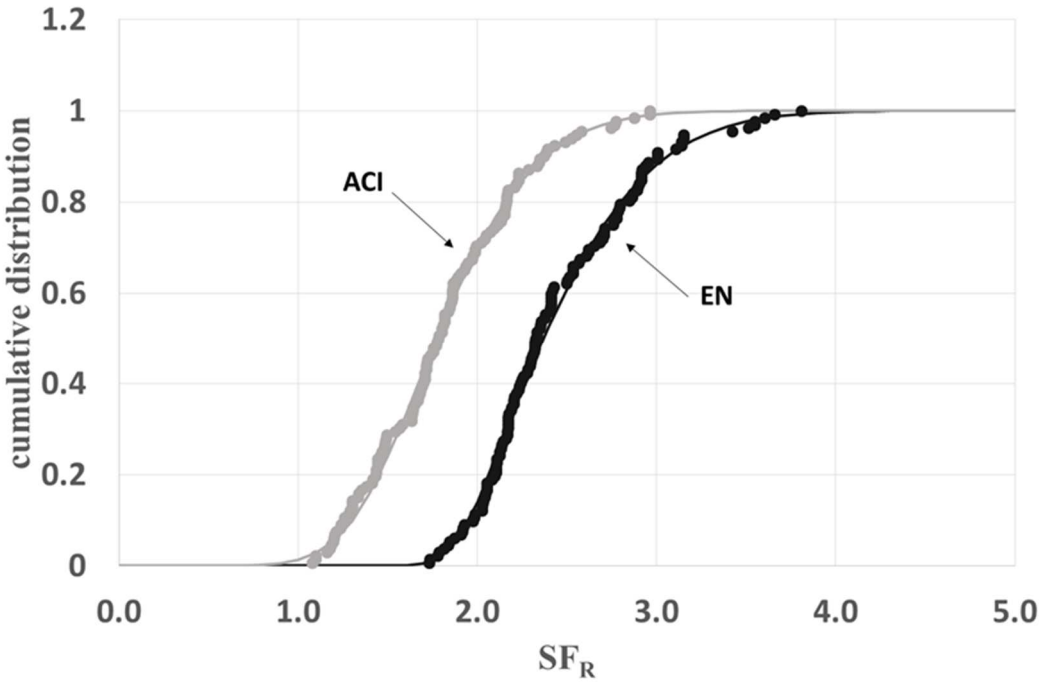

Figure 3-6 – Cumulative skew Normal distribution function adjusted to the resistance safety factor values of EN 1992 and ACI.

Table 3-3 – *p*-values obtained from the Anderson-Darling test applied to the resistance safety factor values (SF_R) of EN 1992 and ACI 318-05 and the probability of $SF_R \leq 1$ (monolithic concrete cracks).

	p-value		*P* ($SF_R \leq 1$)	
	EN	ACI	EN	ACI
Normal	0.000	0.055	-	-
skew Normal	0.335	0.383	8.73×10^{-14}	1.27×10^{-2}
Gumbel	0.176	0.003	-	-
Weibull	0.000	0.002	-	-
log-Normal	0.007	0.250	-	-

Regarding interfaces with different roughness profiles, values of SF_R for both codes decrease when the surfaces are less rough, despite a less pronounced variability in the results for those interfaces (see Figure 3-7 and Table 3-2). The exception occurs in ACI 318-05 proposal for "free" surfaces and interfaces between high strength concretes. Adjustment of *t*-

distribution was better for samples including a very small number of tests and low standard deviation (see Figure 3-8 and Table 3-4). In this context, it is also important to notice two *p*-values below 0.05, the value for which significance level is usually set (Capraro 2006), a fact that implies rejection of the null hypothesis. Finally, we can verify that all values obtained for the probability P ($SF_R \leq 1$) were superior to the target value range.

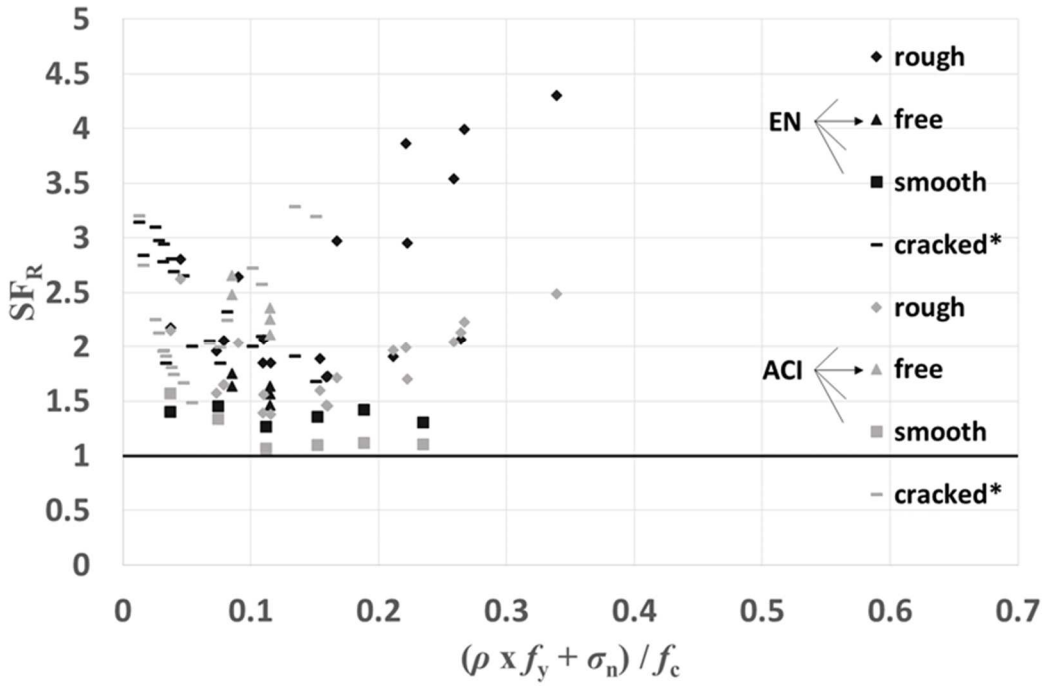

Figure 3-7 – Resistance safety factor obtained from the design expressions of EN 1992 and ACI 318-05 for interfaces with different roughness profiles (*high strength concrete).

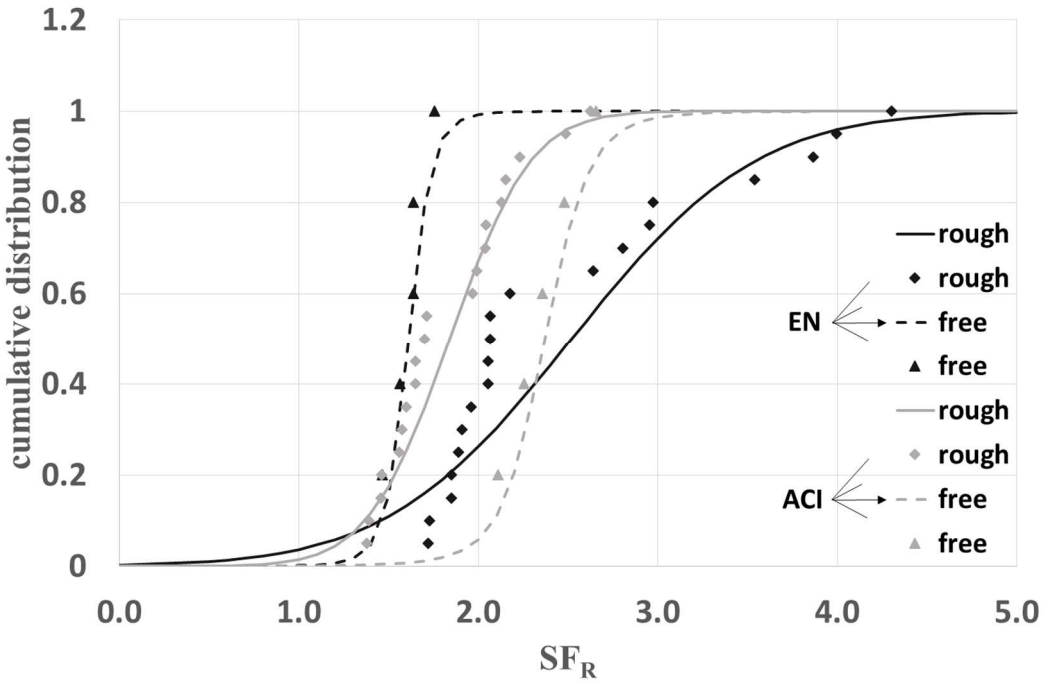

Figure 3-8 – Cumulative *t*-distribution function adjusted to the resistance safety factor values of EN 1992 and ACI for interfaces with different roughness profiles.

Table 3-4 – *p*-values obtained from the Anderson-Darling test applied to the resistance safety factor values of EN 1992 and ACI 318-05 and the probability of $SF_R \leq 1$ (considering a *t*-distribution for interfaces with different roughness profiles).

		p-value		$P\ (SF_R \leq 1)$	
		EN	ACI	EN	ACI
monotonic	rough	0.002	0.182	3.68×10^{-2}	1.43×10^{-2}
	free	0.860	0.976	1.53×10^{-3}	9.17×10^{-4}
	smooth	0.850	0.076	1.10×10^{-3}	1.41×10^{-1}
	cracked*	0.041	0.182	4.46×10^{-3}	1.51×10^{-2}
cyclic	cracked	0.112	-	2.30×10^{-3}	-
	free	0.095	-	6.11×10^{-2}	-

3.4.2 CYCLIC TESTS

Figure 3-9 and Table 3-2 show the EN 1992 SF_R values obtained for cracks in monolithic

concrete, and also "free" surfaces, subjected to cyclic loading. SF_R is somewhat lower in this case, compared with monotonic loading, and slightly decreases with log *N*. Adjustment of *t*-distribution led to *p*-values higher than 0.05 and *P* ($SF_R \leq 1$) superior to the target value range (see Figure 3-10 and Table 3-4).

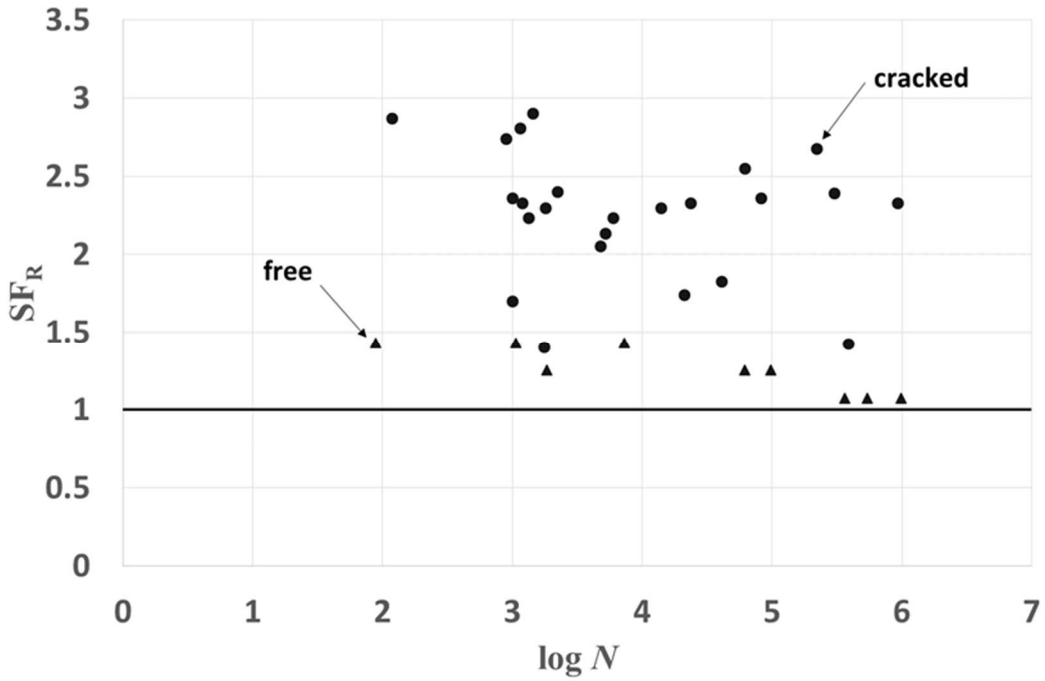

Figure 3-9 – Resistance safety factor obtained from the design expression of EN 1992 for interfaces with different roughness profiles subjected to cyclic loads.

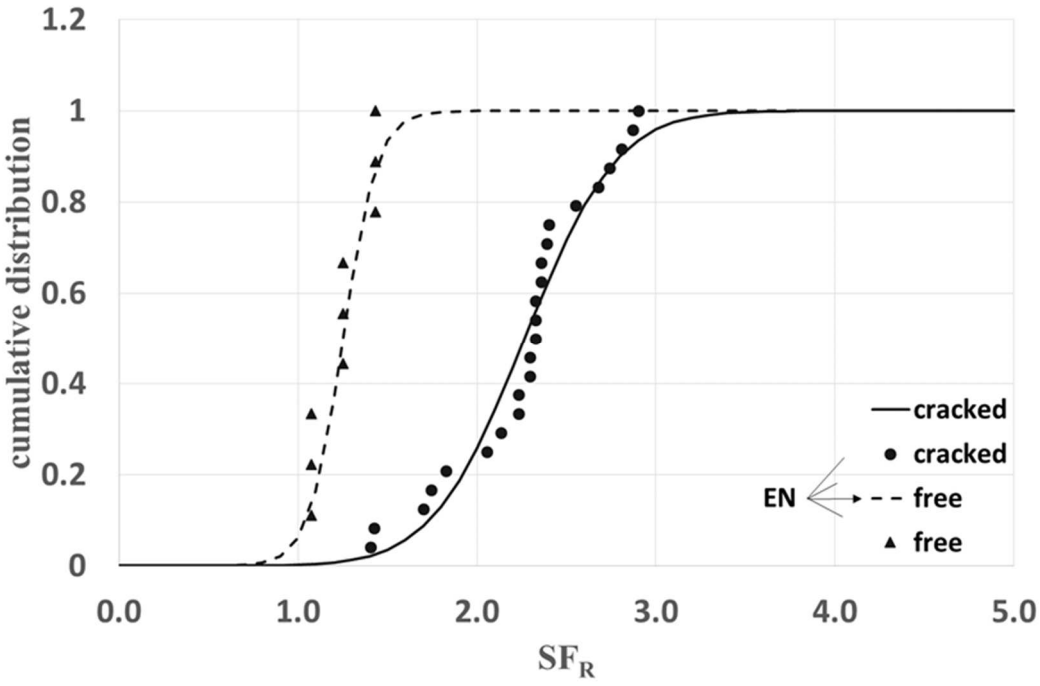

Figure 3-10 – Cumulative *t*-distribution function adjusted to the resistance safety factor values of EN 1992 for interfaces with different roughness profiles subjected to cyclic loads.

3.5 NEW DESIGN RECOMMENDATIONS

The analysis of the design code recommendations in Section 3.4 of this chapter led to values of the probability P ($SF_R \leq 1$) that were significantly higher than the defined target value range. The exception was the EN 1992 proposal for monolithic concrete cracks subjected to monotonic loading, however, the values obtained in this case were substantially lower than the target range, being too conservative. New design recommendations presented in this present work intend to place all the P ($SF_R \leq 1$) values within the target range, through a parametric analysis. The analysis is based on the following design expressions:

$$\tau_{Rd} = \min\{\tau_{Rd1}, \tau_{Rd2}, \tau_{Rd3}\} \tag{3-24}$$

where:

$$\tau_{Rd1} = \mu_1 \times \left(\rho \times f_{yd} + \sigma_n\right) \tag{3-25}$$

$$\tau_{Rd2} = c \times f_{cd} + \mu_2 \times \left(\rho \times f_{yd} + \sigma_n \right) \tag{3-26}$$

$$\tau_{Rd3} = d \times 0.6 \times \left(1 - \frac{f_{ck}}{250} \right) \times f_{cd} \tag{3-27}$$

The above expressions are similar to Equations (3-16), (3-17), (3-18) and (3-19) with the exception of having design values and a coefficient $0.6 \times (1 - f_{ck} / 250)$ to consider concrete strength influence on a reduction factor for strength of diagonal concrete struts subjected to multi-axial stresses. The design values for concrete and reinforcement strength are calculated using partial factors for resistance, as considered in Section 3.4.

The implemented parametric analysis aimed to determine coefficients c, d, μ_1 and μ_2 following two main criteria: reduce to a minimum the variability of SF_R results and set the average SF_R to a value that can provide probabilities P ($SF_R \leq 1$) within the target range. In addition to these two main criteria the analysis took into account the statistical uncertainty associated with the number of tests and prior statistical knowledge.

For cyclic loads, the same procedure was applied. In this case, the design expression is the following:

$$\frac{\tau_{max}}{\tau_{Rd}} = b - a \times \log N \tag{3-28}$$

3.5.1 MONOTONIC TESTS

The parametric analysis was first implemented in the larger available data set, with 132 tests, corresponding to cracks in monolithic concrete. Thus, the conclusions drawn can eventually provide statistical knowledge for further analyses of smaller data sets. For a certain average value of SF_R, coefficients c, d, μ_1 and μ_2 were settled to minimize the sample standard deviation. Figure 3-11 illustrates how the standard deviation σ varied with μ_2 in the analysis. In turn, Figure 3-12 shows how the obtained probability P ($SF_R \leq 1$) varies with the considered average value of SF_R. The dashed lines define the target range for P ($SF_R \leq 1$). Finally, in Figure 3-13, we can see the minimized standard deviation growing with the average value of SF_R.

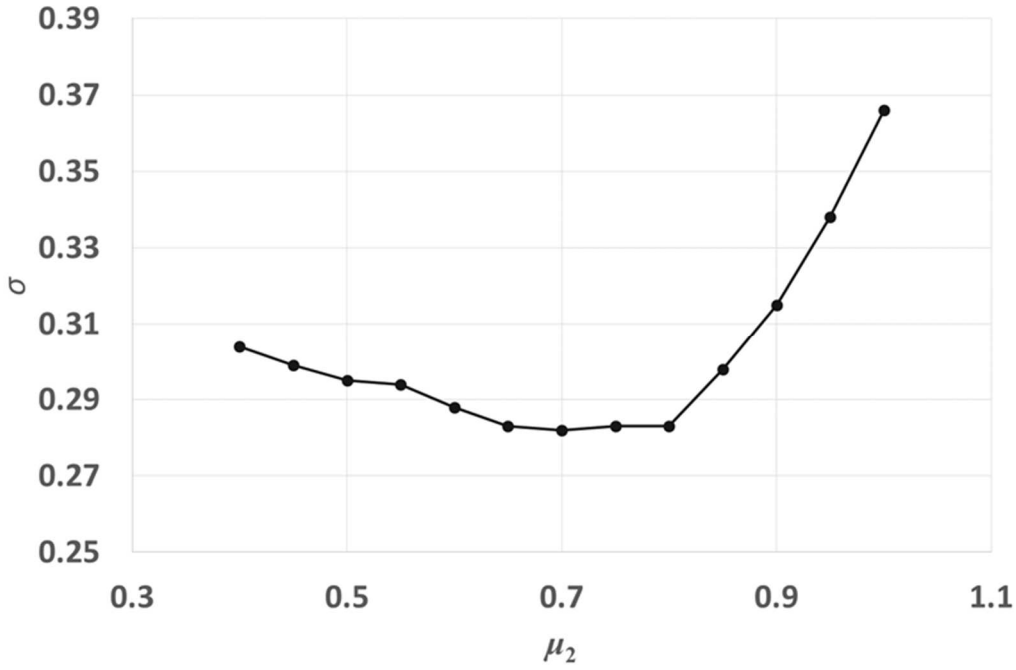

Figure 3-11 – Standard deviation of the resistance safety factor values versus the shear strength design factor μ_2 in monolithic concrete cracks.

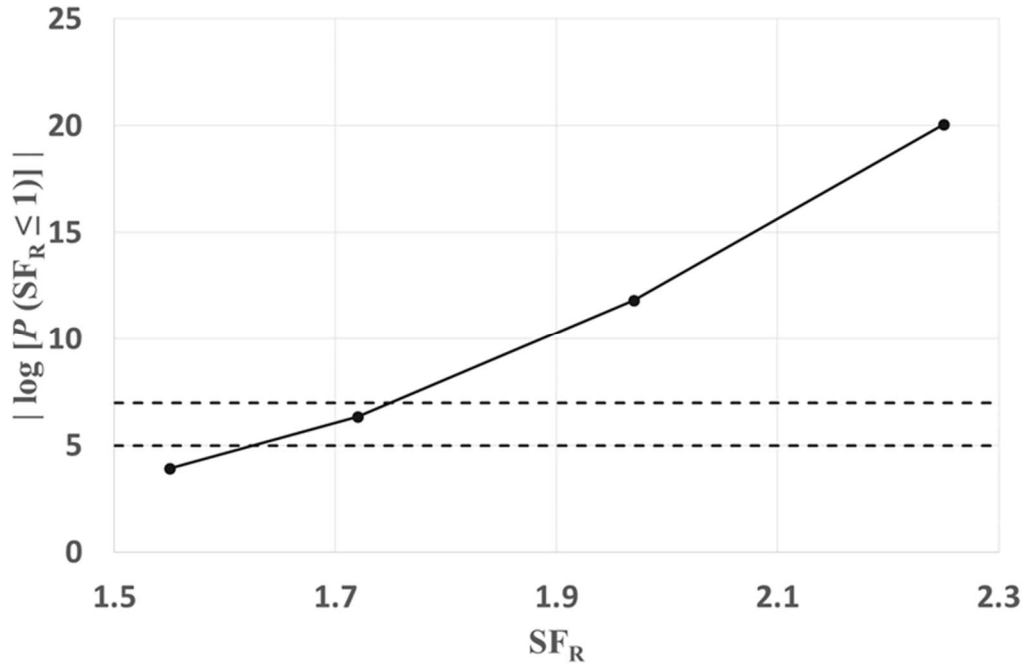

Figure 3-12 – Probability of the resistance safety factor being less than or equal to 1 (SFR $\leq$ 1) versus the average values of SFR in the design of monolithic concrete cracks.

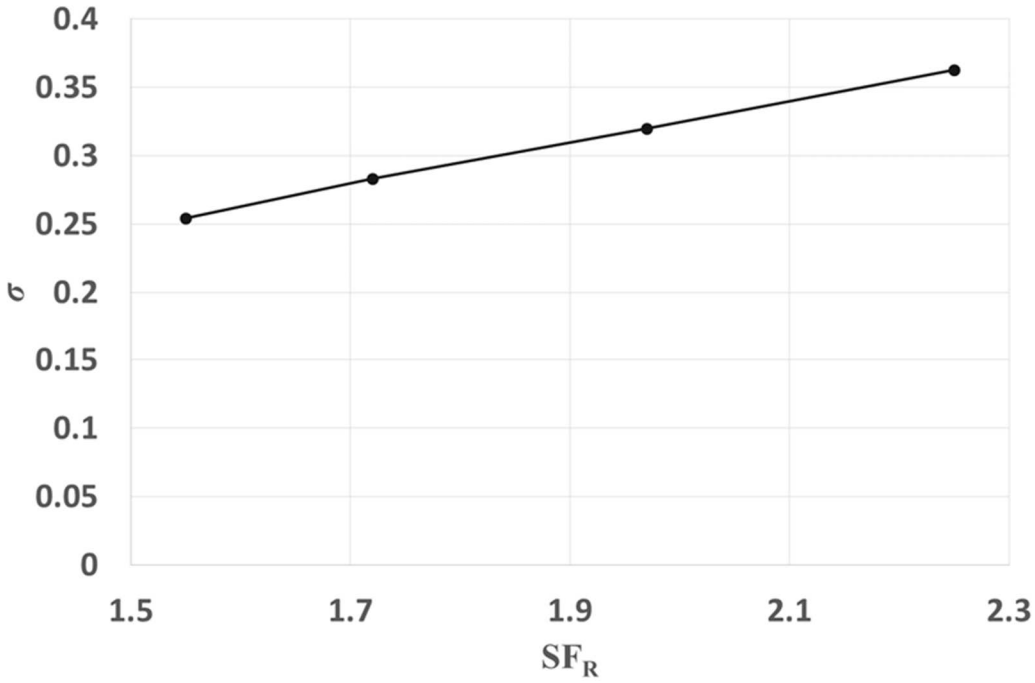

Figure 3-13 – Standard deviation versus the average resistance safety factor values in the design of monolithic concrete cracks.

The values determined for the coefficients c, d, μ_1 and μ_2 are presented in Table 3-5. In Figure 3-14 and Table 3-6, comparing with Figure 3-5 and Table 3-2, we can notice the improvements achieved: a significantly lower variability in SF_R (standard deviation σ = 0.283) and also less conservative results (average μ = 1.72), within the desired reliability. This time, the Gumbel distribution was the one that best fitted the data with a p-value = 0.313 and P ($SF_R \leq 1$) = 4.42 x 10^{-7} (see Figure 3-15 and Table 3-7).

Table 3-5 – Proposed values for the design shear strength factors.

		μ_1	c	μ_2	d	a	b
monotonic	cracked	1.90	0.070	0.80	0.750	-	-
	rough	1.20	0.060	0.65	0.750	-	-
	free	0.50	0.040	0.30	0.750	-	-
	smooth	0.45	0.010	0.30	0.750	-	-
	cracked*	2.20	0.035	0.65	0.750	-	-
cyclic	cracked	-	-	-	-	0.045	0.80
	free	-	-	-	-	0.045	0.80

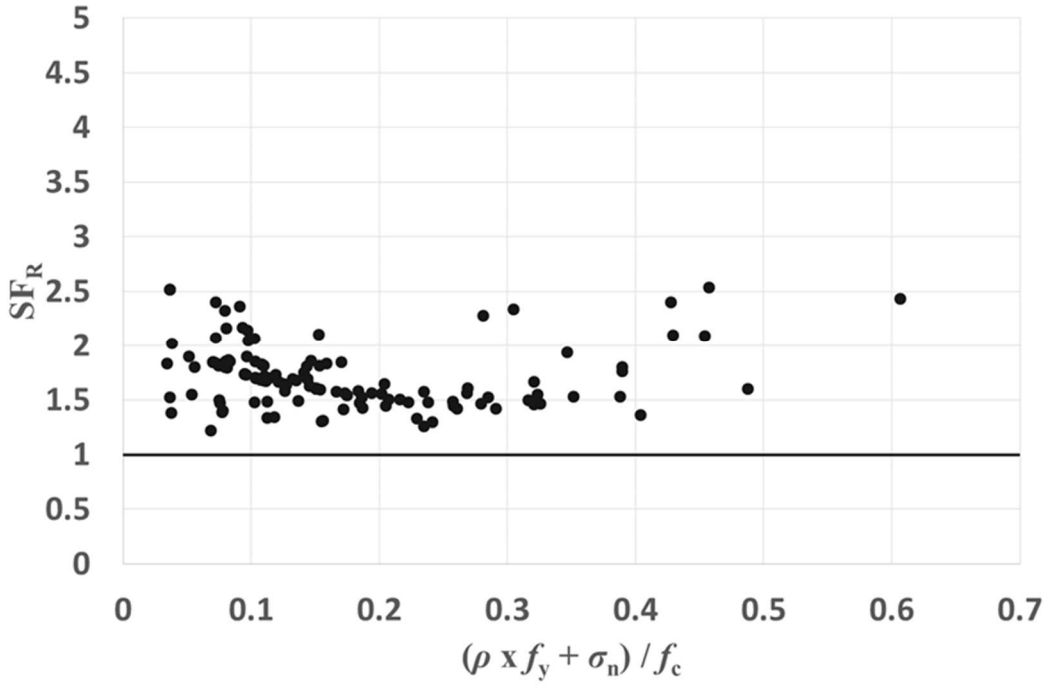

Figure 3-14 – Resistance safety factor obtained from the new design expressions for monolithic concrete cracks.

Table 3-6 – Resistance safety factor values obtained from the application of the new design expressions to interfaces with different roughness profiles.

		SF_R	
		μ	σ
monotonic	cracked	1.72	0.283
	rough	2.00	0.421
	free	2.28	0.111
	smooth	2.26	0.120
	cracked*	2.00	0.215
cyclic	cracked	1.99	0.236
	free	2.58	0.269

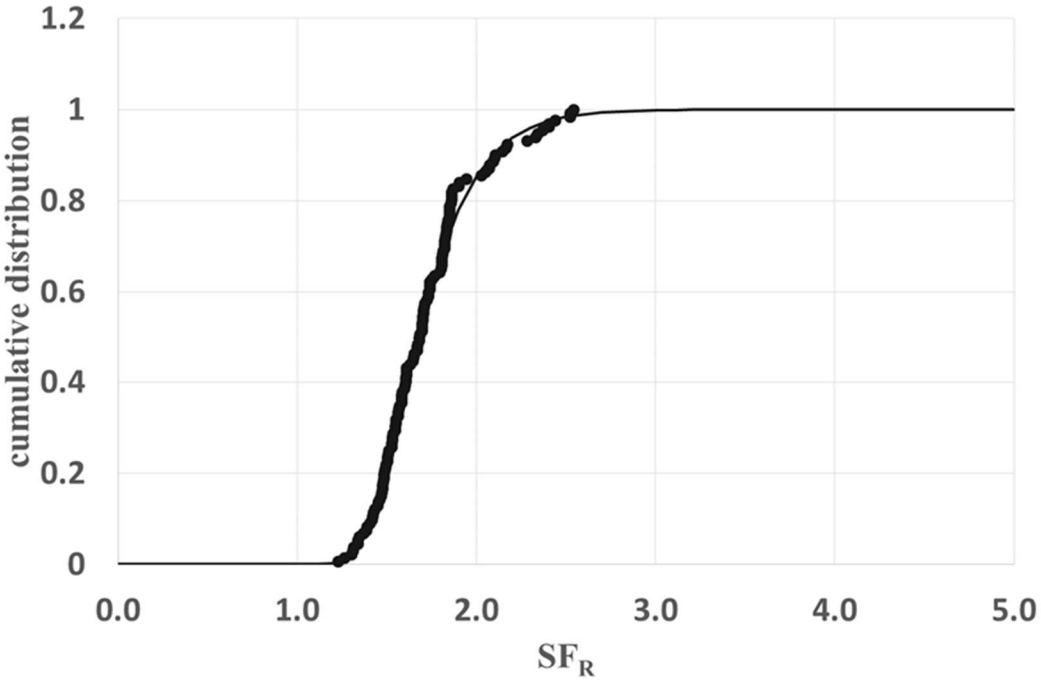

Figure 3-15 – Cumulative Gumbel distribution function adjusted to the resistance safety factor values of the new design expressions for monolithic concrete cracks.

Table 3-7 – *p*-values obtained from the Anderson-Darling test applied to the resistance safety factor values (SF_R) of the new design proposal and the probability of $SF_R \leq 1$ (monolithic concrete cracks).

		p-value	$P\ (SF_R \leq 1)$
monotonic	Normal	0.000	-
	skew Normal	0.003	-
	Gumbel	0.313	4.42×10^{-7}
	Weibull	0.000	-
	log-Normal	0.002	-
cyclic	*t*	0.724	1.68×10^{-4}

For different interface roughness profiles, the same analysis was implemented. In this case, due to the small data sets size, a *t*-distribution was adjusted to the results providing, as expected, high values for the probability $P\ (SF_R \leq 1)$. Therefore, to set that probability within the target range, a significantly higher average value of SF_R was achieved, comparing with the value 1.72 obtained for monolithic concrete cracks. Thus, coefficients c, μ_1 and μ_2 turned out to be significantly lower in this circumstance losing coherence with the results presented in Table 3-1. For that reason, prior statistical knowledge, mainly taken from monolithic concrete cracks, was used to formulate new design recommendations for interfaces with different roughness profiles. In these cases, the mean SF_R value is fixed arbitrarily based on similar information.

"Rough" interfaces, despite presenting a greater variability, are known to have a roughness profile approximate to a monolithic concrete crack (see Section 3.3.1 of this present chapter and Mattock 2001). For that motive, the Gumbel distribution was also tested to the 20 available results and, despite still being very small, a higher *p*-value was reached comparing to the *t*-distribution (see Figure 3-16 and Table 3-8). A probability $P\ (SF_R \leq 1) = 6.91 \times 10^{-6}$ was obtained for an average value $SF_R = 2.00$.

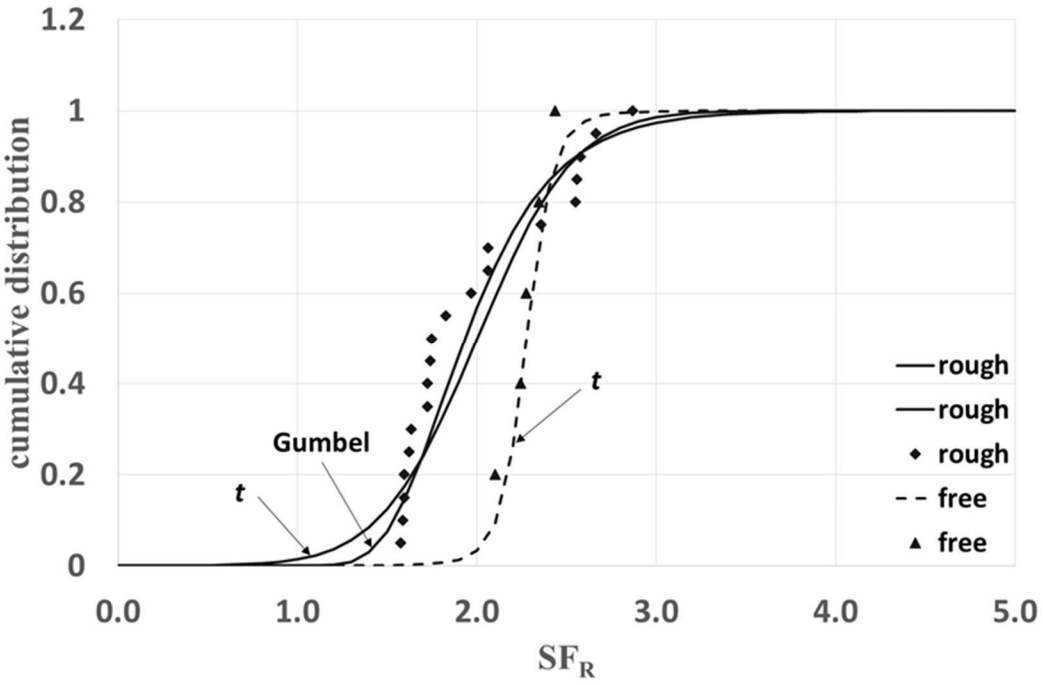

Figure 3-16 – Cumulative distribution functions adjusted to the resistance safety factor values of the new design expressions for interfaces with different roughness profiles.

Table 3-8 – *p*-values obtained from the Anderson-Darling test applied to the resistance safety factor values of the new design proposal and the probability of $SF_R \leq 1$ (for interfaces with different roughness profiles).

		p-value	$P\ (SF_R \leq 1)$	distribution
monotonic	rough	0.003	1.40×10^{-2}	*t*
		0.015	6.91×10^{-6}	Gumbel
	free	0.946	1.65×10^{-4}	*t*
	smooth	0.893	6.75×10^{-5}	*t*
	cracked*	0.113	1.10×10^{-4}	*t*
cyclic	free	0.933	1.87×10^{-4}	*t*

For cracks in monolithic high strength concrete, a similar $SF_R = 2.00$ average value was considered since the number of available data (18 tests) is approximately the same. For "free" and "smooth" surfaces, with very small available experimental data (5 and 6 tests, respectively), $SF_R = 2.25$ was settled. In all cases, $P\ (SF_R \leq 1)$ was not far from the target

range. Since no tests with low reinforcement ratio were available, coefficient μ_1 was defined through a branch connecting the origin of axes ($(\rho \times f_{yd} + \sigma_n) / f_{cd}$; τ_{Rd} / f_{cd}) with the data set point with the lowest $(\rho \times f_{yd} + \sigma_n) / f_{cd}$ value. τ_{Rd} was determined considering c and μ_2 values of Table 3-5. Results obtained in this procedure were coherent with the values presented in Table 3-1 for roughness coefficients c, μ_1 and μ_2.

Comparing Figure 3-17 and Table 3-6 with Figure 3-7 and Table 3-2, we can finally notice the main improvements achieved this time: a significantly lower variability in SF_R for most cases and also closer SF_R values between interfaces with different roughness profiles.

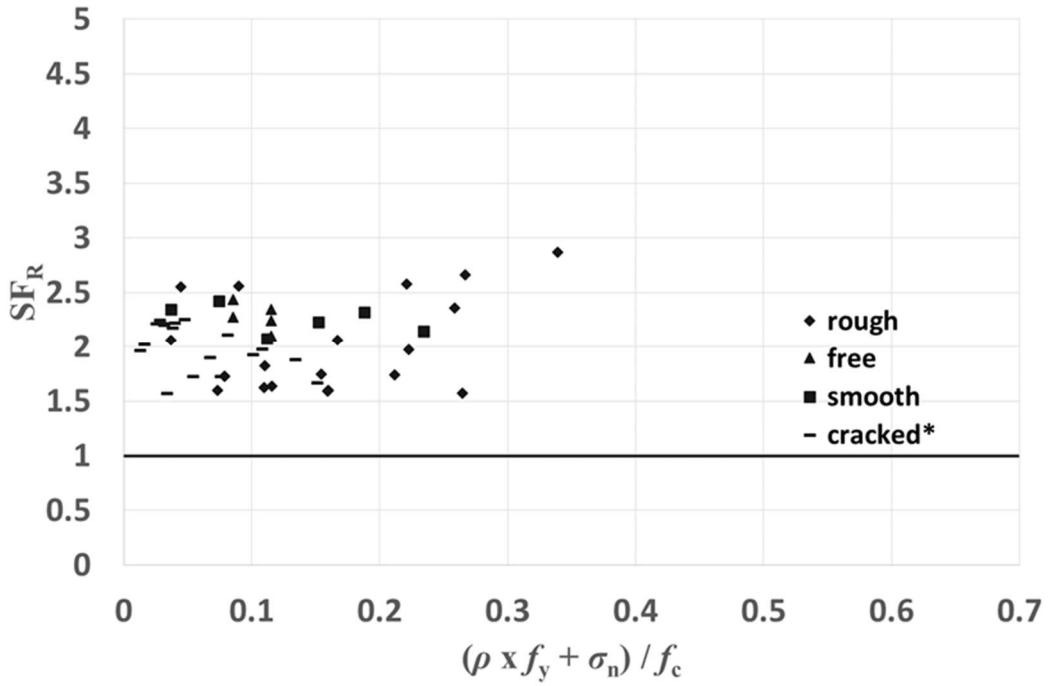

Figure 3-17 – Resistance safety factor obtained from the new design expressions for interfaces with different roughness profiles.

3.5.2 CYCLIC TESTS

A similar procedure was implemented for cyclic tests. Firstly, monolithic concrete cracks were analyzed. Since the number of available data in this case (24 tests) is not far from the number regarding "rough" surfaces (20 tests) and monolithic high strength concrete cracks (18 tests), the same criteria was used. An average value of SF_R = 2.00 was considered,

resulting in a probability P ($SF_R \leq 1$) = 1.68×10^{-4} through a *t*-distribution fitting with a *p*-value equal to 0.724 (see Figure 3-18 and Table 3-7). The values of coefficients *a* and *b* that minimized the sample standard deviation were 0.045 and 0.80, respectively (see Table 3-5). These values were the starting point for a similar analysis on the 9 "free" surface tests, resulting in an average SF_R = 2.58, a higher and more conservative value than the one achieved in the monotonic loading analysis for these interfaces (approximately 2.25). A probability P ($SF_R \leq 1$) = 1.87×10^{-4} was obtained through a *t*-distribution fitting with a *p*-value equal to 0.933 (see Figure 3-18 and Table 3-8).

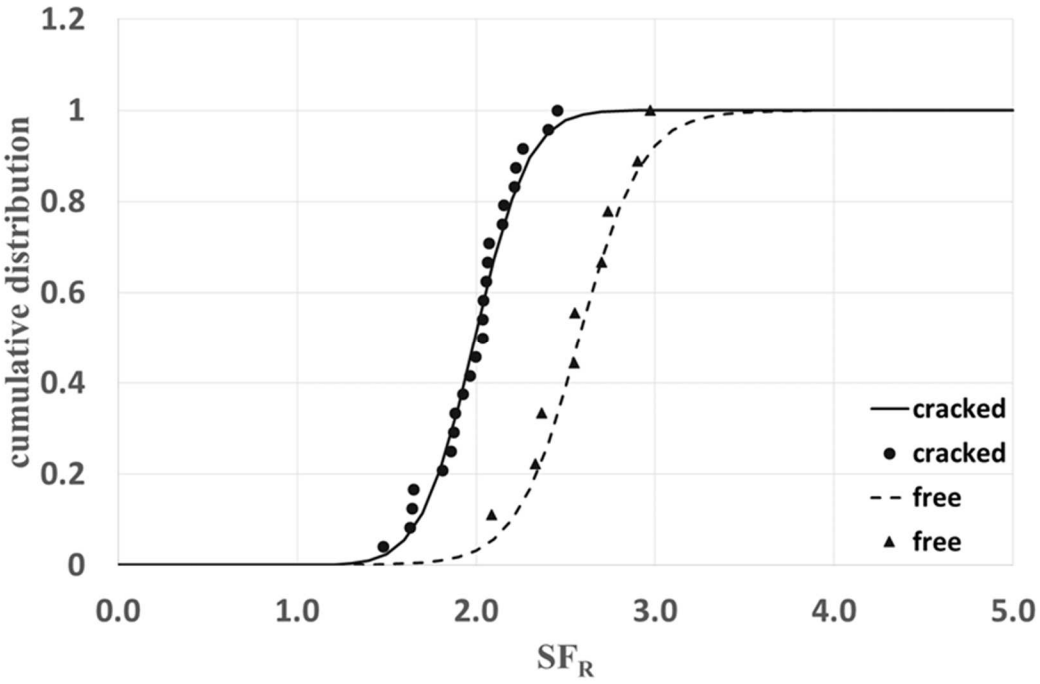

Figure 3-18 – Cumulative *t*-distribution function adjusted to the resistance safety factor values of the new design expressions for interfaces subjected to cyclic loads.

Finally, Figure 3-19 and Table 3-6 show the new SF_R values for each experimental fatigue test. For monolithic concrete cracks, a lower variability can be noticed comparing to Figure 3-9 and Table 3-2. For "free" surfaces, more conservative values can be seen.

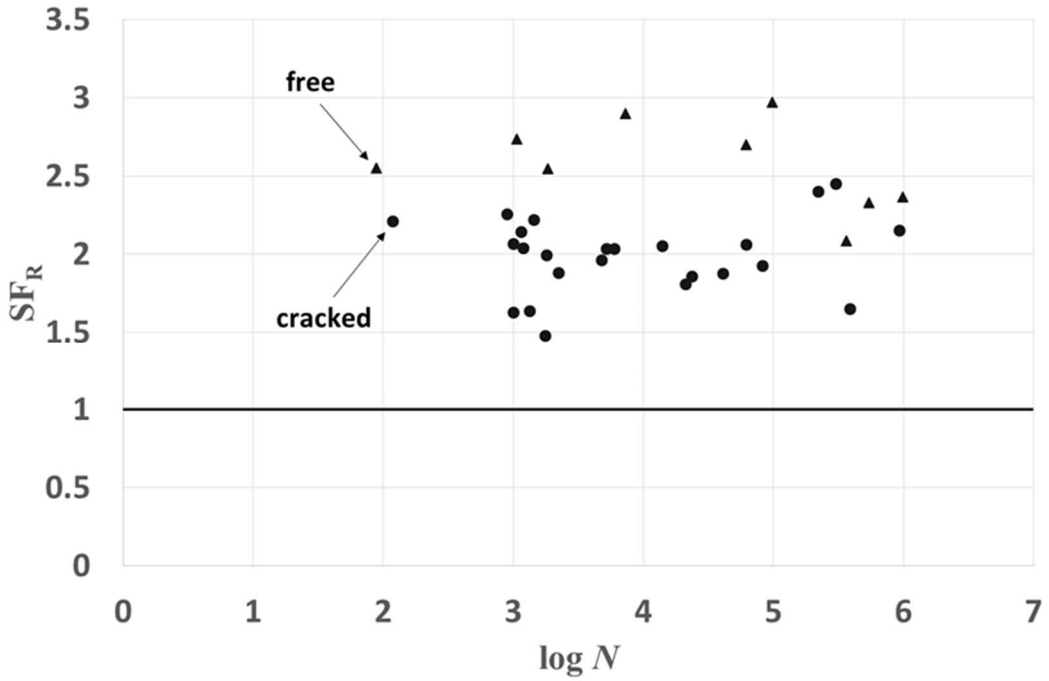

Figure 3-19 – Resistance safety factor obtained from the new design expressions for interfaces with different roughness profiles subjected to cyclic loads.

3.6 CONCLUSIONS

The amount of existing experimental data for interfaces resulting from cracks in monolithic concrete is significantly higher than the number of data referring to interfaces with a different roughness profile. The same conclusion is obtained when the available data for interfaces subjected to monotonic loads is compared with the available data for interfaces subjected to cyclic loads. Further research, to fill that gap, is therefore justified.

In interfaces resulting from cracks in monolithic concrete, the amount of available experimental data provides statistical knowledge that reveals a special importance when dealing with interfaces with different roughness profiles. In monolithic concrete cracks, the observed resistant behavior clearly discloses a nonlinear growth of the shear strength versus the existing normal stress. However, the mathematical fitting of a nonlinear function for this behavior, besides having inherent complexity, does not clearly express the corresponding physical phenomenon, and the resistant mechanisms that interact in shear strength mobilization. In turn, a function consisting of 3 linear branches seeks to overcome these

shortcomings, although the fit to the experimental values is not so perfect.

Analysis of experimental results obtained by various authors showed that interfaces resulting from monolithic concrete cracks and interfaces between concretes cast at different times subjected to treatment, have a significantly higher resistance than others, with values for the first case slightly higher than those relating to the second case. Interfaces resulting from a free surface and smooth interfaces have a lower resistance, with slightly lower values for the smooth interfaces. When the concrete has high strength properties, some differences in the obtained results are observed, mainly related to the cohesion and friction mobilized.

Application of design code expressions (from EN 1992 and ACI 318-05) to the experimental results revealed a higher average resistance safety factor for rougher interfaces, for which the number of available data is also higher. However, the results dispersion and variability were always greater in such cases. It was also concluded that the design code expressions are less conservative than the target defined in the present study, which was based on the EN 1990 recommendations regarding statistical modelling of data and failure probabilities. The only exception was the EN 1992 proposal for interfaces resulting from monolithic concrete cracks subjected to monotonic loads, which provided too conservative values (according to the same criteria).

In order to minimize the variability of results and put the average resistance safety factor in a range that provide failure probability values within the desired target, a new proposal for the design of concrete interfaces is presented. The proposal is characterized by 3 linear branches and came from a parametric analysis of existing experimental data, also following EN 1990 recommendations regarding this subject.

4

FINITE ELEMENT MODELING OF THE DOWEL MECHANISM FOR STATIC LOADING

A nonlinear finite element modeling approach is developed to assess the behavior of a dowel bar embedded on a single concrete block substrate, subjected to monotonic loading. In this approach, a discrete representation of the steel reinforcing bar is considered, using beam finite elements with nonlinear material behavior. The bar is connected to the concrete embedment through nonlinear Winkler spring elements. This modeling approach can only be used if a new constitutive model is developed for the spring elements, to simulate the deformability and strength of the concrete substrate. To define this constitutive model, an extensive literature review was conducted, as well as 3 experimental tests, in order to select the experimental data which can be used in the calibration of the model. Based on this data, an empirical model was established to predict the global dowel response, for a wide range of bar diameters and concrete strengths. This empirical model provided the information needed for calibration of the nonlinear Winkler spring model, valid for dowel displacements up to 4 mm. This new constitutive model is composed by 5 stages, in order to reproduce the concrete substrate response.

4.1 INTRODUCTION

Modeling of shear transfer across cracks in reinforced concrete is a difficult problem, due to the complexity of the shear strength mechanisms involved and their numerical simulation (Dias-da-Costa et al. 2012, Kazaz 2011, Pimentel et al. 2008). The shear force, *V*, transferred

through a crack, either in monolithic concrete or in a concrete joint, is mainly carried by two different mechanisms (Maekawa and Qureshi 1997, Rahal et al. 2016, Santos and Júlio 2014):

$$V = V_{agg} + V_{d} \tag{4-1}$$

in which V_{agg} is the force corresponding to aggregate interlock mechanism and V_{d} the dowel force of steel reinforcing bars.

This present Chapter 4 focuses only on the contribution of dowel action. The strength of a dowel submitted to monotonically increasing load, V_{dR}, has been widely evaluated in several research studies (Bennett and Banerjee 1976, Dei Poli et al. 1992, Dulacska 1972, Engström 1990, Millard and Johnson 1984, Paulay et al. 1974, Randl 1997, Rasmussen 1963, Soroushian et al. 1986, Tanaka and Murakoshi 2011, Vintzeleou and Tassios 1987). This strength is usually predicted through the following analytical expression, whose background theory can be consulted in *fib* Bulletin 43 (*fib* 2008):

$$V_{dR} = K \times A_{s} \times \sqrt{f_{c} \times f_{y}} \tag{4-2}$$

where A_s is the area of reinforcement, f_c the concrete compressive strength and f_y the reinforcement yield stress. K is an empirical constant that depends on the actual confinement existing in the concrete substrate immediately under the dowel bar:

$$K = \frac{4}{\pi} \times \sqrt{\frac{\beta^{*}}{3}} \tag{4-3}$$

with

$$\beta^{*} = \frac{f_{c}^{*}}{f_{c}} \tag{4-4}$$

in which f_c^* is the concrete strength under a biaxial or triaxial stress state caused by confinement due to local compression. Regarding the coefficient K, Randl (2013) reviewed in a recent work the dowel strength experimental data available in literature. He concluded that K = 1.5 agreed the results collected with a rather low scatter. According to *fib* Model Code

(*fib* 2013), K should be less than 1.6. It is important to note that the subscript $_d$ in the variable name V_{dR} does not mean "design value affected by partial safety factors". This subscript means "dowel". In this chapter, Equation (4-2) gives the predicted value for the real dowel strength.

Research studies devoted to modeling of dowel action nonlinear behavior are scarcer. Even though some empirical formulations have been proposed (Dulacska 1972, Millard and Johnson 1984, Vintzeleou and Tassios 1986, Walraven and Reinhardt 1981), modeling of the dowel force – slip (V_d – s) relation is generally based on the Beam resting on an Elastic Foundation (BEF) analogy (Friberg 1938, Guo et al. 1995), see Figure 4-1. In this context, Soroushian et al. (1987) performed tests to assess the elastic stiffness of the Winkler springs corresponding to concrete substrate under the steel bar. The results were the bases for the Dei Poli et al. (1992) nonlinear dowel action behavior proposal, which included a nonlinear coefficient ω multiplying the concrete substrate elastic stiffness in the BEF expressions. Later, Maekawa and Qureshi (1996) developed an analytical model for reinforcing bars under combined axial pullout and transverse displacement. The model includes the effects of bar plasticity and combined axial and shear loading through a damage build-up parameter *DI*.

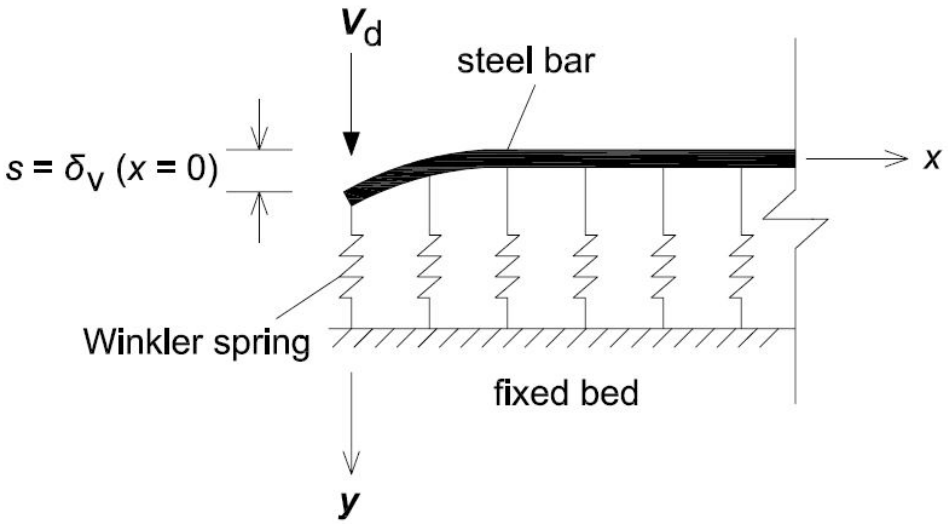

Figure 4-1 – Dowel action of a steel reinforcing bar modeled by the Beam resting on an Elastic Foundation analogy.

Finite element (FE) modeling of dowel action was implemented by Davids and Turkiyyah (1997) through a linear elastic 3D model composed of circular section steel beam elements and concrete regular solid brick embedment elements. Nodes corresponding to the contact area between the two materials had identical displacements. The authors described their approach as an embedded and discrete FE representation of the dowel mechanism. An improved proposal, with plasticity added through a perfect plastic branch in dowel behavior, was published by He and Kwan (2001). In this model, a smeared representation of dowel action is used, in which the effect of reinforcement is spread over the continuum concrete elements. The procedure consists on the direct assemblage of reinforcement dowel stiffness matrix into the stiffness matrices of adjoining concrete elements.

Later, more complex and realistic dowel action modeling was established by Kwan and Ng (2013). To estimate the behavior of a reinforcing bar subjected to both axial and transverse forces, the authors modeled the steel bar as a beam attached to the concrete substrate through interface elements simulating both dowel and bond-slip mechanisms. However, dowel action is considered in the same way as in a smeared representation. Therefore, steel bar elements have no flexural stiffness and no rotational degrees of freedom.

Recently, FE approaches (Magliulo et al. 2014; Zoubek et al. 2014) comprising an embedded and discrete representation of dowel action, similar to the Davids and Turkiyyah (1997) model, have been carried out. The main upgrade of these new approaches relies on the fact that material plasticity is included in the bar and the elements simulating the concrete embedment. Bond slip is accounted for in the tangential direction of the reinforcing bar through interface elements. In the normal direction, a perfect steel/concrete adhesion is assumed. In this context, a recent improvement was implemented by Mackiewicz (2015), in which the interaction between the steel bar and the concrete substrate is modeled through interface gap elements.

Lately, the state-of-art of dowel action modeling for FE analysis is developing at a faster pace comparing to the previous years. This evolution path can be explained by a few factors. In experimental testing, it is difficult to design a setup that can isolate dowel mechanism so it can be the only shear transfer component (Moradi et al. 2012). Additionally, in terms of numerical modeling, a realistic analysis of dowel action implies a discrete representation with

material plasticity included. This type of analysis is complex and time-consuming. Nevertheless, discrete modeling of dowel action is essential to investigate, for example:

- the reinforcement stresses, displacements and curvatures throughout the length of the bar;
- the dowel force for which a plastic hinge is formed in the steel bar, and the position of the hinge relative to the crack section;
- the amount of shear force transferred through kinking of the dowel reinforcement;
- the relative contribution of dowel action and aggregate interlock as a function of crack opening and sliding values.

The objective of this Chapter 4 is to develop a modeling approach that can be a discrete representation of a reinforcing bar dowel action, to be used in those types of applications and analyses. Comparing with other works available in literature, the main achievement of this approach is the inclusion of nonlinear interface Winkler spring FEs simulating the local compression and the confinement conditions of the concrete substrate right under the steel bar. To that end, the chapter presents an exhaustive literature review on experimental data which can be used for model calibration. New experimental test results are also shown. Then, an empirical model to describe the $V_d - s$ relationship is proposed. This model is a modified version of the one originally developed by Dei Poli et al. (1992). After that, the constitutive model for the nonlinear Winkler springs is presented and calibrated. That constitutive model can be directly used in the FE analysis of an isolated steel bar dowel, this being the so called 2D Fixed Bed approach. Finally, a different analysis approach is presented, in which the dowel bar is embedded in a continuum of linear elastic, solid or plane, FEs. This is the designated 3D Embedded Dowel approach.

4.2 REVIEW AND SELECTION OF EXPERIMENTAL DATA

In this Section 4.2, a literature review is carried out in order to collect the available experimental data concerning dowel strength assessment. Then, the data is scrutinized and interpreted, with the aim to arrive at conclusions that can sustain the choice of the tests

suitable to be used in the calibration of the FE analysis methodology introduced in this Chapter 4.

4.2.1 LITERATURE REVIEW ON DOWEL STRENGTH EXPERIMENTAL ASSESSMENT

An extensive literature review allowed to identify 9 publications (Bennett and Banerjee 1976, Dei Poli et al. 1992, Millard and Johnson 1984, Paulay et al. 1974, Randl 1997, Rasmussen 1963, Soroushian et al. 1986, Tanaka and Murakoshi 2011, Vintzeleou and Tassios 1987) with experimental tests aiming to assess the monotonic strength of a steel dowel embedded in concrete.

Three tests (DM1, DM2 and DM3) performed on the present work are also included. This new campaign represents an attempt to remove aggregate interlock and isolate the dowel mechanism of the specimens tested in Chapter 2. Therefore, the same geometry, reinforcement, test setup and loading are considered. The difference with respect to the Chapter 2 specimens (M1, M2 and M3) consists on the placement of 2 brass sheets, 0.3 mm thick, on the shear plane between the concretes of different age, in a similar procedure to Dulacska (1972) and Soroushian et al. (1986) works. Values for f_c measured in cylinder specimens (0.30 m high and 0.15 m diameter) were 87.4 MPa and 31.5 MPa for the concrete of the first and second casting stages of each specimen, respectively.

Table 4-1 presents the data collected. In this context, some notes are relevant:

- All tests considered were performed in reinforcing bars acting against concrete core and not against concrete cover.
- The value of f_c corresponds by default to the concrete compressive strength measured in cylinder specimens. For the publications where only cube specimens were tested, it is adopted $f_c = 0.85 \times f_{cc}$, where f_{cc} is the concrete compressive strength measured in cube specimens. In tests on specimens with two concretes cast at different times, the average compressive strength was considered.
- Dowel behavior depends on the angle between reinforcement axis and the shear plane, particularly due to different confinement conditions in the concrete substrate. In specimens with reinforcement axis not perpendicular to the shear plane, the dowel

strength calculation should follow recommendations presented on Dulacska (1972), and Equation (4-2) is not applicable to predict the strength of such specimens. For that reason, specimens with reinforcement axis not perpendicular to the shear plane were not accounted.

- In cases where the reinforcement yield stress was not measured, f_y is taken as the specified characteristic yield stress value.

- s_1 is the dowel displacement, at the reinforcement section where load is applied (δ_v (x = 0) of Figure 4-1), when maximum force V_R is reached. In turn, s_{max} is the maximum dowel displacement measured in the test. In some published results, s values are not shown.

- c is the lateral cover length (measured in the direction perpendicular to the line of action of the applied load V_d) and ϕ is the bar diameter.

- Single sided dowels correspond to specimens in which the reinforcing bar is embedded on a single concrete block. In double sided dowels, the reinforcing bar is embedded on two concrete blocks and dowel action is mobilized with the relative slipping between the blocks.

Table 4-1 – Dowel strength experimental data collected from literature review.

test	ϕ (mm)	f_c (MPa)	f_y (MPa)	V_{dR} (kN)	K	s_1 (mm)	s_{max} (mm)	c / ϕ	dowel sides
Bennett and Banerjee 1976									
2-6-1	6.4	44.0	410	6.88	1.59	-	-	stirrups	2
2-6-2	6.4	44.0	410	8.33	1.93	-	-	stirrups	2
2-6-3	6.4	44.0	410	10.60	2.45	-	-	stirrups	2
4-6	6.4	44.0	410	6.84	1.58	-	-	stirrups	2
2-13-1	12.7	44.0	410	22.55	1.33	-	-	stirrups	2
2-13-2	12.7	44.0	410	23.73	1.39	-	-	stirrups	2
2-13-3	12.7	44.0	410	27.26	1.60	-	-	stirrups	2
2-16	15.9	44.0	410	39.76	1.49	-	-	stirrups	2
2-19	19	44.0	410	43.75	1.15	-	-	stirrups	2
Dei Poli et al. 1992									
A1	24	29.5	500	76.19	1.39	2.155	3.000	4.5	1
A2	24	29.5	500	80.00	1.46	2.990	2.990	4.5	1

Table 4-1 (continued) – Dowel strength experimental data collected from literature review.

test	ϕ (mm)	f_c (MPa)	f_y (MPa)	V_{dR} (kN)	K	s_1 (mm)	s_{max} (mm)	c / ϕ	dowel sides
A4	18	29.5	500	46.39	1.50	1.131	2.495	6.2	1
A6	18	29.5	500	49.42	1.60	2.120	2.373	6.2	1
A12	18	29.5	500	36.38	1.18	2.080	2.505	6.2	1
A13	18	29.5	500	45.09	1.46	2.046	2.540	6.2	1
A8	14	29.5	500	31.11	1.66	1.088	1.738	8.1	1
A9	14	29.5	500	27.24	1.46	1.429	1.995	8.1	1
A3	24	32.3	500	80.33	1.40	4.213	4.678	4.5	1
B1	24	32.3	500	84.08	1.46	4.951	5.188	4.5	1
B4	24	32.3	500	79.68	1.39	4.164	4.648	4.5	1
A10	18	32.3	500	46.25	1.43	3.441	3.622	6.2	1
B2	18	32.3	500	46.57	1.44	4.491	4.491	6.2	1
B5	18	32.3	500	43.46	1.34	4.092	4.509	6.2	1
B3	14	32.3	500	27.35	1.40	1.414	4.106	8.1	1
B6	14	32.3	500	27.02	1.38	2.728	4.261	8.1	1
E1	24	72.0	500	119.14	1.39	1.052	5.009	4.5	1
E2	18	72.0	500	75.96	1.57	0.829	4.859	6.2	1
E3	14	72.0	500	50.43	1.73	1.041	5.008	8.1	1
Figueira et al.									
DM1	8	59.5	605	19.57	2.05	5.007	5.007	3.6	2
DM2	8	59.5	605	17.82	1.87	1.054	4.993	3.6	2
DM3	8	59.5	605	15.82	1.66	1.315	4.986	3.6	2
Millard and Johnson 1984									
21L	12	32.0	435	22.65	1.70	1.448	1.761	-	2
22L	12	32.7	435	20.55	1.52	1.551	1.752	-	2
23L	12	45.9	435	23.85	1.49	1.254	1.583	-	2
24L	16	23.5	435	32.4	1.60	1.716	1.764	-	2
Paulay et al. 1974									
TA	6.35	24.95	317	6.00	2.13	2.211	2.411	stirrups	2
TB	9.53	24.95	317	11.70	1.85	2.496	2.496	stirrups	2
TC	12.7	24.95	317	19.20	1.70	2.500	2.500	stirrups	2
Randl 1997									
55	6	41.7	653	7.70	1.65	1.090	19.00	stirrups	2
56	12	41.7	600	28.70	1.60	1.860	19.00	stirrups	2
57	12	41.7	600	34.30	1.92	2.330	19.00	stirrups	2
58	20	41.7	524	82.90	1.79	3.020	19.00	stirrups	2
59	12	41.7	600	39.85	2.23	2.380	19.00	stirrups	2
60	12	41.7	600	36.20	2.02	2.000	19.00	stirrups	2

Table 4-1 (continued) – Dowel strength experimental data collected from literature review.

test	ϕ (mm)	f_c (MPa)	f_y (MPa)	V_{dR} (kN)	K	s_1 (mm)	s_{max} (mm)	c / ϕ	dowel sides
61	12	41.7	600	40.33	2.25	2.100	19.00	stirrups	2
62	6	41.7	653	8.10	1.74	1.100	19.00	stirrups	2
63	12	41.7	600	34.60	1.93	2.260	19.00	stirrups	2
64	20	41.7	524	79.90	1.72	3.090	19.00	stirrups	2
81	6	18.3	653	6.00	1.94	1.610	19.00	stirrups	2
82	12	18.3	600	22.40	1.89	2.640	19.00	stirrups	2
83	20	18.3	524	58.10	1.89	3.230	19.00	stirrups	2
Rasmussen 1963									
D1	15.8	11.0	242	16.48	1.63	-	-	stirrups	1
D2	15.8	20.1	242	23.54	1.72	-	-	stirrups	1
D3	15.8	30.5	242	28.94	1.72	-	-	stirrups	1
D4	15.8	43.4	242	31.20	1.55	-	-	stirrups	1
D5	25.1	10.7	221	37.77	1.57	-	-	stirrups	1
D6	25.1	26.6	221	61.31	1.62	-	-	stirrups	1
D7	25.1	28.7	221	68.18	1.73	-	-	stirrups	1
D8	25.1	43.0	221	77.70	1.61	-	-	stirrups	1
D9	16	16.9	431	34.83	2.03	-	-	stirrups	1
D10	25.9	18.4	400	69.16	1.53	-	-	stirrups	1
Soroushian et al. 1988									
T4	12.7	42.8	414	41.99	2.49	5.156	10.08	5.4	2
T6	19.05	42.8	414	59.95	1.58	1.549	8.585	3.4	2
T8	25.4	42.8	414	71.17	1.06	1.981	10.16	2.5	2
Tanaka and Murakoshi 2011									
N2419	19.1	24.5	342	33.30	1.27	-	-	6.0	1
N3010	9.53	33.8	355	9.05	1.16	-	-	12.6	1
N3013	12.7	31.2	338	16.10	1.24	-	-	9.3	1
N3016	15.9	32.8	345	29.05	1.38	-	-	7.4	1
N3019	19.1	33.3	342	40.80	1.33	-	-	6.0	1
N30-345	19.1	33.3	374	39.35	1.23	-	-	6.0	1
N30-390	19.1	33.3	445	41.90	1.20	-	-	6.0	1
N4019	19.1	45.8	342	46.45	1.30	-	-	6.0	1
N5010	9.53	59.2	355	12.00	1.16	-	-	12.6	1
N5013	12.7	59.2	338	20.95	1.17	-	-	9.3	1
N5016	15.9	59.2	345	33.85	1.19	-	-	7.4	1
N5019	19.1	59.1	342	49.00	1.20	-	-	6.0	1
N50-345	19.1	59.1	374	52.85	1.24	-	-	6.0	1
N50-390	19.1	59.1	445	59.20	1.27	-	-	6.0	1
Vintzeleou and Tassios 1987									
150,14-1	14	32	420	30.43	1.71	4.000	4.000	2.9	2

Table 4-1 (continued) – Dowel strength experimental data collected from literature review.

test	ϕ (mm)	f_c (MPa)	f_y (MPa)	V_{dR} (kN)	K	s_1 (mm)	s_{max} (mm)	c / ϕ	dowel sides
150,14-2	14	32	420	31.22	1.75	4.000	4.000	2.9	2
150,14-1	14	45	420	35.70	1.69	4.000	4.000	2.9	2
150,14-2	14	45	420	36.66	1.73	4.000	4.000	2.9	2

4.2.2 SELECTION OF EXPERIMENTAL DATA FOR MODEL CALIBRATION

By comparing values calculated for coefficient K, based on the data provided by the different publications (see Table 4-2, where μ is the average value and σ the standard deviation), a significant scatter can be observed. For a better understanding of the reasons behind the scatter, some aspects concerning the tests performed should be analyzed and compared, such as: specimen geometry, its reinforcement and the test setup. These features and parameters can give information about the presence of other phenomena besides dowel action, like concrete splitting and the aggregate interlock mechanism, which affect the force V_R measured in the test. Moreover, the influence on dowel behavior of the reinforcement kinking effect and the confinement imposed by stirrups can also be deciphered.

Table 4-2 – Average values and standard deviation of the coefficient K obtained from the experimental data.

tests	n	K		concrete splitting	aggregate interlock	kinking effect	confined by stirrups
		μ	σ				
Bennett and Banerjee 1976	9	1.61	0.38	no	unknown	yes	yes
Dei Poli et al. 1992	19	1.45	0.12	no	no	no	no
Figueira et al.	3	1.86	0.20	yes	yes	yes	no
Millard and Johnson 1984	4	1.58	0.09	unknown	unknown	yes	unknown
Paulay et al. 1974	3	1.89	0.22	no	yes	yes	yes
Randl 1997	13	1.89	0.20	no	yes	yes	yes
Rasmussen 1963	10	1.67	0.15	no	no	no	yes
Soroushian et al. 1988	3	1.71	0.73	yes	unknown	yes	no
Tanaka and Murakoshi 2011	14	1.24	0.07	no	no	no	no
Vintzeleou and Tassios 1987	4	1.72	0.03	yes	unknown	yes	no

Concrete splitting cracks were identified by Vintzeleou and Tassios (1987) in the 4 specimens with concrete cover of 40 mm. Moreover, specimen A1 of the Dei Poli et al. (1992) program, and tests T6 and T8 of Soroushian et al. (1986), revealed a sudden decrease in strength, which suggests that splitting failure occurred. Concrete strength and cover length are the main factors affecting splitting.

This phenomenon was also noticed in 2 of the tests (DM2 and DM3) performed on the present work. The test results for the imposed dowel displacement s are shown in Figure 4-2 and Figure 4-3, as a function of dowel force V_d and crack opening w, respectively. In these figures, s is the sum of the slip in the two sides of the dowel. The outlook of specimen DM3 after testing showed wide spread cover detachment of the concrete surrounding reinforcement. Specimen DM2 revealed a similar outlook comparing to DM3, also with clear cover detachment. On the other hand, the outlook of specimen DM1 did not disclose any significant superficial cracking, and consequently higher shear strength was achieved.

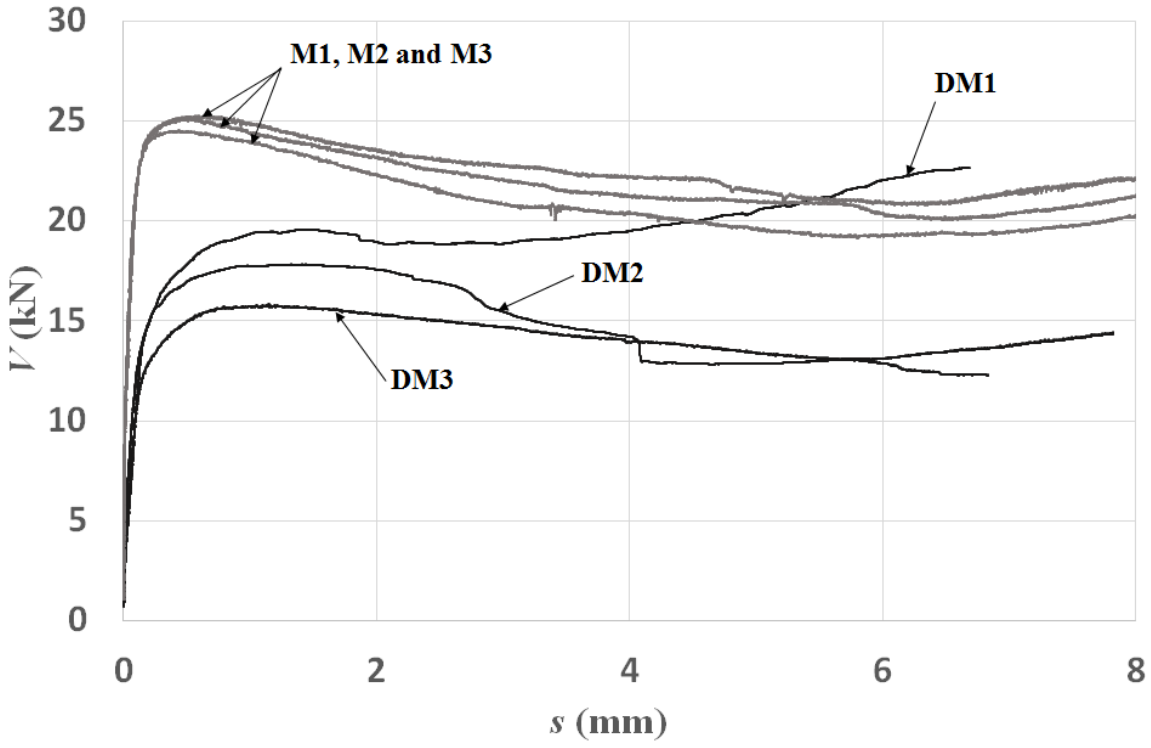

Figure 4-2 – Force – displacement response obtained for the tested dowel specimens.

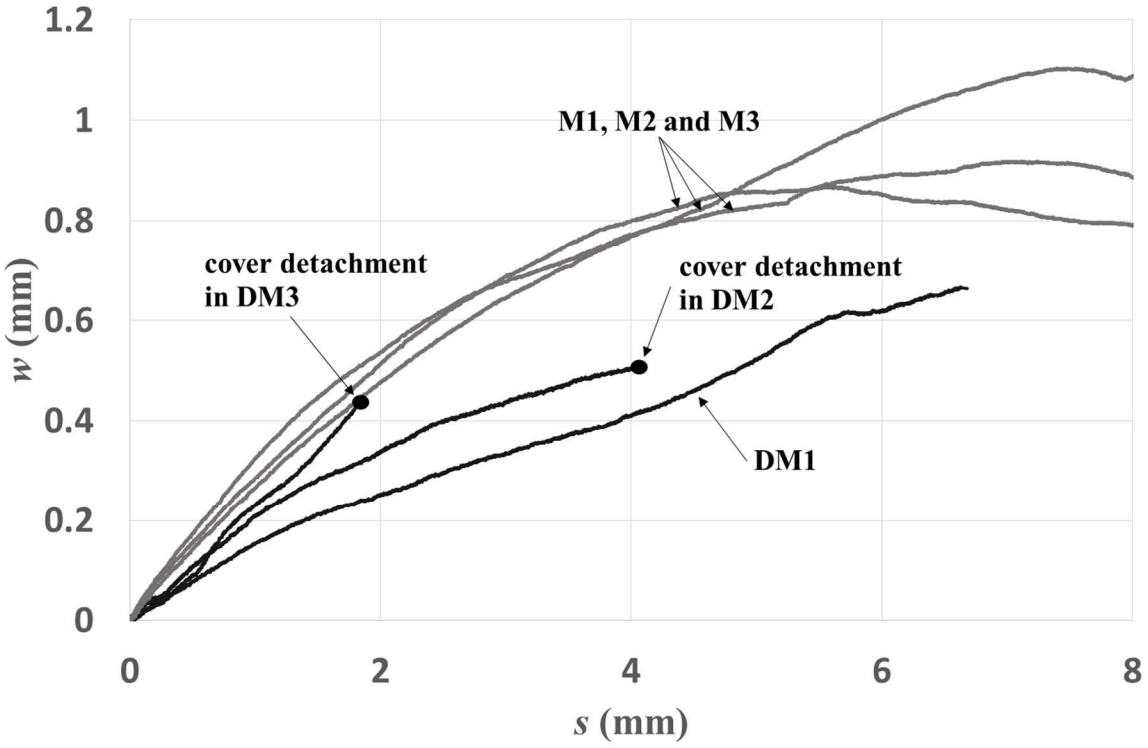

Figure 4-3 – Crack opening – displacement response obtained for the tested dowel specimens.

In Figure 4-3, it can be seen that the crack opening behavior was not the expected for a test without friction at the interface between different concretes. Ideally, in a dowel test with very low friction, crack opening should be minimal. However, the values achieved were significant and not far from the ones relating to tests with interface friction (M1, M2 and M3). This behavior indicates that the execution procedure implemented in the dowel specimens was not totally effective to eliminate roughness in the interface between concretes. Therefore, besides reinforcement dowel action, friction was also present, increasing shear strength.

Another phenomenon influencing dowel behavior can be plainly identified in specimen DM1 for large displacement values, in this case continuously amplifying shear strength. In double sided dowels, in which the reinforcing bar connects two concrete blocks, both slip and crack opening induce axial stress in the bar. With slip developing, the reinforcement axis exhibits an important rotation, in the position where the reinforcement intersects the interface. As a consequence of this rotation, the reinforcement axial force grows the contribution to shear strength, a mechanism typically denoted as kinking or geometric effect of the dowel.

This effect can also be found in specimens M1, M2 and M3. In tests with concrete splitting, DM2 and DM3, the strength increase caused by kinking is not so clear.

Even though the tests DM1 to DM3 were not well succeeded in terms of elimination of aggregate interlock effect, their results were shown here to demonstrate that other test results shown in the bibliography (using similar test procedures, with similar results) are also affected by interlock effects. Concrete splitting and reinforcement kinking can also be present in some of those works. For these reasons, certain criteria should be established in order to select experimental data that can be used in the calibration of a FE model for the dowel mechanism.

Aggregate interlock between concretes does not exist and the kinking effect is greatly minimized in tests performed on single sided dowels. Tests having these characteristics are the ones of Dei Poli et al. (1992), Rasmussen (1963) and Tanaka and Murakoshi (2011). These three experimental campaigns have a significant number of specimens and no signs of concrete splitting, with the exception of Dei Poli et al. (1992) A1 test. However, even for this specimen, 1 out of 19, the value obtained for coefficient K was 1.39, therefore within the standard deviation of the sample.

Differences in dowel strength values between these three campaigns can be explained by a few factors. In Rasmussen (1963) campaign, concrete substrate is more confined since all specimens were reinforced with stirrups. And it is expected that a different amount of stirrups could lead to a variation in dowel strength. Dei Poli et al. (1992) specimens do not have stirrups and are made with a notch, so that the applied dowel force is aligned with the concrete blocks limit, without eccentricity. A notch was not inserted in Tanaka and Murakoshi (2011) specimens and that fact can justify the lower dowel strength values achieved. Moreover, the $V_d - s$ relations for the Rasmussen (1963) and Tanaka and Murakoshi (2011) tests are not available. Force and displacement measurements are very important when the experimental calibration of a dowel action nonlinear FE model is intended.

For the reasons mentioned, and summarized in Table 4-2, Dei Poli et al. (1992) experimental program will be taken as a reference, in the following sections, for FE modeling of dowel action, considering a discrete representation. The test setup designed by Dei Poli et al. (1992) eliminated the main factors or mechanisms interfering with dowel behavior and

strength: concrete splitting, aggregate interlock interaction, kinking effect of reinforcement and confinement induced by stirrups.

4.3 DEFINITION OF AN EMPIRICAL MODEL

Since the aim of the present study is to develop a FE model that can be applied to a wide range of bar diameters and concrete strengths, it is necessary to have a way to predict dowel behavior for cases in which those parameters are different from the ones in the experimental tests considered. In order to interpolate that behavior for several bar diameters and concrete strengths, an empirical model with a very good correlation to the experimental data available must be defined.

Several authors have proposed empirical models resulting from an adjustment to the values measured in their tests, namely: Dei Poli et al. (1992), Dulacska (1972), Millard and Johnson (1984), Vintzeleou and Tassios (1986) and Walraven and Reinhardt (1981). In view of the fact that Dei Poli et al. (1992) campaign will be taken as a reference, its empirical model will also serve as an interpolation tool of dowel behavior. In this context, Dei Poli et al. (1992) compared their proposal with the ones of Vintzeleou and Tassios (1986) and Walraven and Reinhardt (1981), pointing some differences. The model uses the following expression for the $V_d - s$ relation that comes from the BEF analogy:

$$V_d = 2 \times \alpha^3 \times E_s \times I \times s \tag{4-5}$$

in which

$$\alpha = \sqrt[4]{\frac{k_c \times \phi}{4 \times E_s \times I}} \tag{4-6}$$

and where E_s is the steel Young modulus and I the reinforcement moment of inertia. In turn, stiffness k_c of the concrete substrate is the product of a nonlinearity coefficient ω with elastic stiffness k_0:

$$k_c = \omega \times k_0 \tag{4-7}$$

with ω and k_0 given by

$$\omega(s,\phi,f_c)=\left[1.5\times\left(a+\sqrt{d^2\times\left(\frac{40\times s}{\phi}-b\right)^2+c^2}\right)\right]^{-\frac{4}{3}} \tag{4-8}$$

$$k_0=\frac{600\times f_c^{0.7}}{\phi} \tag{4-9}$$

In Equations (4-7) to (4-9), f_c is in MPa, k_0 in MPa/mm and ϕ in mm. The four coefficients a, b, c and d are linear functions of the concrete strength. Nevertheless, the comparison between this empirical model and the Dei Poli et al. (1992) test data allowed to notice that an improvement could be made on stiffness k_0 seeking a better fitting in terms of dowel behavior. Table 4-3 shows values obtained for Equation (4-2) coefficient K considering the experimental results, the empirical model with stiffness k_0 and the empirical model with a slightly changed stiffness k_{0*}:

$$k_{0*}=\frac{700\times f_c^{0.7}}{\phi} \tag{4-10}$$

Table 4-3 – Comparison between Dei Poli et al. (1992) experimental results and its empirical model (with substrate stiffness given by k_0 and k_{0*}) in terms of dowel resistance V_{dR}.

experimental					empirical model - k_0		empirical model - k_{0*}	
test	ϕ (mm)	f_c (MPa)	V_{dR} (kN)	K	V_{dR} (kN)	K	V_{dR} (kN)	K
A1	24	29.5	76.19	1.387	67.51	1.229	75.78	1.379
A2	24	29.5	80.00	1.456	67.51	1.229	75.78	1.379
A4	18	29.5	46.39	1.501	38.36	1.241	43.06	1.393
A6	18	29.5	49.42	1.599	38.36	1.241	43.06	1.393
A12	18	29.5	36.38	1.177	38.36	1.241	43.06	1.393
A13	18	29.5	45.09	1.459	38.36	1.241	43.06	1.393
A8	14	29.5	31.11	1.664	23.26	1.244	26.11	1.397
A9	14	29.5	27.24	1.457	23.26	1.244	26.11	1.397
A3	24	32.3	80.33	1.397	73.45	1.278	82.45	1.434
B1	24	32.3	84.08	1.462	73.45	1.278	82.45	1.434
B4	24	32.3	79.68	1.386	73.45	1.278	82.45	1.434
A10	18	32.3	46.25	1.430	41.65	1.288	46.76	1.446
B2	18	32.3	46.57	1.440	41.65	1.288	46.76	1.446
B5	18	32.3	43.46	1.344	41.65	1.288	46.76	1.446
B3	14	32.3	27.35	1.398	25.37	1.297	28.48	1.456
B6	14	32.3	27.02	1.381	25.37	1.297	28.48	1.456
E1	24	72.0	119.14	1.388	122.56	1.428	137.58	1.603
E2	18	72.0	75.96	1.573	68.94	1.428	77.39	1.603
E3	14	72.0	50.43	1.727	41.71	1.428	46.82	1.603
			μ	1.454		1.289		1.447
			σ	0.123		0.066		0.074

It can be seen that a very good fit is achieved when k_{0*} is considered instead of k_0. The better fitting provided by k_{0*} was not only observed for dowel strength values, V_{dR}, of Table 4-3, but also for the nonlinear $V_d - s$ response (see Figure 4-4 for f_c = 32.3 MPa). The V_{dR} value of the empirical model was calculated as the maximum dowel force predicted by Equation (4-5) until $s = s_{max}$.

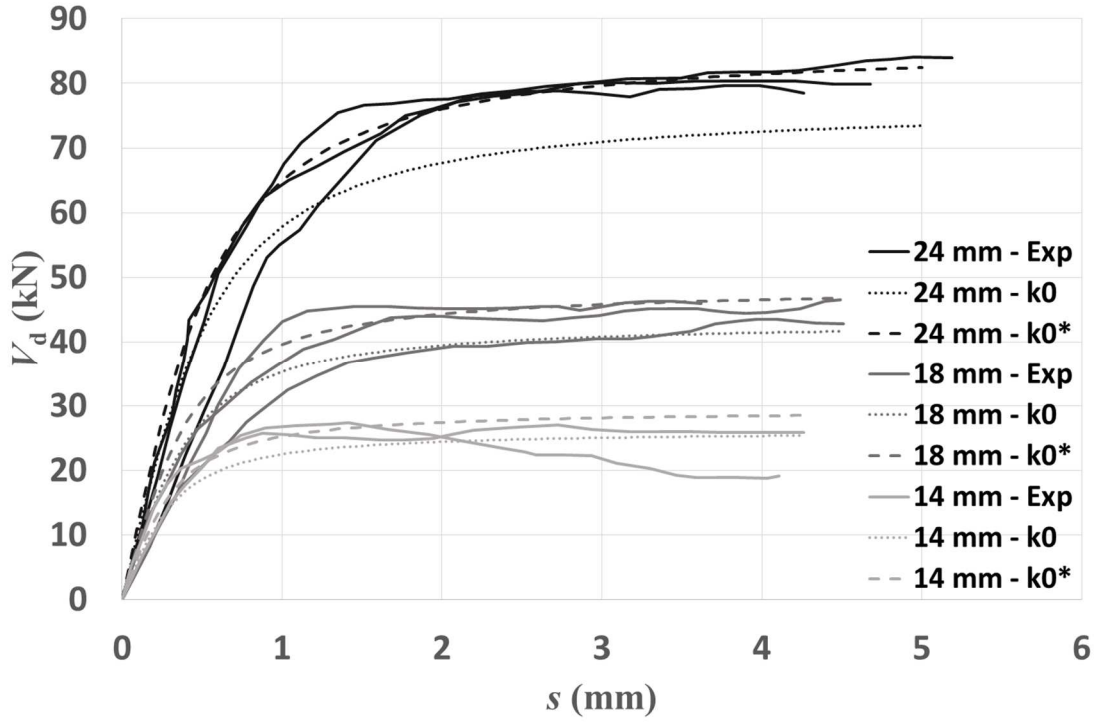

Figure 4-4 – Comparison of empirical model results (having concrete substrate stiffness given by k_0 and k_{0*}) with experimental values obtained by Dei Poli et al. (1992) (f_c = 32.3 MPa).

4.4 2D FIXED BED MODELING APPROACH

Different approaches to model dowel action are possible depending on the purpose of the analysis. If the purpose is the assessment of an isolated dowel, then a simpler approach is sufficient. This one is, in the present work, denoted by 2D Fixed Bed (FB) approach. In this case, the concrete deformation is lumped in several interface spring elements which connect the steel bar to a fixed bed. These springs are designated in this chapter by nonlinear Winkler springs.

4.4.1 FINITE ELEMENT MODEL DESCRIPTION

The implemented 2D FB modeling approach intends to characterize the dowel action mechanism of Figure 4-1. The deformability of the concrete substrate under the reinforcing

bar is modeled through a set of one-node translation nonlinear Winkler springs supported on a fixed bed. Every bar node is connected to one spring.

This 2D FB model is a discrete representation of the dowel mechanism, composed by a single circular steel bar divided into 50 fully numerically integrated Mindlin beam (class-III) (DIANA 2014) FEs with shear deformation contemplated. Each element has a length of 8 mm, 3 nodes, 2 Gauss integration points along its axis and 24 over its cross-section. The cross-section is integrated with a 6-point Trapezium rule in the tangential direction and a 4-point Gauss scheme in the radial direction. The total length of the steel bar is 400 mm in order to match Dei Poli et al. (1992) specimen dimensions.

Five different bar diameters were considered (8, 12, 16, 20 and 25 mm), as well as 3 concrete strengths (29.5, 48.1 and 67.8 MPa), intending to cover a wide and recurrent range for these parameters. The first concrete strength value corresponds to the weaker concrete tested in Dei Poli et al. (1992) campaign, and the last two refer to old and new concretes of Chapter 2 specimens M1, M2 and M3.

Steel reinforcement material properties are the following: Young's modulus E_s = 200 GPa, Poisson's ratio ν = 0.3, yield stress f_y = 605.4 MPa and tensile strength f_t = 631.8 MPa. These strength values were determined in axial tests performed on reinforcing bar specimens, with specified characteristic yield stress of 500 MPa, made with the same steel that was used in specimens DM1, DM2 and DM3. To simulate steel yielding in the FE analyses, a Tresca maximum shear stress condition is adopted (Owen and Hinton 1980). Figure 4-5 shows steel stress-strain ($\sigma_s - \varepsilon_s$) relation assumed in the model, with initial linear-elastic behavior and post-yielding strain-hardening.

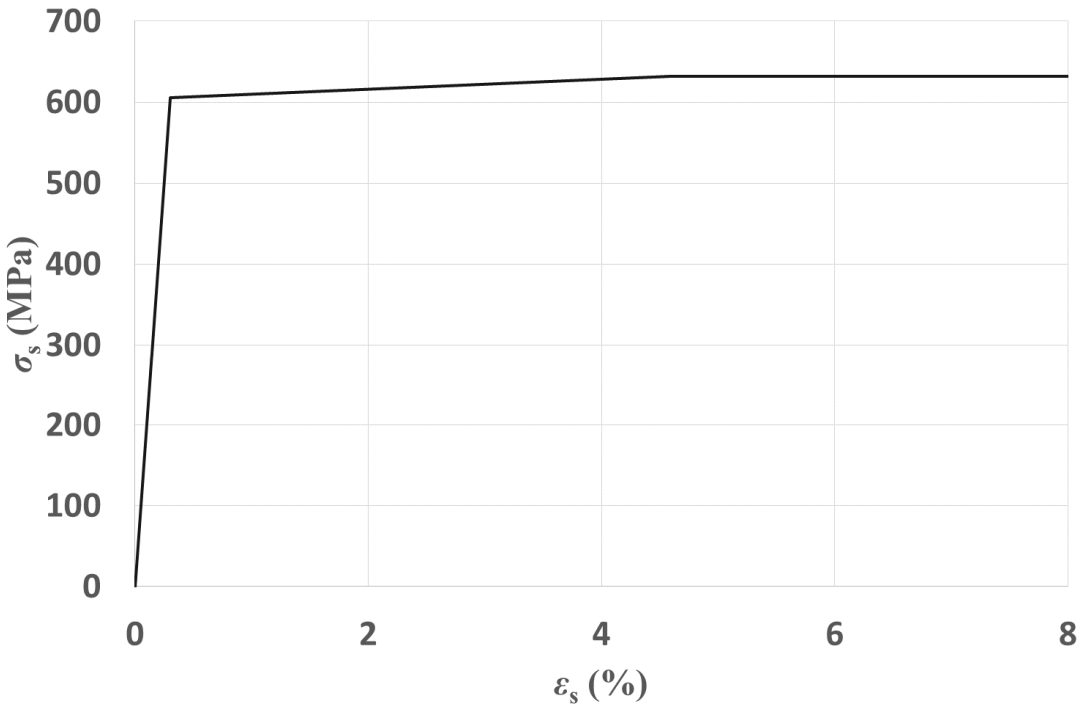

Figure 4-5 – Stress-strain rebar diagram considered in FE analyses.

Since material plasticity is taken into account, the structural analysis involves the solution of a nonlinear analytical problem. Therefore, an iterative procedure is needed. In this work, the BFGS Quasi-Newton (Secant) method is used, with a Line Search algorithm to enhance the robustness of the iteration method (DIANA 2014). When the specified convergence criterion is satisfied, the calculation stops. In this context, an energy norm ratio is used for convergence criteria.

4.4.2 CONSTITUTIVE MODEL FOR THE NONLINEAR WINKLER SPRINGS

4.4.2.1 PROCEDURE FOR CALIBRATION OF THE CONSTITUTIVE MODEL

A procedure is adopted in the present study to set, or adjust, analytical expressions to describe the non-linear behavior of Winkler springs. In the 2D FB modeling approach, all the Winkler springs along the bar length follow the same constitutive behavior. Experimental data from Dei Poli et al. (1992) and its empirical model with elastic stiffness k_{0*} are used to calibrate the adjustment. Since direct determination of those expressions is not possible, an iterative trial-error method was carried out. A mathematical formulation of the spring

response is firstly conceived, and then the approximation between the FE results and the results provided by the empirical model is checked. This procedure aims to reach a balance between the ideal fit to the empirical model and a simple analytical representation of spring force – displacement relation. This procedure can be seen as a retro-analysis methodology.

In the procedure, the dowel force V_d is calculated as the sum of all spring vertical forces F_v in the model:

$$V_d = \sum_{i=1}^{n} F_{v,i} \tag{4-11}$$

with

$$dF_v = k_{sp} \times d\delta_v \tag{4-12}$$

In turn, the spring stiffness k_{sp} is given by:

$$k_{sp} = \psi(\delta_v, \phi, f_c) \times k_{0*} \tag{4-13}$$

where ψ is a nonlinearity coefficient and the elastic stiffness k_{0*} is given in Equation (4-10).

Therefore, the analytical representation of spring behavior will provide the mathematical expressions for the coefficient ψ, depending on the diameter of the steel bar and on the material properties of concrete.

In the following subsection the analytical formulation adopted for the spring constitutive model is explained. Then, the derivation of the values of the various model parameters is presented.

4.4.2.2 ANALYTICAL REPRESENTATION OF SPRING BEHAVIOR

Different possibilities for the nonlinear Winkler spring response were tested. It was concluded that the incremental force – displacement relation of Equation (4-12) can be expressed through five different stages (see Figure 4-6): I – initial linear elastic branch; II – nonlinear branch with increasing force; III – nonlinear branch with decreasing force; IV –

smooth linear branch; V – constant residual branch.

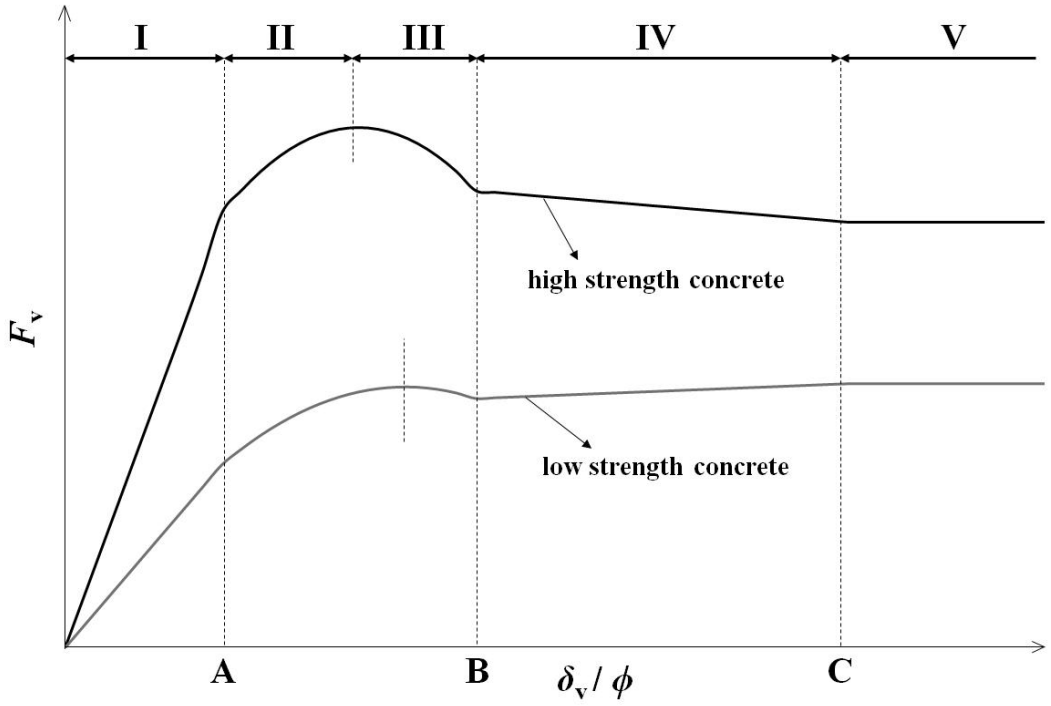

Figure 4-6 – Stages in the constitutive model for nonlinear Winkler springs.

Stages I to III resemble the typical stress – strain relation of concrete subjected to uniaxial compression, where the nonlinear response of stage II is caused by microcracking (Hsu et al. 1963), and the strength decrease of stage III by a vertical crack (Soroushian et al. 1987) appearing right below and along the reinforcing bar axis. The vertical crack seems to be much more pronounced in dowels embedded on high strength concrete, whose model results point to an abrupt decrease in spring force F_v.

Stage IV discloses an increment in spring stiffness k_{sp}, until a residual strength is reached in stage V. This type of behavior is due to the fact that the concrete under the steel bar is subjected to a concentrated load. Therefore, the lateral dilatancy of the locally compressed concrete is hindered by the surrounding mass of non-loaded concrete, which results in a biaxial or triaxial stress state (Mander et al. 1988). In models with the lowest concrete strength considered (f_c = 29.5 MPa), an increase in spring force during stage IV is also observed, showing that the propagation of the vertical crack below the reinforcing bar is more gradual in these cases.

The analyses revealed that a single quadratic function could be used to describe the $F_v - \delta_v$ relation in stages II and III (see Figure 4-6). Therefore, in these stages, the parameter ψ is a linear function of the string displacement δ_v. It was also concluded that a satisfying adjustment is reached if a linear branch is adopted for stage IV. These conclusions are resumed in the subsequent expressions for coefficient ψ:

$$\psi_I = a \Leftarrow \frac{\delta_v}{\phi} < A \tag{4-14}$$

$$\psi_{II,III} = b \times \left(\frac{\delta_v}{\phi} \right) + c \Leftarrow A \le \frac{\delta_v}{\phi} \le B \tag{4-15}$$

$$\psi_{IV} = d \Leftarrow B < \frac{\delta_v}{\phi} < C \tag{4-16}$$

$$\psi_V = 0 \Leftarrow \frac{\delta_v}{\phi} \ge C \tag{4-17}$$

in which *A*, *B* and *C* coefficients mark the transition between stages, as shown in Figure 4-6. Therefore, the values of δ_v at those instants depend on the reinforcing bar diameter. The influence of concrete strength is accounted for on coefficients *a*, *b*, *c* and *d*.

4.4.2.3 DETERMINATION OF THE SPRING MODEL COEFFICIENTS FOR THE 2D FB APPROACH

The constitutive model for nonlinear Winkler springs becomes completely defined once the coefficients *A*, *B* and *C* and also *a*, *b*, *c* and *d* are determined. In order to obtain these coefficients, the retro-analysis methodology explained in section 4.4.2.1 was performed for each different combination of bar diameter and concrete strength. Therefore, 15 retro-analyses were made (3 concretes times 5 diameters). It was concluded that fixed values could be adopted for the coefficients *A*, *B* and *C* of Equations (4-14) to (4-17):

$A = 0.0065$

$B = 0.022$

$C = 0.117$

These coefficient values are thus independent from the bar diameter and the concrete strength. On the other hand, the coefficients *a*, *b*, *c* and *d* to be used in the 2D FB modeling approach can be expressed by the following linear functions of the concrete strength:

$$a = 0.0116 \times f_c + 0.4261 \quad (4\text{-}18)$$

$$b = -1.068 \times f_c - 13 \quad (4\text{-}19)$$

$$c = 0.02275 \times f_c + 0.267 \quad (4\text{-}20)$$

$$d = -0.00184 \times f_c + 0.0825 \quad (4\text{-}21)$$

with f_c in MPa. These expressions are valid for any bar diameter and concrete strength within the upper and lower bounds considered in this work (indicated before): 29.5 MPa $\leq f_c \leq$ 67.8 MPa and 8 mm $\leq \phi \leq$ 25 mm. It should be noted that, in the empirical model proposed by Dei Poli et al. (1992), the parameters which characterize the dowel response (Equation (4-8)) are also linear functions of the concrete strength. Therefore, the shape of the previous Equations (4-18) to (4-21) is not surprising.

Figure 4-7 shows the comparison between the results provided by the empirical model and the outcome of FE analysis (according to the 2D FB approach), considering the constitutive model for the springs defined before (Equations (4-14) to (4-21)). A very good fit can be seen for the 3 concrete strengths and 5 bar diameters considered.

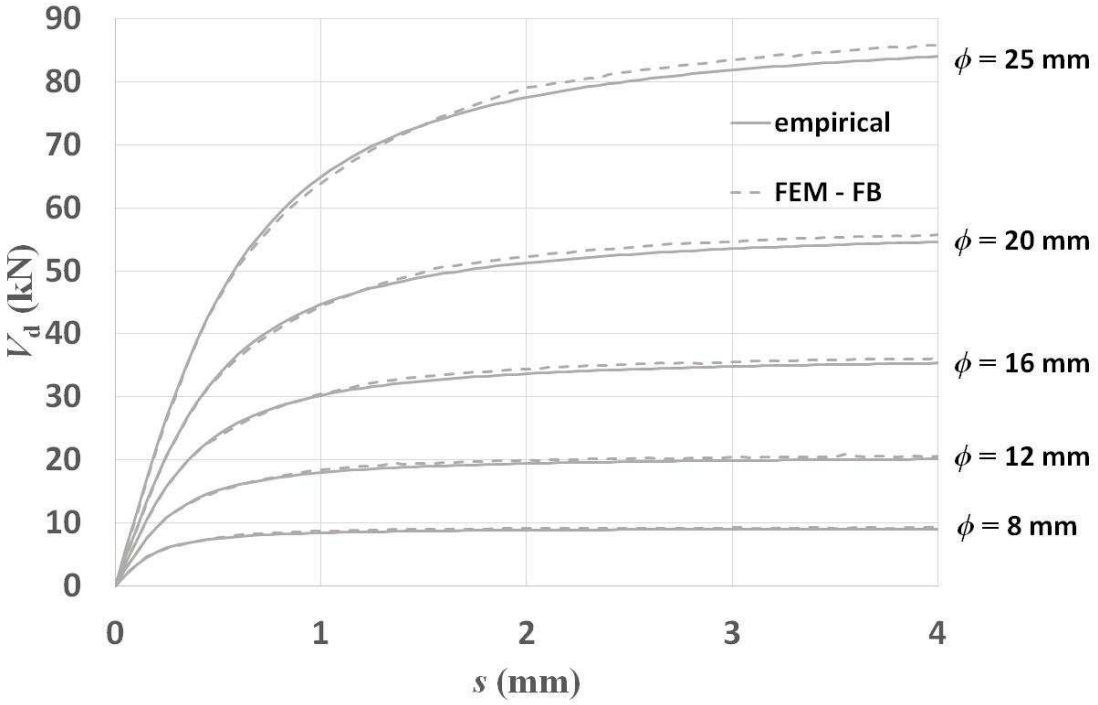
90
80
70
60
50
40
30
20
10
0
V_d (kN)
0
1
2
3
4
s (mm)
empirical
FEM - FB
ϕ = 25 mm
ϕ = 20 mm
ϕ = 16 mm
ϕ = 12 mm
ϕ = 8 mm

a)

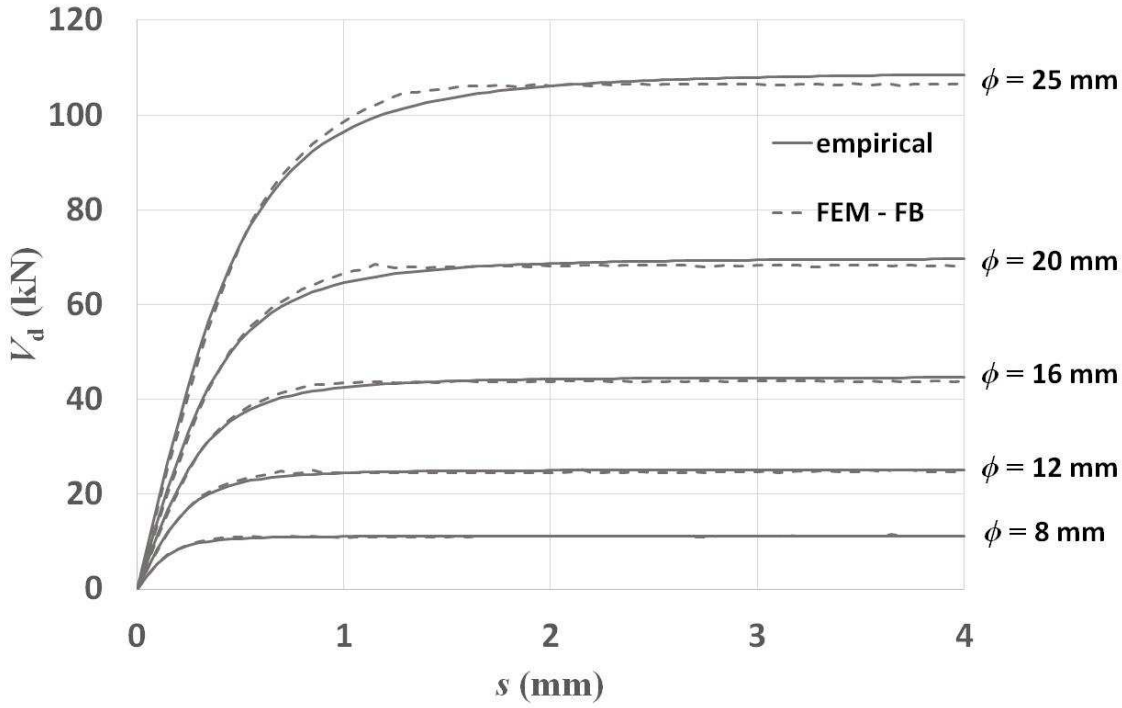
120
100
80
60
40
20
0
V_d (kN)
0
1
2
3
4
s (mm)
empirical
FEM - FB
ϕ = 25 mm
ϕ = 20 mm
ϕ = 16 mm
ϕ = 12 mm
ϕ = 8 mm

b)

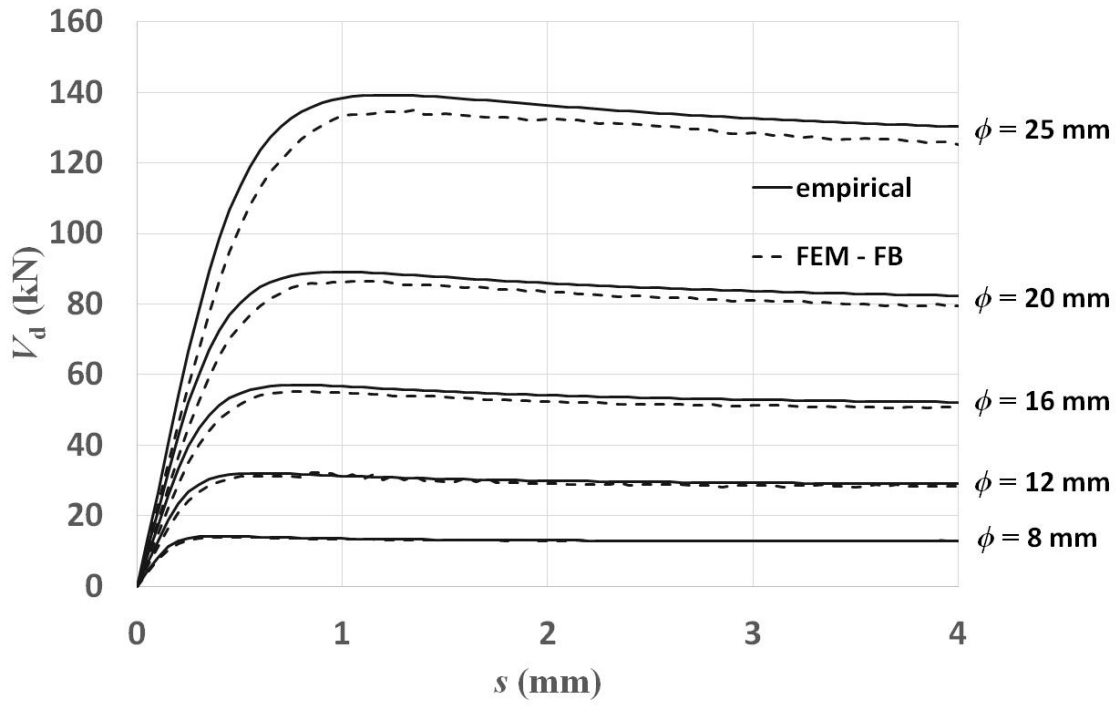

c)

Figure 4-7 – Dowel force values obtained through the empirical model and FE model for the 2D Fixed Bed (FB) approach: a) f_c = 29.5 MPa; b) f_c = 48.1 MPa; c) f_c = 67.8 MPa.

4.5 3D EMBEDDED DOWEL MODELING APPROACH

The 2D Fixed Bed modeling approach cannot be implemented in the analysis of a real structure discretized with solid brick FEs, or plane stress elements. In those cases, the nonlinear Winkler springs are not connected to a rigid element. Instead, they are connected to the deformable solid brick or plane stress FEs. Therefore, a so-called 3D Embedded Dowel (ED) approach is also envisaged in this work. In the example shown below, the concrete substrate is discretized through solid brick elements; however the analysis approach can be applied to structures in which the concrete medium is discretized with plane stress elements without loss of generality.

4.5.1 FINITE ELEMENT MODEL DESCRIPTION

The 3D ED model is illustrated in Figure 4-8. The concrete substrate block has linear elastic behavior. Nonlinearity is accounted for in reinforcement and springs only. In the 3D ED model, interface springs are two-node translation elements which link the steel bar to concrete in the vertical direction only (*y* direction in Figure 4-8). The connected bar and substrate nodes are coincident. In the schematic representation of Figure 4-8 they are not coincident just to make the drawing clear.

In the horizontal *x* direction, the bar and substrate nodes would have to be connected (though a horizontal nonlinear spring) if the bar was subjected to axial force. No axial force is applied to the bar in this example and, for that reason, steel and substrate nodes are not connected in the *x* direction, except in one bar node to avoid instability of the FE model.

The bar is not loaded in the horizontal *z* direction. Therefore, bar and substrate displacements are equal in the horizontal *z* direction.

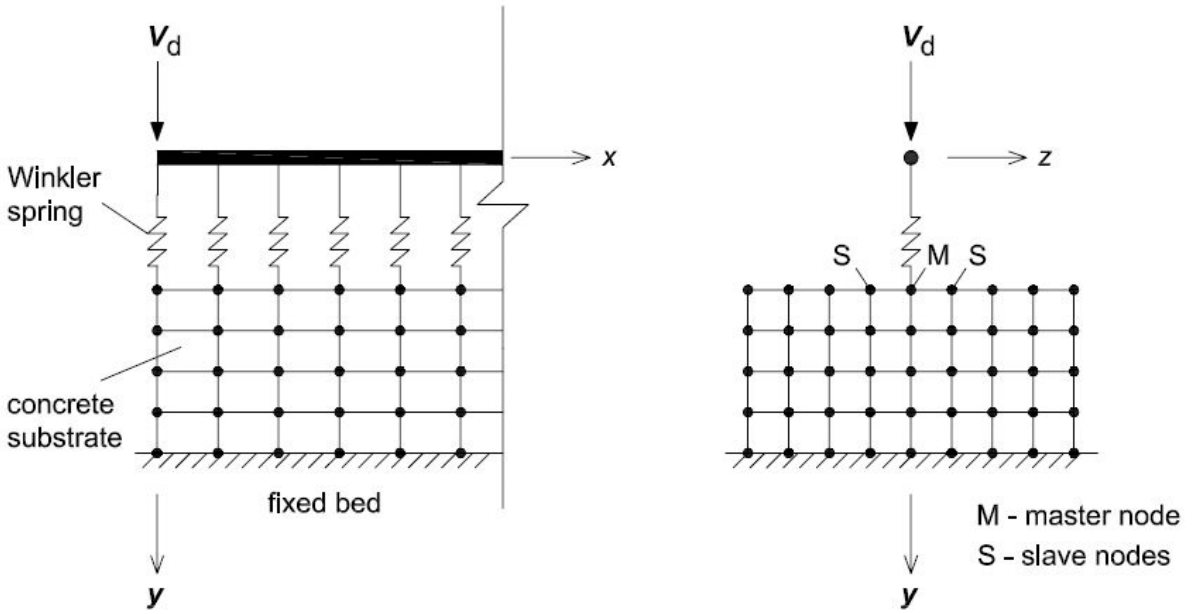

Figure 4-8 – 3D Embedded Dowel (ED) FE model for dowel action analyses.

In this 3D ED approach, each spring links one bar node to a single concrete substrate master node, which then connects to neighboring slave nodes in the transverse *z* direction, as

can be seen in Figure 4-8, through tying conditions included in the model. These tyings impose that the vertical displacement of slave nodes is equal to the displacement of their master node. In turn, the number of slave nodes in each transverse alignment depends on the bar diameter. That number is increased for larger bar diameters in order to get a more realistic load distribution under the reinforcing bar.

4.5.2 Derivation of the constitutive model for the nonlinear Winkler springs

In the 3D ED approach, the constitutive model for the nonlinear Winkler springs depends on the discretization and characteristics of the concrete substrate. In order to take account of this issue, a procedure is proposed in the following paragraphs, to determine the spring constitutive model for a 3D ED modeling approach.

The procedure is based on the fact that Equations (4-14) to (4-21) give the expressions for the approach with fixed bed (the so-called 2D FB approach), which can be taken as a reference for the definition of the constitutive model in the 3D ED approach. Then, it is important to note that, in the 3D ED approach, the reinforcing bar is supported by a system which can be seen as an association in series of a spring and the concrete substrate FEs. Therefore, the deformation of the spring with fixed bed, given by Equations (4-14) to (4-21), has to be equal to the deformation of this association in series. The relationship between the stiffness of a spring in the FB approach, $k_{sp,FB}$, and the corresponding sum of stiffnesses of all springs connecting to a certain bar node in the 3D ED approach, $k_{sp,ED}$, is given by Equation (4-22):

$$\frac{1}{k_{sp,FB}} = \frac{1}{k_{sp,ED}} + \frac{1}{k_{sub}} \tag{4-22}$$

As the constitutive relations for the springs are nonlinear, $k_{sp,FB}$ and $k_{sp,ED}$ are tangent stiffnesses. On the contrary, k_{sub} is the elastic stiffness of the concrete substrate and has a constant value. Thus, to determine in a simple way the values of $k_{sp,ED}$ through Equation (4-22), the constitutive model of the 2D FB approach springs is written as a multilinear function. Moreover, it is necessary to know the value of k_{sub} for the FE model conceived. For that purpose, the following steps should be taken:

1 – Determination of the displacements δ_v, throughout the length of the steel bar, for a certain slip (s) value in the 2D FB FE model.

2 – Imposition of the displacement profile determined in the previous step to the steel bar of the 3D ED FEM model. In this phase, the constitutive relations of the 2D FB approach are assigned to the springs of the 3D ED FE model. In order to impose displacements, vertical supports need to be added to the bar nodes, in the 3D ED FE model.

3 – Calculation of the reactions F_v in the 3D ED model and the corresponding stiffness $k_{sub} = F_v / \delta_{v,sub}$, in which $\delta_{v,sub}$ is the vertical (y direction in Figure 4-8) displacement of the concrete substrate.

4.5.3 EXAMPLE

In this section, an example of dowel behavior assessment through the 3D ED modeling approach is described. A model similar to the one presented in Figure 4-8 is assumed, with concrete substrate modeled through eight node isoparametric solid brick elements and an 8-point (2 x 2 x 2) Gauss integration scheme. The concrete block is 400 mm long, 192 mm high and 240 mm wide, matching Dei Poli et al. (1992) specimens. This block is supported on a fixed bed. The solid brick elements used in the block discretization are 4 mm long and 4 mm high. Their width depends on the bar diameter. In this context, Table 4-4 shows the number of slave nodes N in the transverse z direction, and its spacing s_{sn} considered for each bar diameter.

Table 4-4 – Number of slave nodes in the transverse z direction and its spacing for each bar diameter, in the 3D ED modeling approach.

ϕ (mm)	s_{sp} (mm)	N
8	4	3
12	5	3
16	5	3
20	5	5
25	5	5

The concrete material properties considered are Poisson ratio v = 0.2 and Young's modulus E_c calculated through the *fib* Model Code (*fib* 2013) expression $E_c = 21500 \times (f_c / 10)^{1/3}$ with E_c and f_c in MPa. For the steel properties, the values used in the 2D FB approach are maintained. In turn, the connection between the steel bar and the concrete substrate is established through Winkler springs, whose constitutive relations are calculated using Equation (4-22) and the explained procedure for k_{sub} determination.

Figure 4-9 displays the k_{sub} values obtained for a model with f_c = 48.1 MPa and ϕ = 16 mm (s_{sn} = 4 mm from Table 4-4). It can be seen that the stiffness has a minimum at the specimen theoretical "crack" section (x = 0 mm), rapidly increases near the "crack", and then gradually decreases until reaching negative values at $x / \phi = 2$, when the deformation δ_v of the steel bar starts to have negative values.

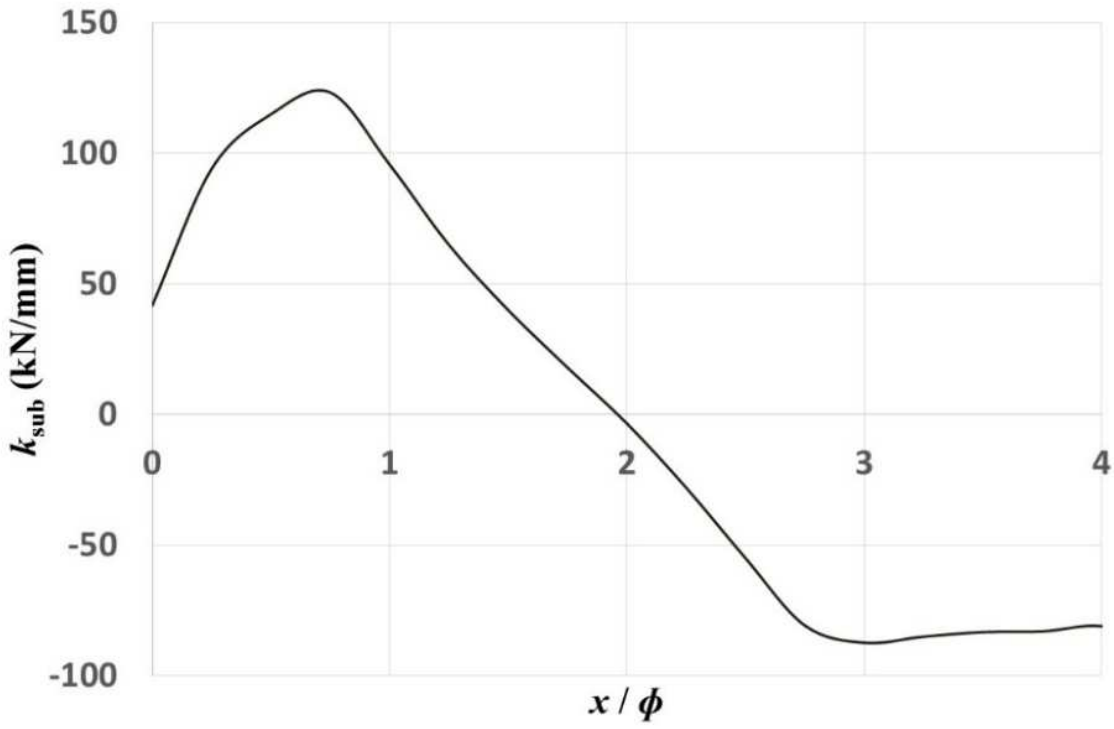

Figure 4-9 – Elastic stiffness k_{sub} of concrete substrate in a 3D ED model with f_c = 48.1 MPa and ϕ = 16 mm (s_{sn} = 4 mm from Table 4-4 and x axis identified in Figure 4-8).

Theoretically, since k_{sub} varies along the steel bar x axis, different constitutive models have to be determined through Equation (4-22) for the nonlinear Winkler springs of the 3D ED

approach. However, very good results can be achieved, with an almost identical dowel response between the 3D ED and the 2D FB approaches, if only two values for k_{sub} are considered: one value $k_{sub1} = k_{sub}$ ($x = 0$) for the first spring at the "crack" section, and a second value k_{sub2} for the remaining springs. For k_{sub2}, it is recommended the average value of k_{sub} calculated for nodes located between $0 < x < \phi$.

Figure 4-10 depicts the obtained constitutive models for the springs, given by Equations (4-14) to (4-22). The figure shows the models for a bar diameter $\phi = 25$ mm and for the three concrete strengths considered in this work. These curves correspond to the constitutive behavior which is represented in Figure 4-6. It can be seen in Figure 4-10 that the constitutive model to be used in 3D ED models has to have a higher stiffness in the first ascending branch, compared to the stiffness in 2D FB models. This is the result of the condition imposed by Equation (4-22). For greater displacement values, the constitutive model for the 3D ED approach is almost coincident with the one of the 2D FB approach.

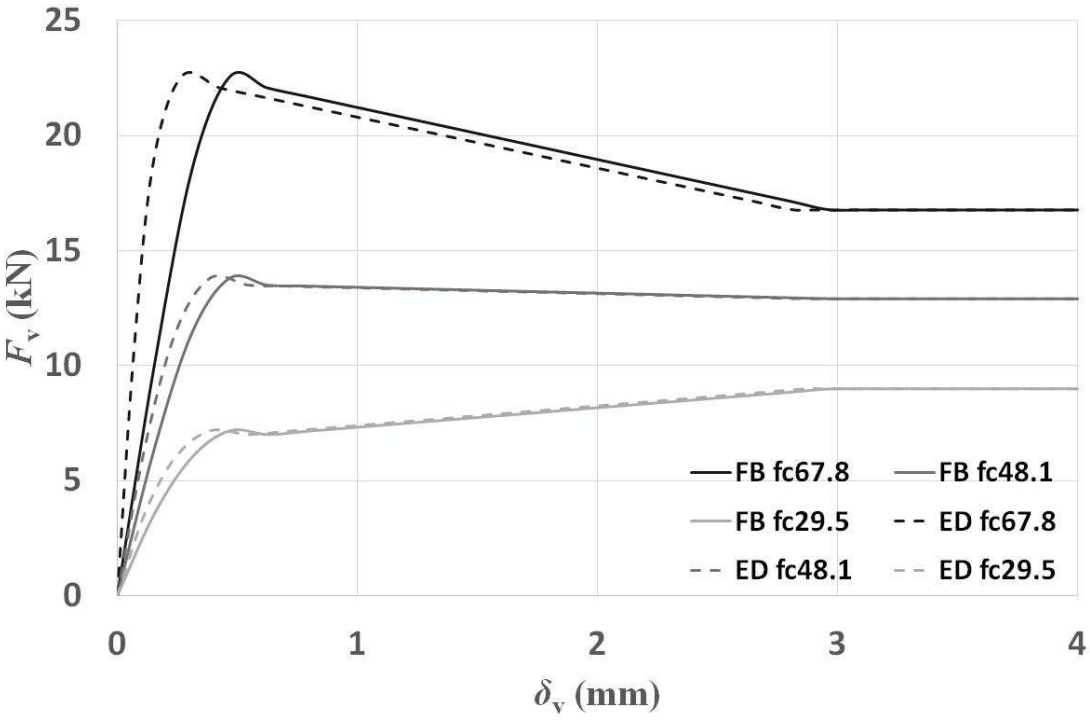

Figure 4-10 – Winkler spring force results achieved in the FE models with $\phi = 25$ mm.

4.6 INFLUENCE OF CONFINEMENT IMPOSED BY STIRRUPS

It was previously mentioned that the dowel strength can be improved and the dowel deformations can be reduced if the concrete is significantly confined by stirrups. This Section 4.6 proposes new expressions to determine the strength of a dowel in concrete confined by stirrups. The expressions are validated through the comparison with experimental data available in the literature.

In this Section 4.6, a new constitutive model is also proposed for the nonlinear Winkler springs, so that the influence of confinement is taken into account.

4.6.1 DOWEL STRENGTH AND DEFORMABILITY

The influence of the confinement provided by stirrups is taken into account by considering an increase of the concrete substrate strength in the expression which gives the dowel strength. That increase of strength can be expressed by a coefficient β_{st} in Equation (4-2), which enhances the effect of confinement provided by local compression (the latter described by the coefficient β^*). Therefore, when stirrups are present, K is expressed as:

$$K = \frac{4}{\pi} \times \sqrt{\frac{\beta^*}{3} \times \beta_{st}} \tag{4-23}$$

with

$$\beta_{st} = \frac{f_{c,c}}{f_c} \tag{4-24}$$

$f_{c,c}$ being the concrete strength under biaxial or triaxial compression caused by confinement due to the presence of stirrups. For $f_{c,c}$ calculation, the following *fib* Model Code (*fib* 2013) expression is considered:

$$\frac{f_{c,c}}{f_c} = 1 + 3.5 \times \left(\frac{\sigma_2}{f_c} \right)^{0.75} \tag{4-25}$$

where the confinement stress σ_2 depends on the transverse section of the concrete specimen dimensions, number of reinforcing longitudinal bars, stirrup spacing and its yield force.

In Table 4-5, Equation (4-25) is applied to Rasmussen (1963) specimens, where s_{st} is the stirrup spacing and ω_c the mechanical reinforcement ratio (*fib* 2013). An average value of β_{st} = 1.28 (with standard deviation σ = 0.145) was achieved. In order to calculate the coefficient K for these tests using Equation (4-23), the value of β^* needs to be determined first. To that end, Dei Poli et al. (1992) program can be taken into account, since stirrups are absent in their experimental program, and the average value of K = 1.45 leads to β^* = 3.89 from Equation (4-3). Consequently, an average K = 1.64 (with standard deviation σ = 0.09) is obtained for Rasmussen (1963) specimens, a value close to the experimentally obtained K value 1.67, with σ = 0.15, as shown in Table 4-2. This suggests that *fib* Model Code (*fib* 2013) recommendations for concrete confined by stirrups can be used in dowel strength calculation.

Table 4-5 – Values of β_{st} and K achieved through the application of *fib* Model Code (*fib* 2013) expression for confinement imposed by stirrups to Rasmussen (1963) test specimens.

	Experimental					*fib* Model Code			
test	ϕ_{st} (mm)	f_c (MPa)	f_y (MPa)	s_{st} (mm)	K	ω_c	σ_2 (MPa)	β_{st}	K
Rasmussen 1963									
D1	10	11.0	242	25	1.63	0.256	0.72	1.45	1.75
D3	10	20.1	242	25	1.72	0.140	0.72	1.29	1.65
D7	10	30.5	242	25	1.72	0.092	0.72	1.21	1.60
D9	10	43.4	242	25	1.55	0.065	0.72	1.16	1.56
D2	10	10.7	221	40	1.57	0.150	0.36	1.27	1.64
D4	10	26.6	221	40	1.62	0.060	0.36	1.14	1.55
D8	10	28.7	221	40	1.73	0.056	0.36	1.13	1.54
D10	10	43.0	221	25	1.61	0.060	0.66	1.15	1.56
D5	10	16.9	431	25	2.03	0.297	1.29	1.51	1.78
D6	10	18.4	400	25	1.53	0.252	1.19	1.45	1.75
				μ	1.67			1.28	1.64
				σ	0.15			0.14	0.09

If the *fib* Model Code (*fib* 2013) criteria for confined concrete is considered also in the estimation of the dowel deformability, a coefficient ξ_{st} can be defined for dowel slip:

$$\xi_{st} = \frac{s_{c1}}{s_1} \tag{4-26}$$

with

$$\frac{s_{c1}}{s_1} = 1 + 5 \times \left(\frac{f_{c,c}}{f_c} - 1 \right) \tag{4-27}$$

in which s_{c1} is dowel slip at maximum force V_{dR} in specimens confined by stirrups. Equation (4-27) reflects an increased ductility in dowel behavior, a fact already observed by Soroushian et al. (1987) in tests to assess bearing strength of reinforced concrete samples.

4.6.2 WINKLER SPRING MODELING

With the addition of stirrups, the dowel force – slip relation is modified. Higher strength and displacement values can be reached in that case. Regarding the constitutive model for the nonlinear Winkler springs, these increased values imply changes such that:

$$\frac{F_{vR,c}}{F_{vR}} = \sqrt{\beta_{st}} \tag{4-28}$$

and

$$\frac{\delta_{v1,c}}{\delta_{v1}} = \xi_{st} \tag{4-29}$$

where F_{vR} and δ_{v1} are spring strength and displacement values corresponding to the peak load, in concrete not confined by stirrups. In turn, $F_{vR,c}$ and $\delta_{v1,c}$ are the corresponding values when concrete is confined by stirrups.

A new constitutive model was derived for springs of the 2D FB modeling approach, with fixed bed. An attempt was made in order to accomplish this altered spring response with only slight adaptations on Equation (4-15). This task was fulfilled with the following expression,

providing a very good approximation for $1 \leq \beta_{st} \leq 1.5$, for the same 5 bar diameters and 3 concrete strengths previously considered in the springs analysis:

$$\psi_{II,III,st} = \frac{b}{\xi_{st}^{\ e}} \times \left(\frac{\delta_v}{\phi} \right) + \frac{c}{\xi_{st}^{\ f}} \Leftarrow A \leq \frac{\delta_v}{\phi} \leq \xi_{st} \times B \tag{4-30}$$

in which *e* and *f*, such as *b* and *c*, are coefficients calculated through a linear interpolation of the concrete strength

$$e = -0.00097 \times f_c + 2.27577 \tag{4-31}$$

$$f = -0.00094 \times f_c + 1.26719 \tag{4-32}$$

with f_c in MPa.

Outside the $1 \leq \beta_{st} \leq 1.5$ range, Equation (4-30) ceases to represent the anticipated spring behavior. However, $\beta_{st} > 1.5$ is only achieved when stirrups amount is very high, and conforms to an uncommon situation in most of the reinforced concrete structures. Rasmussen (1963) program contained specimens with different levels of confinement imposed by stirrups and $1 \leq \beta_{st} \leq 1.5$ in all cases, with the exception of specimen D5 which had $\beta_{st} = 1.51$.

For 3D ED approach, the existence of an elastic concrete substrate imposes a few modifications in the procedure. In this case, and for the example exposed in Section 4.5.3, coefficients *e* and *f* are given by a quadratic interpolation of concrete strength:

$$e = 0.00055 \times f_c^{\ 2} - 0.05998 \times f_c + 3.55273 \tag{4-33}$$

$$f = 0.00055 \times f_c^{\ 2} - 0.05961 \times f_c + 2.53639 \tag{4-34}$$

also with f_c in MPa.

For both 2D FB and 3D ED approaches, coefficients *e* and *f* were determined in order to achieve conditions expressed in Equations (4-28) and (4-29). However, in the 3D ED approach, due to the inclusion of solid brick elements to discretize the concrete substrate, the

fulfillment of Equations (4-28) and (4-29) in the Winkler springs constitutive relations is not sufficient to obtain the same good results. For that reason, spring stiffness $k_{sp,ED,II,III,st}$, calculated through the nonlinearity coefficient $\psi_{II,III,st}$ of Equation (4-30), needs to be adjusted. To achieve that adjustment empirically, the following expression is proposed, depending on concrete substrate stiffness and the concrete strength:

$$k_{sp,ED,II,III,st,adj} = \frac{1}{\frac{1}{k_{sp,ED,II,III,st}} - \frac{1}{g \times k_{sub}\left(x=0\right)}} \tag{4-35}$$

with coefficient g given by

$$g = 0.0008 \times f_c^2 - 0.07702 \times f_c + 1.97544 \tag{4-36}$$

Alternatively, stiffness $k_{sp,ED,st}$ can still be determined from $k_{sp,FB,st}$ through Equation (4-22), assuming an association in series with the concrete substrate stiffness.

Finally, Figure 4-11 illustrates changes introduced by Equation (4-30), with β_{st} = 1.28 (and consequently ξ_{st} = 2.40), in dowel force – slip relation of specimens modeled through the 2D FB approach and with 25 mm reinforcing bars. In turn, Figure 4-12 shows the corresponding spring response. As expected, strength increased, along with ductility.

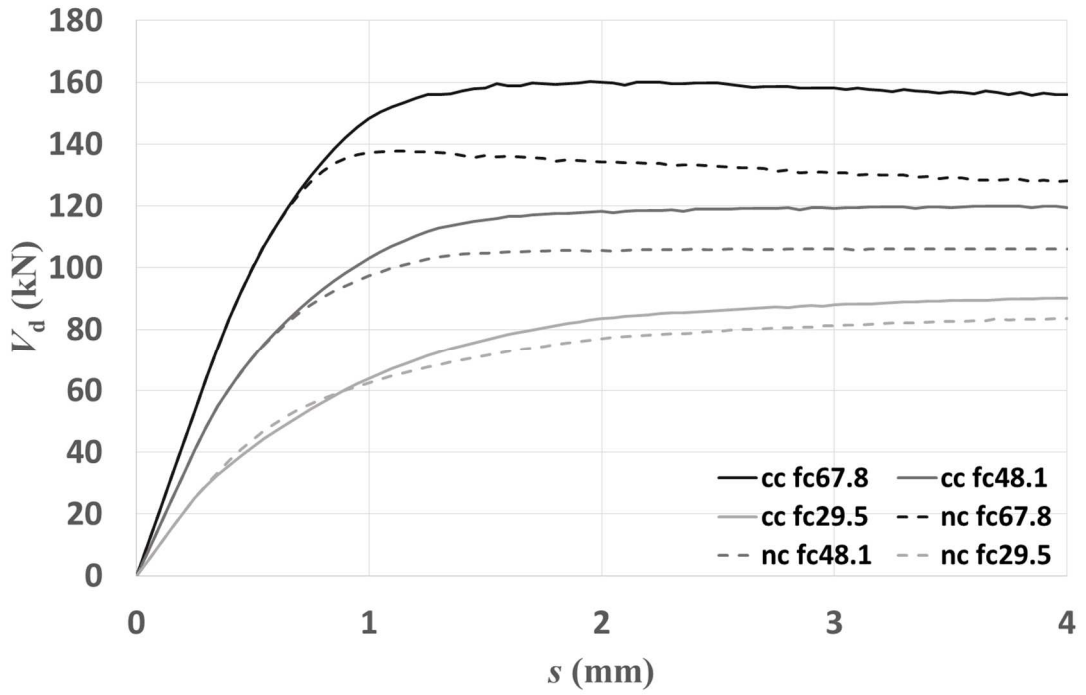

Figure 4-11 – Comparison of dowel force obtained in 2D FB finite element models for specimens confined by stirrups (cc) and without stirrups (nc) – ϕ = 25 mm and β_{st} = 1.28.

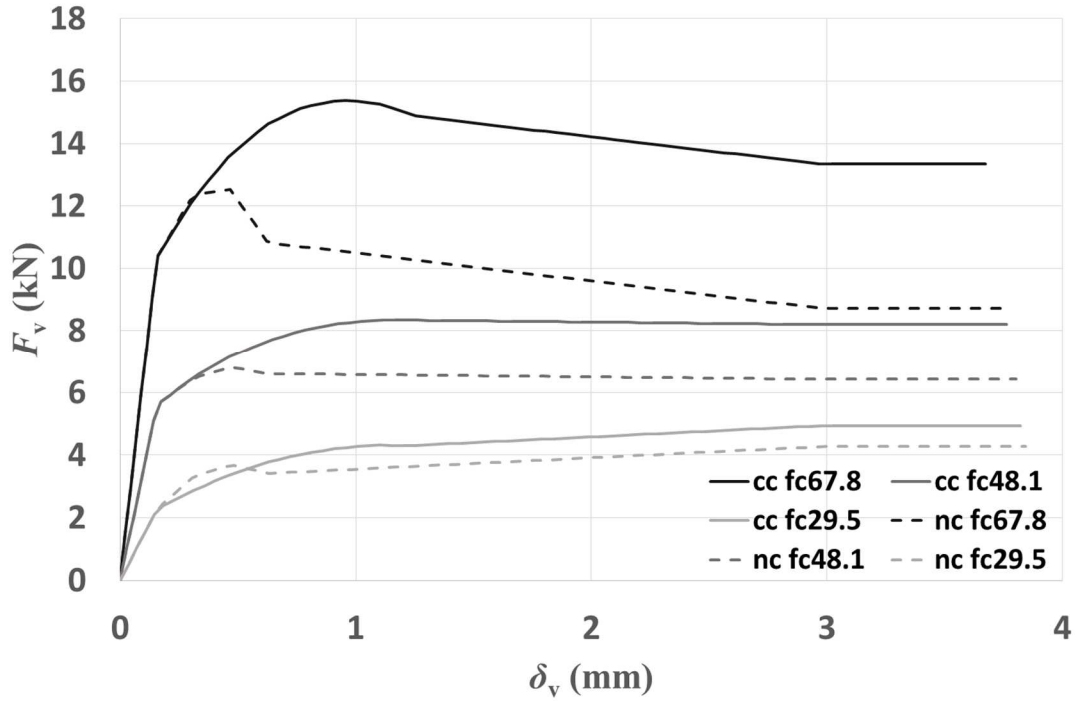

Figure 4-12 – Winkler spring force achieved in the 2D FB finite element models for specimens confined by stirrups (cc) and without stirrups (nc) – ϕ = 25 mm and β_{st} = 1.28.

4.7 INFLUENCE OF LATERAL CONCRETE COVER

Dowel strength can be affected by low concrete substrate confinement due to insufficient lateral cover length *c*. A review of the state-of-art on this subject indicated that solid recommendations for dowel strength reduction, based on experimental data, already exist. Therefore, this Section 4.7 mainly focuses on proposing new endorsements to Winkler spring behavior in order to account for splitting failure in dowel action finite element modeling. The effect of confinement imposed by stirrups is also contemplated.

4.7.1 STATE-OF-ART REVIEW ON DOWEL SPLITTING STRENGTH

When concrete cover is small, since lateral dilatancy of the locally compressed concrete substrate is not so hindered by the surrounding mass of non-loaded concrete, dowel strength decreases. A few research works identified the crack pattern commonly recognized in dowel action failure, and it can be depicted by a major a vertical crack (Millard and Johnson 1984; Soroushian et al. 1987) right below the reinforcing bar. In cases with small cover length, the vertical crack easily reaches the specimen limits and failure is accompanied by splitting cracks (Vintzeleou and Tassios 1987) and cover detachment.

Usually, concrete splitting is taken into account in dowel strength prediction models through a reducing factor. In the present work, the reduction associated to insufficient lateral concrete cover is introduced in a manner consistent with the approach previously followed to describe the influence of confinement provided by stirrups. That is, the influence of concrete cover is taken into account (in the equation to predict the dowel strength) through the modification of the concrete bearing strength. It was explained before that this bearing strength can be adjusted by adding a multiplicative parameter in term under the squared root, in the equation which gives the coefficient *K*. This coefficient is denoted by β_{cov} and the coefficient *K* should therefore be expressed as:

$$K = \frac{4}{\pi} \times \sqrt{\frac{\beta^*}{3} \times \beta_{st} \times \beta_{cov}} \tag{4-37}$$

Soroushian et al. (1987) tested the bearing strength of concrete under a reinforcing bar on specimens with $c / \phi = 1.5$ and $c / \phi = 4.5$. Results collected from the tests showed a 25% decrease in bearing strength in specimens with $c / \phi = 1.5$ compared to specimens where $c / \phi = 4.5$. Those authors then suggested that concrete bearing strength should be multiplied by 0.6 when $c / \phi = 1$, and by 1 only for large c / ϕ values, not specifying any number.

Later, based on experimental data gathered through research projects developed in the National Technical University of Athens, Tsoukantas and Tassios (1989) proposed a reducing factor for dowel strength linearly depending on c / ϕ. According to their recommendations, the reducing factor should be 0.6 for $c / \phi = 0$ and equal to 1 for $c / \phi \geq 3$. This criterion was subsequently adopted in *fib* Bulletin No. 43 – guidance for dowel strength in structural connections (*fib* 2008).

The results presented in Table 4-1 also provide some information about the influence of lateral concrete cover influence on dowel action. A total of 9 tests were identified in which concrete splitting failure occurred:

- In specimen A1 of the Dei Poli et al. (1992) experimental program, having $c / \phi = 4.5$, splitting was observed but no strength decrease is identified in the measured dowel behavior. The dowel response was already in a perfectly plastic state when failure occurred.
- Vintzeleou and Tassios (1987) tested 4 specimens, with $c / \phi = 2.9$, that showed lateral cracks along the reinforcing axis. However, no strength decrease is noticed in the V_d – s graphs. Actually, V_d grew continuously due to reinforcement kinking effect.
- In the 2 tests of the Soroushian et al. (1986) campaign (specimen T6 with $c / \phi = 3.4$ and T8 with $c / \phi = 2.5$), an abrupt failure is visible, which suggests that concrete splitting occurred. Coefficient K calculated for T6 and T8 specimens were 1.58 and 1.06, respectively, while the average value referring to the Dei Poli et al. (1992) tests was 1.45. These results show a clear strength reduction in T8. However, aggregate interlock and kinking can be present in this campaign, affecting dowel decrease determination.
- In 2 tests (DM2 and DM3 having $c / \phi = 3.6$) performed on the present work, cover detachment occurred, but determination of the dowel decrease observed in these tests is also influenced by the interaction with aggregate interlock effects and, therefore, the

influence of concrete cover cannot be isolated.

4.7.2 CRITERIA FOR THE STRENGTH REDUCTION COEFFICIENT

The expression for parameter $\sqrt{\beta_{cov}}$ that will be used hereinafter is:

$$\sqrt{\beta_{cov}} = 0.507 + 0.167 \times \frac{c}{\phi} \leq 1 \tag{4-38}$$

This equation follows Tsoukantas and Tassios (1989) recommendations in terms of setting a linear variation and a superior limit $\sqrt{\beta_{cov}} = 1$ for $c / \phi = 3$. Thus, according to this model, concrete cover values higher than $c = 3\ \phi$ do not give rise to any increase in the dowel strength, since the confinement level remains unchanged.

For the inferior limit of the cover value, when $c / \phi = 0$, confinement is totally absent and concrete substrate is fully compressed. Therefore, coefficient β^* should be equal to 1 in this case. Assuming $\beta^* = 3.89$ obtained from the Dei Poli et al. (1992) tests as a fixed value, a theoretical $\beta^* = 1$ is achieved if $\sqrt{\beta_{cov}} = 0.507$. This is the value provided by Equation (4-38) for $c / \phi = 0$. Obviously, a null concrete cover will never be used in practice.

It is also interesting to note that Equation (4-38) determines $\sqrt{\beta_{cov}} = 0.75$ for $c / \phi = 1.5$, this being a value which matches the results of the Soroushian et al. (1987) tests to evaluate concrete bearing strength. This fact supports the validity of Equation (4-38).

4.7.3 WINKLER SPRING MODELING AND DOWEL SPLITTING BEHAVIOR

The influence of concrete splitting can only be taken into account in finite element modeling approaches (2D FB approach or 3D ED approach) if the constitutive model for Winkler springs is modified accordingly.

Preliminary finite element analyses, aiming at simulating the influence of concrete splitting, were made in which Winkler spring behavior is modeled as a single perfectly plastic branch. The spring force in such plastic branch is denoted by "splitting spring force", $F_{v,split}$. Taking into account the explanations given in Section 4.7.2, $F_{v,split}$ has a constant value, given

by ϕ x s_{sp} x f_c. The results of the various preliminary finite element analyses revealed splitting dowel strength values, $V_{dR,split,}$ very close to 0.507 x V_{dR}. This fact is not surprising, because these finite element "plastic" analyses replicate the assumptions made in the derivation of the expressions proposed to calculate the dowel strength.

The preliminary finite element analyses do not provide results for the dowel deformations under increasing applied actions. Those results can only be calculated if a complete constitutive model is defined for the Winkler springs. Such a definition is proposed in the following sub-sections of this Thesis.

4.7.3.1 SPRING RESPONSE UNTIL SPLITTING FAILURE

In the constitutive model for Winkler springs, the assumption that confinement level has no influence on the initial elastic stiffness is maintained. In the elasto-plastic stage, the same principle is preserved: stiffness is not altered by insufficient concrete cover until splitting failure occurs. This assumption is experimentally supported by Figure 4-2 results, where all of the 3 specimens, including DM1 in which splitting did not occur, showed a similar behavior for low slip values, even at a nonlinear stage.

For the spring force at which splitting takes place, $F_{vR,split}$, the following condition is settled:

$$\frac{F_{vR,split}}{F_{vR}} = \sqrt{\beta_{cov}} \tag{4-39}$$

Afterwards, spring behavior is determined by analyzing experimental data available in literature and in the performed tests.

4.7.3.2 SOFTENING BRANCH AFTER FAILURE

Splitting failure was identified in the tested specimens DM2 and DM3. In these specimens, cover detachment occurred at the instants marked in Figure 4-3. Splitting was more pronounced in DM3, where lower dowel strength was observed. Though, failure was not

abrupt, and a soft descending branch emerged. Concerning Soroushian et al. (1986) T6 and T8 specimens, and Dei Poli et al. (1992) A1 test, a more prominent splitting failure is detected on the $V_d - s$ response. However, the dowel force drop marking the event is not totally sudden, and a softening response can be identified.

These conclusions indicate that the concrete cover detaches gradually, with a progressive loss of confinement in the substrate. Thus, a softening descending linear branch, similar to stage IV of Figure 4-6, is assumed for Winkler spring response in this present work until $F_v = 0$. The branch stiffness is calculated considering the following nonlinearity coefficient, adapted from Equation (4-16):

$$\psi_{IV,cov} = d_{cov} \tag{4-40}$$

in which d_{cov} is given by

$$d_{cov} = d - 0.3824 \times \left(1 - \sqrt{\beta_{cov}}\right) \tag{4-41}$$

for both 2D FB and 3D ED approaches.

Equation (4-41) accounts for the fact that stiffness is reduced when cover length is small and, consequently, β_{cov} acquires low values. Coefficient d_{cov} was determined taking into account that the spring model should comply with Equation (4-39), and the output of finite-element analyses should comply with the condition:

$$\frac{V_{dR,split}}{V_{dR}} = \sqrt{\beta_{cov}} \tag{4-42}$$

During the analysis procedure, it was noted that a sudden splitting failure compels $F_{vR,split}$ to be much superior to $\sqrt{\beta_{cov}}$ x F_{vR} in order to fulfill the premise written in Equation (4-42). This evidence contributed as well to put aside the hypothesis of a fragile and abrupt spring splitting rupture.

Figure 4-13 and Figure 4-14 show results achieved in the 3D ED finite element models, in terms of dowel force and Winkler spring force respectively, for specimens with 25 mm

reinforcing bars and β_{cov} = 0.64. In terms of spring response, cases with higher concrete strength enclosed smaller stiffness values for that branch.

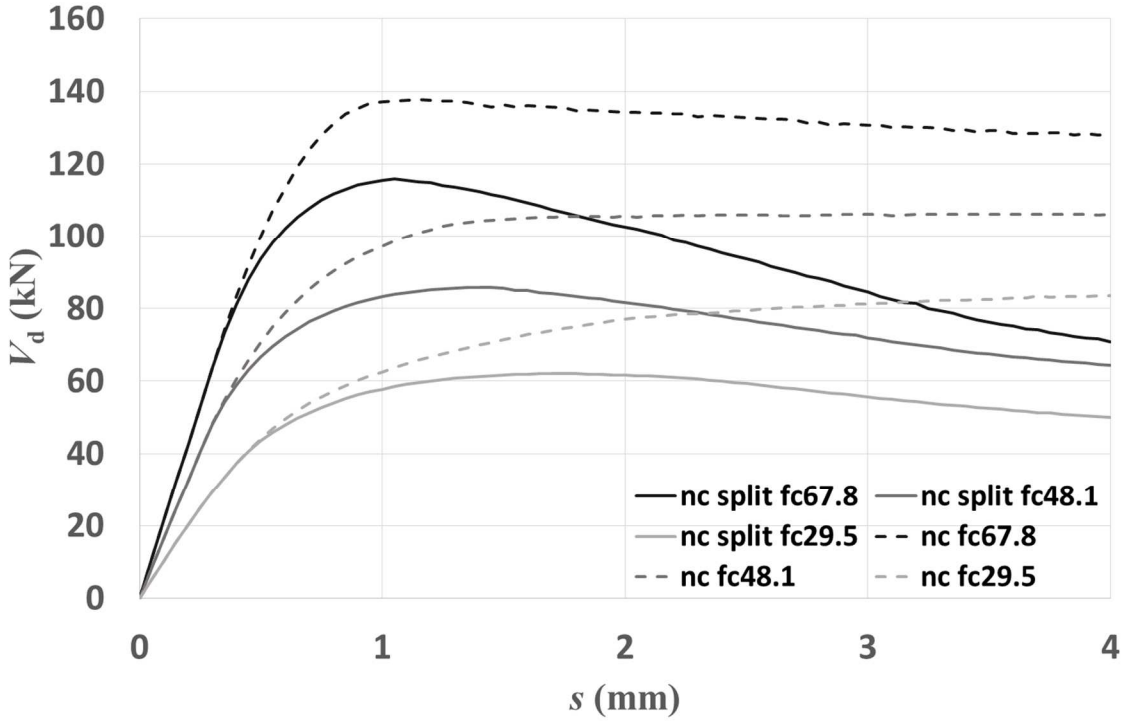

Figure 4-13 – Comparison of dowel force obtained in the 3D ED finite element models for specimens with splitting failure (split) and without (nc) – ϕ = 25 mm and β_{cov} = 0.64.

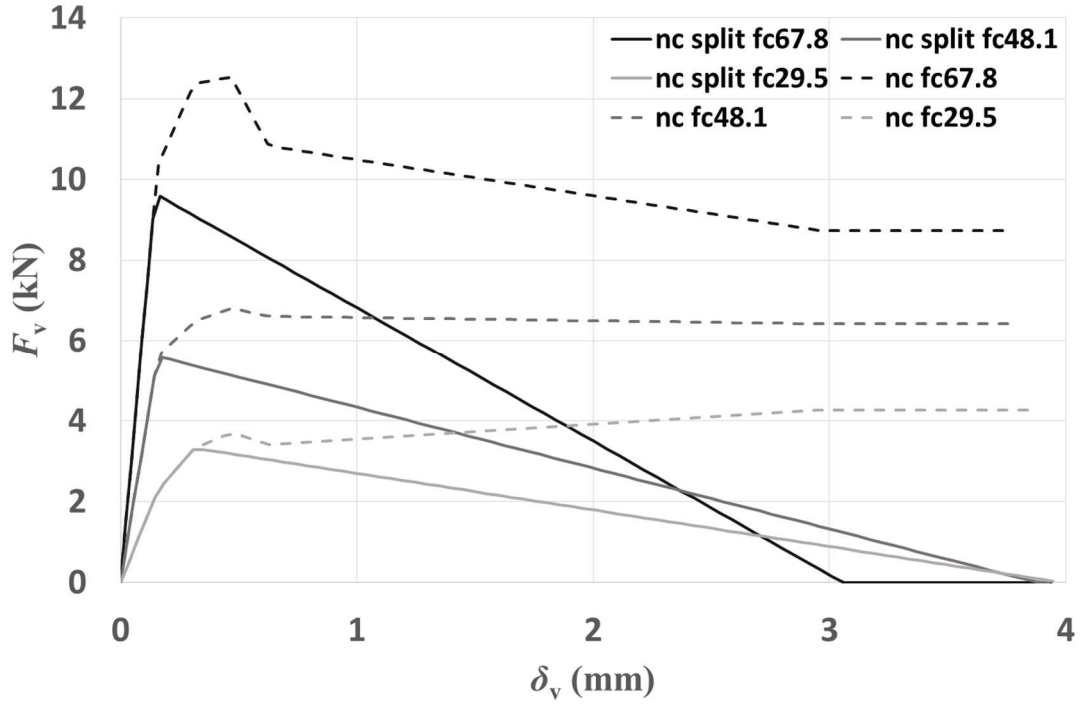

Figure 4-14 – Winkler spring force achieved in the 3D ED finite element models for specimens with splitting failure (split) and without (nc) – ϕ = 25 mm and β_{cov} = 0.64.

4.7.3.3 COMBINED EFFECTS OF LATERAL COVER AND CONFINEMENT IMPOSED BY STIRRUPS

In dowel behavior modeling, the combined effects of lateral cover and confinement due to stirrups should be taken into account, at first place, by considering the assumptions made in Section 4.6 for Winkler spring deformability. It was mentioned there that the influence of confinement imposed by stirrups could be included in the nonlinear constitutive relations of the Winkler springs through a modified stiffness calculation procedure. Changes in the procedure relied on the proposal of a nonlinearity coefficient $\psi_{II,III,st}$, to be used in stiffness calculation for stages II and III of spring behavior (see Figure 4-6), instead of the nonlinearity coefficient $\psi_{II,III}$, which only applies to concrete not confined by stirrups.

Therefore, assuming the nonlinear spring response described in Section 4.6 for concrete confined by stirrups, the following condition is settled for splitting failure force $F_{vR,c,split}$:

$$\frac{F_{vR,c,split}}{F_{vR}} = \sqrt{\beta_{st} \times \beta_{cov}} \tag{4-43}$$

or

$$\frac{F_{vR,c,split}}{F_{vR,c}} = \sqrt{\beta_{cov}} \tag{4-44}$$

For spring displacement values higher than the one corresponding to the force $F_{vR,c,split}$, a softening branch is defined. This branch is characterized through a procedure similar to the one presented in Section 4.7.3.2. In this case, coefficient $d_{cov,st}$ has to be used instead of d_{cov}:

$$d_{cov,st} = d - \frac{0.3824}{\xi_{st}} \times \left(1 - \sqrt{\beta_{cov}}\right) \tag{4-45}$$

The parameter ξ_{st} is added in order to take into account the ductility increment caused by stirrups in spring response. The insertion of ξ_{st} in Equation (4-45) increases dowel force mainly for large displacement values. Its influence on dowel strength V_{dR} is only tenuous.

Comparing to Figure 4-13 and Figure 4-14, Figure 4-15 and Figure 4-16 reveal the effect of the incorporation of stirrups in the modeled specimens so that $\beta_{st} = 1.28$. As can be seen, general dowel and spring behavior are maintained, now having higher force values and a reduced stress softening branch slope, showing the ductility growth.

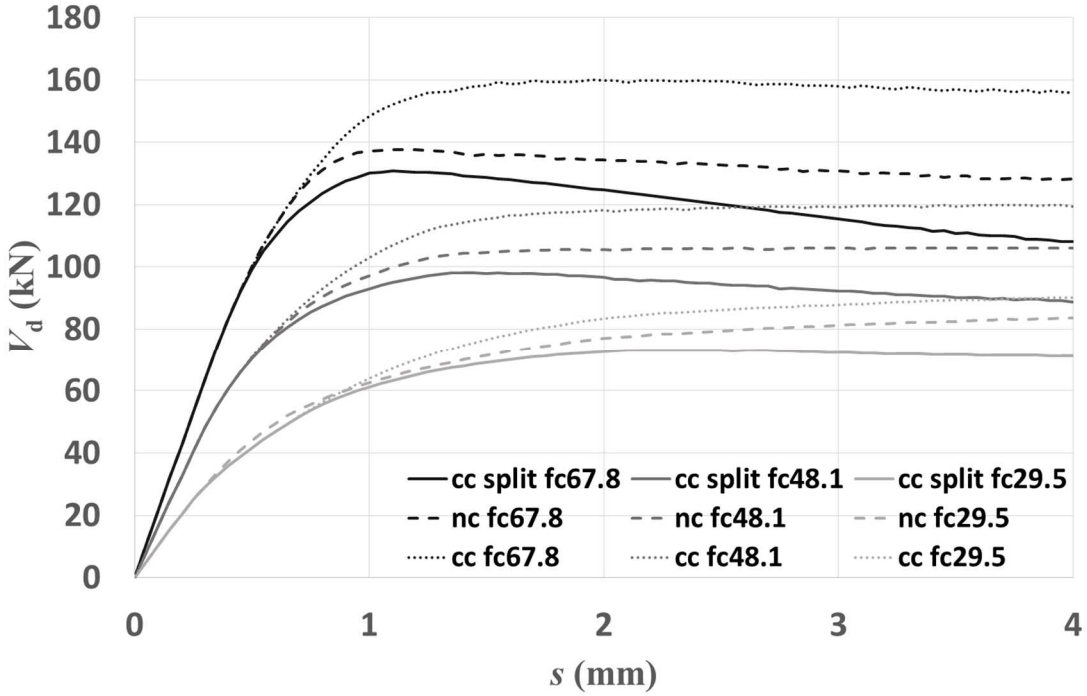

Figure 4-15 – Dowel force obtained in the 3D ED finite element models for specimens with stirrups having splitting failure – ϕ = 25 mm, β_{cov} = 0.64 and β_{st} = 1.28.

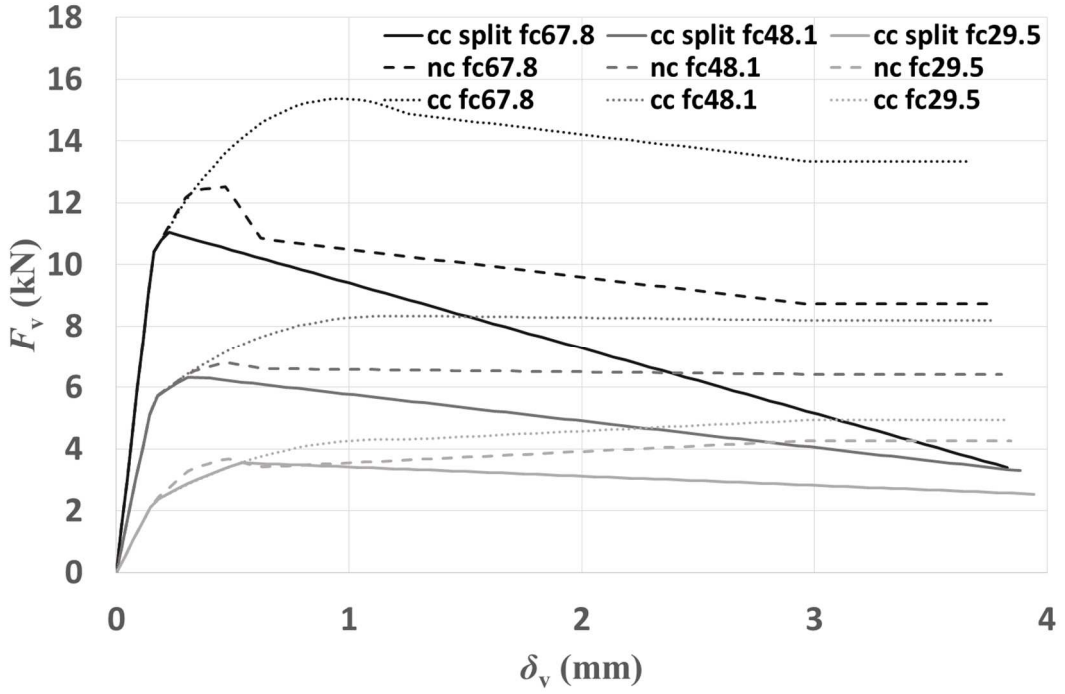

Figure 4-16 – Winkler spring force achieved in the 3D ED finite element models for specimens with stirrups having splitting failure – ϕ = 25 mm, β_{cov} = 0.64 and β_{st} = 1.28.

4.8 CONCLUSIONS

The main conclusions that can be derived from the work on this chapter are the following:

1. Experimental assessment of reinforcing bar dowel action in a concrete interface is a complex task. The conception of a specimen execution procedure that can eliminate interface roughness is hard to accomplish and, consequently, the probability of dowel action interacting with aggregate interlock as an interface strength mechanism is significant. Moreover, reinforcement kinking effect arises in concrete interfaces for large slip values, also contributing for shear strength. The recommended procedure is the evaluation of dowel action in a single concrete block, removing the input of other strength mechanisms.

2. In order to calibrate a finite element model for dowel action that can be applied to a wide range of bar diameters and concrete strengths, the Dei Poli et al. (1992) empirical model was considered. Comparing the model with the tests performed by Dei Poli et al. (1992), it was concluded that a slight change in the proposed stiffness for concrete substrate results in an important improvement in the adjustment to the experimental results.

3. The FE model conceived contains a complete discrete "beam element" representation of the steel reinforcing bar, accounting for flexural stiffness and nonlinear material behavior. The bar is connected to concrete embedment through discrete Winkler spring elements, with nonlinear constitutive relations, to simulate the deformability and strength of the concrete substrate. Two different approaches were proposed: 1 – a 2D Fixed Bed approach, suitable for an isolated analysis of dowel action, in which the concrete deformability is totally lumped in the nonlinear Winkler springs; 2 – a 3D Embedded Dowel approach, suitable for simulation of dowel action is structures (or parts of structures) modeled with solid brick or plane stress finite elements.

4. The constitutive model for the nonlinear Winkler springs was defined and calibrated. In the case of the 2D Fixed Bed modeling approach, this model is given by closed form expressions, valid for a wide and recurrent range of values for bar diameter and concrete strength. In the case of the 3D Embedded Dowel approach, a modified

constitutive model has to be employed. The procedure for definition of such model was also shown in this chapter.

5. Influence on dowel behavior of confinement imposed by stirrups was evaluated and an additional coefficient multiplying dowel strength is suggested, based on recommendations available in literature about this subject. Spring response is also adapted in order to incorporate the existence of stirrups.

6. A state-of-art review about the influence of lateral concrete cover on dowel action provided useful information and background for the definition of a dowel strength reduction factor. Assumptions are made for Winkler spring behavior based on tests performed in this work having concrete splitting failure. Those premises are later introduced in the force – displacement spring relations. Finally, the combined influence of lateral concrete cover and confinement imposed by stirrups is analyzed in terms of dowel and spring response.

5

FINITE ELEMENT MODELING OF CONCRETE INTERFACES SUBJECTED TO STATIC LOADING

A nonlinear finite element model is developed to assess the behavior of an interface between two concretes cast at different times subjected to monotonic loading. Initially, a frictionless interface is considered, in which reinforcement dowel action is the only strength mechanism. This particular and simpler case is useful to achieve a better understanding of how the dowel finite element modeling approach presented in Chapter 4 can be extended to a concrete joint, with the addition of new nonlinear springs in order to account steel/concrete embedment bond behavior. With the analysis of this case, the contribution of the dowel action to the shear strength of an interface between different concretes can be assessed. The influence of crack opening and the relevance of the kinking effect can also be assessed through this type of analysis. Dowel displacements and curvatures of the deformed reinforcing bar are also evaluated. Then, the influence of aggregate interlock effect in rough interfaces is assessed using the same type of modeling approach. The comparison with experimental results available allowed the determination of new constitutive relationships to calculate the shear stress in a concrete interface, due to the aggregate interlock effect.

5.1 INTRODUCTION

The shear stress transferred through a (reinforced) cracked concrete interface can be modeled as the superposition of two different strength mechanisms: dowel action of the

reinforcing bars and aggregate interlock. Therefore, the conception of a finite element model for the behavior of a concrete interface should attain the inputs from both mechanisms.

5.1.1 DOWEL ACTION OF THE REINFORCING BARS

Modeling of dowel action was discussed in Chapter 4, and new prediction equations (models) were proposed. A complete discrete 'beam element' representation of the steel reinforcing bar was adopted, accounting for material plasticity, rotational degrees of freedom and flexural stiffness. The bar is connected to the concrete embedment through several Winkler spring elements, with nonlinear constitutive behavior, to simulate the deformability of the concrete substrate (in the direction perpendicular to the bar) along the bar length. In this Chapter 5, that modeling approach is applied to the study of an interface between concretes cast at different ages, in which the dowel behavior is not only influenced by the slip at the crack, but also by the crack opening displacements are present. In this case, the steel bar is subjected to an axial force which, on the one hand, compresses the concrete interface and, on the other hand, gives rise to the kinking effect of the reinforcing bars, that arises for large displacements. These new features are included in modeling and their effect on dowel behavior is analyzed. The latter is responsible for a significative contribution to the total resistant shear force when the slip at the interface reaches large values. The modeling approach proposed in this work allows to simulate all these effects and understand their contribution to the shear strength of a reinforced concrete interface.

5.1.2 AGGREGATE INTERLOCK

Numerical finite element modeling of the aggregate interlock mechanism was already implemented by Feenstra et al. (1991), either in a single interface element and assemblies of interface elements and plane-stress elements. Five proposals for aggregate interlock modeling were considered: three empirical

– "rough crack model" by Bazant and Gambarova (1980)

– "rough crack model" by Gambarova and Karakoç (1983)

– the aggregate interlock constitutive relations of Walraven and Reinhardt (1981)

and two physical

– "contact density model" by Li et al. (1989)

– "two phase model" by Walraven (1981).

By comparing them with the experimental data of Paulay and Loeber (1974) and Walraven et al. (1979), Feenstra et al. (1991) verified that the aggregate interlock relations (Walraven and Reinhardt 1981) had the best behavior in terms of the stability of the numerical solution and also the stress and displacement distributions along the crack. That proposal allowed the use of a tangential stiffness matrix in the iteration method even for very low displacement values, and a full Newton-Raphson procedure always resulted in converged solutions. Moreover, in the aggregate interlock relations of Walraven and Reinhardt (1981) large load steps were possible even for small displacements in the interface. The relations are the following:

$$\tau_{agg} = C_f \left\{ -0.0333 f_{cc} + \left[1.8 w^{-0.8} + \left(0.234 w^{-0.707} - 0.20 \right) f_{cc} \right] s \right\} \quad (5\text{-}1)$$

$$\sigma_n = C_f \left\{ -0.05 f_{cc} + \left[1.35 w^{-0.63} + \left(0.191 w^{-0.552} - 0.15 \right) f_{cc} \right] s \right\} \quad (5\text{-}2)$$

where τ_{agg} is shear stress due to aggregate interlock and σ_n the normal stress on the interface. Slip s and crack opening w should be in mm, and stresses f_{cc} (concrete compressive strength measured in cube specimens), σ_n and τ_{agg} in MPa. In turn, C_f is an aggregate effectiveness coefficient that should be taken as 0.35 if the crack crosses the aggregates, and 1.0 otherwise. However, those empirical relations were obtained from tests on cracks in monolithic concrete restrained by external steel bars. To the author knowledge, no other relations were proposed in the literature for other interface roughness profiles. Moreover, stiffness provided by the external bars in the normal direction of the interface is different from stiffness provided by embedded bars.

This present chapter intends to make a contribution so that these limitations can be partially overcome. Firstly, are proposed new constitutive relations are proposed for aggregate interlock, for application in the finite element modeling of a crack in monolithic concrete

crossed by embedded bars. Then, the analysis focuses on the case of a cracked interface between concretes cast at different times (Mattock 1976) (i.e. a free surface left without further treatment after vibration) subjected to monotonic loading. The latter type of interface was experimentally studied in Chapter 2 and is particularly common in connections between precast concrete elements (FIP 1982; Tadros et al. 1993) or in connections between precast elements and cast-in-place concrete.

5.2 REVIEW AND SELECTION OF EXPERIMENTAL DATA

In this Section 5.2, a review of the experimental data available in the literature is made, in order to select the tests suitable to be compared with results provided by the finite element models for concrete interfaces. Firstly, the discussion focuses on tests which were devised by their authors to analyze (experimentally) the dowel action as the only strength mechanism. Then, the case of dowel action interacting with aggregate interlock in monolithic concrete cracks is analyzed. Finally, the case of dowel action interacting with aggregate interlock in an interface between concretes cast at different times is brought into focus.

5.2.1 DOWEL ACTION AS THE ONLY STRENGTH MECHANISM

Chapter 4, in Section 4.2, already contains an extensive review on experimental tests devised to analyze the dowel action mechanism. In this Section 5.2.1, the attention goes to the case of double sided dowels. The following comments can be made about such tests:

- It was mentioned in Section 4.2.2 that in some specimens shear strength is significantly influenced by aggregate interlock. Those specimens will not be considered for the analysis.
- In the other tests, contribution from aggregate interlock is not clear. The campaign of Soroushian et al. (1986) (T4, T6 and T8 specimens) is one example. These 3 tests will be considered not only to dissect the presence of aggregate interlock, but also to observe the way phenomena like concrete splitting and reinforcement kinking affect the results.

- In the experimental program of Bennett and Banerjee (1976), as well as the ones of Vintzeleou and Tassios (1987) and Millard and Johnson (1984), aggregate interlock contribution is also not clear enough. However, in the first two cases, $V_d - s$ (dowel shear force – slip) and $w - s$ (crack opening – slip) responses are not available. In the latter case relevant information is unknown, such as the amount of stirrups and lateral concrete cover length.

5.2.2 CRACKS IN MONOLITHIC CONCRETE

Chapter 3, in Section 3.3.1, presented a large collection of experimental data referring to cracks in monolithic concrete subjected to monotonic shear loading. In this Chapter 5, only campaigns with information about the nonlinear $V - s$ (shear force – slip) and $s - w$ interface measurements are considered. Those campaigns are the ones of Mansur et al. (2008), Mattock (1976) and Walraven and Reinhardt (1981). However, some aspects observed in the results of the first two led to put them apart:

- In the Mansur et al. (2008) tests, slip vales at the maximum force were around 3 mm, while the average value of several tests available in literature (Hofbeck et al. 1969; Mattock 1976; Walraven and Reinhardt 1981) with the same characteristics is around 0.5 to 0.6 mm. For the fact, no reason is identified in the publication (Mansur et al. 2008).
- In the Mattock (1976) program, interface slip and crack opening measurements revealed that the transducers used, during an important part of the tests, did not appear to have the desired precision. For that reason, crack opening values acquired were significantly lower than expected. Consequently, their consideration in the constitutive relations for aggregate interlock would be traduced in unrealistic stress values.

Therefore, the Walraven and Reinhardt (1981) campaign will be taken as a reference, in the following sections of this Thesis, for finite element modeling of the shear behavior of a crack in reinforced monolithic concrete. Regarding this experimental program, some notes are relevant:

- As was pointed out in Chapter 3 (Section 3.3.1), when reinforcement ratio is high (ρ x $f_y / f_c > 0.25$), secondary cracks occur, and consequently the structure behavior cannot

be represented through the modeling approach used in this Chapter 5. Tests in which ρ x f_y / f_c > 0.25 will not be considered in the analysis.

- In Chapter 4, it was referred in Section 4.7 that insufficient lateral concrete cover length reduces the reinforcement dowel strength. Therefore, knowledge of this parameter is important. Since the tests on the Walraven and Reinhardt (1981) campaign aimed to assess the concrete interface shear behavior, and not specifically dowel action, exact quantification of lateral cover is not presented. Thus, in the present work, the values of this parameter result from an approximate measurement made in the figures displayed for the specimens in that publication (Walraven and Reinhardt 1981).
- For assessment of concrete compressive strength, only cube specimens were tested. In the aggregate interlock relations of Equations (5-1) and (5-2), that value f_{cc} is taken into account. But for dowel action and bond models, the concrete compressive strength in cylinders is needed. That strength value is therefore estimated as f_c = 0.85 x f_{cc}.

The properties of the 7 specimens considered, as well as their shear strength, are shown in Table 5-1, where: b is the interface width, L the interface length, f_c the concrete compressive strength, f_y the reinforcement yield stress, ρ the reinforcement ratio, ϕ the reinforcing bar diameter, c the lateral concrete cover and V_R the shear strength.

Table 5-1 – Shear strength experimental data of reinforced monolithic concrete cracks collected from the Walraven and Reinhardt (1981) experimental program.

test	b (mm)	L (mm)	f_c (MPa)	f_y (MPa)	ρ (%)	ϕ (mm)	c / ϕ	V_R (kN)
Walraven and Reinhardt 1981								
240208	120	300	16.9	460	0.56	8	1.5	167.4
110208	120	300	26.1	460	0.56	8	1.5	198.8
110408	120	300	26.1	460	1.12	8	1.5	231.8
230208	120	300	47.7	460	0.56	8	1.5	241.9
230408	120	300	47.7	460	1.12	8	1.5	389.9
230608	120	300	47.7	460	1.68	8	1.5	452.2
230808	120	300	47.7	460	2.23	8	1.5	510.8

5.2.3 INTERFACES BETWEEN CONCRETES CAST AT DIFFERENT TIMES

Three roughness profiles are commonly adopted for interfaces between concretes cast at different times: intentionally roughened surface, free surface (left without treatment after vibration of the old concrete) and smooth surface (i.e., a surface cast against steel, plastic or specially prepared wooden molds). Data available in literature for each roughness type is scarce. In this context, the same criteria assumed in the case of monolithic concrete cracks are adopted for interfaces between concretes cast at different times. As a result, the tests considered are only the 3 (M1, M2 and M3) performed on the present work in free surfaces (see Chapter 2). Table 5-2 summarizes the specimen properties and the shear strength values measured, where f_{c1} is the compressive strength of the old concrete and f_{c2} the compressive strength of the new concrete.

Table 5-2 – Shear strength experimental data for reinforced interfaces between concretes cast at different times collected from the tests performed on this Thesis.

test	b (mm)	L (mm)	f_{c1} (MPa)	f_{c2} (MPa)	f_y (MPa)	ρ (%)	ϕ (mm)	c / ϕ	V_R (kN)
Chapter 2 – free surfaces									
M1	150	250	67.8	48.1	605	1.07	8	3.6	202.2
M2	150	250	67.8	48.1	605	1.07	8	3.6	196.2
M3	150	250	67.8	48.1	605	1.07	8	3.6	201.3

5.3 FINITE ELEMENT MODEL FOR A CONCRETE INTERFACE

In this Section 5.3, finite element modeling (FEM) approach used in the analysis of a concrete interface is presented. Initially, the FEM analyses are used to study the case in which the dowel action is the sole strength mechanism. Only the 2D Fixed Bed approach introduced in Chapter 4 is considered, due to its simplicity and applicability to this case in which the local analysis of a reinforced interface is envisaged, and not the global analysis of a real structure. That 2D FB approach is, in Chapter 5, extended in order to account simulate the aspects which affect the behavior of a concrete interface. After that, the model is upgraded to simulate the aggregate interlock between the two concretes.

5.3.1 EXTENSION OF THE DOWEL ACTION MODEL TO CONCRETE INTERFACES

In order to analyze the connection between two concrete blocks, the length of the reinforcing bar is duplicated and same is made for the Winkler springs which reproduce the deformability of the concrete substrate (see Figure 5-1). The bar node at the interface section connects to two springs. The properties of the Winkler springs that simulate each concrete block are not equal, owing to the dissimilar concrete properties.

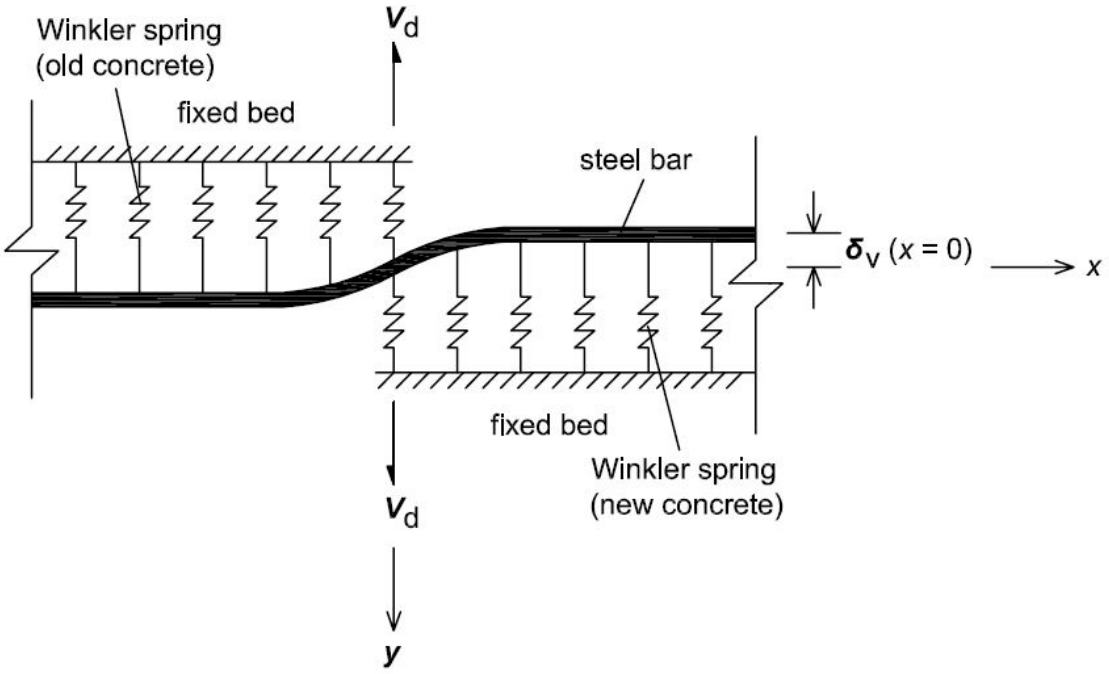

Figure 5-1 – 2D FB finite element model for analysis of the dowel action behavior of a reinforcing bar crossing a concrete interface.

The axial force in the reinforcement, induced by the interface crack opening is accounted for by adding in the model new two-node translation spring elements linking the steel bar to concrete, or to the fixed bed (that simulates the concrete substrate), in the horizontal direction. The two nodes connected are the same of Winkler vertical springs. Then, relative horizontal displacements δ_h between the reinforcement and the fixed bed give rise to bond stresses τ_b along the bar axis through the horizontal springs.

The adopted constitutive model for the bond behavior is the "tension chord model" of Marti et al. (1998), in which the $\tau_b - \delta_h$ relation follows a perfectly plastic branch. After reinforcement yielding, this type of behavior remains but the bond stress is halved. For the horizontal springs, an initial elastic stiffness calculated as $k_{sp,b} = 10^{13} \times \phi \times s_{sp}$, with ϕ and s_{sp} in m and $k_{sp,b}$ in N/m, was considered in the finite element model.

The interface slip and crack opening are simulated by imposing the displacement of the nodes belonging to one fixed bed (new concrete) with respect to the ones of the other fixed bed (old concrete). All the nodes belong to one fixed bed undergo the same displacement.

The analyses whose results are presented in this Chapter were undertaken to simulate the behavior of previously tested concrete specimens. Those analysis were performed with imposed displacements (relative movement between fixed beds which simulate both concrete blocks). The history of slip and crack opening values considered in the analysis reproduces the measured values for those parameters. The intent of the analyses if therefore the determination of the force resisted by the dowel, so that it can be compared with the force measured in the tests. For the sake of simplicity, these displacements are introduced through linear branches fitted to the measured nonlinear $w - s$.

Finally, the influence of reinforcement kinking (geometric effect) in a concrete interface is also considered, so that the model accuracy is improved and the influence of this effect can be quantified and understood. For this purpose, geometric nonlinearity is activated through a classic Total Lagrange formulation, whose background theory is available in detail in de Borst et al. (2012).

5.3.2 MODELING OF AGGREGATE INTERLOCK

The aggregate interlock mechanism can be simulated, in the finite element model, through a single interface finite element which connects two nodes. The two nodes linked are the ones which belong to the fixed bed of old and new concretes and, simultaneously belong to the y axis in Figure 5-1. It is important to note that, these two nodes are represented, in Figure 5-1, in different positions, but that is a schematic representation to improve the figure readability. In the finite element model, the position of both nodes is coincident. That is, the nodes which

represent the fixed beds for the two concretes are aligned and their position coincides, at the start of the analysis, with the *x* axis represented in Figure 5-1.

Two different approaches were followed in this thesis to study the aggregate interlock effect:

- In some of the analyses, the constitutive model to describe the aggregate interlock behavior was defined beforehand – this constitutive model expresses the normal and tangential stresses in the interface element as a function of the relative displacement between the connected nodes, in the normal and tangential direction. The modeling approach described in the previous paragraph (adoption of an interface finite element to model the aggregate interlock effect) was used only in this situation.
- In the other situation, the constitutive model to describe the aggregate interlock effect was not known beforehand. I.e., the purpose of the analysis is, precisely, the quantification of the stresses transferred between concrete blocks through the aggregate interlock mechanism. This job is performed by using the modeling approach described in Section 5.3.1., in which the transferred stresses are calculated as the sum of the reactions in the nodes corresponding to one fixed bed divided by the area of the concrete interface.

As regards the analyses with an interface finite element, an additional remark has to be made. The employed constitutive models to describe the aggregate interlock effect are different from the ones readily available in the used finite element package (TNO DIANA). Therefore, a user-supplied subroutine was utilized to input the new constitutive models in the finite element analyses. User-supplied subroutines are a useful feature of the TNO DIANA software which allow programming user-defined constitutive models to be used in the nonlinear analyses.

5.3.2.1 CONSTITUTIVE RELATION IN THE INTERFACE TANGENTIAL DIRECTION

As was mentioned in Section 5.1, on the study implemented by Feenstra et al. (1991), it was concluded that Walraven and Reinhardt (1981) formulation, among other available alternatives, has the best behavior in terms of the stability of the numerical solution and also the stress and displacement distributions along the crack. For that reason, when cracks in

monolithic concrete are studied, Equation (5-1) is considered, at first place, to define the constitutive model for the interface finite element, in terms of shear stress (stress in the tangential direction – direction *y* in Figure 5-1).

When new constitutive relations need to be determined, the adopted shape for those relations are modified versions of Equation (5-1), obtained through the introduction of new coefficients such that:

$$\tau_{\text{agg,FEM}} = C_{\text{f}*}\left\{a_1 f_{\text{cc}} + \left[b_1 w^{c_1} + \left(d_1 w^{e_1} + f_1\right) f_{\text{cc}}\right] s\right\} \tag{5-3}$$

or

$$V_{\text{agg,FEM}} = C_{\text{f}*}\left\{a_1 f_{\text{cc}} + \left[b_1 w^{c_1} + \left(d_1 w^{e_1} + f_1\right) f_{\text{cc}}\right] s\right\} \times b \times L \tag{5-4}$$

in which coefficients $C_{\text{f}*}$ to f_1 are calculated through the Nonlinear Generalized Reduced Gradient optimization algorithm of Lasdon et al. (1978). The automatic implementation of this algorithm is included in the Microsoft Excel Solver tool and its background theory can be consulted in detail on Coello and Coello (2007). The coefficients $C_{\text{f}*}$ to f_1 are calculated aiming to minimize the difference d

$$d = \left|V - V_{\text{FEM}}\right| \tag{5-5}$$

In this expression for the difference d, V is the shear force measured in experimental tests, and V_{FEM} is the calculation result, given by the sum of $V_{\text{agg,FEM}}$ calculated in Equation (5-4) and the dowel force $V_{\text{d,FEM}}$ obtained in the finite element model described in Section 5.3.1:

$$V_{\text{FEM}} = V_{\text{agg,FEM}} + n \times V_{\text{d,FEM}} \tag{5-6}$$

where n is the number of bars crossing the interface.

It is important to note that lower d values not always correspond to meaningful coefficient values, and very high (tending to infinite) values were reached. Besides that, in some situations different coefficient values resulted in similar differences d. To surpass these issues,

the coefficients in Equation (5-3) take the value displayed in Equation (5-1) whenever possible.

5.3.2.2 CONSTITUTIVE RELATION IN THE INTERFACE NORMAL DIRECTION

The relationship given by Equation (5-2) was derived from tests in which the interface crack opening is restrained by external, unbonded, reinforcing bars. The stiffness of such a confining system can be significantly different from the one provided by embedded reinforcing bars. Therefore, it is not surprising that Equation (5-2) does not provide an accurate representation of the normal stress in interfaces crossed by embedded bars, such as the ones studied in the present chapter. In this work, the actual normal stress at the interface is calculated in analyses according to the approach described in Section 5.3.1. It is therefore given by:

$$\sigma_{\mathrm{n}} = \frac{n \times F_{\mathrm{s,x}}}{b \times L} \tag{5-7}$$

and the corresponding normal force at the interface is given by:

$$N = n \times F_{\mathrm{s,x}} \tag{5-8}$$

where $F_{\mathrm{s,x}}$ is the bar force component at the interface section ($x = 0$) in the x axis direction (see Figure 5-1).

5.4 RESULTS FOR DOWEL ACTION IN CONCRETE INTERFACES

The assessment of dowel action behavior in a concrete interface will be made at first in a finite element model reproducing the characteristics of the specimens M1, M2 and M3 tested in the present Thesis (see Table 5-2 and Chapter 2). This evaluation will mainly focus on the following issues: dowel strength, displacements and curvatures, influence of crack opening and influence of the reinforcement kinking effect. Although the case study corresponds to an

interface crossed by 8 reinforcing bars, dowel force values presented in this Section 5.4 will refer to a single bar.

Later, the finite element model results will be compared with the experimental data of Soroushian et al. (1986). In this comparison, the model parameters are in correspondence with the properties of those specimens. For the steel stress-strain ($\sigma_s - \varepsilon_s$) relation assumed in the model, the same behavior characterized in Figure 4-8 is maintained, but with yield stress f_y = 414 MPa. In turn, the tensile strength f_t is estimated as 1.05 x f_y.

In all dowel action finite element analyses hereinafter performed in this Thesis, spring spacing s_{sp} is equal to 4 mm.

5.4.1 DOWEL STRENGTH

Figure 5-2 illustrates results obtained for dowel force versus interface slip in the finite element model. Three cases were studied: 1 – both sides of the reinforcing bar embedded in the old concrete (f_c = 67.8 MPa), 2 – both sides of the reinforcing bar embedded in the new concrete (f_c = 48.1 MPa), 3 – bar embedded in the old concrete on one side and in the new concrete on the other side. In the third case, representing an interface between concretes cast at different times, the results revealed that its dowel force $V_{d,old+new}$ is approximately equal to the average of the results for cases 1 and 2, $V_{d,old}$ and $V_{d,new}$. For all the load steps in the analysis, the following ratio r was calculated:

$$r = \frac{V_{d,old+new}}{0.5 \times \left(V_{d,old} + V_{d,new} \right)} \tag{5-9}$$

and a mean value μ = 0.987 was achieved, with a standard deviation σ = 0.007.

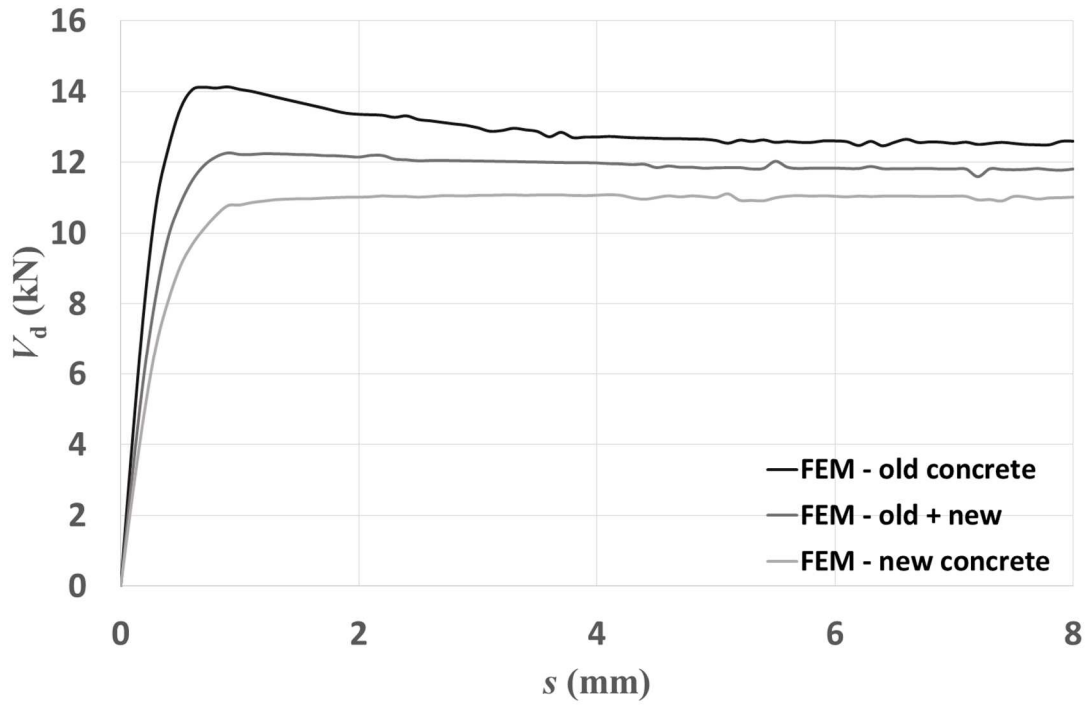

Figure 5-2 – Dowel force versus slip obtained in the finite element model (FEM) for a crack in the old concrete (f_c = 67.8 MPa), a crack in the new concrete (f_c = 48.1 MPa) and for an interface between those two concretes.

5.4.2 DISPLACEMENTS AND CURVATURES

The reinforcement vertical displacements δ_v for the interface between concretes cast at different times obtained in the analysis can be seen in Figure 5-3 for several load steps. As expected, a greater contribution to shear slip is observed in the concrete with lower compressive strength (new concrete).

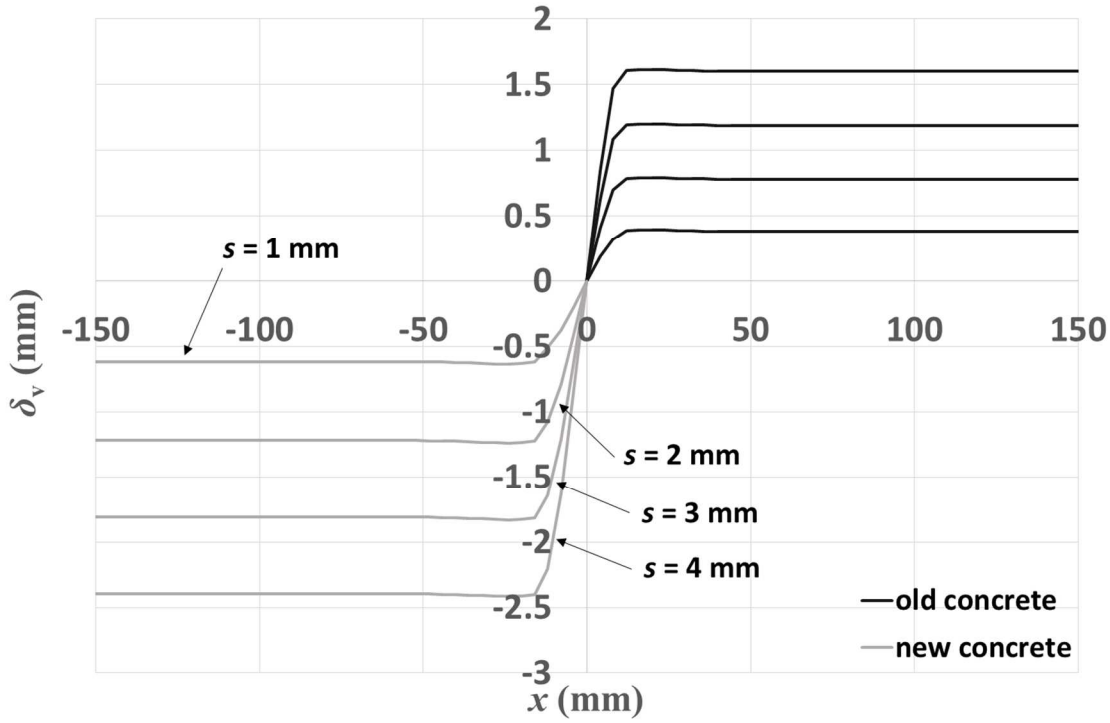

Figure 5-3 – Reinforcement vertical displacement obtained in FEM for a concrete joint.

In turn, Figure 5-4 shows the variation of the vertical displacement along bar axis when s = 1 mm and s = 4 mm, normalized with respect to the displacement at the crack section. As can be seen, the vertical displacement in the concrete with higher compressive strength (old concrete) reaches 0 at a section x closer to the crack. This behavior is coherent with the Beam resting on an Elastic Foundation analogy (BEF), where the section x for which the reinforcement vertical displacement is 0 depends on the concrete strength and is given by $x / \phi = 4.3 / f_c^{0.175}$. However, x values achieved in the two approaches do not exactly match since yielding is very much present when s = 4 mm. The finite element model accounts reinforcement yielding and, because of this effect, the reinforcement vertical displacements become more concentrated at bar sections near the crack.

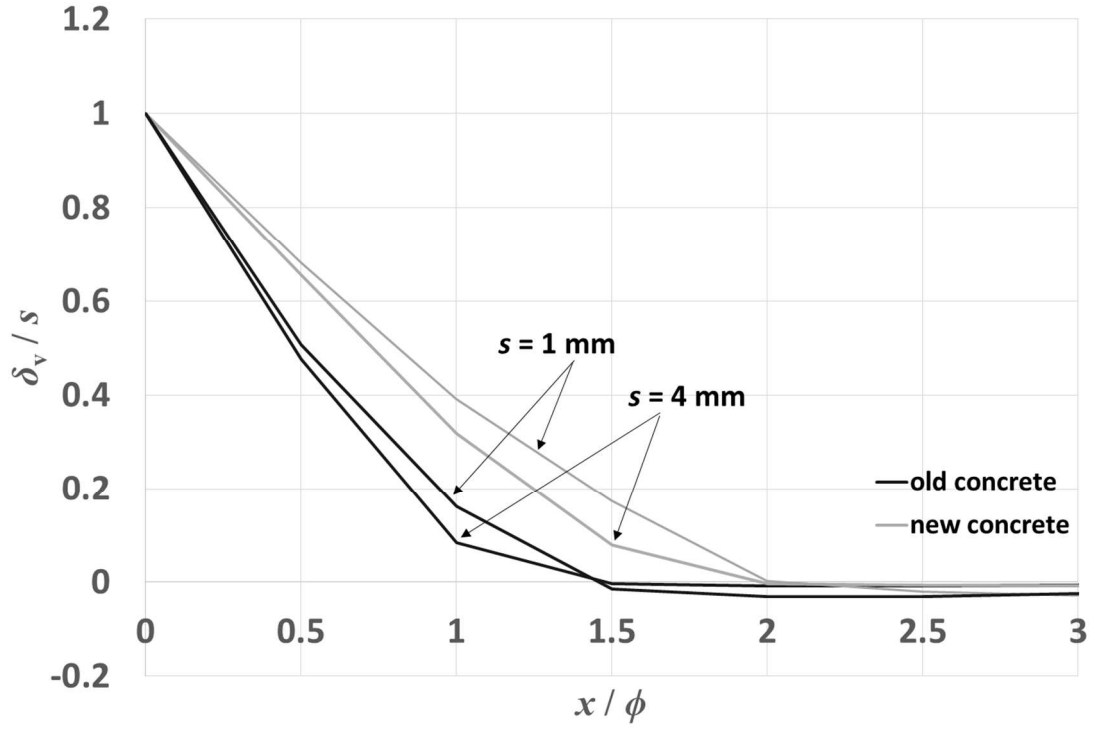

Figure 5-4 – Variation of reinforcement vertical displacement obtained in FEM along bar axis, when s = 1 mm and s = 4 mm.

Figure 5-5 – a) presents the ratio χ / χ_y, where χ is reinforcement curvature and χ_y = 0.757 m^{-1} is the curvature at onset of section yielding. In the old concrete, the steel bar plastic hinge was formed at a distance of 8 mm (equal to the bar diameter) from the interface for low slip values (s < 1 mm). In the new concrete, curvature values are lower and the bar section at which curvature is maximum locates at x = 12 mm (1.5 times the bar diameter).

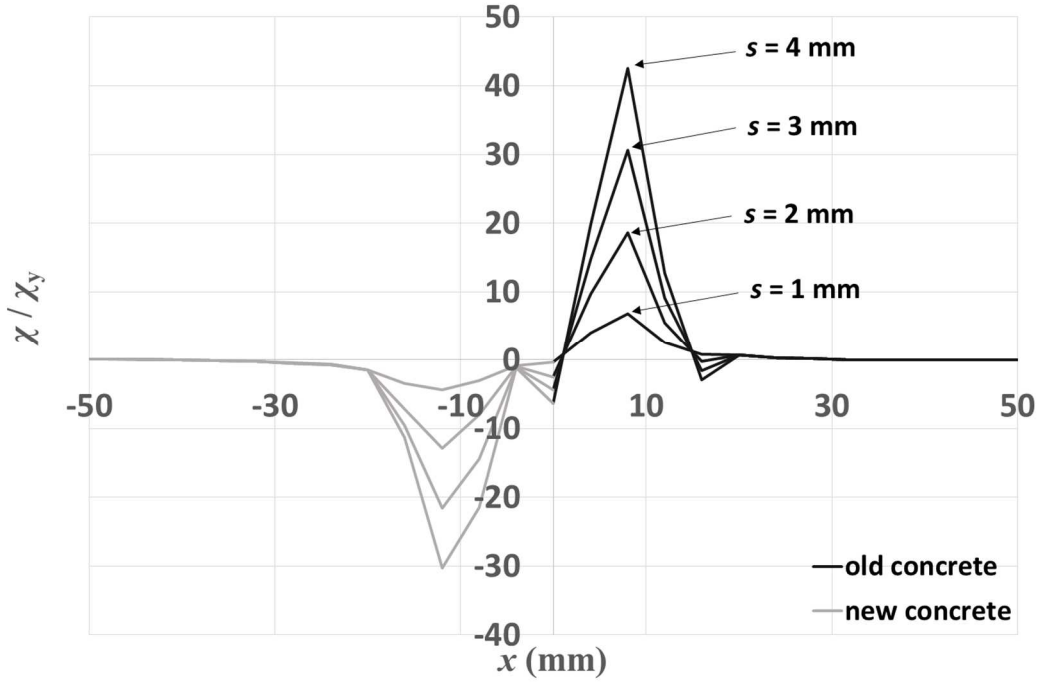

a)

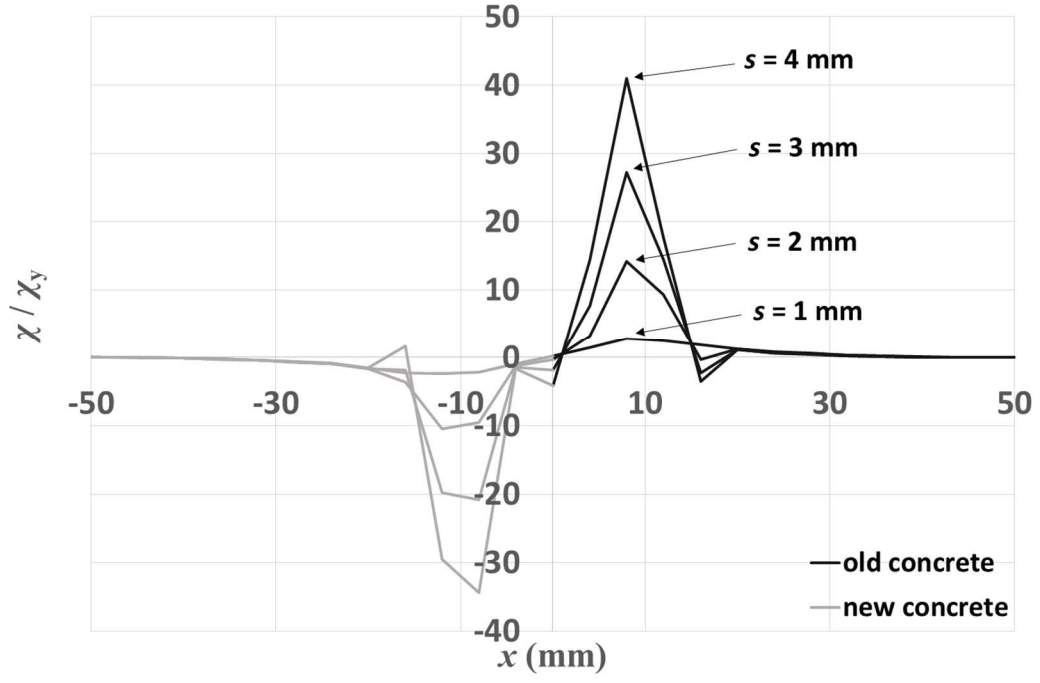

b)

Figure 5-5 – Reinforcement curvature χ obtained in FEM for a concrete joint, where χ_y is curvature at onset of section yielding: a) new concrete of the case study with f_c = 48.1 MPa; b) new concrete having f_c = 29.5 MPa.

Regarding the position of the bar section at which curvature is maximum, it actually varies with slip, besides concrete strength. However, with spring spacing s_{sp} equal to 4 mm, that variation could not be detected for the two concretes studied. When the new concrete compressive strength is altered to f_c = 29.5 MPa (see results in Figure 5-5 – b), the change of the position changing becomes evident. For s = 1 mm, the maximum curvature occurs at x = 16 mm (2 times the bar diameter). These results are consistent with the Dei Poli et al. (1992) curvature measurements on specimens with concrete strength f_c = 30.8 MPa.

The curvature χ_t at the instant when the steel tensile strength is reached is equal to 11.438 m^{-1} and χ_t / χ_y = 15.114. This value was reached at approximately s = 2 mm for both concretes, still an early stage of the total slip imposed.

The FEM results can be sensitive to the discretization adopted for the steel bar, because of yielding effects. The analysis approach and discretization adopted were considered to be valid for purposes envisaged in this work, because the calculated bar curvature profiles have a satisfactory agreement with the experimental results measured by Dei Poli et al. (1992). Nevertheless, further analyses of this type of problem should be conducted in the future for a deeper understanding of the implications of the bar discretization approach.

5.4.3 INFLUENCE OF CRACK OPENING

In the analyses whose results were shown before, the crack opening was taken as zero.

In order to evaluate the influence of crack opening in a concrete joint, the experimentally measured $w – s$ relation of specimens M1, M2 and M3 was assumed. Since a small variability was observed in the results of these 3 tests, average values are considered. Figure 5-6 shows the analysis results (labelled with “crack opening”), and compares them with the previously calculated ones (labelled with “no crack opening”).

At the beginning of the imposed displacements, no differences are observed. As the slip grows, the reinforcing bar of the specimen with crack opening yields first, and the resulting dowel force has lower values. For large displacements, most of the Winkler springs enter the residual force branch and reinforcement curvatures and displacements cease to alter the dowel force mobilized. Thus, crack opening influence fades away.

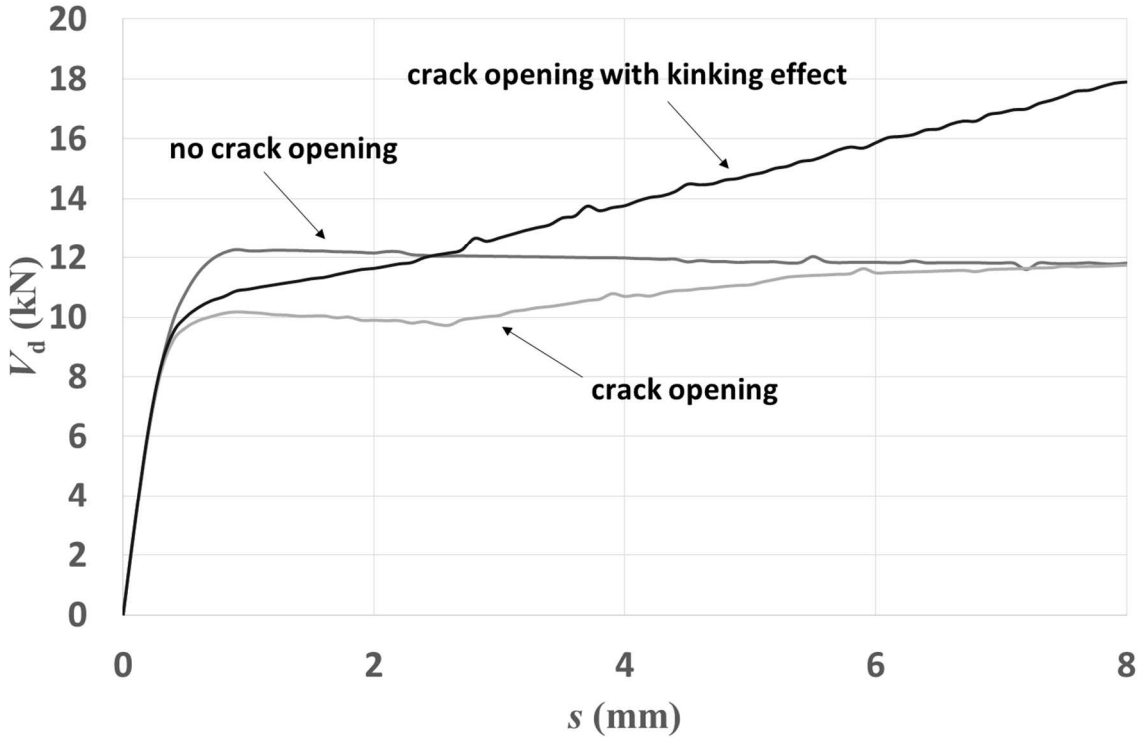

Figure 5-6 – Influence of crack opening and kinking effect in dowel force versus slip behavior of a concrete joint.

In Figure 5-7, reinforcement axial stress, calculated from its axial force F_s and the corresponding transverse section area A_s, can be seen in the response with no kinking effect activated. Initially, the behavior is linear. Then, yielding occurs for a very low slip value (s = 0.30 mm). For $s > 2$ mm, after curvature χ_t is reached, reinforcing bar hinge becomes perfectly plastic and the reinforcement axial force starts to drop significantly until $F_s / A_s = 0$.

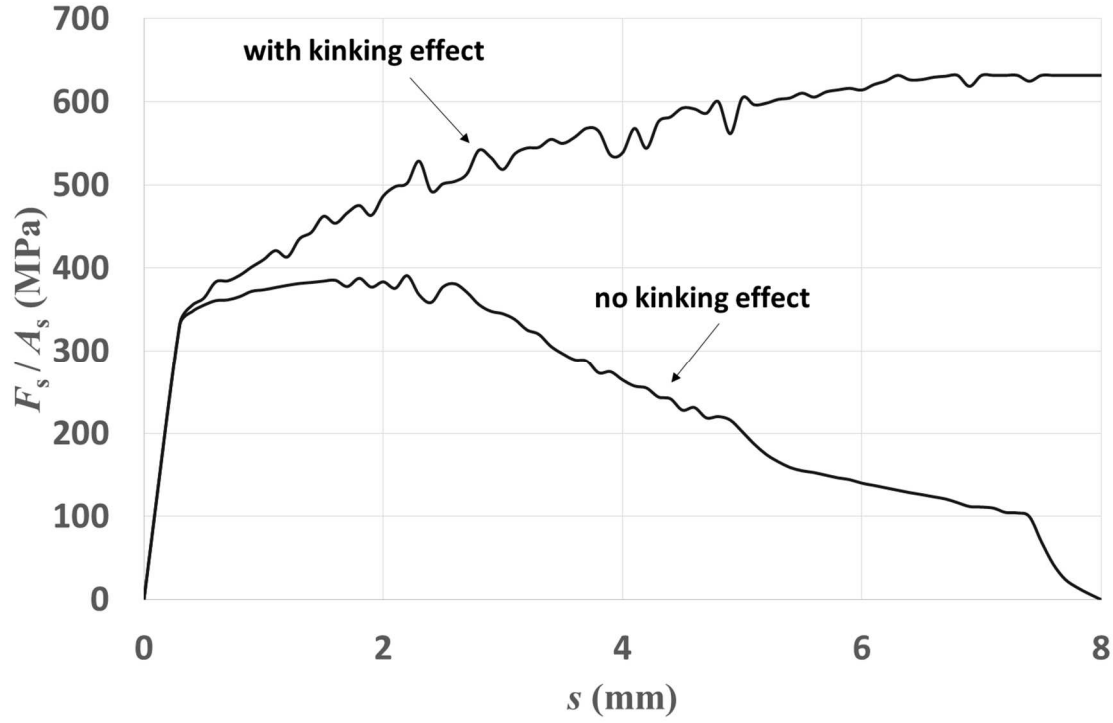

Figure 5-7 – Reinforcement average stress in FEM for an interface subjected to slip and crack opening imposed displacements.

Figure 5-8 – a) depicts the variation of the average axial stress along the length of the reinforcement. A local minimum can be identified near the section of maximum curvature. At s = 2 mm, before curvature χ_t is reached, that local minimum is still not evident. When s > 2 mm, the finite element model equilibrium is established with reinforcing bar bending moment increasing, and consequently dowel force as well, at the expense of a decrease in the bar axial force.

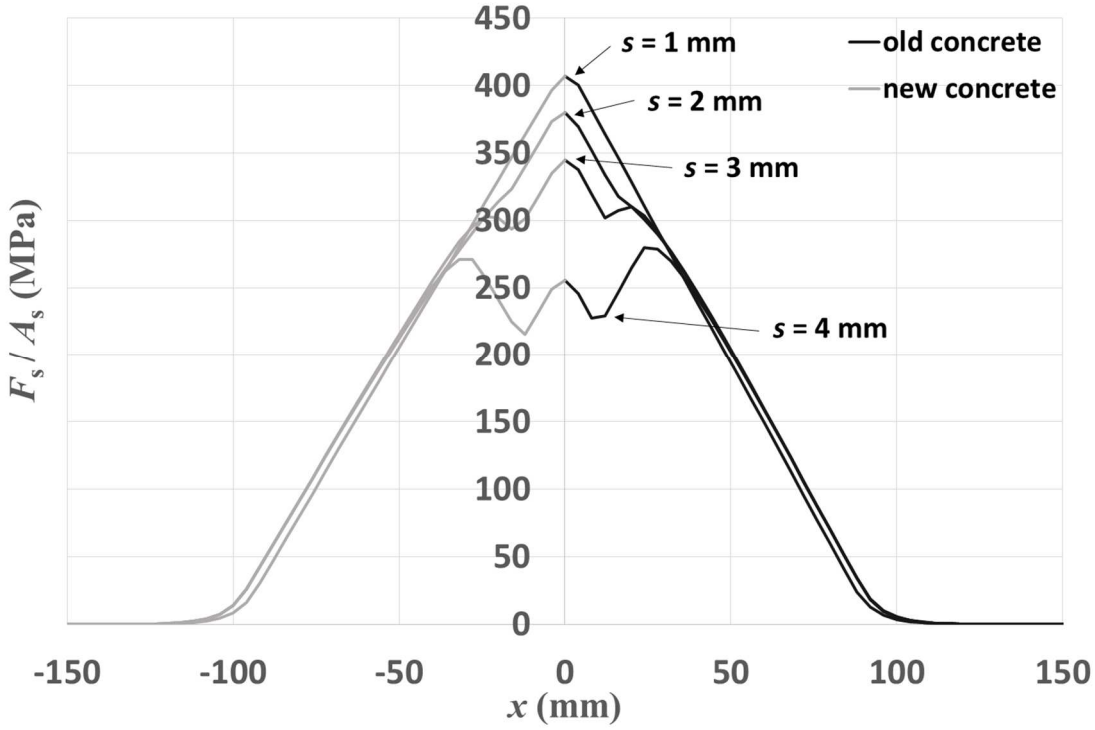

a)

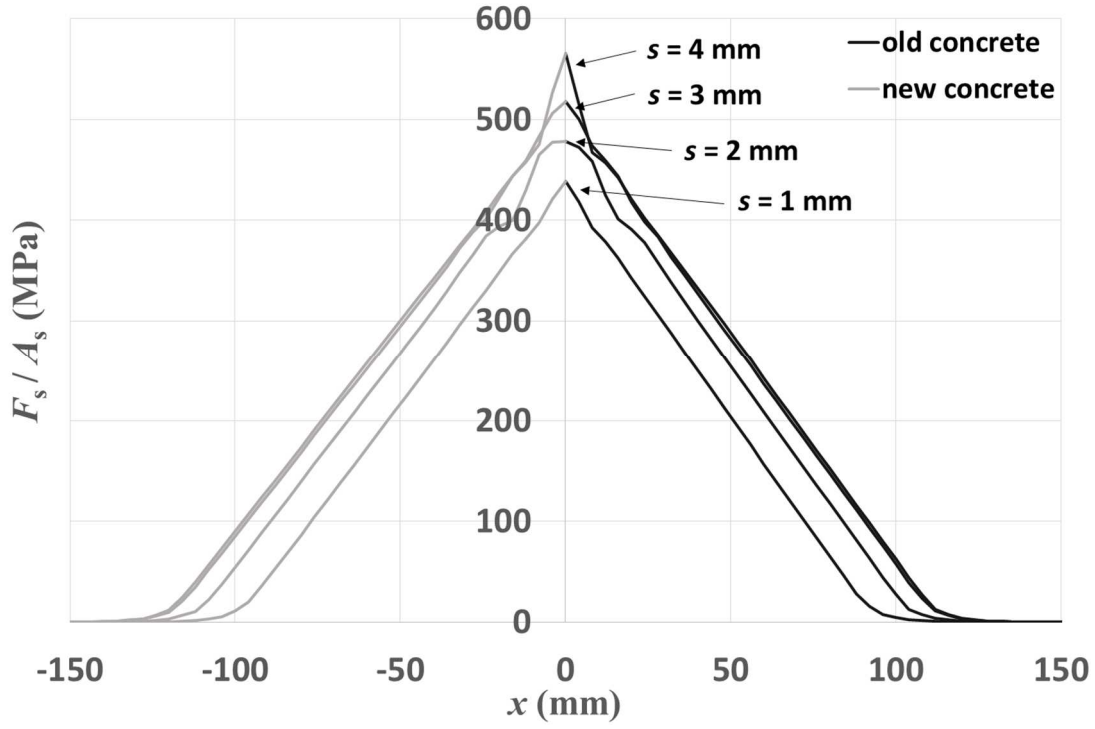

b)

Figure 5-8 – Reinforcement average stress along bar length in FEM for an interface subjected to slip and crack opening displacements: a) no kinking effect; b) with kinking effect.

5.4.4 INFLUENCE OF THE KINKING EFFECT

This section discusses the results of analysis in which the geometrical non-linearity is activated, so that the kinking effect can be assessed.

The FEM results achieved in the analysis showed a substantial influence of the kinking effect on the reinforcement dowel behavior, particularly for large slip values. This type of response (FEM results shown in Figure 5-6) matches experimental results commonly observed in tests of concrete interfaces when the dowel action is the predominant strength mechanism. It was detected in the tests performed on the present work, but also in the tests of Soroushian et al. (1986) and Vintzeleou and Tassios (1987).

The geometric effect becomes significant right after the formation of the plastic hinge, and the rotation of the reinforcement axis at the intersection with the interface starts to be significant. When the bar rotates, its axial force acquires a component in the direction of the interface plane directly contributing to dowel shear strength. With slip growing, rotation increases and dowel strength provided by the kinking effect expands.

Figure 5-7 illustrates reinforcement average axial stress (F_s / A_s) for both conditions (with and without the geometric effect) and a significant difference can be seen in the graphs. When the kinking effect is activated, the model equilibrium conditions change, with the inclusion of the reinforcement axial force component along the direction of the interface plane. Consequently, the average axial stress on the reinforcing bar does not decrease as the slip increases, and the values achieved in this situation resemble the type of response of a steel bar subjected to axial loading. Figure 5-8 – b) also reveals the differences in the reinforcement axial force caused by the activation of geometric nonlinearity in the finite element model. No local minimum in the stress values is now visible.

5.4.5 COMPARISON WITH EXPERIMENTAL DATA

To the author knowledge, no experimental test have been conceived yet to provide a complete characterization of the dowel strength (including kinking effects) without any contribution from the aggregate interlock mechanism. With this limitation in mind, an

exploratory study is presented in this section, by comparing FEM results with the tests of Soroushian et al. (1986).

In the Soroushian et al. (1986) tests (T4, T6 and T8 specimens), the average value obtained for coefficient K in Table 4-2 was 1.71, a high value compared to the reference K = 1.45 of Dei Poli et al. (1992) tests. But since this variation is not as significant as in other experimental campaigns, the reinforcement kinking effect can be an explanation for the difference and not necessarily aggregate interlock. Kinking effect of the reinforcing bars (geometric nonlinearity) is included in the dowel action finite element model developed. Therefore, a comparison of model results with the experimental measurements in those tests may be relevant.

Figure 5-9 presents the finite element model outcomes for specimens T4, T6 and T8, and a good fit is only noticed for low slip values. Aggregate interlock interaction in dowel strength can be seen in specimens T4 and T6, which have greater strength comparing to the models.

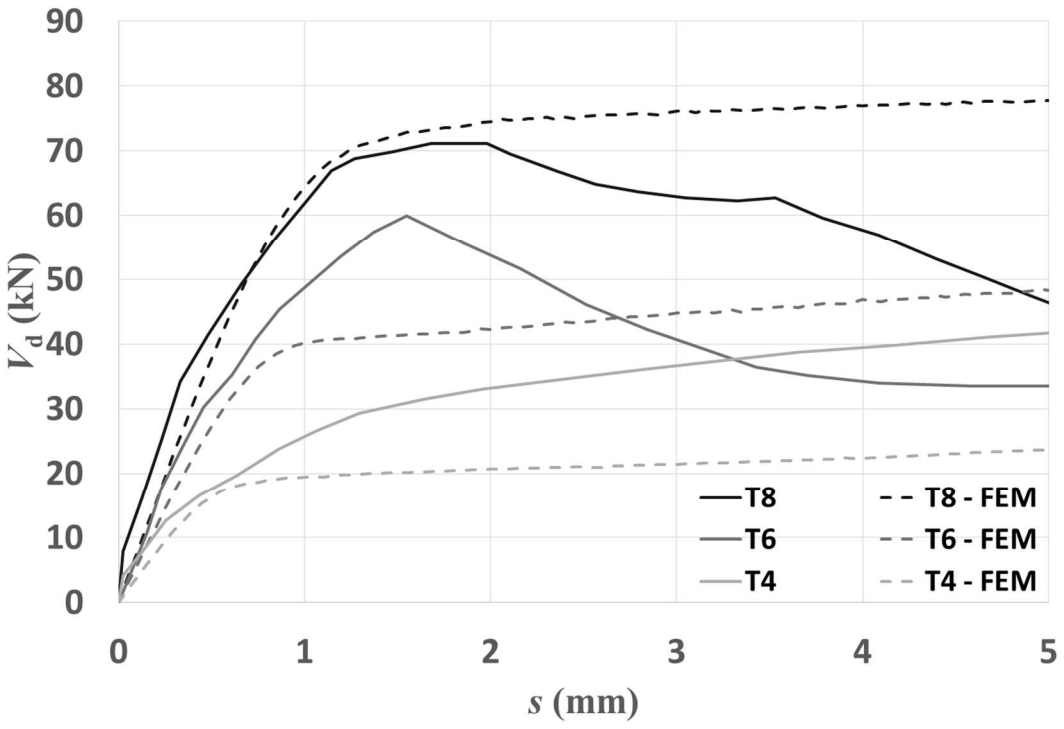

Figure 5-9 – Comparison of the Soroushian et al. (1986) experimental tests on concrete interfaces with FEM results.

In the T6 test, failure by concrete splitting is also identified. This effect was not included in the model, which accounted on Equation 4-48 for the influence of lateral concrete cover length. In the T6 specimen, $c / \phi = 3.4$, which leads in Equation 4-48 to $\sqrt{\beta_{cov}} = 1$. Thus, dowel strength is not affected by insufficient concrete cover. Results acquired for the T6 test did not revealed that behavior, and several reasons can be formulated to understand the fact. In this context, it is relevant to mention that the same situation happened in the tests DM2 and DM3 performed on the present work, which had $c / \phi = 3.6$.

One possible reason is that the theoretically calculated $c / \phi = 3.4$ for test T6, or $c / \phi = 3.6$ for tests DM2 and DM3, were not real due to deviations that can happen in the specimens manufacturing. Other possibility is the variability inherent to the phenomenon, which is still not very much known. Finally, Equation 4-48 may not be the most accurate. However, Equation 4-48 has the advantage of being sustained by experimental data that was obtained in tests specifically developed to assess the influence of lateral concrete cover on dowel strength or concrete bearing strength. Moreover, Vintzeleou and Tassios (1987) (see Table 4-1) tests with $c / \phi = 2.9$, do not show any dowel force decrease caused by insufficient concrete cover. Actually, V_d grew continuously due to reinforcement kinking effect. These tests were not compared with the finite element model because crack opening was not measured by the authors (Vintzeleou and Tassios 1987).

Regarding specimen T8, the crack opening values measured are the highest among the specimens tested by Soroushain et al. (1986). Therefore, presumably the aggregate interlock also contributed to the strength of this specimen. However, the experimental $V_d - s$ graph does not show a clear evidence of that mechanism, since the measured strength is slightly inferior to the one in the FEM results (which do not include any estimate for the aggregate interlock effect). The most reliable explanation for the fact seems to be the effect of lateral concrete cover length ($c / \phi = 3.4$ in this test) and splitting on the dowel behavior. This effect is, presumably, much more significant than the expected in the FEM, which accounted on Equation 4-48. It is also much more significant than what is observed in specimen T6, whose experimental strength is superior comparing to the model results.

5.5 RESULTS FOR AGGREGATE INTERLOCK IN CONCRETE INTERFACES

Once a detailed FEM methodology is available for calculating the contribution of the dowel action mechanism, the aggregate interlock effect in the experimental tests considered in this work can be isolated and determined. Besides the influence of parameters as the concrete strength, steel yield stress and reinforcement ratio, shear transfer by aggregate interlock largely depends on the interface roughness. Therefore, different constitutive relations should be defined for each roughness profile type.

5.5.1 CRACKS IN MONOLITHIC CONCRETE

5.5.1.1 FIRST ANALYSIS USING THE CONSTITUTIVE RELATION OF WALRAVEN AND REINHARDT

In a first analysis, Equation (5-1) with $C_f = 1$ is considered for shear transfer by aggregate interlock in the tangential interface direction. The calculation output showed that the experimental shear strength values V_R are significantly higher than the strength $V_{R,FEM,1}$ achieved in this finite element first analysis (see Figure 5-10 – a)). These results are summarized in Table 5-3, where the relation V_R / $V_{R,FEM,1}$ has an average value of $\mu = 1.31$ and standard deviation $\sigma = 0.15$. This difference between V_R and $V_{R,FEM,1}$ notably increases with the concrete strength. It also increases with reinforcement ratio, but more lightly.

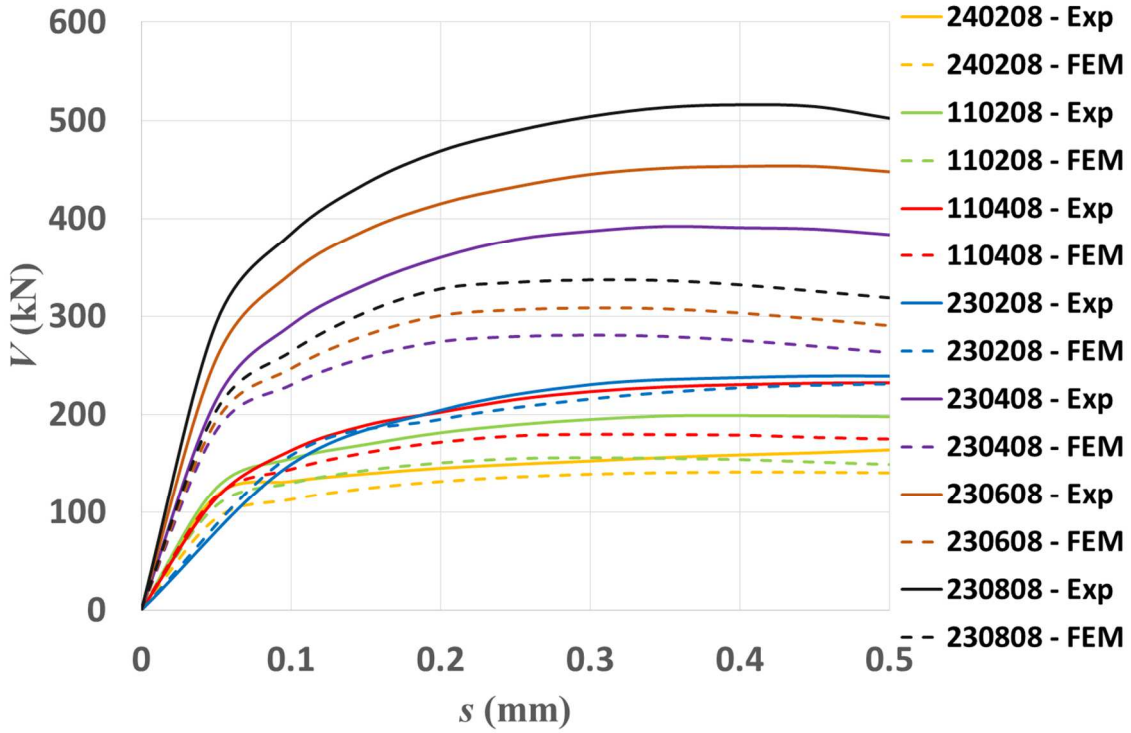
600
500
400
300
200
100
0
V (kN)
0
0.1
0.2
0.3
0.4
0.5
s (mm)
240208 - Exp
240208 - FEM
110208 - Exp
110208 - FEM
110408 - Exp
110408 - FEM
230208 - Exp
230208 - FEM
230408 - Exp
230408 - FEM
230608 - Exp
230608 - FEM
230808 - Exp
230808 - FEM

a)

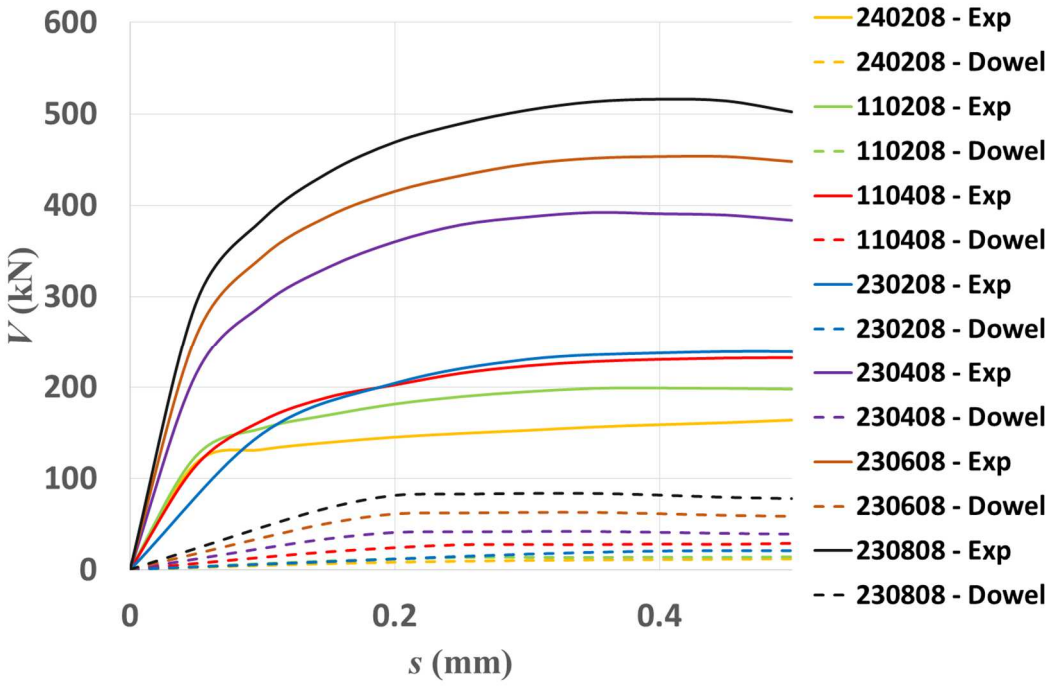
600
500
400
300
200
100
0
V (kN)
0
0.2
0.4
s (mm)
240208 - Exp
240208 - Dowel
110208 - Exp
110208 - Dowel
110408 - Exp
110408 - Dowel
230208 - Exp
230208 - Dowel
230408 - Exp
230408 - Dowel
230608 - Exp
230608 - Dowel
230808 - Exp
230808 - Dowel

b)

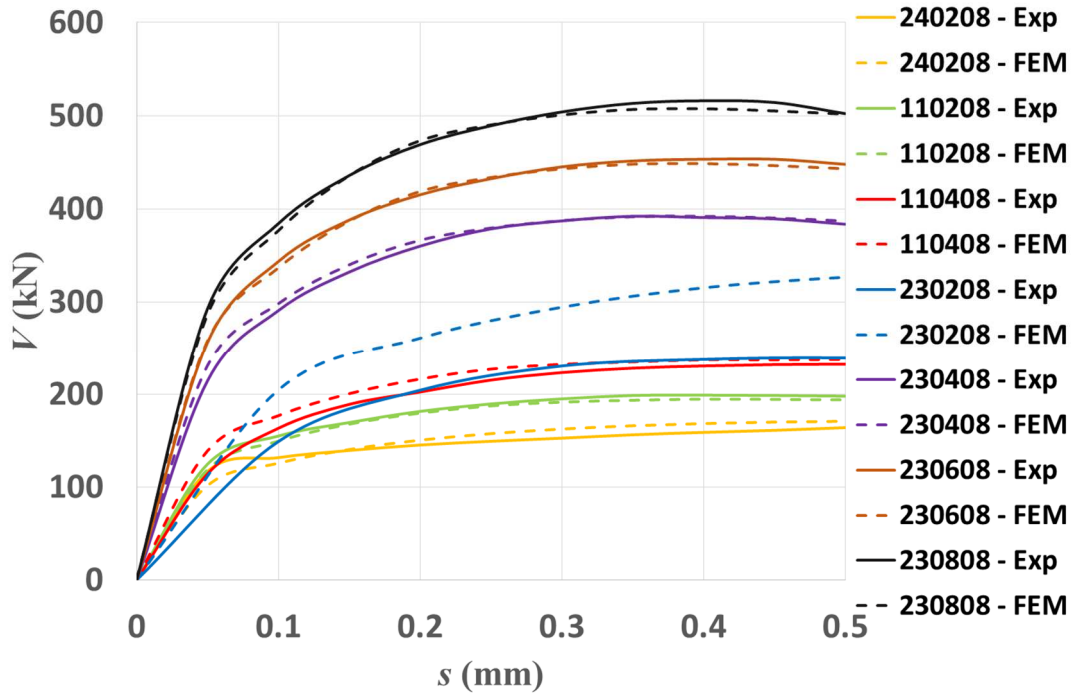

c)

Figure 5-10 – Comparison of Walraven and Reinhardt (1981) experimental tests with FEM results: a) first analysis considering Equation (5-1); b) values for reinforcement dowel action; c) second analysis considering an improved constitutive relation for aggregate interlock.

Table 5-3 – Comparison of Walraven and Reinhardt (1981) experimental values with FEM results obtained in the two analyses implemented: 1 – V_{FEM} considering Equation (1); 2 – V_{FEM} considering the improved constitutive relation for aggregate interlock.

test	V_R (kN)	$V_{R,FEM,1}$ (kN)	V_R / $V_{R,FEM,1}$	$V_{dR,FEM}$ (kN)	$V_{dR,FEM}$ / V_R	$V_{R,FEM,2}$ (kN)	V_R / $V_{R,FEM,2}$
Walraven and Reinhardt 1981							
240208	167.4	140.9	1.19	12.09	0.072	171.1	0.98
110208	198.8	156.1	1.27	14.48	0.073	194.4	1.02
110408	231.8	180.0	1.29	28.95	0.125	237.4	0.98
230208	241.9	231.7	1.04	20.98	0.087	337.5	0.72
230408	389.9	280.5	1.39	41.96	0.108	392.3	0.99
230608	452.2	308.7	1.46	62.94	0.139	448.3	1.01
230808	510.8	337.3	1.51	83.91	0.164	507.5	1.01
		μ	1.31				0.96
		σ	0.15				0.10

In terms of dowel forces, the contribution to interface shear transfer is residual, varying from 7.2 % in the 110208 specimen to 16.4 % in the 230808 specimen (see Figure 5-10 – b)).

The discrepancy between these experimental measurements and the FEM outcome is evident, and can be attributed to the fact that Equation (5-1) is not valid in this case. It should be remembered that the equation was fitted to the results of tests in specimens without embedded reinforcement. The steel/concrete bond increases stiffness in the normal direction of the interface and, consequently, shear strength. In order to include this phenomena in the finite element model, a second analysis is implemented.

5.5.1.2 SECOND ANALYSIS WITH AN IMPROVED CONSTITUTIVE RELATION FOR AGGREGATE INTERLOCK

The Walraven and Reinhardt (1981) constitutive relations of Equations (5-1) and (5-2) result from an empirical approach to the experimental values and are simple to use in a finite element analysis. These relations provide better results in terms of convergence of the numerical solution comparing to other approaches (Feenstra et al. 1991). Therefore, upgrades on Equation (5-1) aiming to include the bond mechanism should maintain the same advantages. These upgrades follow the procedure described in section 5.3.2.1 when new constitutive relations for aggregate interlock are needed.

Different possibilities for the new improvements in Equation (5-1) were tested. It was concluded that the discrepancy between the experimental measurements and the finite element outcome mainly occurs in the shear strength values. Thus, a change in the coefficient C_f should be considered at first place, with the inclusion of the parameters interacting in the bond mechanism: concrete strength, reinforcement ratio and steel yield stress. In this context, it was mentioned that concrete strength has a bigger influence on the difference between V_R and $V_{R,FEM,1}$ than the reinforcement ratio. To take this fact into account, the contribution of the two parameters were separated and the following expression for the new coefficient C_{f*} was reached:

$$C_{f*} = 1 + a_2 \times f_{cc} + b_2 \times \rho \times f_y \tag{5-10}$$

where a_2 and b_2 are coefficients determined through optimization algorithms (Coello Coello 2007; Lasdon 1978) in order to approximate $V_{R,FEM}$ to V_R. For that purpose, a good experimental basis is available in the experimental tests of Walraven and Reinhardt (1981) (see Table 5-1), since four reinforcement ratios (2.57 %, 5.14 %, 7.71 % and 10.28 %) and three concrete strengths (16.9 MPa, 26.1 MPa and 47.7 MPa) were considered for the specimens. The values attained for the coefficients a_2 and b_2 were:

$$a_2 = 0.00422$$

$$b_2 = 0.0395$$

It was concluded that additional improvements could be made in the aggregate interlock model in order to fit the experimental behavior. A much better adjustment to the experimental results was achieved with new values for the coefficients e_1 and f_1 expressed in Equation (5-3). Instead of e_1 = -0.707 and f_1 = -0.20, these new values are proposed:

$$e_1 = -0.673$$

$$f_1 = -0.17$$

Then, aggregate interlock contribution in a monolithic concrete crack with reinforcing bars can be calculated as:

$$\tau_{agg} = C_{f*}\left\{-0.0333 f_{cc} + \left[1.8 w^{-0.8} + \left(0.234 w^{-0.673} - 0.17\right) f_{cc}\right] s\right\} \quad (5\text{-}11)$$

The improvements achieved with these new coefficients are represented in Figure 5-10 – c) and in Table 5-3, where $V_{R,FEM,2}$ is the shear strength obtained in the finite element model for this second analysis. Now, the relation V_R / $V_{R,FEM,2}$ has an average value of μ = 0.96 and standard deviation σ = 0.10.

It can be noticed in the results that specimen 230208 diverges from all the others, having $V_{R,FEM,2}$ significantly higher than V_R. In this case, the difference between the two values occurs because the ratio (ρ x f_y) / f_c for the test is equal to 0.054 and very low. In Chapter 3 (Section 3.3.1), it was mentioned that when (ρ x f_y) / f_c < 0.075, approximately, normal stress on the interface is not enough to cause plasticity in the contact areas between the two concretes. Therefore, the cohesion mechanism is not mobilized and aggregate interlock is only provided by shear friction. Since the aggregate interlock behavior is different in these

situations, Equation (5-10) and the new coefficients e_1 and f_1 should apply exclusively when $0.075 < (\rho \times f_y) / f_c < 0.25$. For $(\rho \times f_y) / f_c < 0.075$, the conception of an aggregate interlock modeling approach requires more experimental data than just one single test.

It is important to mention that Equation (5-1) was calibrated by Walraven and Reinhardt (1981) for slip values up to 2.5 mm in tests on cracks in monolithic concrete restrained by external bars. In the tests on cracks with embedded bars only slip values up to 0.5 mm are available. The new coefficients of Equation (5-11) were calibrated for the interface response in that range. Nevertheless, the stress softening behavior traduced in Equation (5-1) for large slip values is maintained in Equation (5-11), as is depicted in Figure 5-11 referring to the 230808 test (see Table 5-1).

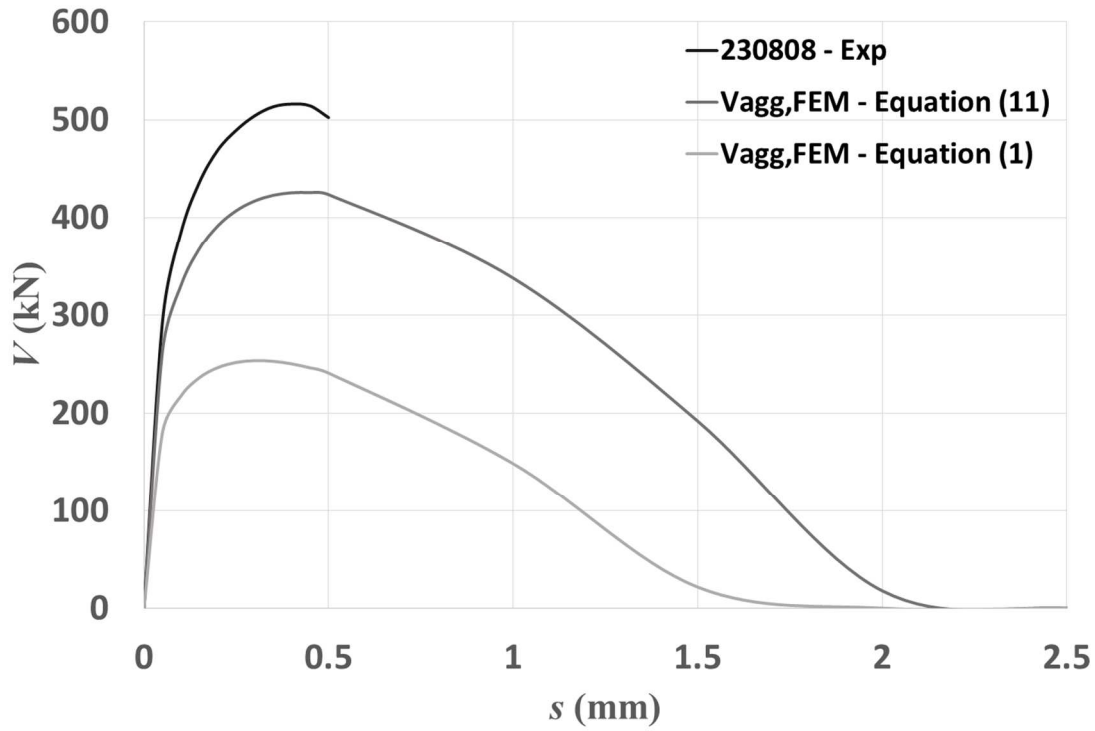

Figure 5-11 – Comparison of Walraven and Reinhardt (1981) experimental test 230808 with FEM results for aggregate interlock force calculated by Equation (5-1) and Equation (5-11).

Figure 5-12 – a) presents $\tau_{agg} - s$ graphs calculated from Equation (5-11) for several crack opening values, with $C_{f^*} = 1.64$ and $f_{cc} = 56.1$ MPa corresponding to the 230808 test (see Table 5-1). The same type of graphs are shown in Figure 5-12 – b) with τ_{agg} calculated from

Equation (5-1), in which C_f = 1 and f_{cc} = 56.1 MPa. As can be seen, the linear response observed in the Equation (5-1) graphs is conserved when the new coefficients are introduced. Differences are mainly detected in the fact that Equation (5-11) provides higher values for τ_{agg}.

As a final remark, it is important to note that, even though the database of experimental results considered in the calibration of Equation (5-11) includes different f_{cc} and ρ values, all the test specimens have embedded reinforcement with a diameter of 8 mm. Therefore, in the scope of this Thesis, it was not possible to extend the calibration and validation of the aggregate interlock model to different bar diameters. The stiffness of the reinforced interface in the direction normal to the crack not only depends on the f_{cc} and ρ values but also on the bar diameter. For that reason, further calibration is recommended before the proposed model can be applied in accurate calculations of stresses due to aggregate interlock, in interfaces crossed by bars of significantly different diameter.

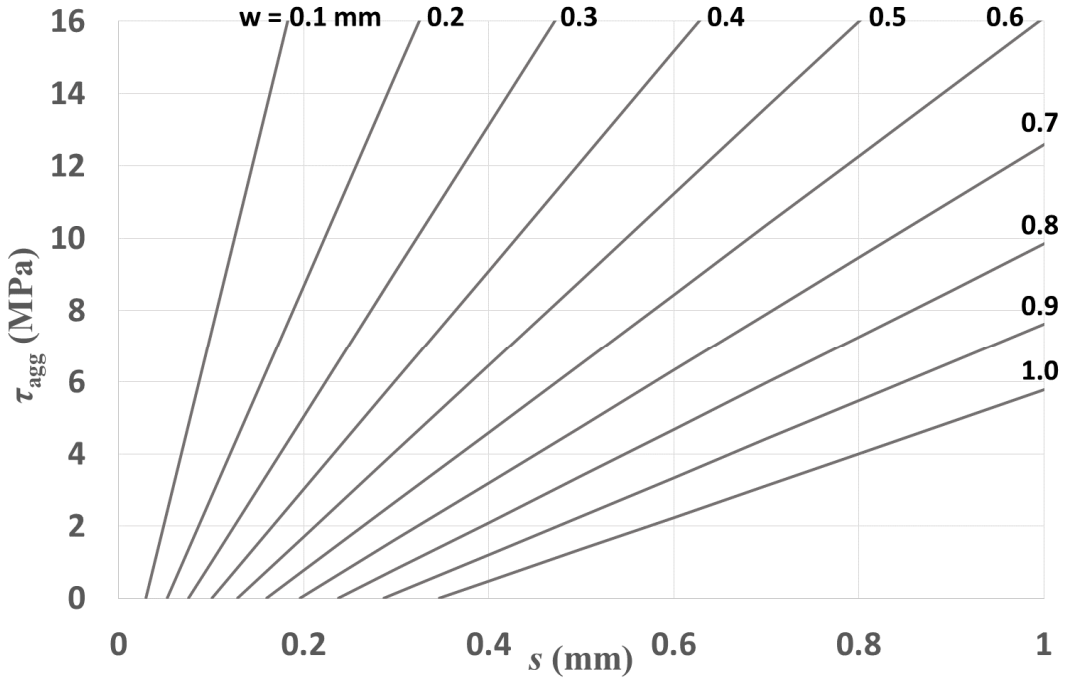

a)

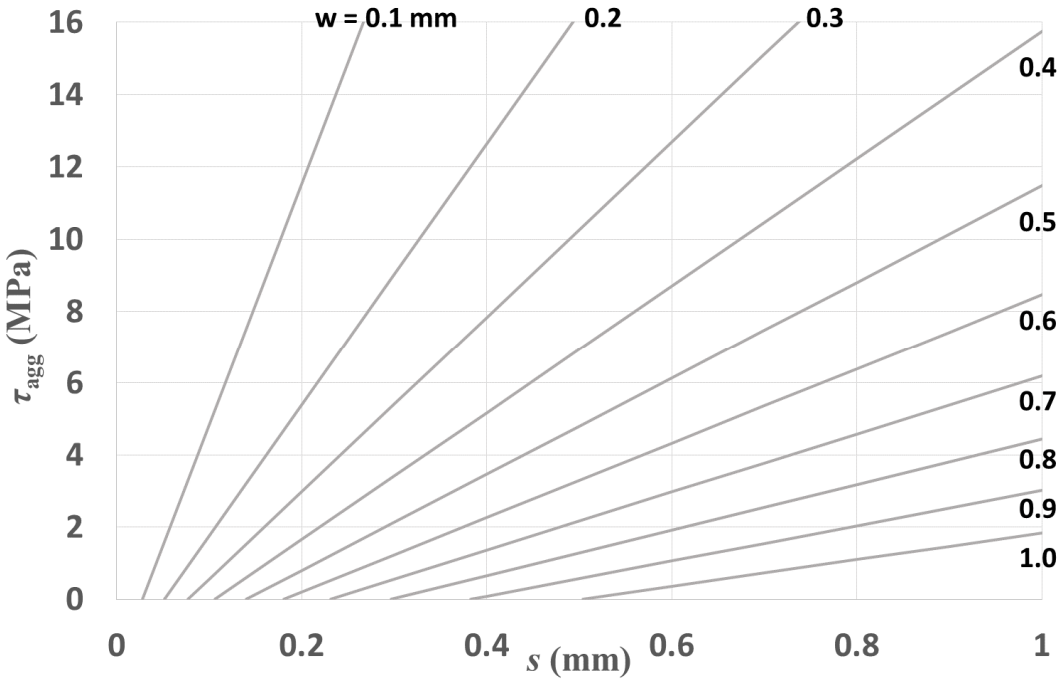

b)

Figure 5-12 – Aggregate interlock shear stresses for several crack opening values: a) calculated from Equation (5-11) with C_{f*} = 1.64 and f_{cc} = 56.1 MPa; b) calculated from Equation (5-1) with C_f = 1 and f_{cc} = 56.1 MPa.

5.5.2 FREE SURFACES

Dowel action contribution to shear transfer in an interface between concretes cast at different times, whose roughness profile is a free surface (left without treatment after vibration of the old concrete), is illustrated in Figure 5-13, where the average experimental response of specimens M1, M2 and M3 (see Table 5-2) is included. It can be noticed that dowel action weight in the global, or complete, interface behavior is much more substantial in comparison with cracks in monolithic concrete. At the peak experimental shear force (V = 199.9 kN), dowel contribution ($V_{d,FEM}$ = 84.38 kN) represents 42.2 %. The influence increases with slip until dowel action becomes the predominant strength mechanism acting for s > 3.5 mm, approximately. For very large slip values (s > 7 mm), dowel strength growth due to the reinforcement kinking effect coincides with an increase in shear force on the complete interface experimental behavior.

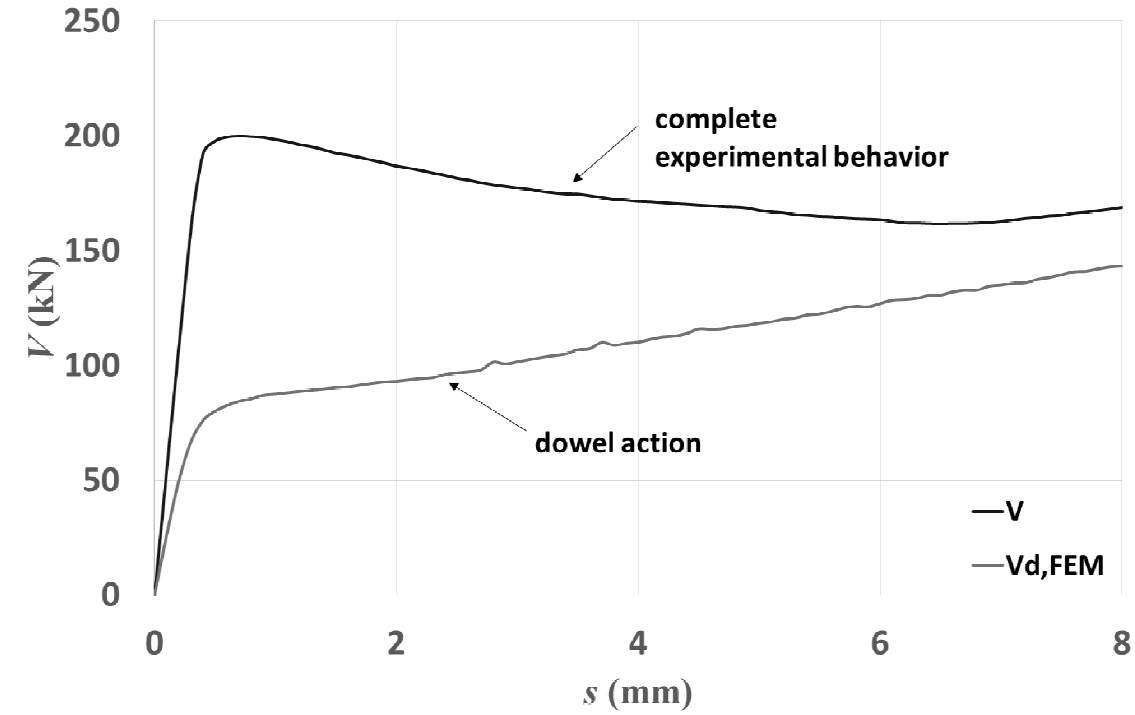

r

Figure 5-13 – Dowel action contribution to shear force, obtained in FEM, for an interface between concretes cast at different times – free surface.

Figure 5-14 presents the aggregate interlock contribution, which is obtained from the difference between the experimentally measured shear force on the concrete joint and the dowel action force calculated in the finite element modeling. It can be observed that the maximum shear force V_{agg} for the aggregate interlock mechanism occurs at a low slip value (s = 0.5 mm). Afterwards, the force decreases continuously with slip, until a residual value is achieved.

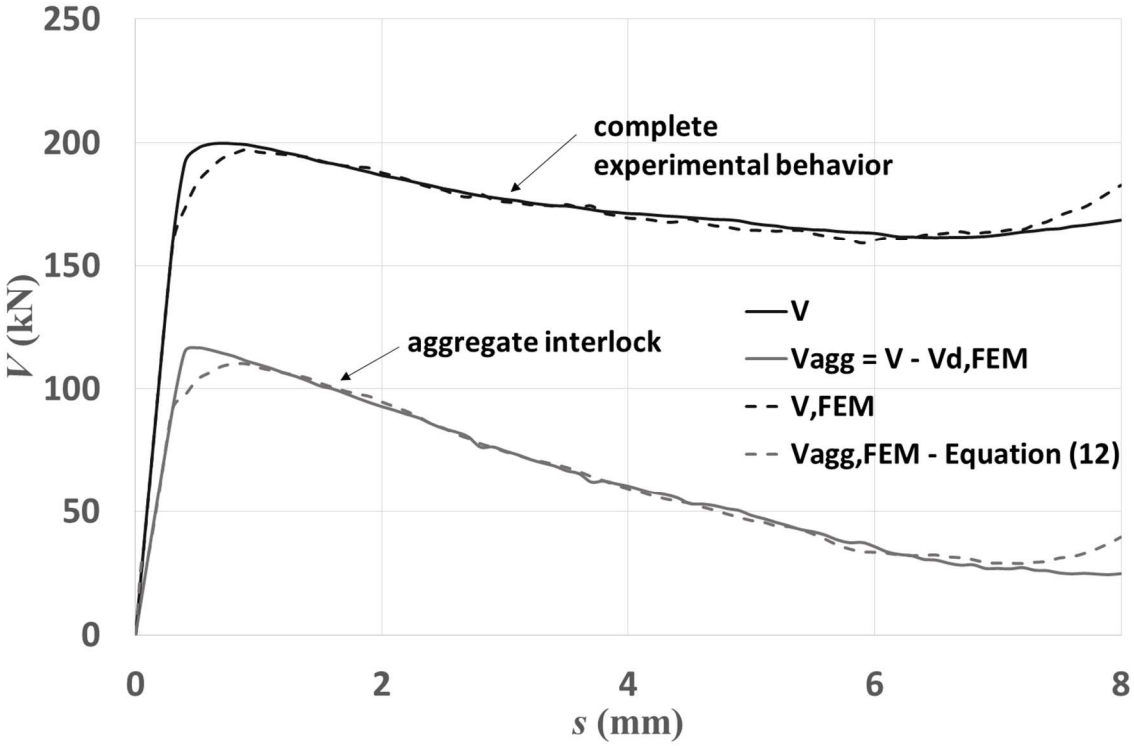

Figure 5-14 – Aggregate interlock contribution to shear, and the corresponding adjustment by Equation (5-12), in an interface between concretes cast at different times – free surface.

For interfaces with this type of roughness profile (free surface), no constitutive relations for shear transfer by aggregate interlock are available in the literature. Therefore, new relations are formulated in the present work. During the procedure, similar to the one implemented for cracks in monolithic concrete on the previous section, it was verified that in order to get a very good fit, all coefficients from Equation (5-11) should be altered. In this context, the expression that provides the best results is the following:

$$\tau_{agg} = 0.058 \times \left\{ -0.157 f_{cc} + \left[2.753 w^{-0.524} + \left(0.478 w^{-0.896} - 0.453 \right) f_{cc} \right] s \right\} \quad (5\text{-}12)$$

where f_{cc} is the average value, between the two concretes, of compressive strength measured in cube specimens.

Figure 5-14 reveals the values calculated from Equation (5-12) and a very good adjustment is achieved until s = 7 mm, approximately. However, it is important to refer that Equation (5-12) is calibrated for a single set of parameters interfering in aggregate interlock mobilization

corresponding to tests M1, M2 and M3: average concrete strength f_c = 58.0 MPa and ρ x f_y = 6.47 MPa. For a specimen with properties that differ significantly from these, it is expected the coefficients of Equation (5-12) change, especially C_{f^*}, as was perceived in the analyses performed on the previous section.

Finally, τ_{agg} – s graphs calculated from Equation (5-12) for several crack opening values can be seen in Figure 5-15, with f_{cc} = 58.0 / 0.85 = 68.2 MPa corresponding to the M1, M2 and M3 tests. Comparing with Figure 5-12 for cracks in monolithic concrete, a linear response is also observed for free surfaces, which provide much lesser values for τ_{agg}.

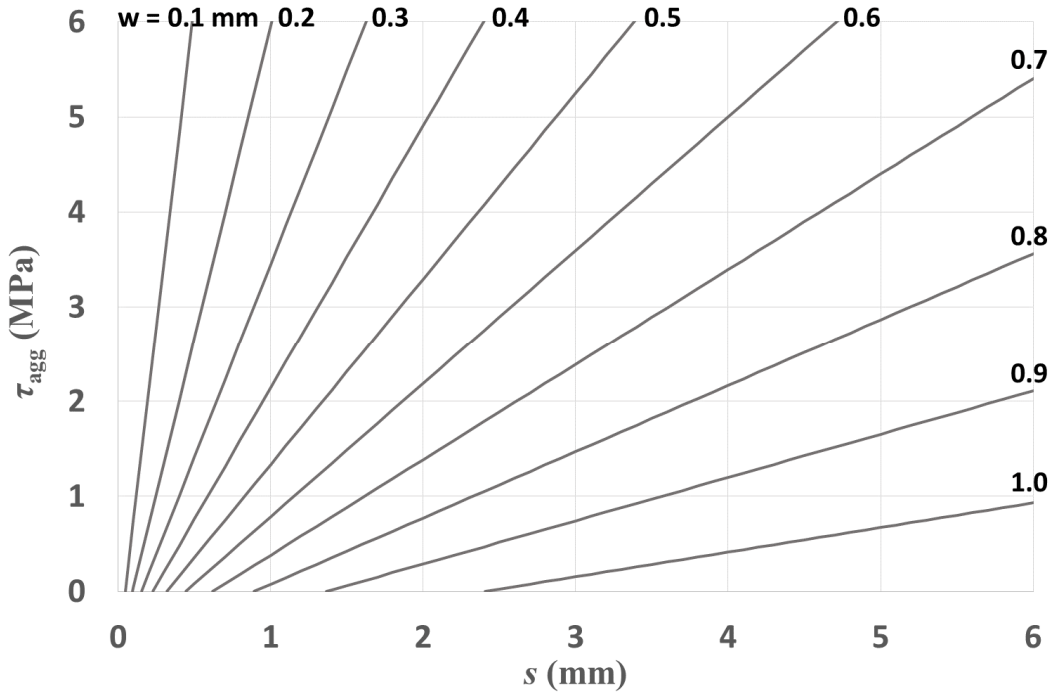

Figure 5-15 – Aggregate interlock stresses calculated from Equation (5-12), with f_{cc} = 68.2 MPa, for several crack opening values.

5.6 CONCLUSIONS

In this chapter, the following conclusions were reached:

1. The number of experimental tests available in literature that are suitable to be used in the calibration of a finite element model to assess the behavior of an interface between concretes cast at different times is scarce. Only the three tests performed in this

present work on free surfaces could be considered, a fact that limits the conception of constitutive relations for those interfaces.

2. A finite element model for the case of a concrete joint with embedded reinforcing bars, subjected to slip and crack opening displacements, was formulated and achieved. Dowel action modeling conceived in Chapter 4 was extended for the purpose, where different Winkler spring constitutive relations were assumed for the two concretes. Bond between the steel bars and the surrounding concrete was taken into account, and an interface element included to simulate aggregate interlock.

3. From the finite element model developed to assess dowel action in an interface between concretes cast at different times, the following statements could be drawn: dowel force is approximately the average of the dowel forces in each concrete separately; the reinforcement kinking effect (geometric non-linearity) has a substantial influence on dowel strength in a concrete interface.

4. Changes were introduced in the aggregate interlock empirical constitutive relations already available for cracks in monolithic concrete restrained by external bars. The modifications were implemented in order to include the contribution of the steel/concrete bond. With this upgrade, the constitutive relations become applicable to the case of an interface with embedded bars (in the range $0.075 < (\rho \times f_y) / f_c < 0.25$), and can effectively predict the stress-displacement behavior observed in the experimental tests on those interfaces.

5. New constitutive relations were also proposed for shear transfer by aggregate interlock in a concrete joint, whose roughness profile corresponds to a free surface. The expressions were calibrated for a single set of parameters interacting in aggregate interlock mobilization: average concrete strength $f_c = 58.0$ MPa and $\rho \times f_y = 6.47$ MPa. For specimens with properties that differ significantly from these, it is expected a discrepancy between results of the constitutive relations and experimental measurements.

6
CONCLUSIONS AND FUTURE RESEARCH

6.1 CONCLUSIONS

The study of reinforced concrete interfaces subjected to shear loading implemented during this work started with an experimental evaluation, then design approaches were analysed bases on statistical and probabilistic methods, and finally, finite element modeling procedures and tools were conceived and calibrated. The main conclusions reached in each of these tasks are described below.

6.1.1 EXPERIMENTAL ASSESSMENT

Knowledge about the resistant behavior of interfaces between concretes cast at different times, particularly those that result from a free surface left without further treatment after vibration of the old concrete, is still very limited. Research carried out in this Thesis allowed to acquire important and pertinent information on the phenomenon through an experimental campaign especially designed to represent the case of an interface between the precast beam and a cast-in-place of a railway bridge deck. Reproduction of that bridge structural detail included the most significant parameters of the strength mechanisms acting in interface shear transfer: surface roughness, material strength, reinforcement rate and bar diameter.

A total of 15 specimens were tested with both monotonic and cyclic loading. Monotonic tests were performed on all the 15 specimens in order to assess interface cracking load, the instant in which behavior significantly changes from being similar to monolithic concrete into a crack ruled by aggregate interlock and transverse reinforcement dowel action strength

mechanisms. An initial crack was induced at the concrete joints and higher shear stress values were observed than those subsequently performed in monotonic tests with the interface already cracked. Variability of results obtained was smaller in the latter. Moreover, when a certain slip value is s_2 reached, a local minimum takes place in the slip-shear stress variation. This occurrence demonstrates the influence and predominance of dowel action effect of the transverse reinforcement for large slip values. This mechanism, particularly due to its kinking geometric effect, causes an increase in interface strength even when roughness degradation and reinforcement yielding are underway.

Regarding fatigue tests, two main failure modes were detected. One of them was observed in the case of high amplitude loads ($\tau_{max}/\tau_R = 0.80$ and $\tau_{min}/\tau_R = 0.05$), where some similarities compared to monotonic behavior were revealed. For high amplitude cyclic loads, the dowel action mechanism (and especially the kinking effect) plays an important role, even after relevant damage occur, such as severe cracking and detachment of the concrete cover to the reinforcement. For large slip values, this mechanism causes an increase in interface fatigue strength. In turn, in the second failure mode, which governs the response under low amplitude cyclic loads ($\tau_{max}/\tau_R = 0.60$ and $\tau_{min}/\tau_R = 0.05$), some differences manifest: the steel bars fail due to fatigue and shear strength decreases abruptly with no significant damage observed in the exterior concrete surface. Also under low amplitude cyclic loading, it was verified that the slip value corresponding to the transition into the third stage, which precedes fatigue failure and slip progresses very rapidly, is slightly higher than the slip value corresponding to the peak stress in the monotonic tests, s_1. These results suggest that s_1, can be taken as a safe (conservative) indicator of an upcoming fatigue failure.

For medium amplitude load cycles ($\tau_{max}/\tau_R = 0.70$ and $\tau_{min}/\tau_R = 0.05$), results were not so clear in terms of interface behavior prediction and some variability appeared. A total of 3 specimens were subjected to cyclic loading of medium amplitude and two of them showed a similar behavior to that observed in the case of low amplitude loads, while the other one revealed a similar behavior to that observed in the case of high amplitude loads.

Conclusions can also be drawn about the evolution of crack openings in the experimental tests. Lower crack openings are observed under cyclic loading, by comparison with monotonic loading tests. Within the cyclic loads, crack openings tend to decrease as the

maximum shear stress level decreases. That tendency reveals the roughness damage caused by the fatigue cycles, which gives rise to a smoother surface as the cyclic loading progresses.

Still regarding the experimental cyclic tests performed, a tendency was noticed for an increased number of resisting load cycles when the applied shear stress amplitude decreases. In turn, within the same amplitude, the number of resisting load cycles decreases when the minimum shear stress level decreases. An S-N curve describing the average number of cycles to failure could be settled, quantifying the expected fatigue resistance under constant amplitude cyclic loading for this type of interface.

6.1.2 DESIGN RECOMMENDATIONS

The amount of existing experimental data for interfaces resulting from cracks in monolithic concrete is significantly higher than the number of data referring to interfaces with a different roughness profile. The same conclusion is obtained when the available data for interfaces subjected to monotonic loads is compared with the available data for interfaces subjected to cyclic loads.

In interfaces resulting from cracks in monolithic concrete, the amount of available experimental data provides statistical knowledge that reveals a special importance when dealing with interfaces with different roughness profiles. In interfaces corresponding to cracks in monolithic concrete, the observed resistant behavior clearly points up a nonlinear growth of the shear strength versus the existing normal stress. However, the mathematical fitting of a nonlinear function for this behavior, besides having inherent complexity, does not clearly express the physical phenomenon in study, and the resistant mechanisms that interact in shear strength mobilization. In turn, a function consisting of 3 linear branches seeks to overcome these shortcomings, although the fit to the experimental values is not so perfect.

Analysis of experimental results obtained by various authors showed that interfaces resulting from cracks in monolithic concrete and interfaces between concretes cast at different times subjected to treatment, have a significantly higher resistance than others, with values for the first case slightly higher than those relating to the second case. Interfaces resulting from a free surface and smooth interfaces have a lower resistance, with slightly lower values for the smooth interfaces. When the concrete has high strength properties, some differences in the

obtained results are observed, mainly related to the mobilization of cohesion and friction mechanisms. The results turn out to reveal the differences in the roughness profile due to fracture of high strength concrete aggregate particles.

Application of design code expressions (from EN 1992 and ACI 318-05) to the experimental results revealed a higher average resistance safety factor for rougher interfaces, for which the number of available data is also higher. However, the results dispersion and variability were always greater in such cases. It was also concluded that the design code expressions are less conservative than the target defined in the present study, which was based on the EN 1990 recommendations regarding statistical modelling of data and failure probabilities. The only exception was the EN 1992 proposal for interfaces resulting from cracks in monolithic concrete subjected to monotonic loads, which provided too conservative values (according to the same criteria).

In order to minimize the variability of results and put the average resistance safety factor in a range that provide failure probability values within the desired target, a new proposal for the design of concrete interfaces was presented. The proposal is characterized by 3 linear branches and came from a parametric analysis of existing experimental data, also following EN 1990 recommendations regarding this subject.

6.1.3 FINITE ELEMENT MODELING

Regarding dowel action of a reinforcing bar in a concrete interface, its experimental assessment is a complex task. The conception of a specimen execution procedure that can eliminate interface roughness is hard to accomplish and, consequently, the probability of dowel action interacting with aggregate interlock as an interface strength mechanism is significant. Moreover, reinforcement kinking effect arises in concrete interfaces for large slip values, also contributing for shear strength. The recommended procedure is the evaluation of dowel action in a single concrete block, removing the input of other strength mechanisms.

In order to calibrate a finite element model for dowel action that can be applied to a wide range of bar diameters and concrete strengths, the Dei Poli et al. (1992) empirical model was considered. Comparing the model with the tests performed by Dei Poli et al. (1992), it was concluded that a slight change in the proposed stiffness for concrete substrate results in an

important improvement in the adjustment to the experimental results. The finite element model conceived contains a complete discrete "beam element" representation of the steel reinforcing bar, accounting for material plasticity, rotational degrees of freedom and flexural stiffness. The bar is connected to concrete embedment through discrete Winkler spring elements, with nonlinear constitutive relations, to simulate the deformability and strength of the concrete substrate. Two different approaches were studied: 1 – simpler 2D models with concrete substrate included only on Winkler springs; 2 – 3D models with concrete substrate treated through a block of linear elastic finite elements and plasticity simulated on the Winkler springs. The 3D Embedded Dowel approach is more complex, but also capable of being included in more global analyses with other structural phenomena.

Comparison with the calibrated empirical model allowed the definition of force-displacement relations for the nonlinear Winkler spring response, considering a wide and recurrent range of values for bar diameter and concrete strength. Influence on dowel behavior of confinement imposed by stirrups was evaluated and an additional coefficient multiplying dowel strength is suggested, based on recommendations available in literature about this subject. Spring response is also adapted in order to incorporate the existence of stirrups. A state-of-art review about the influence of lateral concrete cover on dowel action provided useful information and background for the definition of a dowel strength reduction factor. Assumptions are made for Winkler spring behavior based on tests performed in this work having concrete splitting failure. Those premises are later introduced in the force – displacement spring relations. Finally, the combined influence of lateral concrete cover and confinement imposed by stirrups is analyzed in terms of dowel and spring response.

Concerning finite element modeling to assess the behavior of an interface between concretes cast at different times, the calibration of a model and the conception of constitutive relations for aggregate interlock is limited by the scarce experimental data available. In this context, only the three tests performed in this present work on free surfaces could be considered. Nevertheless, a finite element model for the case of a concrete joint with embedded reinforcing bars, subjected to slip and crack opening displacements, was formulated and achieved. Dowel action modeling previously conceived for the case of a single concrete block acting as substrate was extended for the purpose, with different Winkler spring constitutive relations assumed for the two concretes and geometric nonlinearity (kinking effect) considered for the reinforcing bars. Bond between the steel bars and the

surrounding concrete was also taken into account, and an interface element included to simulate aggregate interlock. From the finite element model developed to assess dowel action in an interface between concretes cast at different times, it was concluded that the interface dowel force is approximately the average of the dowel forces in each concrete separately. Moreover, the reinforcement kinking effect has a substantial influence on dowel strength in a concrete interface.

In terms of aggregate interlock modeling, changes were introduced in the aggregate interlock empirical constitutive relations already available for cracks in monolithic concrete restrained by external bars. The modifications were implemented in order to include the contribution of the steel/concrete bond. With this upgrade, the constitutive relations become applicable to the case of an interface with embedded bars (in the range $0.075 < (\rho \times f_y) / f_c < 0.25$), and can effectively predict the stress-displacement behavior observed in the experimental tests on those interfaces. New constitutive relations were also proposed for shear transfer by aggregate interlock in a concrete joint, whose roughness profile corresponds to a free surface. In this case, the expressions were calibrated for a single set of parameters interacting in aggregate interlock mobilization: average concrete strength f_c = 58.0 MPa and $\rho \times f_y$ = 6.47 MPa.

6.2 FURTHER RESEARCH

Despite the scientific contributions achieved in this Thesis, several aspects regarding its theme and main subject, experimental and numerical assessment of concrete interfaces still need further research. The actual state-of-art concerning to interfaces subjected to monotonic loading is significantly different from the state-of-art for cyclically loaded interfaces. Therefore, further contributions that can be made on the topic are described separately for monotonic and cyclic loads.

6.2.1 INTERFACES SUBJECTED TO MONOTONIC LOADING

In terms of experimental evaluation, in the case of interfaces subjected to monotonic loading, more tests are justified in order to fulfill the scarce database available in literature

concerning the topic. This present work only tested 3 specimens with the same strength parameters (surface roughness, concrete strength, reinforcement ratio and bar diameter). So, an extended experimental campaign, with greater variability in the strength parameters would be relevant. That campaign would be useful, mainly, to provide more extensive information and data for ULS design using statistical and probabilistic methods, and also for a more complete calibration of constitutive relations for aggregate interlock. In this context, the empirical relations proposed by Walraven and Reinhardt (1981) were considered as the basis for the finite element analyses due to its better results in terms of convergence of the numerical solution comparing to other approaches. Since the expressions proposed are totally empirical, other constitutive relations based on a physical approach to the aggregate interlock phenomena would be favorable, as long as they retain the same advantages and results in terms of convergence of the numerical solution in the finite element models.

Furthermore, it is important to note that, even though the database of experimental results considered in the calibration of Equation (5-11) includes different f_{cc} and ρ values, all the test specimens have embedded reinforcement with a diameter of 8 mm. The stiffness of the reinforced interface in the direction normal do the crack not only depends on the f_{cc} and ρ values but also on the bar diameter. In the scope of this Thesis, it was not possible to extend the calibration and validation of the aggregate interlock model to different bar diameters. For that reason, further calibration is recommended for more bar diameters, before the proposed model can be applied in accurate calculations of stresses due to aggregate interlock, in interfaces crossed by bars of significantly different diameter.

Still on concrete joints subjected to monotonic loading, it is now known that the cracking loads are high, even higher than post-cracking strength. Therefore, during structure service life uncracked interface behavior is recurrent. To identify the instant at which cracking can happen, a cracking envelope for this type of interface needs to be known. However, information about that envelope is scarce in literature. In this Thesis, cracking loads were determined only for joints without any normal stress externally applied. In order to have a complete cracking envelope, more results are needed for interfaces with compressive and tensile normal stress. Concerning the issue, some data is available in literature (Saldanha et al. 2013) but only for cracks in monolithic concrete and intentionally roughened surfaces.

Regarding dowel action mechanism, Dei Poli et al. (1992) tests were very complete,

evaluating several specimens with different strength parameter values. However, data related to dowel action in specimens confined by stirrups, or when lateral concrete cover is insufficient, could be vaster. In the first case, Rasmussen (1963) provided valuable data, but only regarding dowel strength. The corresponding force – displacement responses are not available. This information would turn more complete the calibration of the proposed constitutive relations for dowel action in concrete confined by stirrups. In the case of specimens with insufficient lateral cover, there are already in literature recommendations regarding the dowel strength reduction caused by this phenomena. Nevertheless, data analyzed in the present work showed signs of high variability associated to the lateral concrete cover influence on dowel action, compared to the few experimental tests available in literature where this influence is evident. Moreover, it would be also useful to plan further tests where both effects, confinement imposed by stirrups and insufficient lateral concrete cover, are combined. The extensive literature review that was carried out in this Thesis could not find any publication where this combined effect was studied. Furthermore, it would be also interesting to extend this finite element modeling approach to two particular situations: dowel action of reinforcing bars whose axis is not perpendicular to the shear plane (Dulacska 1972), and dowel action against concrete cover (Dei Poli et al. 1993) and not against concrete core.

6.2.2 INTERFACES SUBJECTED TO CYCLIC LOADING

For cyclic loading, a more extended experimental campaign would be relevant to assess shear transfer in reinforced concrete interfaces. Concerning fatigue strength, 9 specimens were tested in this present work for free surfaces, and the data collected, along with previous tests performed by Pruijssers (1988) for cracks in monolithic concrete, provided important information that allowed the setting of an S-N curve. Nevertheless, the total number of experimental data is still far from the desired $n > 100$ condition recommended by EN 1990 (CEN 2002). Although the proposed S-N relationship is independent of the interface roughness, for those additional tests, it would be useful the consideration of specimens with different roughness profiles (intentionally roughened surfaces and smooth surfaces) from the ones already tested (cracks in monolithic concrete and free surfaces). Also to provide for this interfaces with different roughness profiles information for stress – displacement modeling.

Regarding the modeling of an interface subjected to fatigue loading, expressions are available in the work of Pruijssers (1988) relating interface slip and crack opening displacements with maximum shear stress τ_{max} in each load cycle and shear strength τ_R. The expressions were obtained for the case of "high cycle" loading in cracks in monolithic concrete. But since they consider the relation τ_{max} / τ_R to calculate the interface displacements during the cyclic loading, as the proposed S-N curve also considers for interface fatigue strength, their values should be compared in a further research with experimental results on interfaces with different roughness profiles.

In terms of aggregate interlock contribution, Walraven (1994) extended his "two phase model" to cyclic loading, but only for "low cycle" earthquake loading in cracks in monolithic concrete. For dowel action contribution, Vintzeleou and Tassios (1987) tested specimens subjected to "low cycle" loading in order to assess seismic strength, and then recommended that dowel strength should be halved in those cases. Also for dowel behavior in "low cycle" loading, some empirical modeling considerations were purposed by Pruijssers (1988).

From this brief state-of-art review, we can conclude that research on aggregate interlock and dowel action modeling was mainly performed on specimens subjected to "low cycle" loading, for which some recommendations are already available. However, a study with greater depth, robustness and versatility would be important. Particularly, a study that could be an extension of the finite element modeling approach carried out in this Thesis on Chapter 4 (for dowel action) and Chapter 5 (for concrete interfaces and aggregate interlock). In those models, each mechanism contributing to strength is discretized in finite elements suitable to be used in a 3D structural analysis with other structural phenomena. Moreover, the finite elements contain very complete constitutive relations, with plasticity and stress softening, which provide good results in terms of convergence of the model numerical solution. For "high cycle" loading, the research performed on interface modeling is scarcer and the same statements applies: a study with greater depth, robustness and versatility would be important.

REFERENCES

ACI. (2005). *ACI 318-05, Building code requirements for structural concrete*. American Concrete Institute, Farmington Hills, Michigan, United States of America, 438 p.

Anderson, A. R. (1960). *Composite designs in precast and cast-in-place concrete*. Progressive Architecture, 41(9), p. 172-179.

Anderson, T. W. and Darling, D. A. (1954). *A test of goodness of fit*. Journal of the American Statistical Association, 49(268), p. 765-769.

Azzalini, A. and Dalla Valle, A. (1996). *The multivariate skew-normal distribution*. Biometrika, 83(4), p. 715-726.

Banagher. (2015). *http://www.bancrete.com/wp-content/uploads/2011/12/P1010355.jpg*. Banagher Precast Concrete, Co. Offaly, Ireland.

Bazant, Z. P. and Gambarova, P. G. (1980). *Rough cracks in reinforced concrete*. Journal of the Structural Division, American Concrete Institute, 106(4), p. 819-842.

Bennett, E. W. and Banerjee, S. (1976). *Strength of beam-column connections with dowel reinforcement*. The Structural Engineer, 54(4), p. 133-139.

Birkeland, P. W. and Birkeland, H. W. (1966). *Connections in precast concrete construction*. ACI Journal Proceedings, American Concrete Institute, 63(3), p. 345-368.

Capraro, R. M. (2006). *Significance level*. Encyclopedia of measurement and statistics. SAGE, California, United States of America, p. 890-893.

CEB. (1988). *Bulletin 188: Fatigue of concrete structures – state of art report*. Comite Euro-International du Beton, Lausanne, Switzerland, 312 p.

CEB-FIP. (1978). *International system of unified standard codes of practice for structures. Volume I, 'Common unified rules for different types of construction and material'*, Comite Euro-International du Beton – Fédération Internationale de la Precontrainte, Lausanne, Switzerland, 348 p.

CEN. (2004). *EN 1992-1-1, Eurocode 2: Design of concrete structures – Part 1-1: General rules and rules for buildings*. European Committee for Standardization, Brussels, Belgium, 225 p.

CEN. (2002). *EN 1990, Eurocode – Basis of structural design*. European Committee for Standardization, Brussels, Belgium, 118 p.

CEN. (2005). *EN 1992-2, Eurocode 2: Design of concrete structures – Part 2: Concrete bridges – Design and detailing rules*. European Committee for Standardization, Brussels, Belgium, 95 p.

CIRIA. (1977). *Rationalization of safety and serviceability factors in structural codes*. Construction Industry Research and Information Association, Report 63, Delft, The Netherlands, 208 p.

Clímaco, J. C. T. S. and Regan, P. E. (2001). *Evaluation of bond strength between old and new concrete in structural repairs*. Magazine of Concrete Research, 53(6), p. 377-390.

Coello Coello, C. A., Lamont, G. B. and Van Veldhuizen, D. A. (2007). *Evolutionary algorithms for solving multi-objective problems*. 2nd Edition, Springer, New York, United States of America, 800 p.

CPCI (2015). http://www.cpci.ca/en/precast_solutions/girder_bridges. Canadian Precast Prestressed Concrete Institute, 2015.

D'Agostino, R. B. and Stephens, M. A. (1986). *Goodness-of-fit techniques*. Marcel Dekker, New York, United States of America, 560 p.

Dalla Valle, A. (2007). *A test for the hypothesis of skew-normality in a population*. Journal of Statistical Computation and Simulation, 77(1), p. 63-77.

Davids, W. G. and Turkiyyah, G. M. (1997). *Development of embedded bending member to model dowel action*. Journal of Structural Engineering, American Society of Civil Engineers, 123(10), p. 1312-1320.

de Borst, R., Crisfield, M. A., Remmers, J. J. and Verhoosel, C. V. (2012). *Nonlinear finite element analysis of solids and structures*. 2nd Edition, John Wiley & Sons, Chichester, United Kingdom, 540 p.

Dei Poli, S., Di Prisco, M. and Gambarova, P. G. (1992). *Shear response, deformations and subgrade stiffness of a dowel bar embedded in concrete*. ACI Structural Journal, American Concrete Institute, 89(6), p. 665-675.

Dei Poli, S., Di Prisco, M. and Gambarova, P. G. (1993). *Cover and stirrup effects on the shear response of dowel bar embedded in concrete*. ACI Structural Journal, American Concrete Institute, 90(4), p. 441-450.

DIANA. (2014). *DIANA finite element analysis user's manual release 9.6*. TNO DIANA BV, Delft, The Netherlands.

Dias-da-Costa, D., Alfaiate, J. and Júlio, E. N. B. S. (2012). *FE modeling of the interfacial behaviour of composite concrete members*. Construction and Building Materials, 26, p. 233-243.

Dulacska, H. (1972). *Dowel action of reinforcement crossing cracks in concrete*. ACI Journal Proceedings, American Concrete Institute, 69(12), p. 754-757.

Engström, B. (1990). *Combined effect of dowel action and friction in bolted connections*. Nordic Concrete Research, 9, p. 14-33.

Fardis, M. N. and Chen, E. S. (1986). *A cyclic multiaxial model for concrete*. Computational Mechanics, 1(4), p. 301-315.

Feenstra, P. H., de Borst, R. and Rots, J. G. (1991). *Numerical study on crack dilatancy. I: Models and stability analysis*. Journal of Engineering Mechanics, 117(4), p. 733-753.

Feenstra, P. H., de Borst, R. and Rots, J. G. (1991). *Numerical study on crack dilatancy. II: Applications*. Journal of Engineering Mechanics, 117(4), p. 754-769.

fib (2004). *Bulletin 29: Precast concrete bridges*. fédération internationale du béton, Lausanne, Switzerland, 84 p.

fib (2008). *Bulletin 43: Structural connections for precast concrete buildings*. fédération internationale du béton, Lausanne, Switzerland, 370 p.

fib (2013). *fib Model Code for concrete structures 2010*. Ernst & Sohn, Berlin, Germany, 434 p.

Figueira, D., Sousa, C., Calçada, R. and Serra Neves, A. (2015). *Push-off tests in the study of the cyclic behavior of interfaces between concretes cast at different times*. Journal of Structural Engineering, American Society of Civil Engineers, 142(1), 04015101.

FIP. (1982). *Shear at the interface of precast and in situ concrete*. Fédération Internationale de la Precontrainte, Lausanne, Switzerland, 32 p.

Friberg, B. F. (1938). *Design of dowels in transverse joints of concrete pavements*. Proceedings of the American Society of Civil Engineers, 64(9), p. 1809-1828.

Fronteddu, L., Léger, P. and Tinawi, R. (1998). *Static and dynamic behavior of concrete lift joint interfaces*. Journal of Structural Engineering, American Society of Civil Engineers, 124(12), p. 1418-1430.

Galloway, J. W., Harding, H. M. and Raithby, K. D. (1979). *Effects of age on flexural, fatigue and compressive strength of concrete.* Transport and Road Research Laboratory, Report No. 865, 20 p.

Gambarova, P. G. and Karakoç, C. (1983). *A new approach to the analysis of the confinement role in regularly cracked concrete elements*. Transactions of the 7th International Conference on Structural Mechanics in Reactor Technology, International Association for Structural Mechanics in Reactor Technology, Volume H, Chicago, United States of America.

Gebreyouhannes, E., Kishi, T. and Maekawa, K. (2008). *Shear fatigue response of cracked concrete interface*. Journal of Advanced Concrete Technology, 6(2), p. 365-376.

Guo, H., Sherwood, J. A. and Snyder, M. B. (1995). *Component dowel-bar model for load-transfer systems in PCC pavements*. Journal of Transportation Engineering, American Society of Civil Engineers, 121(3), p. 289-298.

Hanson, N. W. (1960). *Precast-prestressed concrete bridges – 2. Horizontal shear connections*. Journal of the PCA Research and Development Laboratories, Portland Cement Association, 2(2), p. 38-58.

Hartl, H. and Feix, J. (2011). *Bemessungs- und Ausführungshinweise für Aufbeton auf Brückenfahrbahnplatten*. Beton- und Stahlbetonbau, 106(4), p. 250-259.

He, X. G. and Kwan, A. K. H. (2001). *Modeling dowel action of reinforcement bars for finite element analysis of concrete structures*. Computers & Structures, 79, p. 595-604.

Hofbeck, J. A., Ibrahim, I. O. and Mattock, A. H. (1969). *Shear transfer in reinforced concrete*. ACI Journal Proceedings, American Concrete Institute, 66(2), p. 119-128.

Horvatis, J., Andreatta, A. and Feix, J. (2010). *Economic strengthening of bridges by additional concrete layers*. 6th CCC Congress, p. 59-65.

Hsu, T. C., Mau, S. T. and Chen, B. (1986). *Theory of shear transfer strength of reinforced concrete*. ACI Structural Journal, American Concrete Institute, 84(2), p. 149-160.

Hsu, T. T., Slate, F. O., Sturman, G. M. and Winter, G. (1963). *Microcracking of plain concrete and the shape of the stress-strain curve*. ACI Journal Proceedings, American Concrete Institute, 60(2), p. 209-224.

ISO (1998). *ISO 2394, General principles on reliability for structures*. International Standard Organization, Geneva, Switzerland, 75 p.

Júlio, E. N. B. S., Dias-da-Costa, D., Branco, F. A. B. and Alfaiate, J. M. V. (2010). *Accuracy of design code expressions for estimating longitudinal shear strength of strengthening concrete overlays*. Engineering Structures, 32, p. 2387-2393.

Kahn, L. F. and Mitchell, A. D. (2002). *Shear friction tests with high-strength concrete*. ACI Structural Journal, American Concrete Institute, 99(1), p. 98-103.

Kazaz, I. (2011). *Finite element analysis of shear-critical reinforced concrete walls*. Computers & Structures, 8(2), p. 143-162.

Kwan, A. K. H. and Ng, P. L. (2013). *Modelling dowel action of discrete reinforcing bars for finite element analysis of concrete structures*. Computers and Concrete, 12(1), p. 19-36.

Lasdon, L. S., Waren, A. D., Jain, A. and Ratner, M. (1978). *Design and testing of a generalized reduced gradient code for nonlinear programming*. ACM Transactions on Mathematical Software (TOMS), 4(1), p. 34-50.

Lenz, P. (2012). *Beton-Beton-Verbund Potenziale für Schubfugen*. Technischen Universität München, Ph.D. Thesis, 294 p.

Li, B., Maekawa, K. and Okamura, H. (1989). *Contact density model for stress transfer across cracks in concrete*. Journal of the Faculty of Engineering, 40(1), p. 9-52.

Lockhart, R. A. and Stephens, M. A. (1994). *Estimation and tests of fit for the three-parameter Weibull distribution*. Journal of the Royal Statistical Society, Series B(Methodological), p. 491-500.

Loov, R. E. and Patnaik, A. K. (1994). *Horizontal shear strength of composite concrete beams with a rough interface*. PCI Journal, Precast/Prestressed Concrete Institute, 39(1), p. 48-69.

Mackiewicz, P. (2015). *Finite-element analysis of stress concentration around dowel bars in jointed plain concrete pavement*. Journal of Transportation Engineering, 141(6), 06015001.

Maekawa, K. and Qureshi, J. (1996). *Computational model for reinforcing bar embedded in concrete under combined axial pullout and transverse displacement*. Journal of Materials, Concrete Structures and Pavements, 31(538), p. 227-239.

Maekawa, K. and Qureshi, J. (1997). *Stress across interfaces in reinforced concrete due to aggregate interlock and dowel action*. Journal of Materials, Concrete Structures and Pavements, 34(557), p. 159-172.

Maekawa, K., Pimanmas, A. and Okamura, H. (2003). Nonlinear mechanics of reinforced concrete. Spon Press, London, United Kingdom, 766 p.

Maekawa, K., Fukuura, N. and Soltani, M. (2008). *Path-dependent high cycle fatigue modeling of joint interfaces in structural concrete*. Journal of Advanced Concrete Technology, 6(1), p. 227-242.

Magliulo, G., Ercolino, M., Cimmino, M., Capozzi, V. and Manfredi, G. (2014). *FEM analysis of the strength of RC beam-to-column dowel connections under monotonic actions*. Construction and Building Materials, 69, p. 271-284.

Mander, J. B., Priestley, M. J. and Park, R. (1988). *Theoretical stress-strain model for confined concrete*. Journal of Structural Engineering, American Society of Civil Engineers, 114(8), p. 1804-1826.

Mansur, M. A., Vinayagam, T. and Tan, K.-H. (2008). *Shear transfer across a crack in reinforced high-strength concrete*. Journal of Materials in Civil Engineering, American Society of Civil Engineers, 20(4), p. 294-302.

Marti, P., Alvarez, M., Kaufmann, W. and Sigrist, V. (1998). *Tension chord model for structural concrete*. Structural Engineering International, 8(4), p. 287-298.

Mattock, A. H. and Kaar, P. H. (1961). *Precast-prestressed concrete bridges – 4. Shear tests of continuous girders*. Journal of the PCA Research and Development Laboratories, Portland Cement Association, 3(1), p. 19-46.

Mattock, A. H. and Hawkins, N. M. (1972). *Shear transfer in reinforced concrete - recent research*. PCI Journal, Precast/Prestressed Concrete Institute, 17(2), p. 55-75.

Mattock, A. H. (1974). *Shear transfer in concrete having reinforcement at an angle to the shear plane*. ACI Special Publication 42-2, American Concrete Institute, p. 17-42.

Mattock, A. H., Johal, L. and Chow, H. C. (1975). *Shear transfer in reinforced concrete with moment or tension acting across the shear plane*. PCI Journal, Precast/Prestressed Concrete Institute, 20(4), p. 76-93.

Mattock, A. H. (1976). *Shear transfer under monotonic loading across an interface between concretes cast at different times*. SM 76-3, University of Washington, Seattle, United States of America, 70 p.

Mattock, A. H., Li, W. K. and Wang, T. L. (1976). *Shear transfer in lightweight reinforced concrete*. PCI Journal, Precast/Prestressed Concrete Institute, 21(1), p. 20-39.

Mattock, A. H. (1981). *Cyclic shear transfer and type of interface*. Journal of the Structural Division, American Society of Civil Engineers, 107(10), p. 1945-1964.

Mattock, A. H. (1988). *Influence of concrete strength and load history on the shear friction capacity*

of concrete members - comments. PCI Journal, Precast/Prestressed Concrete Institute, 33(1), p. 165-166.

Mattock, A. H. (2001). *Shear friction and high-strength concrete*. ACI Structural Journal, American Concrete Institute, 98(1), p. 50-59.

Millard, S. G. and Johnson, R. P. (1984). *Shear transfer across cracks in reinforced concrete due to aggregate interlock and to dowel action*. Magazine of Concrete Research, 36(126), p. 9-21.

Miller, R. A., Castrodale, R., Mirmiran, A. and Hastak, M. (2004). *Connection of simple-span precast concrete girders for continuity*. National Cooperative Highway Research Program, Report 519, Washington, D. C., United States of America, 202 p.

Mohamad, M. E., Ibrahim, I. S., Abdullah, R., Rahman, A. B. A., Kueh, A. B. H. and Usman, J. (2015). *Friction and cohesion coefficients of composite concrete-to-concrete bond*. Cement & Concrete Composites, 56, p. 1-14.

Moradi, A. R., Soltani, M. and Tasnimi, A. A. (2012). *A simplified constitutive model for dowel action across RC cracks*. Journal of Advanced Concrete Technology, 10, p. 264-277.

Muller, A. (2008). *Zum Zug- und Schubtragverhalten von Betonfugen*. Technischen Universität München, Ph.D. Thesis, 205 p.

Newhouse, C. D. (2005). *Design and behavior of precast, prestressed girders made continuous – an analytical and experimental study*. Virginia Polytechnic Institute and State University, United States of America, 271 p.

Owen, D. R. J. and Hinton, E. (1980). *Finite elements in plasticity: theory and practice*. 1st Edition, Pineridge Press Limited, Swansea, United Kingdom, 594 p.

Park, R. and Paulay, T. (1975). *Reinforced concrete structures*. John Wiley & Sons, New York, United States of America, 783 p.

Patnaik, A. K. (2001). *Behavior of composite concrete beams with smooth interface*. Journal of Structural Engineering, American Society of Civil Engineers, 127(4), p. 359-366.

Paulay, T. and Loeber, P. J. (1974). *Shear transfer by aggregate interlock*. ACI Special Publication, American Concrete Institute, V. 42, p. 1-16.

Paulay, T., Park, R. and Phillips, M. H. (1974). *Horizontal construction joints in cast-in-place reinforced concrete*. ACI Special Publication 42-27, American Concrete Institute, p. 599-616.

Paris, P. C. (1964). *The fracture mechanics approach to fatigue*. 10th Sagamore Army Material Research Conference, Syracuse University Press, New York, United States of America, 26 p.

Pimentel, M., Cachim, P. and Figueiras, J. (2008). *Deep-beams with indirect supports: numerical modeling and experimental assessment*. Computers and Concrete, 5(2), p. 117-134.

Pruijssers, A. F. and Lung, G. L. (1985). *Shear transfer across a crack in concrete subjected to repeated loading. Experimental results: Part I*. Stevin Report 5-85-12, University of Technology,

Delft, The Netherlands, 186 p.

Pruijssers, A. F. (1988). *Aggregate interlock and dowel action under monotonic and cyclic loading*. University of Technology, Delft, The Netherlands, 193 p.

Puntel, E. and Saouma, V. E. (2008). *Experimental behavior of concrete joint interfaces under reversed cyclic loading*. Journal of Structural Engineering, American Society of Civil Engineers, 134(9), p. 1558-1568.

Rahal, K. N., Khaleefi, A. L. and Al-Sanee, A. (2016). *An experimental investigation of shear-transfer strength of normal and high strength self compacting concrete*. Engineering Structures, 109, p. 16-25.

Randl, N. (1997). *Investigations on load transfer between old and new concrete at different surface roughnesses*. Leopold-Franzens-Universität Innsbruck, Tirol, Austria, 379 p.

Randl, N., Münger, F. and Wicke, M. (2005). *Verstärkung von Brückentragwerken durch Aufbeton*. Bauingenieur, 4, p. 207-214.

Randl, N. (2013). *Design recommendations for interface shear transfer in fib Model Code 2010*. Structural Concrete, 14(3), p. 230-241.

Rasmussen, B. H. (1963). *The carrying capacity of transversely loaded bolts and dowels embedded in concrete*. Bygningsstatiske Meddelser, 34(2), p. 39-55.

Ribeiro, D. (2014). *Dynamic effects induced by traffic on railway bridges: numerical modeling, calibration and experimental validation*. SEI – Structural Engineering International, IABSE, 24(2), p. 298.

Saldanha, R., Júlio, E., Dias-da-Costa, D. and Santos, P. (2013). *A modified slant shear test designed to enforce adhesive failure*. Construction and Building Materials, 41, p. 673-680.

Santos, P. M. D. and Júlio, E. N. B. S. (2011). *Factors affecting bond between new and old concrete*. ACI Materials Journal, American Concrete Institute, 108(4), p. 449-456.

Santos, P. M. D. and Júlio, E. N. B. S. (2012). *A state-of-the-art review on shear-friction*. Engineering Structures, 45, p. 435-448.

Santos, P. M. D. and Júlio, E. N. B. S. (2013). *A state-of-the-art review on roughness quantification methods for concrete surfaces*. Construction and Building Materials, 38, p. 912-923.

Santos, P. M. D. and Júlio, E. N. B. S. (2014). *Interface shear transfer on composite concrete members*. ACI Structural Journal, 111(1), p. 113-121.

Schneider, J. (1997). *Introduction to safety and reliability of structures*. International Association for Bridge and Structural Engineering, Zurich, Switzerland, 109 p.

Shorack, G. R. and Wellner, J. A. (1986). *Empirical processes with application to statistics*. John Wiley & Sons, New York, United States of America, 956 p.

Silfwerbrand, J. (2003). *Shear bond strength in repaired concrete structures*. Materials and Structures,

36, p. 419-424.

Soroushian, P., Obaseki, K., Rojas, M. C. and Sim, J. (1986). *Analysis of dowel bars acting against concrete core*. ACI Journal Proceedings, American Concrete Institute, 83(4), p. 642-649.

Soroushian, P., Obaseki, K. and Rojas, M. C. (1987). *Bearing strength and stiffness of concrete under reinforcing bars*. ACI Materials Journal, American Concrete Institute, 84(3), p. 179-184.

Soroushian, P., Obaseki, K., Baiyasi, M. I., El-Sweidan, B. and Choi, K. (1988). *Inelastic cyclic behavior of dowel bars*. ACI Structural Journal, American Concrete Institute, 85(1), p. 23-29.

Sousa, C. (2012). *Analysis of cyclic and long-term effects in continuous precast railway bridge decks*. University of Porto – Faculty of Engineering, Portugal, 371 p.

Sousa, C., Rocha, J. F., Calçada, R. and Serra Neves, A. (2013). *Fatigue analysis of box-girder webs subjected to in-plane shear and transverse bending induced by railway traffic*. Engineering Structures, 54, p. 248-261.

Tadros, M. K., Ficenec, J. A., Einea, A. and Holdsworth, S. (1993). *A new technique to create continuity in prestressed concrete members*. PCI Journal, Precast/Prestressed Concrete Institute, 38(5), p. 30-37.

Taiwan. (2015). *http://www.taiwan.gov.tw/public/data/310915414953.jpg*. Ministry of Foreign Affairs, Republic of China (Taiwan).

Tanaka, Y. and Murakoshi, J. (2011). *Reexamination of dowel behavior of steel bars embedded in concrete*. ACI Structural Journal, American Concrete Institute, 108(6), p. 659-668.

Tassios, T. P. and Vintzeleou, E. N. (1987). *Concrete-to-concrete friction*. Journal of Structural Engineering, American Society of Civil Engineers, 113(4), p. 832-849.

Tsoukantas, S. G. and Tassios, T. P. (1989). *Shear resistance of connections between reinforced concrete linear precast elements*. ACI Structural Journal, American Concrete Institute, 86(3), p. 242-249.

Vintzeleou, E. N. and Tassios, T. P. (1986). *Mathematical models for dowel action under monotonic and cyclic conditions*. Magazine of Concrete Research, 38(134), p. 13-22.

Vintzeleou, E. N. and Tassios, T. P. (1987). *Behavior of dowels under cyclic deformations*. ACI Structural Journal, American Concrete Institute, 84(3), p. 18-30.

Walraven, J. C., Vos, E. and Reinhardt, H. W. (1979). *Experiments on shear transfer in cracks in concrete. Part I: Description of results*. Stevin Laboratory Report 5-79-3, University of Technology, Delft, The Netherlands, 98 p.

Walraven, J. C. (1981). *Fundamental analysis of aggregate interlock*. Journal of the Structural Division, American Society of Civil Engineers, 107(11), p. 2245-2270.

Walraven, J. C. and Reinhardt, H. W. (1981). *Theory and experiments on the mechanical behaviour of cracks in plain and reinforced concrete subjected to shear loading*. Heron, 26(1A), 68 p.

Walraven, J. C., Frenay, J. and Pruijssers, A. (1987). *Influence of concrete strength and load history on the shear friction capacity of concrete members*. PCI Journal, Precast/Prestressed Concrete Institute, 32(1), p. 66-84.

Walraven, J. C. (1994). Rough cracks subjected to earthquake loading. Journal of Structural Engineering, American Society of Civil Engineers, 120(5), p. 1510-1524.

Walraven, J. C. and Stroband, J. (1994). *Shear friction in high-strength concrete*. ACI Special Publication 149-17, American Concrete Institute, p. 311-330.

Zoubek, B., Fahjan, Y., Fischinger, M., and Isaković, T. (2014). *Nonlinear finite element modelling of centric dowel connections in precast buildings*. Computers and Concrete, 14(4), p. 463-477.

A. EXPERIMENTAL DATA FOR STRENGTH ANALYSIS

A.1 MONOTONIC TESTS

A.1.1. CRACKED SURFACES (132 + 18 TESTS)

Hofbeck et al. (1969) – 20 specimens: 2.1; 2.2; 2.3; 2.4; 2.5; 2.6; 3.2; 3.3; 3.4; 3.5; 4.1; 4.2; 4.3; 4.4; 4.5; 5.1; 5.2; 5.3; 5.4; 5.5.

Kahn and Mitchell (2002) – 3 specimens: SF-4-1C; SF-4-2-C; SF-4-3-C.

Mansur et al. (2008) – 7 specimens: AN-2; AN-4; AN-6; AM-2; AM-3; AM-4; B1-4.

Mattock (1974) – 3 specimens: 1.1; 3.1; 4.4.

Mattock (1976) – 8 specimens: A1; A2; A3; A4; A5; A6; A6A; A7.

Mattock (1981) – 6 specimens: MN2M; MN2C; MN3M; MN3C; MN4M; MN4C.

Mattock et al. (1975) – 3 specimens: A1; E1C; F1C.

Mattock et al. (1976) – 6 specimens: N1; N2; N3; N4; N5; N6.

Pruijssers (1988) – 42 specimens: A/4L/.61/6.1; A/4L/.63/6.0; A/4H/.64/7.0; A/4L/.65/6.0; A/4H/.66/6.9; A/4L/.70/7.0; A/4L/.73/7.2; A/4L/.74/7.0; A/4L/.76/7.0; A/4H/.76/7.7; A/4L/.77/7.2; A/4H/.78/8.0; A/4L/.79/8.6; A/4L/.80/7.3; A/4L/.80/7.5; A/4L/.82/7.4; A/4L/.90/9.0; A/6L/.51/6.0; A/6L/.56/6.7; A/6L/.58/6.8; A/6L/.61/7.2; A/6L/.62/8.0; A/6H/.66/7.9; A/6L/.66/8.6; A/6L/.67/8.2; A/6L/.68/8.0; B/4L/.57/7.0; B/4L/.59/7.0; B/4L/.60/7.0; B/4L/.60/7.4; B/4L/.61/7.3; B/4H/.61/8.5; B/4L/.63/7.3; B/4L/.65/8.0; B/4H/.66/9.0; B/4L/.75/8.4; B/4L/.79/8.8; B/4L/.81/9.1; B/6L/.46/6.9; B/6L/.52/7.9; B/6L/.53/8.0; B/6L/.56/8.9.

Pruijssers and Lung (1985) – 3 specimens: 15; 16; 48.

Walraven and Reinhardt (1981) – 31 specimens: 110208t; 110208; 110208g; 110408; 110608; 110808h; 110808hg; 110706; 210204; 210608; 210216; 210316; 210808h; 120208; 120408; 120608; 120808; 120706; 120216; 230208; 230408; 230608; 230808; 240208; 240408; 240608; 240808; 250208; 250408; 250608; 250808.

Mansur et al. (2008) – 12 specimens (high strength concrete): AH-2; AH-3; AH-4; B2-2; B2-4; B2-5; B2-6; B3-4; B4-2; B4-4; B4-5; B4-6.

Walraven and Stroband (1994) – 6 specimens (high strength concrete): 10; 11; 12; 13; 14; 15.

A.1.2. Rough surfaces (20 tests)

Mattock (1976) – 14 specimens: B1; B2; B3; B4; B5; B6; D1; D2; D3; D4; D4A; D5; D6; D6A.

Mattock (1981) – 6 specimens: CB2M; CB2C; CB3M; CB3C; CB4M; CB4C.

A.1.3. Free surfaces (5 tests)

Figueira et al. (2015) (see Chapter 2) – 3 specimens: M1; M2; M3. The properties of the other 2 specimens (PM1; PM2) are the following: f_{c1} = 70.8 MPa; f_{c2} = 43.3 MPa; ρ = 0.80 x 10^{-2}; f_y = 605.4 MPa; τ_R = 4.19 MPa for the specimen M-4 and τ_R = 4.49 MPa for the specimen M-5.

A.1.4. Smooth surfaces (6 tests)

Mattock (1976) – 6 specimens: C1; C2; C3; C4; C5; C6.

A.2 CYCLIC TESTS

A.2.1. Cracked surfaces (24 tests)

Pruijssers (1988) – 24 specimens: A/4L/.73/7.2; A/4L/.76/7.0; A/4H/.76/7.7; A/4L/.77/7.2; A/4H/.78/8.0; A/4L/.79/8.6; A/4L/.80/7.3; A/4L/.80/7.5; A/4L/.82/7.4; A/4L/.90/9.0; A/6L/.56/6.7; A/6H/.66/7.9; A/6L/.66/8.6; A/6L/.67/8.2; A/6L/.68/8.0; B/4L/.59/7.0; B/4L/.60/7.4; B/4L/.61/7.3; B/4L/.63/7.3; B/4L/.65/8.0; B/4H/.66/9.0; B/4L/.75/8.4; B/4L/.79/8.8; B/4L/.81/9.1.

A.2.2. Free surfaces (9 tests)

Figueira et al. (2015) (see Chapter 2) – 9 specimens: C-5-80-1; C-5-80-2; C-5-80-3; C-5-70-1; C-5-70-2; C-5-70-3; C-5-60-1; C-5-60-2; C-5-60-3.